Towards Understanding Lymphocyte Biology – Lessons from Murine Models and Primary Immunodeficiencies

Institut für Immunologie
der Ludwig-Maximilians-Universität München

Schrift zur Erlangung der *venia legendi*
im Fachgebiet „Immunologie"

von

Marcin Łyszkiewicz, PhD

München, 2021

Die in dieser Habilitationsschrift beschriebenen Arbeiten wurden von mir an folgenden Institutionen durchgeführt:

2008 bis 2015:

Als Research Fellow in der Arbeitsguppe von Prof. Andreas Krueger am Institut für Immunologie, Medizinische Hochschule Hannover, Hannover

2015 bis 2018:

Als Research Fellow in der Arbeitsguppe von Prof. Christoph Klein am Dr. von Haunersches Kinderspital, Ludwig-Maximilians-Universität München

seit 2018:

Als DFG-Projektleiter und Research Fellow in der Arbeitsgruppe von Prof. Ludger Klein am Institut für Immunologie (Leiter: Prof. Thomas Brocker), Medizinische Fakultät, Ludwig-Maximilians-Universität München

In der vorliegenden kumulativen Habilitationsschrift werden die folgenden vier Publikationen zusammenfassend beschrieben und im Kontext diskutiert:

(1) Blume J, Ziętara N, Witzlau K, Liu Y, Sanchez OO, Puchałka J, Winter SJ, Kunze-Schumacher H, Saran N, Düber S, Roy B, Weiss S, Klein C, Wurst W, **Łyszkiewicz M** ***, ****, Krueger A. miR-191 modulates B-cell development and targets transcription factors E2A, Foxp1, and Egr1. *Eur J Immunol, 49: 121–132 (2019). *equal contribution, **corresponding author*

(2) **Łyszkiewicz M *,** Kotlarz D *, Ziętara N *, Brandes G, Diestelhorst J, Glage S, Hobeika E, Reth M, Huber L.A., Krueger A, Klein C. LAMTOR2 (p14) controls B cell differentiation by orchestrating endosomal BCR trafficking. *Front Immunol* (eCollection 2019). *equal contribution

(3) **Łyszkiewicz M** ***, ****, Ziętara N *, Frey L, Pannicke U, Liu Y, Fan Y, Puchałka P, Hollizeck S, Somekh I, Rohlfs M, Yilmaz T, Ünal E, Karakukcu M, Patiroğlu T, Keller C, Karasu E, Sykora K-W, Somech R, Roesler J, Hoenig M, Schwarz K, Klein C **. Human FCH domain only 1 (FCHO1) deficiency reveals an essential role for clathrin-mediated endocytosis for the development and function of T cells. *Nat Comm* (2020). *equally contributing first author, **corresponding author

(4) **Łyszkiewicz M**, Ziętara N, Föhse L, Puchałka J, Diestelhorst J, Witzlau K, Prinz I, Schambach A, Krueger A. Niche availability promotes intrathymic dendritic-cell development from Early T lineage Progenitors. *Blood*, 125(3):457-64 (2015).

TABLE OF CONTENTS

      6.1. miR-191 modulates B-cell development and targets transcription factors E2A, Foxp1, and Egr1

      6.2 LAMTOR2 (p14) controls B cell differentiation by orchestrating endosomal BCR trafficking. *Front Immunol* (eCollection 2019). *equal contribution

      6.3 Human FCH domain only 1 (FCHO1) deficiency reveals an essential role for clathrin-mediated endocytosis for the development and function of T cells.

      6.4 Niche availability promotes intrathymic dendritic-cell development from Early T lineage Progenitors

1. Summary

B and T lymphocytes constitute two essential components of the adaptive immune system. Both lineages arise from haematopoietic progenitors which reside in the bone marrow. Although final commitment and differentiation steps happen in different lymphoid organs, B and T cells share remarkable similarities. Both utilise Rag genes for somatically rearrange genes that encode their antigen recognition receptors. While B and T cells recombine different sets of genes, the Rag1/Rag2 genes complex recognises the same short motif in DNA to catalyse the reaction. Also, final commitment processes and selection of newly emerged receptors are similar and unique to them. Deriving a picture of the regulatory network of lymphocytes might also be seen as a model allowing to understand the basic mechanisms of non-coding RNA action. Moreover, it permits to deepen our understanding of fundamental processes in which B and T lymphocytes act.

The first study summarised here describes the impact of microRNA-191 on the transcriptional regulatory network and posttranscriptional gene regulation. The transcription factors FoxP1, E2A and Egr1, were identified as direct downstream targets of miR-191. Deletion, as well as ectopic expression of miR-191, resulted in a developmental arrest in B lineage cells, indicating that fine-tuning of the combined expression levels of Foxp1, E2A, and Egr1, which in turn control somatic recombination and cytokine-driven expansion, constitutes a prerequisite for efficient B-cell development. Two other studies explored the molecular mechanism behind primary immunodeficiencies. The pivotal role of the LAMTOR2 (p14) protein on B-lymphocytes development was linked to the aberrant internalisation of BCR from the cell membrane, subsequently leading to abnormal phosphorylation of BCR-associated kinases. Further, by studying the case of unknown entities, the unexpected significance of FCHO1 protein and clathrin-mediated endocytosis during T-lymphocyte development and function in humans was revealed. The last paper delineates the lineage relationship between myeloid cells and T lymphocytes. Development of cellular barcoding experiments allowed to follow hematopoietic lineage decisions and to answer the query about the origin of thymic DC and the mechanisms of thymic progenitor commitment.

2. ZUSAMMENFASSUNG

B- und T-Lymphozyten stellen zwei wesentliche Komponenten des adaptiven Immunsystems dar. Beide Linien gehen aus hämatopoetischen Vorläuferzellen hervor, die sich im Knochenmark befinden. Obwohl die endgültige Festlegung und die Differenzierungsschritte in unterschiedlichen lymphatischen Organen stattfinden, weisen B—und T-Zellen bemerkenswerte Ähnlichkeiten auf. Beide nutzen Rag-Gene zur somatischen Rekombination von Genen, die für ihre Antigenerkennungsrezeptoren kodieren. Während B- und T-Zellen verschiedene Sets an Genen rekombinieren, erkennt der Rag1/Rag2-Gen-Komplex dasselbe kurze DNA-Motiv, um die Reaktion zu katalysieren. Des Weiteren sind ihre endgültigen Festlegungsprozesse und ihre Selektion der neu entstandenen Rezeptoren ähnlich und einzigartig. Die Abbildung des regulatorischen Netzwerks von Lymphozyten könnte auch als Modell angesehen werden, das es erlaubt, grundlegende Mechanismen der ncRNA-Wirkungsweise zu verstehen. Außerdem gestattet es, unser Verständnis der wesentlichen Prozesse zu vertiefen, in denen B- und T-Lymphozyten beteiligt sind.

Die erste hier zusammengefasste Studie beschreibt den Einfluss der microRNA-191 auf das transkriptionelle Regulationsnetzwerk und die posttranskriptionelle Genregulation. Die Transkriptionsfaktoren FoxP1, E2A und Egr1 wurden als direkte nachgeschaltete Ziele von miR-191 identifiziert. Sowohl die Deletion als auch die ektopische Expression von miR-191 hatten einen Entwicklungsstillstand bei Zellen der B-Zelllinie zur Folge, was zeigt, dass die Feinabstimmung der kombinierten Expressionslevels von Foxp1, E2A und Egr1, die wiederum die somatische Rekombination und die zytokingesteuerte Expansion kontrollieren, eine Voraussetzung für eine effiziente B-Zellentwicklung darstellt. Zwei weitere Studien haben die molekularen Mechanismen von primären Immundefizienzen untersucht. Die zentrale Rolle des LAMTOR2 (p14)-Proteins in der Entwicklung von B-Lymphozyten wurde mit der aberranten Internalisierung des BCRs von der Zellmembran in Verbindung gebracht, die eine abnormale Phosphorylierung von BCR-assoziierten Kinasen zur Folge hat. Des Weiteren wurde durch die Untersuchung unbekannter Entitäten die unerwartete Bedeutung des FCHO1-Proteins und der Clathrin-vermittelten Endozytose für die Entwicklung und Funktion

von T-Lymphozyten im Menschen aufgedeckt. Die letzte Veröffentlichung beschreibt die Abstammungsbeziehung von myeloiden Zellen und T-Lymphozyten. Die Etablierung von zellulären Barcodes erlaubte es, die Entscheidung der hämatopoetischen Abstammungslinie nachzuvollziehen und die Frage nach dem Ursprung von thymischen DCs, sowie den Mechanismen der Festlegung der Thymus-Vorläuferzellen zu beantworten.

3. INTRODUCTION

B cells are essential players of the immune system. They are among the most omnipotent immune cells, widely appreciated as a source of antibodies. Their abilities to create antibodies against virtually any antigen is a fundament of adaptive immune response and vaccination. B cells are also recognised as crucial cells for optimal T-cell responses by their ability to present antigens, secrete cytokines and regulate the formation of the lymphoid tissue structures. At the same time, perturbations in B-cell function are manifested as allergy or malignancies. Thus, the process of B-cell development is tightly controlled on the transcriptional and posttranscriptional levels (Busslinger, 2004; Lanzavecchia, 1990; Melchers, 2015).

Transcriptional and posttranscriptional regulation of B-cell development

B cells are continuously generated in the bone marrow from uncommitted hematopoietic progenitors. The process of B cell differentiation is characterised by phases of intensive proliferation in response to extracellular and intracellular signals. Since immunoglobulin heavy and light chain loci rearrange during this process, B cells undergo developmental defined states characterised by a predisposition to genomic instability. If ill-conducted, it can lead to the generation of non-functional cells or malignancies. Therefore, B cell differentiation must be tightly controlled by regulatory networks of transcription factors and cytokines as well as non-coding RNAs (Busslinger, 2004; Lin et al., 2010; Matthias and Rolink, 2005; Turner et al., 2014). Furthermore, the quality of B-cell receptor and the signal it transduces have to be tested to ensure its productivity and removal of self-reactive B cells (Melchers, 2015; Osmond et al., 1998; Reth, 2001).

E2A and Ebf1 are considered to be the earliest determinants of B lineage (O'Riordan and Grosschedl, 1999). B-lineage commitment is completed upon expression of Pax5 (Nutt et al., 1999; Nutt et al., 1997; Urbanek et al., 1994). Once committed, developing B cells undergo a series of defined differentiation events centred on somatic recombination of immunoglobulin (Ig) heavy (IgH) and light (IgL) chain loci. Productive rearrangement of the IgH locus results

in assembly of the pre-BCR consisting of IgH and the VpreB and λ5 surrogate light chain components (Karasuyama et al., 1993; Kitamura et al., 1992; Winkler et al., 1995). Expression of the pre-BCR promotes proliferation, cell survival and developmental progression. Signalling via the IL-7 receptor (IL-7R) induces additional survival and proliferation cues. Upon productive IgL rearrangement, immature B cells undergo negative selection, which can be overcome by a further round of IgL recombination termed receptor editing and finally exit from bone marrow. During these processes, expression of key elements of the recombination machinery, such as Rag1 and Rag2, is regulated by E2A, Ebf1, and Pax5 (Bain et al., 1994; Beck et al., 2009; Fuxa et al., 2004; Goebel et al., 2001; Greenbaum and Zhuang, 2002; Lin and Grosschedl, 1995; Lin et al., 2010; Matthias and Rolink, 2005; Shen and Kadesch, 1995). In addition, the transcription factor Foxp1 contributes to the expression of Rag1 and Rag2 by binding to an enhancer region within the Rag locus (Bain et al., 1994). In consequence, the deletion of Foxp1 results in a B-lineage developmental block.

In contrast to transcription factors and cytokines, the orchestrating role of micro-RNAs (mRNA), representing another level of developmental control, remains poorly understood. Regulation of B cell development by miRNA has not been systematically addressed, and among the ~1900 known miRNAs, only a few are described to influence particular steps during the development and activation of B cells. MicroRNAs are small, non-coding RNA molecules which act as negative regulators of translation. Targeting of cognate mRNA molecules usually leads to their degradation or posttranscriptional repression. Mice deficient for Dicer, an enzyme required for processing of pre-miRNA into mature form, display defects in the development of B, T and NK cells (Koralov et al., 2008). Although it is clear that B cell development and function critically depends on miRNAs, the role of individual miRNAs in these processes remains to be determined (Chen et al., 2004; Turner et al., 2014). Some of the miRNA, comprising the miRNA cluster miR-17~92, miR-34a, miR-155, and miR-150, have been reported to regulate B cell development at different stages of differentiation directly and by targeting distinct transcriptional regulators or effectors of cell survival and proliferation

(Costinean et al., 2006; Jin et al., 2017; Loeb et al., 2012; Rao et al., 2010; Ventura et al., 2008; Xiao et al., 2008). Furthermore, abnormal expression of miRNAs has been associated with the development of B-cell malignancies. For example, overexpression of miR-17~92 cluster (also known as oncomiR-1) resulted in lymphoproliferative disease leading to B-cell lymphoma (Olive et al., 2010; Xiao et al., 2008). Similarly, overexpression of miR-155 resulted in the development of B-cell leukaemia (Loeb et al., 2012). Number of reports indicated the aberrant expression of miR-191 in solid tumours (Brown et al., 2008). Although the functional role of miR-191 has been implicated in erythroid enucleation and T cell development, the function of miR-191 in B cell development or malignancy remains unclear (Cubedo et al., 2012; Gururajan et al., 2005).

Here we describe the impact of microRNA-191 on the transcriptional regulatory network and posttranscriptional gene regulation. We show that transcription factors FoxP1, E2A and Egr1 are direct downstream targets of miR-191. Deletion, as well as ectopic expression of miR-191, results in a developmental arrest in B lineage cells, indicating that fine-tuning of the combined expression of three transcription factors which in turn control somatic recombination and cytokine-driven expansion, constitutes a prerequisite for efficient B-cell development.

Impact of B-cell receptor internalisation on B-cell differentiation and activation

In addition to the transcriptional and posttranscriptional control, the fate of developing B-cell is tightly bunded to the quality of the signal provided by newly rearranged B-cell antigen receptor (BCR) (Campbell, 1999; Melchers, 2015; Osmond et al., 1998; Reth, 2001). During development, upon successful recombination of the immunoglobulin heavy chain locus (IgH), so-called pre-BCR is assembled by pairing with surrogate light chain and expressed on the surface of the pre-B1 cells. It is signalling through the pre-BCR that promotes the transition to the next stage (pre-B2) where recombination of immunoglobulin light chain occurs. If successful, it results in formation of BCR and emergence of immature B cells. Here, BCR signalling serves to test the productivity of the light chain recombination as well as to remove self-reactive B cells in bone marrow and spleen. Finally, recognition of non-self antigens by

BCR leads to the cell activation, presentation of the foreign antigen to T cells. Further, concert action of B and T cells results in affinity maturation of B cells, subsequent differentiation into plasma cells, antibody secretion and formation of memory cells (Melchers, 2015; Osmond et al., 1998; Reth, 2001). Activation of BCR is associated with signal transduction and amplification through tyrosine phosphorylation and Ca^{2+} release including cascades like PLCγ/Ca^{2+}/NF-κB/NFAT, Rho family, PI3-K/Akt as well as Ras/Raf-1/Erk pathway (Campbell, 1999).

Yet another layer of complexity adds the fact that the BCR is not statically expressed, but rather continuously internalised from the plasma membrane and recycled or degraded via endosomal-lysosomal route. Although the process of receptor internalisation is well-described for TCR (reviewed in Brownlie and Zamoyska, 2013; Miosge and Zamoyska, 2007), surprisingly little is known about it in the context of BCR and B cells. It has been proposed that spatio-temporal distribution of the BCR is required to ensure proper signal transduction, suggesting that inhibition of BCR internalisation may result in dysregulation of kinase activation (Chaturvedi et al., 2011). However, the exact molecular mechanism involved in this process is poorly described and even controversial. In one study, the entire idea of interdependence between signalling and BCR internalisation has been questioned, describing both processes as mutually exclusive (Hou et al., 2006). Here we provided evidence that LAMTOR2 (p14)-mediated BCR internalisation is indeed required to deliver signal of appropriate quality for developing B cells as well as for activation of peripheral B lymphocytes.

Significance of clathrin-adaptor FCHO1 in human T-cell development

The quality of signal provided by T cell receptor (TCR) is essential for T-lymphocyte development and function. During thymopoiesis, there are three key selection points in which such signal is required to test both functionality and autoreactivity of newly emerged TCR (Brownlie and Zamoyska, 2013; Miosge and Zamoyska, 2007). At first, signalling through the pre-TCR indicates productive recombination of TCR beta locus and promotes the transition from CD4 CD8 double-negative (DN) 3a to DN3b developmental stage. Later, at so-called

double-positive stage (DP), where both CD4 and CD8 co-receptor molecules are co-expressed on the surface of thymocytes, signalling serves to test for successful rearrangement of TCR alpha locus. Finally, DP and later single-positive (SP) CD4 and CD8 thymocytes are tested for autoreactivity in the process of negative selection. Similarly to the BCR discussed above, the dynamic of TCR internalisation from the plasma membrane and the exact localisation is of utmost importance for the quality of signal transduced (Miosge and Zamoyska, 2007). The internalisation of TCR upon MHC-peptide complex recognition serves several purposes. It can facilitate amplification of the signal by scaffolding of TCR complexes on early endosomes. Alternatively, the signal could be down-tuned via TCR-degradation in lysosomes. Finally, recirculation of the TCR to the immune synapses may modulate TCR-dependent activation signal while interacting with antigen presenting cells.

Clathrin, a primary structural component of clathrin-coated pits (CCP), plays an essential role in the reorganisation of cellular membranes and transport between a variety of compartments, including cell membrane, trans-Golgi-network and endosomes (Robinson, 2015). Clathrin-dependent endocytosis (CME) is initiated on the plasma membrane by the recruitment of the adaptors and cargo-selecting proteins, of which most important one are the heterotetrameric AP-2 complex, CALM (clathrin assembly lymphoid myeloid leucaemia), EPS15 (epidermal growth factor receptor substrate 15) as well as FCHO1 and FCHO2 (FCH domain only 1 and 2) (Cocucci et al., 2012; Henne et al., 2010; Pechstein et al., 2010). These proteins are concentrated around PIP2 (phosphatidylinositol 4,5-biphosphate) reach regions of the plasma membrane where they trigger assembly of the clathrin triskelion into vesicles. During vesicle maturation, membrane near which the vesicle is formed undergoes invagination, and once the formation of the vesicle is completed, it is detached by dynamin (McMahon and Boucrot, 2011). Both FCHO1 and FCHO2 plays a pivotal role in CME by triggering the process and selecting the cargo. Contrary to their name, they consist of two domains. N' F-BAR domain non-covalently anchor the protein to the plasma membrane, while localised at 5' end μHD domain facilitates interaction with EPS15/EPS15R and intersectin. Ill-structured central part of

the FCHO1 (but not FCHO2) is responsible for interaction with the AP-2 protein (Koh et al., 2007; Pechstein et al., 2010).

Studies on elements orchestrating clathrin-mediated endocytosis proved that deficiencies in central elements like clathrin, AP-2 complex or Epsin are deleterious and result in embryonic lethality (Henne et al., 2010). Mutations in other, less pivotal proteins involved in this process have been associated with a variety of diseases ranging from cancer, through neuro-psychiatric disorders to metabolic syndromes, but not to inherited defects of the immune system (Cavrois et al., 2002; Henne et al., 2010; Henne et al., 2007; Mulkearns and Cooper, 2012; Pearse, 1976; Reider et al., 2009). It was proposed that TCR is internalised in clathrin-dependent (Boyer et al., 1991; Dietrich et al., 1994; Ohno et al., 1995; Telerman et al., 1987) or clathrin-independent way (Compeer et al., 2018). In our study, we show that FCHO1 is a first protein central for the process of clathrin-mediated endocytosis, the function of which can be directly linked to the adaptive immune system. Thus, the initial genetic discovery followed by human cellular models allows us to show new principle governing the immune system: endocytosis of T cell receptor depends on clathrin and its mediated via a specific adaptor.

The origin of thymic dendritic cells

In order to avoid the generation of autoreactive or non-productive T-cells, thymocytes developing in the thymus are subjected to a strict selection process. T cells reacting too strongly to a self-peptide in the context of MHC I or II molecules are either deleted in the process of negative selection or converted to so-called regulatory T cells. Those thymocytes which fail to recognise self dye by neglect. The entire process solely depends on the interaction of thymocytes with non-thymocytes, mainly thymic epithelial cells, B lymphocytes and thymic dendritic cells (tDC). Thymic DC compartment consists of plasmacytoid DCs (pDCs) and two subsets of so-called conventional DCs. The later can be distinguished by differential expression of CD8α and SIRPα (Wu and Shortman, 2005). The origin of conventional DCs in peripheral lymphoid organs is well described. Both populations derived from the common myeloid pathway, starting from myeloid progenitors (MPs) via

macrophages/DC progenitors (MDPs) and common DC progenitors through pre-DC (Geissmann et al., 2010).

Whereas thymic epithelial cells are an integral part of the thymus, B lymphocytes populating thymus are of bone marrow origin, the developmental origin of tDC was controversial. There is strong evidence supporting the hypothesis of their lymphoid origin. It has been shown that tDC, but not peripheral cDC, have partially rearranged D_H to J_H TCR beta locus (Corcoran et al., 2003). Furthermore, both human and murine tDC express pre-TCRa chain (Wu et al., 2001). Besides, early T-lineage progenitors (ETP) retain DC potential and given right environment can robustly differentiate into cDC with kinetic similar to that of T cells (Ardavin et al., 1993; Bell and Bhandoola, 2008; Donskoy and Goldschneider, 2003; Wada et al., 2008; Wu et al., 1995). However, the analysis of mouse models expressing lineage-specific reporter genes under the control of Cre recombinase suggested non-lymphoid origin of tDCs. Using *Il7r*-based fate mapping, which labels essentially all thymocytes, revealed that although the majority of pDC has a lymphoid past, very few conventional tDC stem from progenitors with *Il7r* history (Schlenner et al., 2010). Along this line, fate mapping of progenitors with Ptcra history showed that tDC did not originate from T-cell committed progenitors (Luche et al., 2013). Finally, the only DC progenitor population of origin independent from ETP is very advanced in development, in that it already express CD207 (Langerin), CD11c and MHC II, albeit on a low level (Luche et al., 2011). In our study, we have addressed this controversy and show that thymic DCs and T cell have a distinct origin. However, in permissive microenvironment when appropriate niches are open, some of the early thymic progenitors retaining myeloid potential can differentiate into dendritic cells.

4. Overview and discussion of research works

1/ Posttranscriptional regulation of B-lymphocyte biology by microRNA

Blume J, Ziętara N, Witzlau K, Liu Y, Sanchez OO, Puchałka J, Winter SJ, Kunze-Schumacher H, Saran N, Düber S, Roy B, Weiss S, Klein C, Wurst W, **Łyszkiewicz M** *, **, Krueger A. miR-191 modulates B-cell development and targets transcription factors E2A, Foxp1, and Egr1. *Eur J Immunol, 49: 121–132 (2019). *equal contribution, **corresponding author*

B-lymphocyte development can be used as a model for studying the interplay between coding and non-coding part of the genome. Here, in order to identify miRNA relevant in lymphocyte ontogeny, we performed miRNA transcriptome analysis of numerous haematopoietic progenitors. Among sixty-three differentially expressed miRNAs, expression of miR-191 appears to be strongly regulated at the branching point between T- and B-cell commitment.

To test the significance of miR-191 in B cell development, we generated two murine models. In the first approach, utilising programmable endonucleases (CRISPR/Cas9), we deleted a critical fragment of the miR-191 stem-loop to generate knock out mice. In the second approach, we created competitive bone marrow chimaeras, where miR-191 was ectopically overexpressed. Surprisingly, in both loss- and gain-of-function approaches, we observed a reduction in frequencies of B cells. At the same time, we could not identify any significant perturbation in the development of T lymphocytes or myeloid cells. We concluded that a balanced expression of miR-191 is required for efficient B-cell development, but dispensable for other haematopoietic lineages.

Further, we have investigated the molecular mechanism through which miR-191 modulates B-cell development. Using a gain-of-function approach, we have shown that miR-191 targets three transcription factors which are essential for B cell differentiation: E2A, FoxP1 and Egr1. We demonstrated that an elevated level of miR-191 resulted in block of B-cell development at the early progenitor stage. Pre-B1 cells are the first B-cell committed precursors in the BM. Successful recombination of immunoglobulin heavy chain leads to assembly of pre-B cell receptor (pre-BCR). Signalling via pre-BCR allows progression to pre-B2 stage, where immunoglobulin light chain loci are rearranged, and pre-BCR is replaced by the B cell receptor

(BCR). Developing B cells initially proliferate in response to IL-7 signalling, which is produced by bone marrow stromal cell. Later, expansion of preB2 progenitors is promoted by pre-BCR; however, they are still IL-7 dependent (Clark et al., 2014). We could show that enforced expression of miR-191 results in a blockade of the early B cell development, due to lowered expression of IL-7R and delayed recombination of IgH locus.

We hypothesised that this effect might be secondary to reduced expression of key components of the recombination machinery. In agreement, a computational analysis demonstrated that 3' UTRs of Rag1, Rag2 and TdT are devoid of miR-191 putative seeding regions, and thus make them unlikely to be its direct targets. However, lowered expression of FoxP1 and E2A, which directly regulate the expression of those genes allows to explain this observation.

The development of early B cell progenitors depends on the gene dosage of transcription factors, and even mild perturbation may cause severe effects (Matthias and Rolink, 2005). Heterozygosity for E2A affects the transcriptional program of early B cell progenitors, including lowered expression of Rag2 and mb-1 genes, which leads to a partial block in development (O'Riordan and Grosschedl, 1999). Although heterozygosity of the FoxP1 locus alone does not influence directly on B cell lymphopoiesis, we cannot rule out that distorted expression of both E2A and FoxP1 acts synergistically and deepen the observed effect. Such synergistic action was described for E2A and EBF, where double heterozygosity almost entirely ablates B cell development (O'Riordan and Grosschedl, 1999). The significance of a distorted expression pattern of E2A by miR-191 is further supported by a rescue experiment, where enforced expression of E2A alone abolished the developmental block of pre-B1 progenitors in miR-191 chimaeras. In agreement with previously published reports, E2A restored expression of pre-BCR and thus allowed progression to next differentiation step, while IL-7R expression remains E2A-independent (O'Riordan and Grosschedl, 1999).

In contrast to E2A and FoxP1, the consequences of perturbed expression of Egr-1 are challenging to assess directly. Four highly homologous members constitute the Egr family

(Egr-1, Egr-2, Egr-3 and Egr-4) and may substitute for each other. Single knockout of Egr-1 does not result in any developmental perturbation, presumably because the effect is masked by other gene family members (Lee et al., 1995). Dominant-negative mutation in Egr-1 locus resulted in decreased B lymphopoiesis in BM, associated with a reduced number of mature B cells in spleen (Gururajan et al., 2008). Those results as well as another report, where overexpression approach has been used, link Egr-1 function with BCR signalling (Dinkel et al., 1998). Taken together, regulation of Egr-1 expression by miR-191 might be in part responsible for a block of B cell development.

Our results suggest a model whereby miR-191 acts as a rheostat for transcriptional factors crucial for early B-cell development. It is in line with a proposed, but not well-documented role of miRNAs in fine-tuning and stabilising transcriptional factor networks. MiR-191 allows for timely and precise regulation of crucial processes like the proliferative expansion of progenitors, responsiveness to survival cues as well as expression of key components of the recombination machinery.

2/ The molecular basis of primary immunodeficiencies

Łyszkiewicz M *, Kotlarz D *, Ziętara N *, Brandes G, Diestelhorst J, Glage S, Hobeika E, Reth M, Huber L.A., Krueger A, Klein C. LAMTOR2 (p14) controls B cell differentiation by orchestrating endosomal BCR trafficking. *Front Immunol* (eCollection 2019). *equal contribution

Łyszkiewicz M *, **, Ziętara N *, Frey L, Pannicke U, Liu Y, Fan Y, Puchałka P, Hollizeck S, Somekh I, Rohlfs M, Yilmaz T, Ünal E, Karakukcu M, Patiroğlu T, Keller C, Karasu E, Sykora K-W, Somech R, Roesler J, Hoenig M, Schwarz K, Klein C **. Human FCH domain only 1 (FCHO1) deficiency reveals an essential role for clathrin-mediated endocytosis for the development and function of T cells. *Nat Comm* (2020). *equally contributing first author, **corresponding author

Primary immunodeficiencies (PID), which predominantly result from recessive monogenic mutations, give a unique insight into the mechanism governing the human immune system. To take them as the initial point of the inquiry has a significant advantage, as it allows us to work on the genes and mechanism which are directly linked to humans. However, limited access to the primary material and obvious ethical considerations permit only limited scale *ex vivo* and *in vitro* experiments. Thus, to fully understand the mechanisms underlying disease, experimental animal models have to be employed. This section summarises the studies where the starting point to understand the biology of lymphocytes were primary immunodeficiencies.

In the first of the discussed project, the intimal trigger of the inquiry was a previous discovery of the PID associated with a mutation localised in the 3' untranslated region of LAMTOR2 locus (also known as P14). Such a mutation results in massively reduced expression of the protein, leading to numerous defects including partial albinism, short stature as well as complex haematopoietic phenotype. These include congenital neutropenia, defects in functionality of cytotoxic T lymphocytes, and defects in B-cell development and function (Bohn et al., 2007).

Here, we took advantage of B-lymphocyte specifics conditional knock out models to decipher the otherwise complex phenotype of LAMTOR2 deficiency. To assess the impact of LAMTOR2 on B-cell development, we crossed mice carrying floxed allele with two different Cre deleter strains. Mice carrying mb-1-cre are very efficient deleters, starting at the early stage of B-cell

development, ensuring virtually complete deletion of floxed allele at the pre-B1 stage (Hobeika et al., 2006). On the contrary, CD19-cre mice delete floxed alleles inefficiently, also starting at the pre-B1 stage. However, continues the expression of the cre through the B lineage development results in almost complete deletion reached in splenic B-cells (Rickert et al., 1997; Schmidt-Supprian and Rajewsky, 2007). Our analysed show that loss LAMTOR2 early in B-cell ontogeny result in a profound block in B-lineage development during the transition from pre-B1 to the pre-B2 stage. The depth of the effect is comparable to that in $Rag2^{-/-}$ mice; however, the underlying mechanism differs. Rag2-deficiency is manifested by complete lack of immunoglobulin heavy and light chain recombination, whereas $LAMTOR2^{mb-1/mb-1}$ is due to a defect in pre-BR signalling. Stepwise deletion in $LAMTOR2^{CD19/CD19}$ resulted in an approximately 2-fold reduction of B-cells in bone marrow, mostly on the expense of the mature, $IgM^{lo}IgD^{hi}$ B cells. In spleen, we observed further reduction of B-cell in $LAMTOR2^{CD19/CD19}$ mice; the most affected were follicular (Fo) B cell, while the absolute number of marginal zone (MZ) B cells remain almost intact.

Given the role of LAMTOR2 in the process of the spatial organisation of the endosomal compartment and the fact that signalling downstream of B-cell receptor (BCR) depends on its internalisation, we tested whether LAMTOR2 deficiency impacts on BCR signalling kinetic. Interestingly, and somewhat unexpectedly, we found that phosphorylation of main BCR-associated kinases, Syk (pSyk) and Erk (pErk), as well as overall phosphorylation of tyrosines upon BCR triggering (pY) is elevated in LAMTOR-deficient B cells. Conversely, Ca^{2+} mobilisation from intracellular stores upon BCR stimulation was curtailed, resulting in an overall misbalanced signalling pathway, rather than general weakening or strengthening of signalling machinery. Mechanistic explanation of this phenomenon comes from the transmission electron microscopy analysis, where we followed intracellular trafficking of BCR upon stimulation. Here, in the absence of LAMTOR2, we could show retention of the BCR on the plasma membrane and subsequently in the early endosomes resulting in delayed degradation of BCR molecules. Taken together, we concluded that lack of LAMTOR2 results

in aberrant internalisation of BCR from the cell membrane, subsequently leading to abnormal phosphorylation of BCR-associated kinases. These observations are in line with human patients, where hypomorphic mutation allows for residual protein expression leading to a partial block in B-cell development and defects in class-switch recombination. This, combined with the defect in the formation of memory cells, support the idea that LAMTOR2 controls BCR signalling in both mice and human.

In the second approach, by studying a case of human immunodeficiency, we recently discovered that gene coding for FCHO1 (F-BAR domain only protein 1) is essential for human T cell development and activation. Here, we identified six distinct autosomal recessive mutations in the FCHO1 locus of 10 unrelated patients, all of which resulted in combined immunodeficiency (CID). The nature of these mutations varies from point mutations resulting in single amino acid substitution, through premature stop codons, to variants affecting pre-mRNA splicing. Yet, all of these mutations were deleterious for protein function. T-cell deficiency in all patients, as well as hypogammaglobulinemia, observed in all but one patient predisposed them to be severe and persistent viral and fungal infections. While we can directly link the FCHO1 mutations to the T-cell deficiency, it remains open whether B-cell defects are intrinsic or are caused by defective T cells.

Although FCHO1 has been previously recognised to act in an early stage of clathrin-mediated endocytosis, we provided mechanistic insight into the structural and functional biology of FCHO1 in the context of the human immune system. Patient-associated point mutations were located in two distinct domains that facilitate the essential function of the protein. First of them, leading to a single amino acid substitution in the µHD domain (R679P) alters FCHO1 interaction with its main interacting partners EPS15 and EPS15R, preventing the productive formation of clathrin-coated vesicles. Alteration of the proximal fragment of the FCHO1, so-called F-BAR domain, also proved to be deleterious, although in a different way. Here, A34P substitution was breaking an alpha-helix structure of the domain, leading to dissociation of the protein from the plasma membrane, hence abolishing its function.

FCHO1 deficiency in patients is predominantly manifested by severe T-cell insufficiency. Given that the quality of the TCR-mediated signalling is a key factor during T-cell ontogeny and FCHO1-deficiency leaves the other cells of the immune system largely unaffected, we explored the impact of FCHO1 on TCR internalisation. To this end, we took advantage of CD4 positive human Jurkat cell lymphoma line where FCHO1 loci were disrupted to generate knock out clones. Such modified cells were tested for their abilities to internalise and cluster the TCR upon CD3-stimulation. Consistent with our hypothesis, both internalisation and formation of TCR aggregates were perturbed in FCHO1-deficient cells when compared to their wild type counterparts. Of note, reconstitution of FCHO1 expression in knock out clones restores TCR functionality.

Given the crucial role of the FCHO1 in the initiation of the CME, it is somewhat surprising that the effect of the FCHO1 deficiency is manifested in T cells only (and presumably limited to the TCR internalisation) rather than leading to more global defects of development. Deficiency in FCHO orthologues in *Caenorhabditis elegans* leads to severe body malformation (Hollopeter et al., 2014). In *Danio rerio*, knock-down of either Fcho1 or its paralogue Fcho2 results in embryonic lethality (Umasankar et al., 2012). These observations prompted us to hypothesise that function of FCHO has changed during evolution. The emergence of two paralogues (Dergai et al., 2016) allows that one of them (FCHO1) evolved together with the adaptive immune system to modulate T cell receptor endocytosis, while second paralogue (FCHO2) maintained its original function. This notion is further supported by the fact, that FCHO2 deficiency results in early embryonic lethality of mice (unpublished observation) and FCHO paralogues may act as receptor-specific adaptors rather than global regulators of CME (Umasankar et al., 2012).

Taken together, we provided evidence for an unexpected and critical role of FCHO1 in orchestrating the T-cell development and activation. It also exemplifies how systematic studies in patients with inborn disorders help to uncover the importance of genes and pathways, previously not associated with the function of the immune system.

3/ The origin of thymic dendritic cells

The origin of thymic dendritic cells (tDC) and other myeloid cells remained controversial. To address this question, we tested whether the thymus contains myeloid progenitors similar to that in the bone marrow. Here we employed CX3CR1[GFP] reporter mouse and concluded that myeloid progenitors, macrophage/DC progenitors and common DC progenitors, although readily detectable in bone marrow, are absent in thymus. Since expression of CX3CR1 is common for almost all DC progenitors (except for the earliest MP), and maintained through ontogeny, we tested whether noncanonical DP progenitors, expressing CX3CR1 exist in the thymus. Indeed, we identified a population of the early T-lineage progenitors (ETP) positive for CX3CR1 (ETP CX3CR1[+]). There were virtually identical to canonical ETPs and devoid of expression of any typical myeloid markers such as CD115 (M-CSFR), CD11c and CD11b.

Further, we employed the OP9 coculture system to test myeloid and B-cell potential of CX3CR1[+] ETP and compare to that of CX3CR1[-] ETP as well as other canonical myeloid progenitors. Overall, both population of ETPs have comparable and strong potential to generate all main subsets of DCs. However, not only ETP subsets but all tested myeloid progenitors retain robust B-cell potential. Besides, limiting dilution assay showed that CX3CR1[+] ETP progenitors contained a slightly higher proportion of myeloid-lineage progenitors when compared to their canonical counterparts.

Since all thymic and bone marrow DC progenitors retain at least some B-lymphoid potential, we assessed whether they could also differentiate towards T lymphocytes. To evaluate it, we took advantage of the OP9-DL1 coculture system. Here we show that both CX3CR1[+] ETP and CX3CR1[-] ETP have similar and robust T-cell potential. Interestingly, just after six days of coculture in the presence of DL1, T-lineage progenitors dominate all the cultures, irrespective

of the starting population. These data suggest that strong, instructive signal from the environment (Notch1) may critically contribute to the DC vs T-cell lineage decision.

Further, we wanted to assess *in vivo* to which extend tDC and T cells are developmentally related. Here, we employed retrogenic mice system combined with molecular barcoding and next-generation sequencing to trace the origin of tDC quantitatively. The barcoding system contains approximately 10^6 different tags, allowing for faithful detection of small differences in clone size. This, combined with limited colonisation potential of the thymus by blood-derived progenitors (quantified to be approximately one progenitor per day, (Zietara et al., 2015), allows us to determine whether the thymocytes and tDC share a common intrathymic precursor. Analysis of barcodes recovered from bone marrow chimaeras where each initially transplanted progenitor was individually tagged, revealed minimal lineage relationship between tDC and T-cells. We concluded, that the large majority of tDC do not arise from intrathymic progenitors, but instead migrate to the thymus once committed to DC-lineage in the bone marrow.

The minimal lineage relationship between tDCs and thymocytes and yet strong myeloid potential of thymic resident ETPs suggest that robust and instructive signal like Notch in OP9-DL1 coculture determine the fate of the progenitors. Thus, we asked if also thymic microenvironment transmits such inductive signals and whether it can be manipulated towards non-T lineage. To this end, we transferred congenically marked bone marrow or thymic progenitors and followed their fate 21 days after transfer. Here, all tested progenitors, regardless of their origin (MP, MDP, CDP, ETP CX3CR1$^-$, ETP CX3CR1$^+$) gave rise exclusively into T-lineage. Of note, in such conditions, even myeloid-primed progenitors develop only to T- but not DC-lineage. To test whether it is possible to induce intrathymic DC differentiation, we took advantage of the CD11c-DOG mice, where mature DC can be depleted by administration of diphtheria toxin. In such settings, 21 days after transfer, all donor populations gave rise predominantly to T-lineage. However, in DC-depleted environment, all transferred progenitors gave also rise into CD11c$^+$ and CD11b$^+$ myeloid cells. Thus, the

depletion of DCs generate the permissive state for myelopoiesis and allows for DC development despite the presence of Notch signal.

Taken together, here we show that at steady state vast majority of tDC is of external, myeloid origin. Furthermore, we have identified and characterise a subset of early T-lineage progenitors (ETP) expressing CX3CR1, a bona fide marker of DC progenitors. Such progenitors can efficiently develop into tDC in permissive conditions when appropriate thymic niches are available. Hence, our data support a model in which the adoption of T-lineage fate by noncommitted progenitors at steady state is enforced by signals from the thymic microenvironment unless niches promoting alternative lineage fates become available.

REFERENCES

Ardavin, C., Wu, L., Li, C.L., and Shortman, K. (1993). Thymic dendritic cells and T cells develop simultaneously in the thymus from a common precursor population. Nature *362*, 761-763.

Bain, G., Maandag, E.C., Izon, D.J., Amsen, D., Kruisbeek, A.M., Weintraub, B.C., Krop, I., Schlissel, M.S., Feeney, A.J., van Roon, M., and et al. (1994). E2A proteins are required for proper B cell development and initiation of immunoglobulin gene rearrangements. Cell *79*, 885-892.

Beck, K., Peak, M.M., Ota, T., Nemazee, D., and Murre, C. (2009). Distinct roles for E12 and E47 in B cell specification and the sequential rearrangement of immunoglobulin light chain loci. J Exp Med *206*, 2271-2284.

Bell, J.J., and Bhandoola, A. (2008). The earliest thymic progenitors for T cells possess myeloid lineage potential. Nature *452*, 764-767.

Bohn, G., Allroth, A., Brandes, G., Thiel, J., Glocker, E., Schaffer, A.A., Rathinam, C., Taub, N., Teis, D., Zeidler, C.*, et al.* (2007). A novel human primary immunodeficiency syndrome caused by deficiency of the endosomal adaptor protein p14. Nat Med *13*, 38-45.

Boyer, C., Auphan, N., Luton, F., Malburet, J.M., Barad, M., Bizozzero, J.P., Reggio, H., and Schmitt-Verhulst, A.M. (1991). T cell receptor/CD3 complex internalisation following activation of a cytolytic T cell clone: evidence for a protein kinase C-independent staurosporine-sensitive step. Eur J Immunol *21*, 1623-1634.

Brown, P.J., Ashe, S.L., Leich, E., Burek, C., Barrans, S., Fenton, J.A., Jack, A.S., Pulford, K., Rosenwald, A., and Banham, A.H. (2008). Potentially oncogenic B-cell activation-induced smaller isoforms of FOXP1 are highly expressed in the activated B cell-like subtype of DLBCL. Blood *111*, 2816-2824.

Brownlie, R.J., and Zamoyska, R. (2013). T cell receptor signalling networks: branched, diversified and bounded. Nat Rev Immunol *13*, 257-269.

Busslinger, M. (2004). Transcriptional control of early B cell development. Annu Rev Immunol *22*, 55-79.

Campbell, K.S. (1999). Signal transduction from the B cell antigen-receptor. Curr Opin Immunol *11*, 256-264.

Cavrois, M., De Noronha, C., and Greene, W.C. (2002). A sensitive and specific enzyme-based assay detecting HIV-1 virion fusion in primary T lymphocytes. Nat Biotechnol *20*, 1151-1154.

Chaturvedi, A., Martz, R., Dorward, D., Waisberg, M., and Pierce, S.K. (2011). Endocytosed BCRs sequentially regulate MAPK and Akt signaling pathways from intracellular compartments. Nat Immunol *12*, 1119-1126.

Chen, C.Z., Li, L., Lodish, H.F., and Bartel, D.P. (2004). MicroRNAs modulate hematopoietic lineage differentiation. Science *303*, 83-86.

Clark, M.R., Mandal, M., Ochiai, K., and Singh, H. (2014). Orchestrating B cell lymphopoiesis through interplay of IL-7 receptor and pre-B cell receptor signalling. Nat Rev Immunol *14*, 69-80.

Cocucci, E., Aguet, F., Boulant, S., and Kirchhausen, T. (2012). The first five seconds in the life of a clathrin-coated pit. Cell *150*, 495-507.

Compeer, E.B., Kraus, F., Ecker, M., Redpath, G., Amiezer, M., Rother, N., Nicovich, P.R., Kapoor-Kaushik, N., Deng, Q., Samson, G.P.B.*, et al.* (2018). A mobile endocytic network connects clathrin-independent receptor endocytosis to recycling and promotes T cell activation. Nat Commun *9*, 1597.

Corcoran, L., Ferrero, I., Vremec, D., Lucas, K., Waithman, J., O'Keeffe, M., Wu, L., Wilson, A., and Shortman, K. (2003). The lymphoid past of mouse plasmacytoid cells and thymic dendritic cells. J Immunol *170*, 4926-4932.

Costinean, S., Zanesi, N., Pekarsky, Y., Tili, E., Volinia, S., Heerema, N., and Croce, C.M. (2006). Pre-B cell proliferation and lymphoblastic leukemia/high-grade lymphoma in E(mu)-miR155 transgenic mice. Proc Natl Acad Sci U S A *103*, 7024-7029.

Cubedo, E., Gentles, A.J., Huang, C., Natkunam, Y., Bhatt, S., Lu, X., Jiang, X., Romero-Camarero, I., Freud, A., Zhao, S.*, et al.* (2012). Identification of LMO2 transcriptome and interactome in diffuse large B-cell lymphoma. Blood *119*, 5478-5491.

Dergai, M., Iershov, A., Novokhatska, O., Pankivskyi, S., and Rynditch, A. (2016). Evolutionary Changes on the Way to Clathrin-Mediated Endocytosis in Animals. Genome Biol Evol *8*, 588-606.

Dietrich, J., Hou, X., Wegener, A.M., and Geisler, C. (1994). CD3 gamma contains a phosphoserine-dependent di-leucine motif involved in down-regulation of the T cell receptor. EMBO J *13*, 2156-2166.

Dinkel, A., Warnatz, K., Ledermann, B., Rolink, A., Zipfel, P.F., Burki, K., and Eibel, H. (1998). The transcription factor early growth response 1 (Egr-1) advances differentiation of pre-B and immature B cells. J Exp Med *188*, 2215-2224.

Donskoy, E., and Goldschneider, I. (2003). Two developmentally distinct populations of dendritic cells inhabit the adult mouse thymus: demonstration by differential importation of hematogenous precursors under steady state conditions. J Immunol *170*, 3514-3521.

Fuxa, M., Skok, J., Souabni, A., Salvagiotto, G., Roldan, E., and Busslinger, M. (2004). Pax5 induces V-to-DJ rearrangements and locus contraction of the immunoglobulin heavy-chain gene. Genes Dev *18*, 411-422.

Geissmann, F., Manz, M.G., Jung, S., Sieweke, M.H., Merad, M., and Ley, K. (2010). Development of monocytes, macrophages, and dendritic cells. Science *327*, 656-661.

Goebel, P., Janney, N., Valenzuela, J.R., Romanow, W.J., Murre, C., and Feeney, A.J. (2001). Localised gene-specific induction of accessibility to V(D)J recombination induced by E2A and early B cell factor in nonlymphoid cells. J Exp Med *194*, 645-656.

Greenbaum, S., and Zhuang, Y. (2002). Identification of E2A target genes in B lymphocyte development by using a gene tagging-based chromatin immunoprecipitation system. Proc Natl Acad Sci U S A *99*, 15030-15035.

Gururajan, M., Chui, R., Karuppannan, A.K., Ke, J., Jennings, C.D., and Bondada, S. (2005). c-Jun N-terminal kinase (JNK) is required for survival and proliferation of B-lymphoma cells. Blood *106*, 1382-1391.

Gururajan, M., Simmons, A., Dasu, T., Spear, B.T., Calulot, C., Robertson, D.A., Wiest, D.L., Monroe, J.G., and Bondada, S. (2008). Early growth response genes regulate B cell development, proliferation, and immune response. J Immunol *181*, 4590-4602.

Henne, W.M., Boucrot, E., Meinecke, M., Evergren, E., Vallis, Y., Mittal, R., and McMahon, H.T. (2010). FCHo proteins are nucleators of clathrin-mediated endocytosis. Science *328*, 1281-1284.

Henne, W.M., Kent, H.M., Ford, M.G., Hegde, B.G., Daumke, O., Butler, P.J., Mittal, R., Langen, R., Evans, P.R., and McMahon, H.T. (2007). Structure and analysis of FCHo2 F-BAR domain: a dimerising and membrane recruitment module that effects membrane curvature. Structure *15*, 839-852.

Hobeika, E., Thiemann, S., Storch, B., Jumaa, H., Nielsen, P.J., Pelanda, R., and Reth, M. (2006). Testing gene function early in the B cell lineage in mb1-cre mice. Proc Natl Acad Sci U S A *103*, 13789-13794.

Hollopeter, G., Lange, J.J., Zhang, Y., Vu, T.N., Gu, M., Ailion, M., Lambie, E.J., Slaughter, B.D., Unruh, J.R., Florens, L., and Jorgensen, E.M. (2014). The membrane-associated proteins FCHo and SGIP are allosteric activators of the AP2 clathrin adaptor complex. Elife *3*.

Hou, P., Araujo, E., Zhao, T., Zhang, M., Massenburg, D., Veselits, M., Doyle, C., Dinner, A.R., and Clark, M.R. (2006). B cell antigen receptor signaling and internalisation are mutually exclusive events. PLoS Biol *4*, e200.

Jin, H.Y., Oda, H., Chen, P., Yang, C., Zhou, X., Kang, S.G., Valentine, E., Kefauver, J.M., Liao, L., Zhang, Y., *et al.* (2017). Differential Sensitivity of Target Genes to Translational Repression by miR-17~92. PLoS Genet *13*, e1006623.

Karasuyama, H., Rolink, A., and Melchers, F. (1993). A complex of glycoproteins is associated with VpreB/lambda 5 surrogate light chain on the surface of mu heavy chain-negative early precursor B cell lines. J Exp Med *178*, 469-478.

Kitamura, D., Kudo, A., Schaal, S., Muller, W., Melchers, F., and Rajewsky, K. (1992). A critical role of lambda 5 protein in B cell development. Cell *69*, 823-831.

Koh, T.W., Korolchuk, V.I., Wairkar, Y.P., Jiao, W., Evergren, E., Pan, H., Zhou, Y., Venken, K.J., Shupliakov, O., Robinson, I.M., *et al.* (2007). Eps15 and Dap160 control synaptic vesicle membrane retrieval and synapse development. J Cell Biol *178*, 309-322.

Koralov, S.B., Muljo, S.A., Galler, G.R., Krek, A., Chakraborty, T., Kanellopoulou, C., Jensen, K., Cobb, B.S., Merkenschlager, M., Rajewsky, N., and Rajewsky, K. (2008). Dicer ablation affects antibody diversity and cell survival in the B lymphocyte lineage. Cell *132*, 860-874.

Lanzavecchia, A. (1990). Receptor-mediated antigen uptake and its effect on antigen presentation to class II-restricted T lymphocytes. Annu Rev Immunol *8*, 773-793.

Lee, S.L., Tourtellotte, L.C., Wesselschmidt, R.L., and Milbrandt, J. (1995). Growth and differentiation proceeds normally in cells deficient in the immediate early gene NGFI-A. J Biol Chem *270*, 9971-9977.

Lin, H., and Grosschedl, R. (1995). Failure of B-cell differentiation in mice lacking the transcription factor EBF. Nature *376*, 263-267.

Lin, Y.C., Jhunjhunwala, S., Benner, C., Heinz, S., Welinder, E., Mansson, R., Sigvardsson, M., Hagman, J., Espinoza, C.A., Dutkowski, J., *et al.* (2010). A global network of transcription

factors, involving E2A, EBF1 and Foxo1, that orchestrates B cell fate. Nat Immunol *11*, 635-643.

Loeb, G.B., Khan, A.A., Canner, D., Hiatt, J.B., Shendure, J., Darnell, R.B., Leslie, C.S., and Rudensky, A.Y. (2012). Transcriptome-wide miR-155 binding map reveals widespread noncanonical microRNA targeting. Mol Cell *48*, 760-770.

Luche, H., Ardouin, L., Teo, P., See, P., Henri, S., Merad, M., Ginhoux, F., and Malissen, B. (2011). The earliest intrathymic precursors of CD8alpha(+) thymic dendritic cells correspond to myeloid-type double-negative 1c cells. Eur J Immunol *41*, 2165-2175.

Luche, H., Nageswara Rao, T., Kumar, S., Tasdogan, A., Beckel, F., Blum, C., Martins, V.C., Rodewald, H.R., and Fehling, H.J. (2013). In vivo fate mapping identifies pre-TCRalpha expression as an intra- and extrathymic, but not prethymic, marker of T lymphopoiesis. J Exp Med *210*, 699-714.

Matthias, P., and Rolink, A.G. (2005). Transcriptional networks in developing and mature B cells. Nat Rev Immunol *5*, 497-508.

McMahon, H.T., and Boucrot, E. (2011). Molecular mechanism and physiological functions of clathrin-mediated endocytosis. Nat Rev Mol Cell Biol *12*, 517-533.

Melchers, F. (2015). Checkpoints that control B cell development. J Clin Invest *125*, 2203-2210.

Miosge, L., and Zamoyska, R. (2007). Signalling in T-cell development: is it all location, location, location? Curr Opin Immunol *19*, 194-199.

Mulkearns, E.E., and Cooper, J.A. (2012). FCH domain only-2 organises clathrin-coated structures and interacts with Disabled-2 for low-density lipoprotein receptor endocytosis. Mol Biol Cell *23*, 1330-1342.

Nutt, S.L., Heavey, B., Rolink, A.G., and Busslinger, M. (1999). Commitment to the B-lymphoid lineage depends on the transcription factor Pax5. Nature *401*, 556-562.

Nutt, S.L., Urbanek, P., Rolink, A., and Busslinger, M. (1997). Essential functions of Pax5 (BSAP) in pro-B cell development: difference between fetal and adult B lymphopoiesis and reduced V-to-DJ recombination at the IgH locus. Genes Dev *11*, 476-491.

O'Riordan, M., and Grosschedl, R. (1999). Coordinate regulation of B cell differentiation by the transcription factors EBF and E2A. Immunity *11*, 21-31.

Ohno, H., Stewart, J., Fournier, M.C., Bosshart, H., Rhee, I., Miyatake, S., Saito, T., Gallusser, A., Kirchhausen, T., and Bonifacino, J.S. (1995). Interaction of tyrosine-based sorting signals with clathrin-associated proteins. Science *269*, 1872-1875.

Olive, V., Jiang, I., and He, L. (2010). mir-17-92, a cluster of miRNAs in the midst of the cancer network. Int J Biochem Cell Biol *42*, 1348-1354.

Osmond, D.G., Rolink, A., and Melchers, F. (1998). Murine B lymphopoiesis: towards a unified model. Immunol Today *19*, 65-68.

Pearse, B. (1976). Clathrin: a unique protein associated with intracellular transfer of membrane by coated vesicles PNAS *73*, 1255-1259.

Pechstein, A., Bacetic, J., Vahedi-Faridi, A., Gromova, K., Sundborger, A., Tomlin, N., Krainer, G., Vorontsova, O., Schafer, J.G., Owe, S.G.*, et al.* (2010). Regulation of synaptic vesicle

recycling by complex formation between intersectin 1 and the clathrin adaptor complex AP2. Proc Natl Acad Sci U S A *107*, 4206-4211.

Rao, D.S., O'Connell, R.M., Chaudhuri, A.A., Garcia-Flores, Y., Geiger, T.L., and Baltimore, D. (2010). MicroRNA-34a perturbs B lymphocyte development by repressing the forkhead box transcription factor Foxp1. Immunity *33*, 48-59.

Reider, A., Barker, S.L., Mishra, S.K., Im, Y.J., Maldonado-Baez, L., Hurley, J.H., Traub, L.M., and Wendland, B. (2009). Syp1 is a conserved endocytic adaptor that contains domains involved in cargo selection and membrane tubulation. EMBO J *28*, 3103-3116.

Reth, M. (2001). Oligomeric antigen receptors: a new view on signaling for the selection of lymphocytes. Trends Immunol *22*, 356-360.

Rickert, R.C., Roes, J., and Rajewsky, K. (1997). B lymphocyte-specific, Cre-mediated mutagenesis in mice. Nucleic Acids Res *25*, 1317-1318.

Robinson, M.S. (2015). Forty Years of Clathrin-coated Vesicles. Traffic *16*, 1210-1238.

Schlenner, S.M., Madan, V., Busch, K., Tietz, A., Laufle, C., Costa, C., Blum, C., Fehling, H.J., and Rodewald, H.R. (2010). Fate mapping reveals separate origins of T cells and myeloid lineages in the thymus. Immunity *32*, 426-436.

Schmidt-Supprian, M., and Rajewsky, K. (2007). Vagaries of conditional gene targeting. Nat Immunol *8*, 665-668.

Shen, C.P., and Kadesch, T. (1995). B-cell-specific DNA binding by an E47 homodimer. Mol Cell Biol *15*, 4518-4524.

Telerman, A., Amson, R.B., Romasco, F., Wybran, J., Galand, P., and Mosselmans, R. (1987). Internalisation of human T lymphocyte receptors. Eur J Immunol *17*, 991-997.

Turner, M., Galloway, A., and Vigorito, E. (2014). Noncoding RNA and its associated proteins as regulatory elements of the immune system. Nat Immunol *15*, 484-491.

Umasankar, P.K., Sanker, S., Thieman, J.R., Chakraborty, S., Wendland, B., Tsang, M., and Traub, L.M. (2012). Distinct and separable activities of the endocytic clathrin-coat components Fcho1/2 and AP-2 in developmental patterning. Nat Cell Biol *14*, 488-501.

Urbanek, P., Wang, Z.Q., Fetka, I., Wagner, E.F., and Busslinger, M. (1994). Complete block of early B cell differentiation and altered patterning of the posterior midbrain in mice lacking Pax5/BSAP. Cell *79*, 901-912.

Ventura, A., Young, A.G., Winslow, M.M., Lintault, L., Meissner, A., Erkeland, S.J., Newman, J., Bronson, R.T., Crowley, D., Stone, J.R.*, et al.* (2008). Targeted deletion reveals essential and overlapping functions of the miR-17 through 92 family of miRNA clusters. Cell *132*, 875-886.

Wada, H., Masuda, K., Satoh, R., Kakugawa, K., Ikawa, T., Katsura, Y., and Kawamoto, H. (2008). Adult T-cell progenitors retain myeloid potential. Nature *452*, 768-772.

Winkler, T.H., Rolink, A., Melchers, F., and Karasuyama, H. (1995). Precursor B cells of mouse bone marrow express two different complexes with the surrogate light chain on the surface. Eur J Immunol *25*, 446-450.

Wu, L., D'Amico, A., Hochrein, H., O'Keeffe, M., Shortman, K., and Lucas, K. (2001). Development of thymic and splenic dendritic cell populations from different hemopoietic precursors. Blood *98*, 3376-3382.

Wu, L., and Shortman, K. (2005). Heterogeneity of thymic dendritic cells. Semin Immunol *17*, 304-312.

Wu, L., Vremec, D., Ardavin, C., Winkel, K., Suss, G., Georgiou, H., Maraskovsky, E., Cook, W., and Shortman, K. (1995). Mouse thymus dendritic cells: kinetics of development and changes in surface markers during maturation. Eur J Immunol *25*, 418-425.

Xiao, C., Srinivasan, L., Calado, D.P., Patterson, H.C., Zhang, B., Wang, J., Henderson, J.M., Kutok, J.L., and Rajewsky, K. (2008). Lymphoproliferative disease and autoimmunity in mice with increased miR-17-92 expression in lymphocytes. Nat Immunol *9*, 405-414.

Zietara, N., Lyszkiewicz, M., Puchalka, J., Witzlau, K., Reinhardt, A., Forster, R., Pabst, O., Prinz, I., and Krueger, A. (2015). Multicongenic fate mapping quantification of dynamics of thymus colonisation. J Exp Med *212*, 1589-1601.

Appendix 6.1.

miR-191 modulates B-cell development and targets transcription factors E2A, Foxp1, and Egr1

Jonas Blume, Natalia Ziętara, Katrin Witzlau, Yanshan Liu, Oskar Ortiz Sanchez,

Jacek Puchałka, Samantha J Winter, Heike Kunze-Schumacher, Namita Saran,

Sandra Düber, Bishnudeo Roy, Siegfried Weiss, Christoph Klein, Wolfgang Wurst,

Marcin Łyszkiewicz *, **, Andreas Krueger *, **;

* equal contribution, ** corresponding author

Molecular immunology and signaling

Basic

Research Article

miR-191 modulates B-cell development and targets transcription factors E2A, Foxp1, and Egr1

Jonas Blume[1], Natalia Ziętara[1], Katrin Witzlau[1], Yanshan Liu[2], Oskar Ortiz Sanchez[3], Jacek Puchałka[+2], Samantha J. Winter[5], Heike Kunze-Schumacher[5], Namita Saran[1], Sandra Düber[4], Bishnudeo Roy[4], Siegfried Weiss[1,4], Christoph Klein[2], Wolfgang Wurst[3,6,7,8], Marcin Łyszkiewicz[1,2] and Andreas Krueger*[1,5]* iD

[1] Institute of Immunology, Hannover Medical School, Hannover, Germany
[2] Department of Pediatrics, Dr. von Hauner Children's Hospital, University Hospital, LMU Munich, Munich, Germany
[3] Institute of Developmental Genetics, Helmholtz Centre Munich, Germany
[4] Molecular Immunology, Helmholtz Centre for Infection Research (HZI), Braunschweig, Germany
[5] Institute for Molecular Medicine, Goethe University Frankfurt, Frankfurt, Germany
[6] Technische Universität München-Weihenstephan, Neuherberg/Munich, Germany
[7] German Center for Neurodegenerative Diseases (DZNE), Site Munich, Germany
[8] Munich Cluster for Systems Neurology (SyNergy), Munich, Germany

The interdependence of posttranscriptional gene regulation via miRNA and transcriptional regulatory networks in lymphocyte development is poorly understood. Here, we identified miR-191 as direct upstream modulator of a transcriptional module comprising the transcription factors Foxp1, E2A, and Egr1. Deletion as well as ectopic expression of miR-191 resulted in developmental arrest in B lineage cells, indicating that fine tuning of the combined expression levels of Foxp1, E2A, and Egr1, which in turn control somatic recombination and cytokine-driven expansion, constitutes a prerequisite for efficient B-cell development. In conclusion, we propose that miR-191 acts as a rheostat in B-cell development by fine tuning a key transcriptional program.

Keywords: B cells · Lymphocyte development · miRNA · miR-191 · Transcription factors

🖥 Additional supporting information may be found online in the Supporting Information section at the end of the article.

Introduction

Development of B cells from bone marrow derived progenitors as well as final differentiation of mature B cells are characterized by the execution of distinct and tightly controlled transcriptional networks. In consequence, dysregulation of these networks constitutes a frequent cause for generation of B lineage leukemia and lymphomas.

Correspondence: Prof. Andreas Krueger and Dr. Marcin Łyszkiewicz
e-mail: Andreas.Krueger@kgu.de; Marcin.Lyszkiewicz@med.uni-muenchen.de

*These authors contributed equally to this work.
[+] Deceased

In addition to a B-lineage determining transcriptional network comprising E2A (encoded by *Tcf3*), Ebf1, and Pax5, the temporally controlled action of other transcription factors, such as Egr1 and Foxp1 drives development of B cells from bone-marrow derived progenitors [1]. Developmental progression of B lineage cells is centered on somatic recombination of Ig heavy (IgH) and light (IgL) chain loci [2]. Expression of key elements of the recombination machinery, such as Rag1 and Rag2, is regulated by E2A, Ebf1, and Pax5 [3]. In addition, the transcription factor Foxp1 contributes to expression of Rag1 and Rag2 by binding to an enhancer region within the Rag locus [4]. Upon productive IgL rearrangement immature B cells undergo negative selection, which can be partially overcome by receptor editing, and finally exit from BM.

MicroRNAs (miRs) form an additional layer of regulation of B-cell development. Disruption of components of miRNA biosynthesis and concomitant total miRNA deficiency severely impairs B-cell development and differentiation [5]. Aberrant expression of miRNAs has also been linked to the development of B-cell malignancies. Thus, overexpression of miR-17~92, also termed oncomiR-1, resulted in lymphoproliferative disease and exacerbated B-cell lymphoma [6–9]. Furthermore, ectopic expression of miR-155 resulted in development of B-cell leukemia [10].

In the present study, we demonstrated that miR-191 targeted key transcriptional regulators of B-cell development and malignancy, E2A, Egr-1, and Foxp1, in mice and humans. Deletion as well as ectopic expression of miR-191 resulted in impaired early B-cell development, suggesting that expression of miR-191 is tightly controlled and serves to maintain exactly tuned transcriptional programs.

Results

Expression of miR-191 is dynamically regulated during B-cell development and differentiation

We performed miRNA transcriptome analysis to identify miRNAs differentially expressed at the branching point of B- and T-cell development. Sixty-three miRNAs were differentially expressed between noncommitted and progressively committed progenitor cells of the B and T lineage (Fig. 1A). Validation by quantitative RT-PCR showed that expression of miR-191 was developmentally regulated in B cells reaching peak expression levels from proB to immature B cells followed by a decline toward mature B cells (Fig. 1B). In contrast, expression of miR-191 was about tenfold lower in early T-cell progenitors (ETPs) when compared to HSC and remained low during the course of intrathymic T-cell development (Fig. S1). This finding suggests that the thymic environment negatively regulated expression of miR-191. Next, we addressed whether expression of miR-191 was also regulated during activation and differentiation of B cells. Stimulation via the BCR resulted in a twofold upregulation of miR-191 after 1–2 h and remained elevated over a period of 48 h (Fig. 1C). Stimulation via CD40, mimicking T-cell interaction, had a similar but more pronounced effect. However, after immunization with SRBC, a
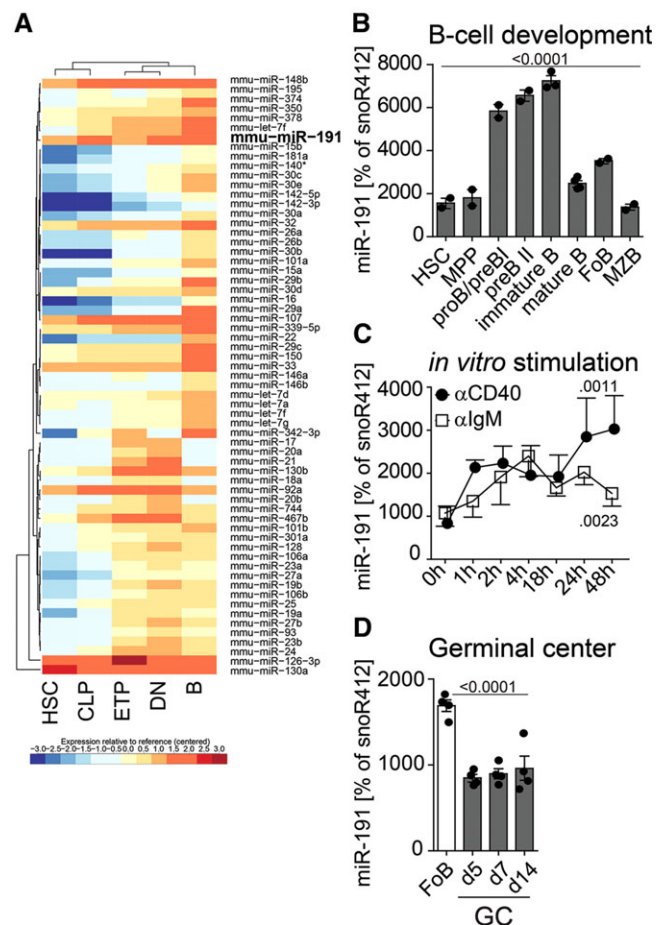

Figure 1. Expression of miR-191 is dynamically regulated during B-cell development and differentiation. (A) Unsupervised clustering of 63 miRNAs differentially expressed between HSC, common lymphoid progenitors (CLP), early T-cell rogenitors (ETP), double negative thymocytes (DN), and B-cell progenitors (B). (B–D) Expression levels of miR-191 relative to snoRNA412 determined by qRT-PCR: (B) in developing B cells, (C) in Fo B cells upon in vitro stimulation, (D) in GC B cells isolated at the indicated time points after immunization of mice with SRBC. Pooled data of four (B), three (C), two (D) independent experiments are depicted. Data are shown as mean relative expression + SD or +/− SD. Statistical analysis was performed using one-way ANOVA. Number above the graphs indicates *p* value.

thymus-dependent antigen, expression of miR-191 was reduced in germinal center derived B cells after extended periods of time (Fig. 1D). Taken together, dynamic regulation of miR-191 suggests that this miRNA constitutes a posttranscriptional regulatory factor of lymphocyte development and differentiation.

Defined expression levels of miR-191 are essential for efficient B-cell development

To understand the role of miR-191 in lymphocyte development we generated mice carrying a targeted deletion of miR-191 using CRISPR/Cas9 technology. To minimize the effect of genetic manipulation on neighboring loci we designed sgRNAs to cut only critical fragments of miR-191 stem-loop. We obtained two mouse lines, in
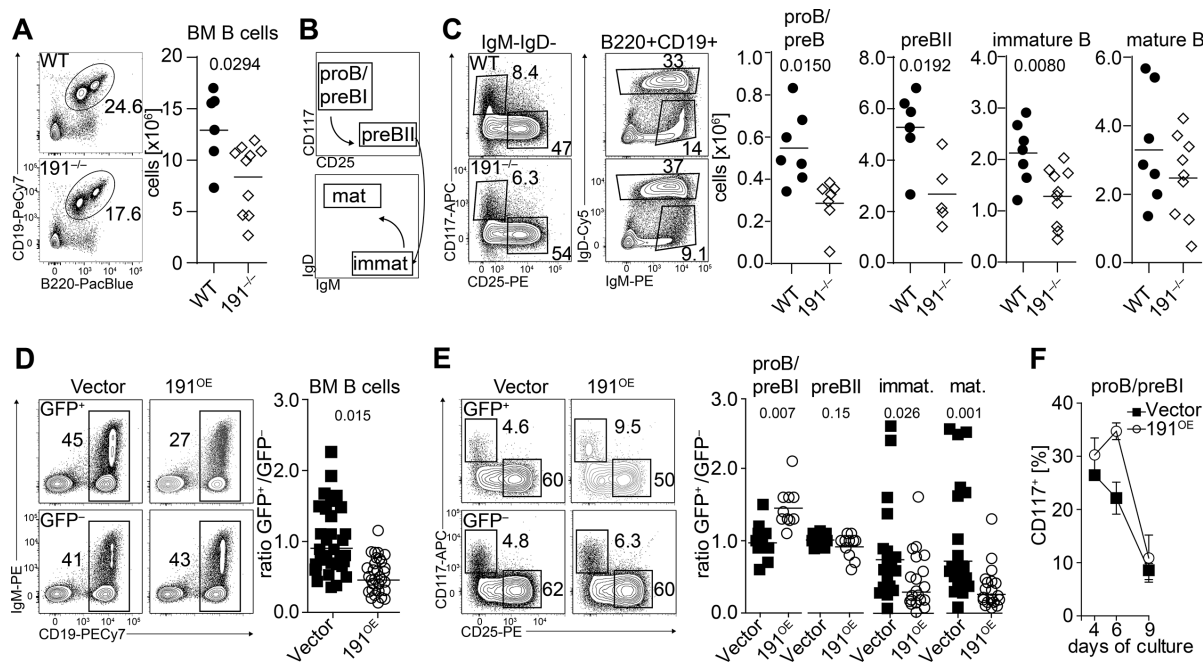
Figure 2. Defined expression levels of miR-191 are essential for efficient B-cell development. (A–C) Analysis of B-cell development in C57BL/6 (WT) and miR-191$^{-/-}$ mice (191$^{-/-}$). (A) Representative contour plots of bone marrow resident B cells indicating frequencies of B cells given as % of total nucleated cells (left) and total number of B cells (right). (B) Schematic gating strategy to identify proB/preBI, preBII, immature, and mature bone marrow B cells. (C) Representative contour plots of bone marrow resident B-cell stages from WT and 191$^{-/-}$ mice and quantification given as % of total nucleated cells (left) and total number (right). (D–F) Analysis of B-cell development of chimeric mice reconstituted with LSK cells transduced with either empty vector (Vector) or miR-191 overexpressing vector (191^{OE}). Approximately 50% of LSK cells were transduced with either of the vectors (GFP$^+$ cells), and remaining nontransduced (GFP$^-$ cells) served as competitor. Eight to ten weeks after transplantation cells were analyzed by FACS. (D) Representative contour plots of bone marrow resident B cells and quantification given as ratio of GFP$^+$/GFP$^-$. (E) Representative contour plots indicating development of early B cells upon overexpression of miR-191 (left) and quantification of two independent experiments with six mice per group (right). ProB/preBI cells were B220$^+$CD19$^{+/-}$CD117$^+$, preBII cells were B220$^+$CD19$^+$CD25$^+$, immature B cells were CD19$^+$IgM$^+$IgD$^-$ and mature were CD19$^+$IgM^{lo}IgD^{hi}. (F) Ex vivo development of proB/preBI cells cocultured with ST-2 stroma cells. Frequency of CD19$^+$CD117$^+$ cells is shown. Each dot represents mean value of three wells ±SD. Data shown are representative of two independent experiments. (A–E) Numbers next to the gates indicate percentages. Numbers above the plots indicate p values. (A, C–E) Each dot represents an individual mouse. Pooled data of three (A, C) or five (D, E) independent experiments with minimum three mice per group are shown. Statistical analysis was performed using unpaired Student's t test.

which either 36 bp or 7 and 15 bp of critical region were deleted resulting in complete loss of mature miR-191 (Fig. S2A). Of note, expression of *Daldr3* and *Ndufa3*, genes located in close proximity to miR-191 (< 2 kb), was not affected (Fig. S2B). Cellularity of BM, thymus and spleen from miR-191$^{-/-}$ mice was indistinguishable from littermate controls (Fig. S2C). Furthermore, T-cell development in these mice was comparable to that in WT littermates (Fig. S2D). However, loss of miR-191 resulted in a 1.4-fold reduction in frequencies and total number of B cells in BM (Fig. 2A). Analysis of BM B-cell subsets showed that B-lineage deficiency became apparent starting at the proB/preBI stage (defined as B220$^+$CD19$^+$CD117$^+$CD25$^-$), which represents the earliest subset of B-lineage committed progenitors (Fig. 2B, C). Of note, B-cell frequencies and total numbers recovered at the transition between the immature and mature stage in BM from miR-191$^{-/-}$ mice (Fig. 2C). Thus, the effect of deletion of miR-191 directly correlates with physiological expression levels of miR-191 in B-cell progenitors.

In a complementary approach we next addressed the function of miR-191 in lymphocyte development upon overexpression in competitive BM chimeras. Ectopic expression using a retroviral vector resulted in an approximately twofold overexpression of miR-191 in B lineage cells isolated from chimeric mice (Fig. S2E). Surprisingly, we observed a reduction in frequencies of bone marrow B cells by 40% within the subset of cells ectopically expressing miR-191 (Fig. 2D). At the same time, we did not observe any significant changes in developing T cells and myeloid cells (Fig. S2F and not depicted). Analysis of recipient mice after 8 weeks revealed no differences in B-cell ratios upon overexpression of unrelated miRNAs miR-126 and miR-22 (Fig. S2G). Next, we examined B-cell progenitors in BM of chimeric mice. We detected an accumulation of GFP$^+$ proB/preBI cells upon overexpression of miR-191 indicating a developmental block induced by miR-191 (Fig. 2E). Ratios of preBII cells in chimeric mice remained unaltered upon overexpression of miR-191, presumably due to compensatory effects (Fig. 2E). Furthermore, a significant (∼twofold) reduction in both immature and postselection mature B cells overexpressing miR-191 was detected (Fig. 2E).

Accumulation of early B-cell precursors might be a result of delayed B-cell development or augmented proliferation of proB/preBI cells. To be able to distinguish between these alternative scenarios, we differentiated preBI precursors on ST-2 stromal

cells. Declining surface expression of CD117 served as signature marker for differentiation. Control cells lost CD117 more rapidly while not declining in numbers when compared to cells overexpressing miR-191. This observation further supported the notion that elevated expression of miR-191 induces a partial developmental arrest at the preBI to preBII cell transition (Fig. 2F). Taken together, these data show that neither complete loss nor even moderate overexpression of miR-191 are conducive to efficient early B-cell development. In contrast, development of other lymphocyte lineages is completely independent of miR-191.

Overexpression but not loss of miR-191 affect B cells in the periphery

Next, we tested whether perturbed development of B cells in the absence of miR-191 penetrates to the periphery. Frequencies and total number of splenic B cells were unaffected by loss of miR-191 (Fig. S3A). Given the dynamic regulation of miR-191 upon BCR stimulation and during germinal center formation we studied the response of miR-191$^{-/-}$ mice to SRBC, a well-characterized T-cell dependent model antigen. Seven and 14 days postimmunization both WT and miR-191$^{-/-}$ mice generated comparable numbers of germinal center B cells (Fig. S3B).

Analysis of peripheral lymphocytes from competitive overexpression chimeras revealed a reduction in frequencies of splenic B cells, equally affecting follicular B cells (Fo B) and marginal zone B cells (MZ B), upon overexpression of miR-191 (Fig. S3C). This finding is consistent with the observed miR-191-dependent retardation of BM B-cell development, given that T-cell development remained unaffected by overexpression of miR-191 (Fig. S2C). Antigen-specific B-cell expansion and class switch of B cells upon immunization of chimeras with the T-cell dependent antigen TNP-KLH as well as overall production of IgM and IgG by Fo B cells were unaffected by overexpression of miR-191 (Fig. S3D). Furthermore, stimulation of follicular B cells overexpressing miR-191 and respective control cells in vitro revealed a similar proliferation potential (Fig. S3E). These findings imply that once B-cell development is completed, elevated levels of miR-191 do not impair activation, proliferation, or class switch of mature B cells. Taken together, these results indicate that miR-191 controls development but not peripheral activity of B cells. Consistent with its expression pattern across the B lineage, ectopic expression, but not deletion of miR-191 resulted in developmental defects penetrating into the periphery.

Transcription factors Foxp1, Egr1, and E2A are bona fide targets of miR-191

The sequence of mature miR-191 is broadly conserved across species (Fig. S4A). Using the target prediction tools miRanda and TargetScan, we identified the transcription factors Egr1, Foxp1, and E2A as potential targets. All of them contain at least two conserved potential-binding sites for miR-191 (Fig. S4B–D) and
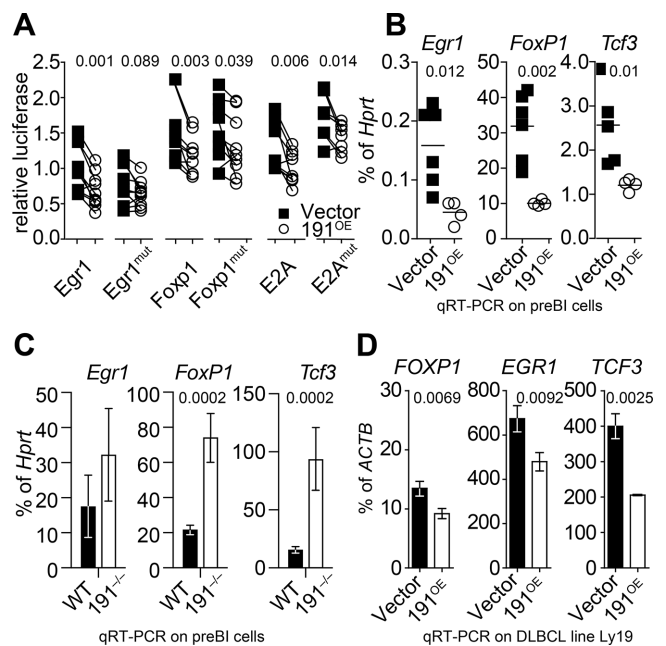
Figure 3. Transcription factors Egr1, Foxp1, and E2A are bona fide targets of miR-191. (A) Dual luciferase assay in 3T3 cells with 3'UTR of Egr1, Foxp1, and E2A and respective mutated 3'UTRs lacking miR-191 binding sites. Pairwise comparison of relative luciferase activity in control (Vector) and cells overexpressing miR-191 (191^{OE}). Pooled data of a minimum nine independent experiments are shown. (B–C) Relative expression of *Egr1*, *Foxp1*, and *Tcf3* (E2A) assessed by qRT-PCR in sorted preBI cells from (B) chimeric mice expressing Vector or 191OE vector or from (C) miR-191$^{-/-}$ mice (191$^{-/-}$) or littermate controls (WT). Expression levels are shown as percentage of *Hprt*. Each point represents a pool of cells from two to three mice. (D) Relative expression of *FOXP1*, *EGR1*, and *TCF3* in in vitro cultured DLBCL Ly19 line assessed after transduction with Vector or 191^{OE} vector. (B) Each dot represents data from an individual mouse. (C–D) Pooled data of two independent experiments (mean ± SD). Statistical analysis was performed using paired Student's *t* test. Numbers above the charts indicate *p* values.

sequences surrounding putative miR-191 binding sites in the 3'UTRs of *Egr1* and *Foxp1* were enriched in CLIP-Seq data obtained from naïve CD4 T cells [11]. To assess whether miR-191 directly targeted these transcription factors, we established 3T3 cell lines overexpressing miR-191 by using a retroviral vector that encodes miR-191 along with GFP (Fig. S4E). Dual-luciferase assays using psiCheck vectors encoding a luciferase cDNA fused to the respective 3′UTRs revealed that luciferase activity was lower in 3T3 cells that overexpressed miR-191 when compared to control cells (Fig. 3A). Deletion of candidate binding sites resulted in derepression of luciferase activity. Partial derepression in case of Foxp1 and E2A can be attributed to additional noncanonical-binding sites in the 3′UTR of those genes (Fig. S4B–D).

To validate that miR-191 was effectively repressing its targets Foxp1, Egr1, and E2A in vivo we ectopically expressed miR-191 together with GFP as reporter in hematopoietic progenitors and generated developing B cells by injection into irradiated mice. Ten days after reconstitution, we examined expression of Foxp1, Egr1, and E2A in FACS-sorted proB/preBI subsets by qRT-PCR. Ectopic expression of miR-191 resulted in a two to threefold decrease in expression of all three transcription factors (Fig. 3B). In contrast,

expression of other key mediators of B-cell development, such as Ebf1 and Pax5, was not affected by ectopic expression of miR-191 (Fig. S4F). Conversely, expression levels of Foxp1 and E2A were elevated in preBI cells isolated from miR-191⁻/⁻ mice when compared to WT controls, whereas a trend toward, but no statistically significant elevation of expression of Egr1 was observed (Fig. 3C). The high degree of conservation of miR-191 across species (Fig. S4A) and preserved miR-191-binding sites in the 3'UTRs of the three target genes (Fig. S4B–D) implied a functional relevance for miR-191 in human B cells. Consistent with our data from murine hematopoietic cells, expression of the three target genes *FOXP1*, *EGR1*, and *TCF3* was decreased upon overexpression of miR-191 in Ly19 DLBCL cells (Fig. 3D). Collectively, these data indicate that Foxp1, Egr1, and E2A are conserved targets of miR-191.

miR-191 regulates V(D)J recombination and IL-7-dependent expansion of preBI cells

Next, we addressed the molecular mechanisms through which miR-191 modulates B-cell development. First we tested the hypothesis that *Igh* rearrangement, which occurs prior to the preBI–preBII transition, might be impaired upon overexpression of miR-191. To this end, we assessed expression of *Rag1*, *Rag2*, and *Dntt* (encoding TdT), which constitute key components of the recombination machinery. Expression of these genes, but not other components of the recombination machinery, such as *Xrcc6* and *Lig1*, in preBI cells was substantially decreased upon overexpression of miR-191 (Fig. 4A and Fig. S5A). Furthermore, expression of surrogate light chain components was not affected (Fig. S5B). Direct analysis of V-to-DJ_H rearrangements in preBI cells revealed that the occurrence of complete V-DJ rearrangements in miR-191 overexpressing preBI progenitors was substantially lower than in controls (Fig. 4B, Fig. S5C), irrespective of the V gene position in the *Igh* locus.

Clonal expansion and developmental progression at the preBI stage are driven by IL-7 signaling. We observed reduced expression of IL-7Rα (CD127) on preBI cells overexpressing miR-191 (Fig. 4C). To test whether this reduction affected expansion of B-cell progenitors, purified preBI cells were cultured for ten days in methylcellulose supplemented with IL-7. Expansion of preBI cell colonies was reduced by approximately 2.5-fold upon miR-191 overexpression (Fig. 4D).

In summary, our findings indicate that elevated levels of miR-191 impair development of early B-cell progenitors by inhibiting *Igh* recombination as well as by reducing their responsiveness to IL-7.

Overexpression of E2A and Foxp1 rescue the developmental block induced by miR-191

Next, we directly assessed the interdependence of miR-191 and transcription factors E2A and Foxp1. To this end, we generated
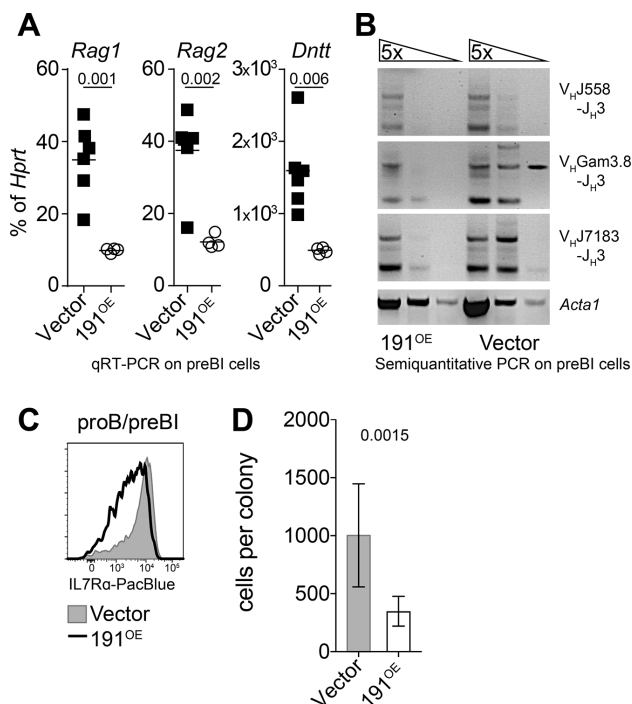

Figure 4. miR-191 regulates V(D)J recombination and IL-7-dependent expansion of preBI cells. (A) Relative expression of *Rag1*, *Rag2*, and *Dntt* in proB/preBI cells isolated from chimeric mice assessed by qRT-PCR. Expression levels are shown as percentage of *Hprt*. Pooled data of two individual experiments. Each point represents a pool of sorted cells from two to three mice. (B) Semiquantitative PCR analysis of genomic DNA for V_HJ558, V_HGam3.8, or V_HJ71833 to J_H3 rearrangements from sorted proB/preBI cells. Expression of recombination-independent *Acta1* serves as loading control. Data shown are representative of 3 independent experiments. (C) FACS analysis of IL-7Rα (CD127) expression on surface of proB/preBI cells isolated from Vector and 191^OE bone marrow chimeras. Representative histogram of two independent experiments is shown. (D) Sorted proB/preBI cells from Vector and 191^OE chimeras were cultured in methyl cellulose supplemented with 10 ng/mL of IL-7. After ten days colonies were harvested and the number of cells per colony was assessed by flow cytometry. Pooled data of two independent experiments are shown ($n = 46$ and $n = 49$), indicating median cellularity and 95% CI. (A, D) Statistical analysis was performed using unpaired Student's *t* test. Numbers above the plots indicate *p* values.

chimeras with cells cooverexpressing miR-191 and its targets E2A or Foxp1. Cells overexpressing miR-191, its targets or both could be detected based on GFP, hCD25 or both reporter genes, respectively. In order to avoid development of leukemia by enforced expression of E2A, we assessed B-cell development 10 days after transfer of BM precursors. B-cell development in these short-term chimeras was arrested at the same developmental check point as in long-term chimeras upon ectopic expression of miR-191 resulting in an even more pronounced accumulation of proB/preBI precursors (Fig. 5A). Development of preBII cells was delayed in short-term chimeras, an effect that was presumably compensated by the increased pool of proB/preBI cells at steady state in long-term chimeras. Ectopic expression of E2A alone strongly promoted B-cell development indicated by increased frequencies of preBII cells at the expense of the preBI subset (Fig. 5B). Interestingly, combined expression of E2A and miR-191 resulted in a distribution of preBI and preBII subsets comparable to that
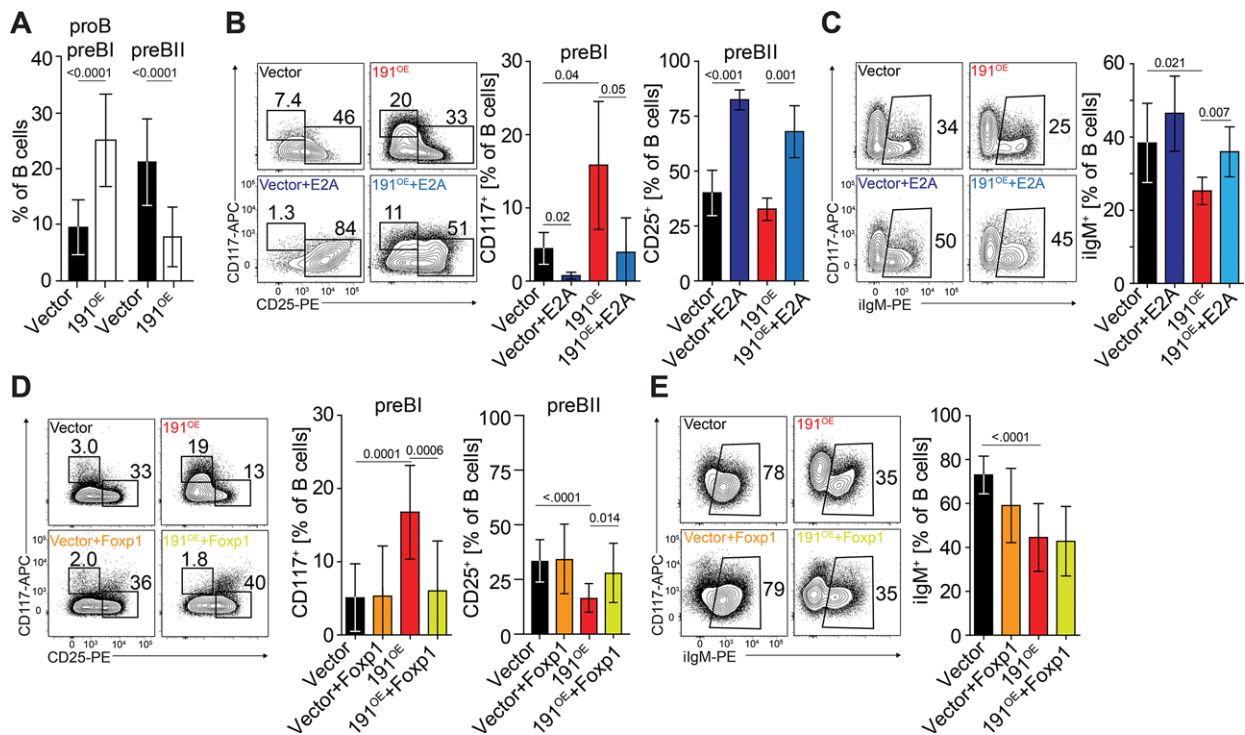
Figure 5. Overexpression of E2A and Foxp1 rescue the developmental block induced by miR-191. (A) LSK precursors were transduced with Vector or 191[OE] vector and transfer red into lethally irradiated recipient mice. Development of early B-cell progenitors was assessed ten days after transplantation. Representative data of five independent experiments are shown. (B) Similar to A, LSK precursors were transduced with Vector or 191[OE] vectors with or without E2A vector and transfer into lethally irradiated host. Ten days after transplantation development of proB/preBI and preBII precursors was assessed by FACS. (C) Bone marrow cells of chimeric mice depicted in (B) were fixed and intracellularly stained for IgM. Representative contour plots of B-cell progenitor. (D–E) Analo to B and C but replacement of E2A with Foxp1 vector. (B–C) Representative contour plots of early B-cell progenitors (left panel) and statistical analysis of one of three independent experiments (right panel) is shown ($n = 4$, average + SD). (D–E) Representative contour plots of early B-cell progenitors (left panel) and statistical analysis of two independent experiments (right panel) is shown ($n = 10$–12, average + SD). Statistical analysis was performed using unpaired Student's t test. Numbers above the charts indicate p values.

observed in control chimeras (Fig. 5B). Furthermore, coexpression of E2A and miR-191 rescued expression of intracellular IgM, indicating that restoration of E2A expression is sufficient to overcome miR-191-induced inhibition of *Igh* rearrangement (Fig. 5C). Ectopic expression of Foxp1 alone did not result in alterations in B-cell development in short-term chimeras (Fig. 5D). However, coexpression of Foxp1 and miR-191 was able to specifically overcome the B-lineage developmental block induced by ectopic expression of miR-191 alone (Fig. 5D). Of note, expression of Foxp1 did not restore *Igh* rearrangement (Fig. 5E). In summary, we conclude that coexpression of E2A as well as Foxp1 were sufficient to rescue early B-cell development in cells ectopically expressing miR-191, albeit in part via distinct mechanisms. These data establish that miR-191 acts opposingly to E2A and Foxp1 and, together with in silico prediction, luciferase assays and expression analyis, suggest that both transcription factors are functionally relevant targets of miR-191.

Discussion

In this study, we have identified miR-191 as an upstream regulator of key B lineage transcription factors, E2A, Foxp1, and Egr1. We

demonstrated that, paradoxically, both deletion as well as elevated levels of miR-191 prevented efficient developmental progression prior to and at the pre-B cell stage. Thus, our data suggest that miR-191 acts as a rheostat to create a tight window of transcription factor expression to robustly execute the B lineage developmental program. This notion is consistent with earlier studies investigating B-cell development in models with graded levels of transcription factor expression. Thus, lowering the gene dosage of E2A in heterozygous gene-targeted mice affects B-cell development by reducing expression of the E2A targets *Rag2* and *mb-1* [12]. Concomitant heterozygosity for E2A and Ebf1 results in a virtually complete block in B-cell development, underscoring the synergistic function of these transcription factors. Although no gene dosage effect of Foxp1 on B-cell development has been described, at least part of its function overlaps with that of E2A. Both transcription factors bind to the Erag enhancer and control expression of Rag genes [4, 13]. Interestingly, expression of all three transcription factors identified as targets was substantially increased or downregulated in preBI cells deficient in miR-191 or ectopically expressing miR-191, respectively. In contrast, luciferase assays indicated only a rather modest effect of miR-191 on posttranscriptional modulation via the 3'UTRs. Although these assay systems cannot be compared directly, our data suggest that miR-191 may

interfere with positive feedback regulation of at least some of its target transcription factors. Furthermore, we noticed that the substantial repression of target mRNA showing two- to threefold lower levels resulted in comparatively moderate effects. Thus, the developmental block observed here is of a similar magnitude, if not smaller, than heterozygous deletion of E2A alone [12].Given a miRNA's propensity to act on multiple targets simultaneously this apparent discrepancy might be explained by engagement of other, yet to be identified, targets that might account for compensatory effects. That such effects might play a role here is supported by our finding that in short-term chimeras the B-lineage developmental block is stronger when compared to the steady-state in long-term chimeric mice. In addition, still comparatively little is known about complex gene regulatory networks and the direct interplay of multiple transcription factors. Combined ChIPseq analysis has only recently resulted in identification of regulatory networks and new modes of regulation, such as redirection and capture of transcription factors by competing factors, are only beginning to emerge [14, 15]. Ultimately, we cannot exclude that expression of Foxp1, E2A, and/or Egr1 mRNA does not completely reflect protein expression, which we were not able to directly test due to a lack of suitable reagents. Such divergence might occur in case of uncoupling of transcription and translation due to posttranscriptional mechanisms or posttranslationally due to targeted degradation or selective stabilization of protein. Such means of selective regulation on the protein level have not been reported for the three transcription factors in question. Nevertheless, restriction of expression analysis to mRNA levels represents a limitation to our study.

In conclusion, targeting of this transcriptional module by miR-191 is well in line with a proposed role of miRNAs in fine-tuning and stabilizing transcriptional networks or signaling pathways. The rescue of B-cell development by cooverexpression of E2A and miR-191 supports this model. Of note, whereas rescue by E2A restored pre-BCR expression it did not affect expression levels of IL-7R, which is line with previous reports [12]. The contribution of Egr1 as a third target of miR-191 identified in this study is more difficult to assess. Whereas the role of Egr family members in B-cell development has been well established through transgenic expression of dominant-negative Egr mutants, deletion of individual family members including Egr1 had no apparent effect on B-cell development. These data suggest that other Egr family proteins can compensate for loss of Egr1 [16, 17]. Egr proteins function downstream of BCR signaling [18]. Thus, it is conceivable that miR-191 not only acts upstream of pre-BCR signaling via regulation of somatic recombination but also downstream by limiting the expression of Egr1.

Cooperativity of transcription factor action and thus the formation of transcription factor coregulatory networks has been well established at the level of loss-of-function mutations and cotargeting of critical effector genes of B-cell development [14]. In contrast, little is known about the consequences of compound overexpression of transcription factors in the course of B-cell development. An increase in Foxp1 expression alone due to downregulation of miR-34 did not abrogate B-cell development but

rather displayed a B-lineage promoting function [19]. In contrast, deletion of miR-191 paradoxically showed a similar phenotype as overexpression of the same miRNA. Analysis of miR-191-deficient developing B cells revealed elevated expression of Foxp1, E2A, and Egr1, which was consistent with overexpression data, but cannot be easily reconciled with the phenotype observed. To date, combined transcription factor action is difficult to analyze quantitatively and combined ectopic expression of transcription factors acting in parallel is usually not analyzed. Thus, there is currently no precendence for a combined negative effect of individually positively acting transcription factors. Combined ChIPseq experiments might provide insight into such scenarios. In addition, we cannot exclude that although overexpression and deletion of miR-191 result in corresponding changes in expression of the three targets identified here, other targets yet to be identified might act predominantly upon deletion of miR-191. Accordingly, it has recently been proposed for miR-17~92 that not all targets react equally sensitive to deletion or overexpression of the miRNA cluster [20].

Upon ectopic expression of miR-191 developing B-cell precursors displayed limited responsiveness to survival cues from the IL-7R as well as reduced expression levels of components of the recombination machinery resulting in impaired IgH rearrangement. Computational analysis indicated that the 3'UTRs of *Rag1*, *Rag2,* and *Dntt* (encondingTdt) lack candidate-binding sites for miR-191, suggesting that reduced expression of these genes is likely to be an indirect effect. In fact, it has been shown that both E2A and Foxp1 transcriptionally regulate Rag genes by binding to the Erag enhancer region [19, 21, 22]. In conclusion, we propose that miR-191 is at the top of a hierarchy of transcriptional control of the recombination machinery comprising the transcription factors E2A and Foxp1 as key intermediates. Interestingly, restoring expression of Foxp1 alone did not rescue somatic recombination, suggesting that repression of E2A by miR-191 plays a dominant role in this regulatory network.

Expression levels of miR-191 increased with developmental progression toward B cells, but also substantially decreased once progenitors entered the T lineage. These findings are in good agreement with an earlier study describing the overall dynamics of miRNA expression during hematopoiesis [23]. Therefore, it was somewhat surprising that ectopic expression of miR-191 did not influence T-cell development to any detectable degree. Our data suggest a model, in which miR-191 downmodulates E2A and Foxp1, thus limiting IgH rearrangement. Interestingly, both transcription factors regulate Rag expression by binding to an enhancer element (Erag), which is only required for optimal Rag gene expression in cells of the B lineage but not in T lineage cells [24]. Furthermore, Foxp1 has no apparent function during early T-cell development. Thus, the effect on Foxp1 may best explain why ectopic expression of miR-191 constrains B cell but not T-cell development. In addition, it is possible that alternative transcripts of E2A required at different stages of B and T-cell development are selectively targeted by miR-191 [25–28]. Further work is required to test this hypothesis.

Materials and methods

Mice

All animal experiments were conducted in accordance with local and institutional regulations (Nds. Landesamt f. Verbraucherschutz und Lebensmittelsicherheit, 33.14-42502-04-08-1480, −11-0533, −14/1431). C57BL/6J and NOD.Cg-$Prkdc^{scid}Il2rg^{tm1}$Wjl/SzJ (NSG) mice were purchased from Charles River or bred at the animal facility of Hannover Medical School. Animals were maintained under specific-pathogen-free conditions. To generate miR-191$^{-/-}$ mice two single guide RNAs (sgRNAs) targeting miR-191 locus were designed with an online CRISPR design tool (http://crispr.mit.edu/) to disrupt hairpin structure and minimize off-target effects. sgRNAs were generated via in vitro transcription based on previously published protocol [29]. Briefly, T7 promoter sequence was added to the forward primers containing sgRNA sequence. PCR was performed with T7-sgRNA forward primer (5′-TAATACGACTCACTATAGGG N20GTTTAAGAGCTATGCTGGAAACAGC-3′) and reverse primer (5′-AAAAAAAGCACCGACTCGGTG-3′), using the pX330-U6-Chimeric_BB-CBh-hSpCas9 plasmid (Addgene #42230, a gift from Feng Zhang) [30] as template, to generate a 133bp PCR product. The product was purified and in vitro transcribed (MEGAshortscipt T7 Transcription Kit, Thermofisher Scientific). Two T7-sgRNAs and Cas9 Nuclease (IDT) were combined to generate an RNP complex. Microinjection of embryos was performed as previously described [31].Two mouse lines carrying a 36 bp or 7 + 15 bp deletion in the miR-191 locus were established. Deletions resulting in disruption of miR-191 hairpin structure in both founder lines were confirmed by Sanger sequencing after purification of PCR product using (forward) AACACCTACTCCTTCCTACTCAGC and (reverse) CTTCAGAGAGAGGACCCAGGACC primers. Quantitative RT-PCR with primers recognizing mature miR-191 showed that both deletions in miR-191 locus resulted in essentially complete absence of miR-191. To minimize off-target effects founder F0 mice were bred to heterozygocity with wild-type C57BL/6 mice. miR-191$^{-/-}$ mice were maintained under specific-pathogen-free conditions at Central Animal Facility of LMU. To exclude off-target deletions potential targeting sites were assessed using the MIT online webtool. Five sites with the highest score were selected and subjected to Sanger sequencing using the following primer sets:

191-T1-OT1-F-GTTGCTGAGCATGGCCATCTTTC	365bp
191-T1-OT1-R-CTACCAGGGACACACAGGTCTG	
191-T1-OT2-F-GCTGAGGGTGGTGTGTTCTTTG	284bp
191-T1-OT2-R-TAACGTGGAGTTCTGGTTGGC	
191-T1-OT3-F-ACCCTTTTCCGTCTTTAGCCCA	426bp
191-T1-OT3-R-AGCATCATACTGATCCCCCAGC	
191-T1-OT4-F-AGGTGGGAAACAGGTTAAGGGG	341bp
191-T1-OT4-R-GCCCCCTCTACCCATCTCATTC	
191-T1-OT5-F-ACTGCTTCCTCTCTGCTTCCTG	351bp
191-T1-OT5-R-GCTGGAAGCCCTCAACAAGTTT	
191-T2-OT1-F-AGAAACGGCCTCCACTTACCTC	391bp

191-T2-OT1-R-CTCTGATATGGTCTCTGGGGCG	
191-T2-OT2-F-TTGCTGTTGACTGGAGCATTGC	305bp
191-T2-OT2-R-GACACACTTAGTCCACCAGGCT	
191-T2-OT3-F-TTTCCGAAAACAGAGTGCGCTC	283bp
191-T2-OT3-R-AAGGTGGAGGCGATCTGTTTCA	
191-T2-OT4-F-GCTGCTAAGCCAGTAGTGTCTG	363bp
191-T2-OT4-R-CCTGTGCTTGGCATGTCTGTTT	
191-T2-OT5-F-AGCTTTTTGTGCCTGAACCTCG	257bp
191-T2-OT5-R-TCTTCCTCTCCTCCCTGACACT	

Bone marrow chimeras

Bone marrow chimeras were established as previously described [32]. Irradiated C57BL/6 mice (9 Gy) were analyzed 10 days or 8–10 weeks after reconstitution.

Purification of lin⁻ BM cells and enrichment of developing thymocytes

Lin⁻ cells were isolated from total BM by staining cell suspensions with a lineage-specific antibody cocktail including TCRβ, CD19, CD11b, CD11c, Gr-1, Ter-119, and NK1.1, all eBioscience or BioLegend (followed by incubation with sheep anti-rat IgG conjugated to magnetic beads (Dynal, Invitrogen) and magnetic bead depletion of mature lineages. DN thymocytes were enriched by complement lysis of DP and SP cells using anti-CD4 and anti-CD8 antibodies (clones RL1.72 and 31M) and incubation with LowTox-M rabbit complement (Cedarlane) followed by gradient separation using Lympholyte M (Cedarlane).

Cloning and production of retroviruses

HEK293T cells were transfected using the Calcium Phosphate Method (CalPhos, Clontech). As a packaging plasmid pCLEco (coexpressing MLV gag, pol and env) was used. MDH1-PGK-GFP_2.0, a gift from Chang-Zheng Chen [33], served as empty vector control (Addgene plasmid # 11375) and was used to generate MDH1-PGK-GFP-2.0-miR-191 and MDH1-PGK-GFP-2.0-miR-126 containing pre-miRNAs and flanking regions of miR-191 and miR-126, respectively, under control of an H1 promoter. pHuE47TAC – encoding human E47 cDNA in combination with an IRES-linked hCD25 reporter [34, 35] and MSCV-mFoxp1-IRES-Thy1.1 were based on Addgene plasmids # 17442 and # 35170. MSCV-IRES-Thy1.1 DEST was a gift from Anjana Rao (Addgene plasmid # 17442) [36]; pCMV10-mFoxp1 was a gift from Benjamin Blencowe (Addgene plasmid # 35170) [37].

Transduction of cells

For competitive bone marrow chimeras, bead-enriched lin⁻ bone marrow cells were cultured overnight in complete α-MEM medium

(Life Technologies) supplemented with 10% heat inactivated FCS (GE Healthcare), 50 U/mL and 50 µg/mL Penicillin-Streptomycin, 1 mM Sodium Pyruvate (both Life Technologies), 60 µM β-mercaptoethanol and SCF (50 ng/mL), IL-7 (25 ng/mL), Flt3L (25 ng/mL) and IL-6 (20 ng/mL) (all cytokines from Peprotech). Spin infections were conducted with retrovirus supernatants in 24 well plates in the presence of 8 µg/mL of polybrene (Sigma Aldrich). For short-term and most long-term chimeras, lin$^-$Sca-1$^+$CD117^{hi} (LSK) cells were sorted from lineage-depleted BM and cultured overnight in complete α-MEM medium supplemented with SCF (50 ng/mL), IL-7 (25 ng/mL), Flt3L (25 ng/mL), and IL-6 (20 ng/mL). LSK cells were then transferred into 96-well plates (Sarstedt) preloaded with retroviral vector attached to RetroNectin (Takara) according to the manufacturer's protocol.

Immunization

Germinal center B cells (CD95$^+$GL7$^+$) were sorted from spleen on day 5, 7, and 14 after induction by i.v. injection of 200 µL PBS-washed SRBC suspension (Acila). For ELISPOT analysis of class switch recombination, mice were immunized i.p. with 200 µL TNP-KLH (Biosearch Technologies) emulsified in Complete Freund's Adjuvant (Sigma Aldrich). After 7 and 14 days splenic B cells were analyzed for TNP specific IgM$^+$ or IgG$^+$ B cells. Transduced and nontransduced cells were seeded onto plates coated with TNP. Cells were incubated overnight at 37°C in 5% CO$_2$. After washing, biotin-conjugated rat anti–mouse IgM (LO-MM-9; AbDSerotec) or goat-anti-mouse IgG (Sigma Aldrich) were added and developed with streptavidin- HRP (BD Biosciences) using 3-amino- 9-ethyl-carbazole (Sigma Aldrich) in N,N-dimethylformamide (Sigma Aldrich) diluted in 0.1 M acetate solution and with H$_2$O$_2$ as substrate [38].

Cells

Primary cells from wild-type or chimeric mice were sorted and cultured at 37°C, 5% CO$_2$. Mature B cells were stimulated in complete α-MEM supplemented with cross-linking 20 µg/mL F(ab')$_2$ fragment goat anti-mouse IgM (Jackson Immuno Research), anti-CD40 (clone FGK4T) and fully thiolated CpG 2006 type B (24mer 5′-TCGTCGTTTTGTCGTTTTGTCGTT-3′, TIB MOLBIO). Proliferation was assessed by staining of cells with Cell Proliferation Dye eFluor 670 according to manufacturer's instructions (eBioscience).

Clonal expansion of preB1 cells was assessed in methyl cellulose containing IL-7 (MethoCult M3630, Stemcell Technologies) according to the manufacturer's instructions with a starting cell number of 5000–20 000 sorted cells. Cellularity was assessed by picking single colonies and flow cytometric cell counting after 7 days.

Cell death of immature and transitional B cells was assessed in plain α-MEM (Life Technologies) supplemented with cross-linking F(ab')$_2$ fragments of goat anti-mouse IgM antibodies (20 µg/mL) overnight. Dead cells were identified by flow cytometry by loss

of GFP expression and reduction in size (FSC) and increased granularity (SSC).

For T-cell differentiation OP9-DL1 stromal cells transduced LSK cells were cultured in complete α-MEM supplemented with IL-7 (1 ng/mL) and Flt3-L (5 ng/mL) (both Peprotech). At day 4, the culture medium was exchanged and at day 7 cells were transferred onto fresh OP9-DL1 monolayers. Differentiation was assessed every 2–3 days by flow cytometry.

OCI-Ly19 were cultured in RPMI (Life Technologies) supplemented with 1% PenStrep, 1% Pyruvate and 20% (FCS #080150, Lot# 115654, Wisent INC).

Flow cytometry

Flow cytometry and cell sorting were performed on LSRII and FACSAriaIIu (BD), respectively, and followed the "Guidelines for the use of flow cytometry and cell sorting in immunological studies" [39]. Monoclonal antibodies specific for CD4 (RM4-5, GK1.5), CD8 (53-6.7), CD25 (PC61), CD44 (IM7), Gr-1 (RB6-8C5), erythroid cell marker (Ter-119), CD19 (1D3), CD11b (M1/70), NK1.1 (PK136), CD11c (N418), CD45.1 (A20), CD45.2 (104), B220 (RA3-6B2), CD117 (ACK2), Sca-1 (E13-161.7), CD135 (A2F10), CD127 (A7R34), CD95 (15A7), Thy-1.1 (OX-7), T- and B-cell activation marker (GL7), human CD25 (BC96) were used purified or as various fluorescent or biotin conjugates. Antibodies were purified from hybridoma supernatants or were purchased from eBioscience, BD Biosciences, Biolegend, or Miltenyi Biotech. Flow cytometry was conducted on an LSRII (Becton Dickinson) and analyzed in FlowJo (9.3 or X, TreeStar). Cell sorting was done using a FACSAriaIIu (Becton Dickinson).

Bone marrow B-cell stages were defined as follows: proB (B220$^+$CD19$^-$), preBI (B220$^+$CD19$^+$CD117$^+$CD25$^-$), preBII (B220$^+$CD19$^+$CD25$^+$CD117$^-$), immature B (CD19$^+$IgM^{lo}IgD$^-$), transitional (CD19$^+$IgM^{hi}IgD$^{+/-}$), mature (CD19$^+$IgM$^{int/-}$IgD$^+$). Splenic B-cell stages were defined as: Fo B cells (CD19$^+$CD23$^+$CD21/35$^-$), MZ B cells (CD19$^+$CD23$^-$CD21/35$^+$). Thymic T-cell stages: ETP (CD44$^+$ CD117$^+$CD25$^-$), DN2 (CD44$^+$CD117$^+$CD25$^+$), DN3 (CD44$^-$CD25$^+$), DN4 (CD44$^-$CD25$^-$), DP (CD4$^+$CD8$^+$), SP4 (CD4$^+$), SP8 (CD8$^+$). Intracellular staining, preserving GFP fluorescence, was carried out according to Heinen et al. [40].

miRNA microarrays

miRNA microarray (miRCURY LNA Arrays v. 10.0) transcriptional profiling was carried out by Exiqon. RNA samples from progenitor populations (200 ng each) were labeled with Hy3 and compared to Hy5-labeled skewed common reference sample consisting of an RNA mixture from total BM and thymus. Populations of interest were defined as follows: HSC, lin$^-$Sca-1$^+$CD117^{hi}CD135$^-$; CLP, lin$^-$Sca-1$^+$CD117$^+$CD127$^+$CD135$^+$; pre-pro-B, lin$^-$B220$^+$CD19$^-$; ETP, lin$^-$CD44$^+$CD117^{hi}CD25$^-$; DN2, lin$^-$CD44$^+$CD117^{hi}CD25$^+$. Analysis of scanned microarray images was performed by Exiqon

using the ImaGene software. Downstream data analysis was performed the "R" statistical analysis software package. Normalization and computation of significantly differentially expressed genes analysis was performed with the "limma" package from the Bioconductor suite. Genes whose absolute log2 fold change exceeded 1 and the adjusted p-value (using "Benjamini-Hochberg" method) was lower than 0.05 were assumed to be differentially expressed in a given pair-wise comparison. For hierachical clusterings only those probes were used that in a particular dataset were rated as differentially expressed in at least one pairwise comparison and to which a murine miRNA identifier was assigned.

Gene expression and rearrangement PCR

Total RNA was extracted with miRNeasy (Qiagen) followed by RT of mRNA (SuperScript II and random hexamers, Life Technologies) and miRNAs (TaqMan® MicroRNA Reverse Transcription Kit). Real-Time quantification was conducted using TaqMan Universal PCR master mix, MicroAmp™ 96-well fast reaction plates and optical adhesive covers in a StepOnePlus™ Instrument (Applied Biosystems) with TaqMan-probes for hsa-miR-191 (000490), snoR412 (001243), U6 (001973), *Rag1* (Mm01270936_m1), *Rag2* (Mm00501300_m1), *Dntt* (encoding TdT) (Mm00493500_m1), *Ebf1* (Mm00432648_m1), *Egr1* (Mm00656724_m1), *EGR1* (Hs00152928_m1), *Foxp1* (Mm00474848_m1), *FOXP1* (Hs00212860_m1), *Tcf3* (encoding E2A) (Mm01175588_m1), *TCF3* (Hs00413032_m1), *Pax5* (Mm00435502_m1), *Hprt* (Mm00446968_m1), *ACTB* (Hs99999903_m1). Heavy chain rearrangement was assessed on three V_H gene families: V_HJ558, V_HGam3.8 and V_HJ7183 to DJ_H3. The genes belonging to the V_HJ558 family are located at the most 5′ end of the V_H locus and belong to the most frequently used V_H families. Genes belonging to the V_HGam3.8 are located at the center of the V_H locus; the genes belonging to V_HJ7183 family are located at the most 3' end of the V_H locus and are the first used to rearrange with DJ_H [4, 41, 42] Genomic DNA was isolated using QIAamp micro kit (Qiagen) and the PCR was carried out on 20 000; 4000; and 800 cells using 1 nM of primers as previously described [43, 44] in 1x PCR reaction buffer (B9004S, Thermopol) for 40 cycles (annealing 59°C).

Luciferase Assay

Wild type and mutated 3'UTRs (Fig. S2) of Egr1, FoxP1, and E2A were synthesized by GeneArt (Regensburg) and cloned into PsiCheck2.0. 3T3 cells overexpressing miR-191 or control cells were cultured in DMEM (Life Technologies) (10% FCS, 1% Pen-Strep, 1% Na-Pyruvate, 25 g/mL Geneticin (Life Technologies)). A total of 250 000 cells were electroporated with 0.1 μg Plasmid (250 V, 950 μF, Biorad Gene Pulser II) and cultured for 24 h in six-well plates. Dual-Luciferase Reporter assay (Promega) was conducted according to manufacturer's instructions. Luciferase activities were normalized to empty PsiCheck2.0 to control for variances between cell lines.

Statistics

Statistical significance of differences between two groups was analyzed using paired or nonpaired *t*-tests where applicable. For comparison of multiple groups statistical significance was determined using ANOVA followed by *t*-tests to assess significance between groups.

Author contributions: M.Ł., J.B., N.Z., S.W., and A.K. designed research; M.Ł., J.B., N.Z., Y.L., O.O.S., S.J.W., H.K.-S., N.S., S.D., B.R., and K.W. performed research; M.Ł., J.B., N.Z., J.P., and A.K. analyzed data; W.W. and C.K. gave critical advice and lab resources; M.Ł., J.B., and A.K. wrote the manuscript.

Conflict of interest: The authors have declared that no conflict of interest exists.

References

1 **Busslinger, M.**, Transcriptional control of early B cell development. *Annu. Rev. Immunol.* 2004. **22**: 55–79.

2 **Matthias, P. and Rolink, A. G.**, Transcriptional networks in developing and mature B cells. *Nat. Rev. Immunol.* 2005. **5**: 497–508.

3 **Fuxa, M., Skok, J., Souabni, A., Salvagiotto, G., Roldan, E. and Busslinger, M.**, Pax5 induces V-to-DJ rearrangements and locus contraction of the immunoglobulin heavy-chain gene. *Genes Dev.* 2004. **18**: 411–422.

4 **Hu, H., Wang, B., Borde, M., Nardone, J., Maika, S., Allred, L., Tucker, P. W. and Rao, A.**, Foxp1 is an essential transcriptional regulator of B cell development. *Nat. Immunol.* 2006. **7**: 819–826.

5 **Koralov, S. B., Muljo, S. A., Galler, G. R., Krek, A., Chakraborty, T., Kanellopoulou, C., Jensen, K. et al.**, Dicer ablation affects antibody diversity and cell survival in the B lymphocyte lineage. *Cell* 2008. **132**: 860–874.

6 **Olive, V., Jiang, I. and He, L.**, mir-17-92, a cluster of miRNAs in the midst of the cancer network. *Int. J. Biochem. Cell Biol.* 2010. **42**: 1348–1354.

7 **He, L., Thomson, J. M., Hemann, M. T., Hernando-Monge, E., Mu, D., Goodson, S., Powers, S. et al.**, A microRNA polycistron as a potential human oncogene. *Nature* 2005. **435**: 828–833.

8 **Ventura, A., Young, A. G., Winslow, M. M., Lintault, L., Meissner, A., Erkeland, S. J., Newman, J. et al.**, Targeted deletion reveals essential and overlapping functions of the miR-17 through 92 family of miRNA clusters. *Cell* 2008. **132**: 875–886.

9 Xiao, C., Srinivasan, L., Calado, D. P., Patterson, H. C., Zhang, B., Wang, J., Henderson, J. M. et al., Lymphoproliferative disease and autoimmunity in mice with increased miR-17-92 expression in lymphocytes. *Nat. Immunol.* 2008. **9**: 405–414.

10 Costinean, S., Zanesi, N., Pekarsky, Y., Tili, E., Volinia, S., Heerema, N. and Croce, C. M., Pre-B cell proliferation and lymphoblastic leukemia/high-grade lymphoma in E(mu)-miR155 transgenic mice. *Proc. Natl. Acad. Sci. USA* 2006. **103**: 7024–7029.

11 Loeb, G. B., Khan, A. A., Canner, D., Hiatt, J. B., Shendure, J., Darnell, R. B., Leslie, C. S. and Rudensky, A. Y., Transcriptome-wide miR-155 binding map reveals widespread noncanonical microRNA targeting. *Mol. Cell* 2012. **48**: 760–770.

12 O'Riordan, M. and Grosschedl, R., Coordinate regulation of B cell differentiation by the transcription factors EBF and E2A. *Immunity* 1999. **11**: 21–31.

13 Goebel, P., Janney, N., Valenzuela, J. R., Romanow, W. J., Murre, C. and Feeney, A. J., Localized gene-specific induction of accessibility to V(D)J recombination induced by E2A and early B cell factor in nonlymphoid cells. *J. Exp. Med.* 2001. **194**: 645–656.

14 Lin, Y. C., Jhunjhunwala, S., Benner, C., Heinz, S., Welinder, E., Mansson, R., Sigvardsson, M. et al., A global network of transcription factors, involving E2A, EBF1 and Foxo1, that orchestrates B cell fate. *Nat. Immunol.* 2010. **11**: 635–643.

15 Hosokawa, H., Ungerback, J., Wang, X., Matsumoto, M., Nakayama, K. I., Cohen, S. M., Tanaka, T. and Rothenberg, E. V., Transcription factor PU.1 represses and activates gene expression in early T cells by redirecting partner transcription factor binding. *Immunity* 2018. **48**: 1119–1134 e1117.

16 Gururajan, M., Simmons, A., Dasu, T., Spear, B. T., Calulot, C., Robertson, D. A., Wiest, D. L. et al., Early growth response genes regulate B cell development, proliferation, and immune response. *J. Immunol.* 2008. **181**: 4590–4602.

17 Lee, S. L., Tourtellotte, L. C., Wesselschmidt, R. L. and Milbrandt, J., Growth and differentiation proceeds normally in cells deficient in the immediate early gene NGFI-A. *J. Biol. Chem.* 1995. **270**: 9971–9977.

18 Maltzman, J. S., Carmen, J. A. and Monroe, J. G., Transcriptional regulation of the Icam-1 gene in antigen receptor- and phorbol ester-stimulated B lymphocytes: role for transcription factor EGR1. *J. Exp. Med.* 1996. **183**: 1747–1759.

19 Rao, D. S., O'Connell, R. M., Chaudhuri, A. A., Garcia-Flores, Y., Geiger, T. L. and Baltimore, D., MicroRNA-34a perturbs B lymphocyte development by repressing the forkhead box transcription factor Foxp1. *Immunity* 2010. **33**: 48–59.

20 Jin, H. Y., Oda, H., Chen, P., Yang, C., Zhou, X., Kang, S. G., Valentine, E. et al., Differential sensitivity of target genes to translational repression by miR-17~92. *PLos Genet.* 2017. **13**: e1006623.

21 Lin, H. and Grosschedl, R., Failure of B-cell differentiation in mice lacking the transcription factor EBF. *Nature* 1995. **376**: 263–267.

22 Greenbaum, S. and Zhuang, Y., Identification of E2A target genes in B lymphocyte development by using a gene tagging-based chromatin immunoprecipitation system. *Proc. Natl. Acad. Sci. USA* 2002. **99**: 15030–15035.

23 Kuchen, S., Resch, W., Yamane, A., Kuo, N., Li, Z., Chakraborty, T., Wei, L. et al., Regulation of microRNA expression and abundance during lymphopoiesis. *Immunity* 2010. **32**: 828–839.

24 Hsu, L. Y., Lauring, J., Liang, H. E., Greenbaum, S., Cado, D., Zhuang, Y. and Schlissel, M. S., A conserved transcriptional enhancer regulates RAG gene expression in developing B cells. *Immunity* 2003. **19**: 105–117.

25 Bain, G., Maandag, E. C., Izon, D. J., Amsen, D., Kruisbeek, A. M., Weintraub, B. C., Krop, I. et al., E2A proteins are required for proper B cell development and initiation of immunoglobulin gene rearrangements. *Cell* 1994. **79**: 885–892.

26 Shen, C. P. and Kadesch, T., B-cell-specific DNA binding by an E47 homodimer. *Mol. Cell. Biol.* 1995. **15**: 4518–4524.

27 Beck, K., Peak, M. M., Ota, T., Nemazee, D. and Murre, C., Distinct roles for E12 and E47 in B cell specification and the sequential rearrangement of immunoglobulin light chain loci. *J. Exp. Med.* 2009. **206**: 2271–2284.

28 Turner, M., Galloway, A. and Vigorito, E., Noncoding RNA and its associated proteins as regulatory elements of the immune system. *Nat. Immunol.* 2014. **15**: 484–491.

29 Henao-Mejia, J., Williams, A., Rongvaux, A., Stein, J., Hughes, C. and Flavell, R. A., Generation of genetically modified mice using the CRISPR-Cas9 genome-editing system. *Cold Spring Harb. Protoc.* 2016. https://doi.org/10.1101/pdbprot090704.

30 Cong, L., Ran, F. A., Cox, D., Lin, S., Barretto, R., Habib, N., Hsu, P. D. et al., Multiplex genome engineering using CRISPR/Cas systems. *Science* 2013. **339**: 819–823.

31 Wefers, B., Panda, S. K., Ortiz, O., Brandl, C., Hensler, S., Hansen, J., Wurst, W. and Kuhn, R., Generation of targeted mouse mutants by embryo microinjection of TALEN mRNA. *Nat. Protoc.* 2013. **8**: 2355–2379.

32 Lyszkiewicz, M., Zietara, N., Fohse, L., Puchalka, J., Diestelhorst, J., Witzlau, K., Prinz, I. et al., Limited niche availability suppresses murine intrathymic dendritic-cell development from noncommitted progenitors. *Blood* 2015. **125**: 457–464.

33 Chen, C. Z., Li, L., Lodish, H. F. and Bartel, D. P., MicroRNAs modulate hematopoietic lineage differentiation. *Science* 2004. **303**: 83–86.

34 Engel, I. and Murre, C., Ectopic expression of E47 or E12 promotes the death of E2A-deficient lymphomas. *Proc. Natl. Acad. Sci. USA* 1999. **96**: 996–1001.

35 Sayegh, C. E., Quong, M. W., Agata, Y. and Murre, C., E-proteins directly regulate expression of activation-induced deaminase in mature B cells. *Nat. Immunol.* 2003. **4**: 586–593.

36 Wu, Y., Borde, M., Heissmeyer, V., Feuerer, M., Lapan, A. D., Stroud, J. C., Bates, D. L. et al., FOXP3 controls regulatory T cell function through cooperation with NFAT. *Cell* 2006. **126**: 375–387.

37 Gabut, M., Samavarchi-Tehrani, P., Wang, X., Slobodeniuc, V., O'Hanlon, D., Sung, H. K., Alvarez, M. et al., An alternative splicing switch regulates embryonic stem cell pluripotency and reprogramming. *Cell* 2011. **147**: 132–146.

38 Duber, S., Hafner, M., Krey, M., Lienenklaus, S., Roy, B., Hobeika, E., Reth, M. et al., Induction of B-cell development in adult mice reveals the ability of bone marrow to produce B-1a cells. *Blood* 2009. **114**: 4960–4967.

39 Cossarizza, A., Chang, H. D., Radbruch, A., Akdis, M., Andra, I., Annunziato, F., Bacher, P. et al., Guidelines for the use of flow cytometry and cell sorting in immunological studies. *Eur. J. Immunol.* 2017. **47**: 1584–1797.

40 Heinen, A. P., Wanke, F., Moos, S., Attig, S., Luche, H., Pal, P. P., Budisa, N. et al., Improved method to retain cytosolic reporter protein fluorescence while staining for nuclear proteins. *Cytometry A* 2014. **85**: 621–627.

41 Connor, A. M., Fanning, L. J., Celler, J. W., Hicks, L. K., Ramsden, D. A. and Wu, G. E., Mouse VH7183 recombination signal sequences mediate recombination more frequently than those of VHJ558. *J. Immunol.* 1995. **155**: 5268–5272.

42 Wu, G. E. and Paige, C. J., VH gene family utilization in colonies derived from B and pre-B cells detected by the RNA colony blot assay. *EMBO J.* 1986. **5**: 3475–3481.

43 **Schlissel, M.**, Voronova, A. and Baltimore, D., Helix-loop-helix transcription factor E47 activates germ-line immunoglobulin heavy-chain gene transcription and rearrangement in a pre-T-cell line. *Genes Dev.* 1991. **5**: 1367–1376.

44 **Angelin-Duclos, C. and Calame, K.**, Evidence that immunoglobulin VH-DJ recombination does not require germ line transcription of the recombining variable gene segment. *Mol. Cell. Biol.* 1998. **18**: 6253–6264.

Abbreviations: **ETP**: early T-cell progenitor · **MZ**: marginal zone

Full correspondence: Prof. Andreas Krueger, Institute for Molecular Medicine, Goethe University Frankfurt, D-60590 Frankfurt, Germany
e-mail: Andreas.Krueger@kgu.de

Additional correspondence: Dr. Marcin Łyszkiewicz, Institute of Immunology, Biomedical Center Munich,
Ludwig-Maximilians-University Munich, 82152 Planegg-Martinsried, Germany
e-mail: Marcin.Lyszkiewicz@med.uni-muenchen.de

Current Address: Jonas Blume, The Peter Doherty Institute for Infection and Immunity, The University of Melbourne, Melbourne, Victoria 3000, Australia.

Current Address: Natalia Ziętara, Institute of Immunology, Biomedical Center Munich, Ludwig-Maximilians-University Munich, 82152 Planegg-Martinsried, Germany.

Current Address: Namita Saran, King's College London, Immunobiology Department, Guys Hospital, London, UK.

Current Address: Bishnudeo Roy, Centre for Immune Regulation and Department of Immunology, University of Oslo and Oslo University Hospital, 0372 Oslo, Norway.

Appendix 6.2.

LAMTOR2 (p14) Controls B Cell Differentiation by Orchestrating

Endosomal BCR Trafficking

Łyszkiewicz M *, Kotlarz D *, Ziętara N *, Brandes G, Diestelhorst J, Glage S,

Hobeika E, Reth M, Huber L.A., Krueger A, Klein C.

* equal contribution

LAMTOR2 (p14) Controls B Cell Differentiation by Orchestrating Endosomal BCR Trafficking

Marcin Łyszkiewicz [1,2†§], Daniel Kotlarz [2†], Natalia Ziętara [1,2†§], Gudrun Brandes [3], Jana Diestelhorst [2], Silke Glage [4], Elias Hobeika [5], Michael Reth [6], Lukas A. Huber [7], Andreas Krueger [1,8*‡] and Christoph Klein [2*‡]

[1] Institute of Immunology, Hannover Medical School, Hannover, Germany, [2] Department of Pediatrics, Dr. von Hauner Children's Hospital, University Hospital, Ludwig-Maximilians-University Munich, Munich, Germany, [3] Institute of Neuroanatomy and Cell Biology, Hannover Medical School, Hannover, Germany, [4] Institute of Laboratory Animal Science, Hannover Medical School, Hannover, Germany, [5] Institute of Immunology, Ulm University, Ulm, Germany, [6] Max Planck Institute of Immunobiology and Epigenetics, Freiburg, Germany, [7] Division of Cell Biology, Biocenter, Medical University of Innsbruck, Innsbruck, Austria, [8] Institute for Molecular Medicine, Goethe-University Frankfurt, Frankfurt am Main, Germany

B-cell development and function depend on stage-specific signaling through the B-cell antigen receptor (BCR). Signaling and intracellular trafficking of the BCR are connected, but the molecular mechanisms of this link are incompletely understood. Here, we investigated the role of the endosomal adaptor protein and member of the LAMTOR/Ragulator complex LAMTOR2 (p14) in B-cell development. Efficient conditional deletion of LAMTOR2 at the pre-B1 stage using *mb1*-Cre mice resulted in complete developmental arrest. Deletion of LAMTOR2 using *Cd19*-Cre mice permitted analysis of residual B cells at later developmental stages, revealing that LAMTOR2 was critical for the generation and activation of mature B lymphocytes. Loss of LAMTOR2 resulted in aberrant BCR signaling due to delayed receptor internalization and endosomal trafficking. In conclusion, we identify LAMTOR2 as critical regulator of BCR trafficking and signaling that is essential for early B-cell development in mice.

Keywords: B cells, B-cell antigen receptor, LAMTOR2, signal transduction, trafficking, p14

INTRODUCTION

Signals from the B cell antigen receptor (BCR) determine development and function of B cells. During development, a pre-BCR is first assembled by pairing immunoglobulin (Ig) heavy chains with surrogate light chains (VpreB and λ5). Thus, signaling through the pre-BCR indicates successful Ig heavy chain gene rearrangement and promotes transition from the pro-B/pre-B1 to the pre-B2 developmental stage (1–3). Phenotypically, these stages can be discriminated by expression of CD117 and CD25 on the surface of pro-B/pre-B1 and pre-B2 cells, respectively (4). Later during development BCR signaling serves to monitor cells for productive Ig light chain rearrangements and to remove autoreactive B cells in bone marrow and spleen (4). Finally, recognition of antigen by the BCR in combination with T cell help results in B cell activation and eventually differentiation into plasma cells, production of antibodies and memory formation. Signal transduction through the BCR comprises proximal events of tyrosine phosphorylation resulting in downstream activation of multiple signaling cascades including PLCγ/Ca^{2+}/NF-κB/NFAT, Rho family, PI3-K/Akt as well as the Ras/Raf-1/Erk pathway (5). Receptor internalization constitutes

another consequence of BCR engagement (6). However, the interdependence between signaling and internalization of the receptor remains to be fully characterized. On the one hand, it has been reported that both processes are mutually exclusive (7). On the other hand, it has been proposed that internalization of the BCR via the endosomal route is required for proper spatial organization of signal transduction (8). Thus, inhibition of BCR endocytosis resulted in dysregulation of kinase activation.

LAMTOR2 (p14) has been described as an endosomal adaptor protein and forms a part of the late endosomal/lysosomal adaptor and MAPK and mTOR activator (LAMTOR)/Ragulator complex at late endosomes (9). LAMTOR2 contributes to spatial organization of the endosomal compartment and regulates proliferation. As a consequence, constitutive deletion of LAMTOR2 in mice results in embryonic lethality (10). Together with its partner MP-1, LAMTOR2 provides a scaffold for recruitment of the MAP kinase Erk to endosomes (11). Spatial compartmentalization of Erk has been suggested to provide context-dependent specificity for this signaling pathway (12). Deletion of LAMTOR2 results in complete abrogation of the LAMTOR/Ragulator complex (10, 13). The function of the LAMTOR/Ragulator complex in B cells has not been explored.

Of note, humans carrying a homozygous mutation in the $3'$ untranslated region of the gene encoding LAMTOR2, resulting in massively reduced expression of protein, display partial albinism, short stature as well as complex hematologic, and immunologic defects, including congenital neutropenia, defects in cytotoxic T lymphocytes, and defects in B-cell development and function (14).

Given the emerging role of spatial compartmentalization of signaling downstream of the BCR and the yet mechanistically uncharacterized B-lineage defect in humans carrying a mutation in LAMTOR2, we hypothesized that the LAMTOR/Ragulator complex might affect B-cell development and function. To test this hypothesis, we employed B-lineage specific deletion of the gene encoding LAMTOR2 gene in mice to study the function of the LAMTOR/Ragulator complex in B cells. Loss of LAMTOR2 in the B lineage resulted in a profound block at the pre-BI to pre-B2 developmental transition due to a defect in pre-BCR signaling. Furthermore, LAMTOR2-deficient B cells displayed aberrant kinase activation as well as dysregulated trafficking of the BCR upon stimulation. We conclude that aberrant BCR signaling due to a defect in BCR internalization in the absence of LAMTOR2 provides an explanation for the developmental defect observed in the B lineage.

RESULTS

LAMTOR2 Is Critical for B-cell Development

To assess the functional role of LAMTOR2 in B cells we crossed mice carrying floxed alleles of LAMTOR2 with two different Cre deleter strains. CD19-Cre mice are comparatively inefficient deleters in developing B cells but display continuous Cre expression throughout the B lineage starting at the pre-B1 stage (15, 16). In contrast, mb1-Cre mice delete floxed

alleles very efficiently also starting essentially at the pre-B1 stage (17). CD19-Cre-mediated deletion of LAMTOR2 (termed LAMTOR2$^{Cd19/Cd19}$ here) resulted in an ∼2-fold reduced frequency and absolute number of B lineage cells in bone marrow (BM) (**Figure 1A**). In spleen, frequencies and absolute numbers of B cells were further reduced in the absence of LAMTOR2 (**Figure 1B**). Mice carrying a loss of LAMTOR2 through mb-1-mediated deletion (termed LAMTOR2$^{mb-1/mb-1}$ here) lacked B lineage cells altogether, showing virtually identical numbers of B220 and CD19 positive cells as Rag2$^{-/-}$ mice, which display a complete block in immunoglobulin (Ig) gene rearrangement (**Figures 1A,B**). The observed difference between the two Cre deleter strains was not caused by heterozygous modification of the mb-1 locus (encoding the BCR signaling component CD79a), as mb1-Cre-positive mice heterozygous for the floxed LAMTOR2 allele had essentially normal numbers of B cells in BM and spleen (**Figures 1A,B**).

LAMTOR2 Is Required for the Pre-B1-to-Pre-B2 Developmental Transition

The transition between pre-B1 and pre-B2 cells depends on productive Ig heavy chain rearrangement and is characterized by loss of CD117 and induction of expression of CD25. LAMTOR2$^{mb-1/mb-1}$ mice completely lacked pre-B2 cells (showing similar levels as Rag2-deficient mice) but displayed normal numbers of pre-B1 cells (**Figure 2A** and **Figure S1A**). These data indicate that LAMTOR2 was strictly required for the developmental transition between pre-B1 and pre-B2 cells. As a consequence, all later stages of B-cell development were equally absent in LAMTOR2-deficient mice (**Figures 2B,C** and **Figures S1A,B**). In order to assess the effect of LAMTOR2 deletion on later stages of B cell development, we also analyzed LAMTOR2$^{Cd19/Cd19}$ mice, which displayed a partial block at the pre-B1-to-pre-B2 transition, indicated by an increased proportion of pre-B1 cells at the expense of pre-B2 cells (**Figure 2A**). Accordingly, numbers of pre-B2 cells were lower in BM of LAMTOR2$^{Cd19/Cd19}$ mice (**Figure S1**). Frequencies and absolute numbers of immature, transitional, and mature B cells were reduced in these mice at a similar degree as pre-B2 cells when compared to wild-type (WT) controls (**Figure 2B** and **Figure S1**). In addition, we noted a small shift toward the T1 subset, when directly comparing T1 and T2 transitional B cells (**Figure S1C**). Whereas, in spleen numbers of follicular B (Fo B) cells were severely affected by deletion of LAMTOR2, numbers of marginal zone B (MZ B) cells were barely reduced, resulting in increased relative proportions of these cells MZ B cells (**Figure 2C** and **Figure S1**). In order to test whether the partial block in B cell development observed in LAMTOR2$^{Cd19/Cd19}$ mice could be directly attributed to inefficient deletion, residual expression of LAMTOR2 mRNA was assessed using qRT-PCR. Indeed, LAMTOR2 transcripts were detected in all B cell subsets analyzed, indicating a range of deletion efficiency between ∼50% in Fo B cells to more than 80% in pre-B2, immature and MZ B cells (**Figure S2**). These data suggest that different degrees of counter-selection against deletion of LAMTOR2 are in place and that Fo B cells are particularly dependent on LAMTOR2.
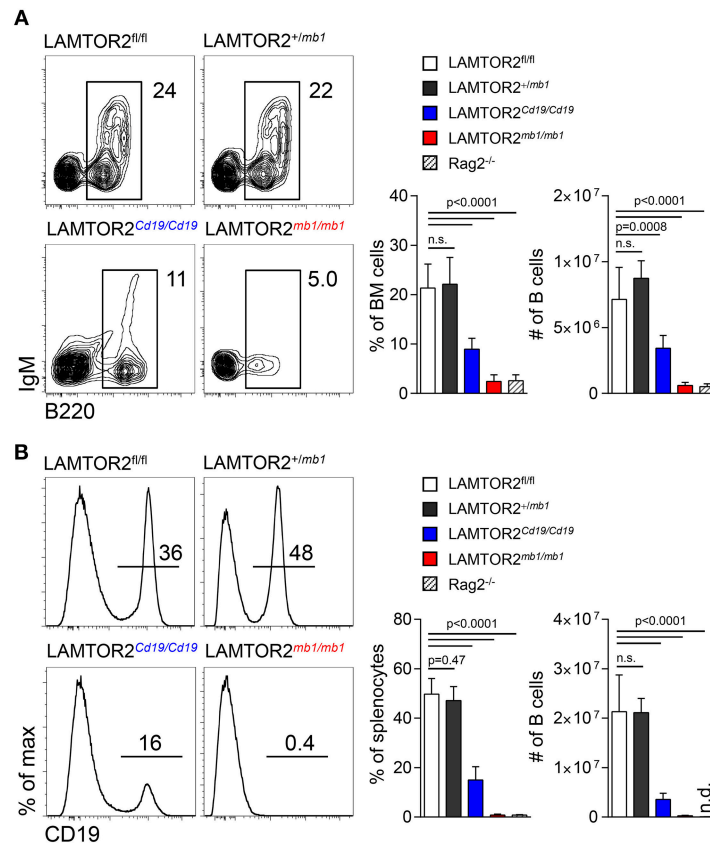
FIGURE 1 | LAMTOR2 is critical for B-cell development. **(A)** FACS analysis of B cells in bone marrow of LAMTOR2$^{fl/fl}$, LAMTOR2$^{+/mb1}$, LAMTOR2$^{Cd19/Cd19}$, and LAMTOR2$^{mb1/mb1}$ mice. Representative plots of multiple experiments (left panel) are depicted. Percentage within all BM cells and total number of pooled two independent experiments (right panel) are shown (mean + SD, $n = 6$–13, Rag2$^{-/-}$ $n = 3$). **(B)** Analogous to A, flow cytometric analysis of B cells in spleen of LAMTOR2-deficient mice. Representative histograms of multiple experiments are shown (left). Frequency of B cells within all splenocytes and total number of B cells from two independent experiments (right panel, mean + SD, sample numbers: $n = 6$–13, Rag2$^{-/-}$ $n = 3$). Statistical analysis was performed using unpaired t-test.
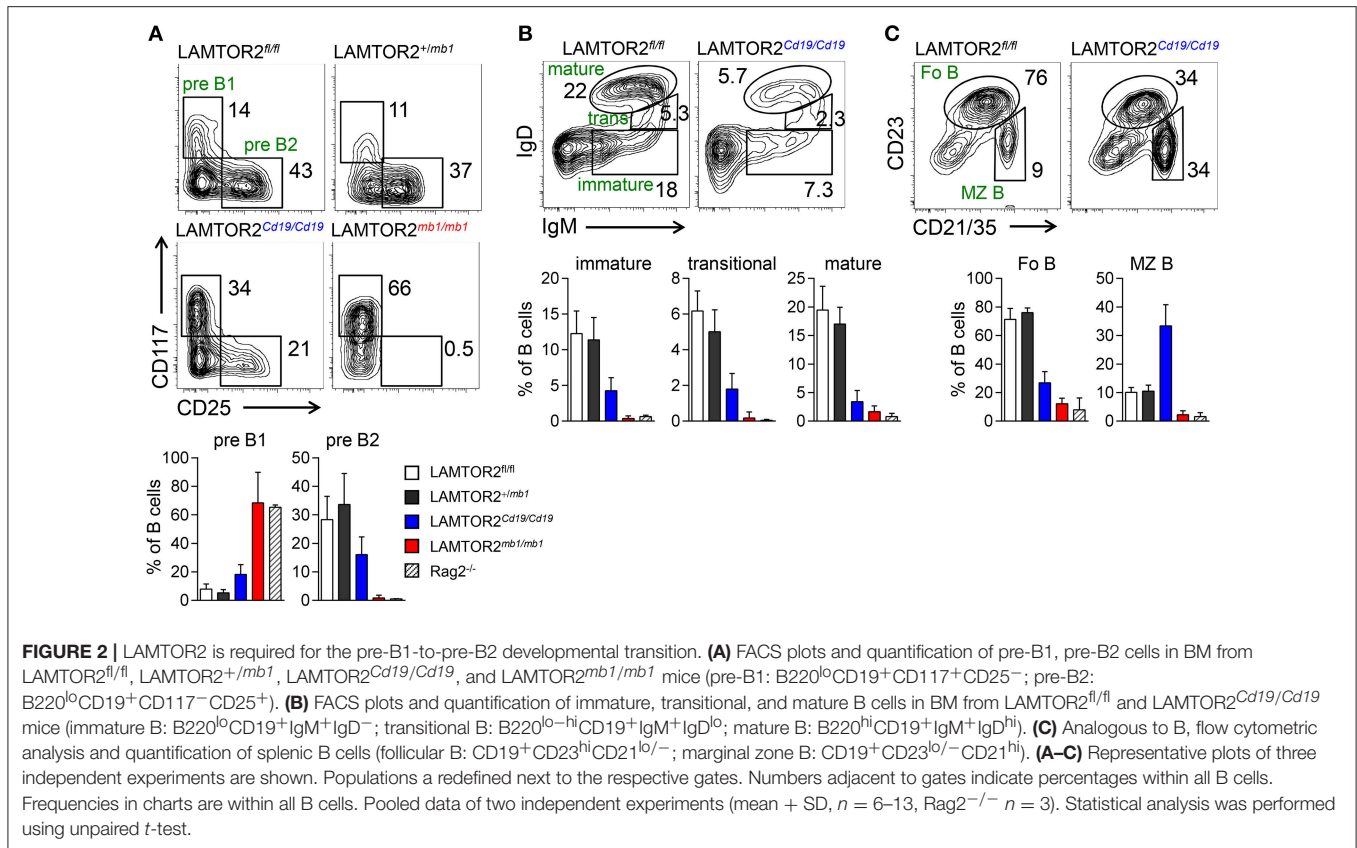
LAMTOR2 Regulates Pre-BCR-Dependent Events

In order to address the molecular mechanism, by which LAMTOR2 regulates B cell development we employed methylcellulose cultures of pre-B1 cells in the presence of IL-7. After 9 days of culture, colonies were assessed for expression of IgM (**Figure 3A**). In this assay expansion of colonies is dependent on IL-7 and differentiation into IgM$^+$ cells depends on signaling through the pre-BCR, thus allowing us to discriminate between the two central signaling pathways that are critical for developmental progression at this stage. Whereas, in control cultures on average 20% of cells had retained expression of CD117, in cultures from LAMTOR2$^{Cd19/Cd19}$ cells, 40% had retained a pre-B1 phenotype. In turn, control colonies contained on average 8% IgM$^+$ cells, whereas LAMTOR2-deficient colonies had generated on average 2% IgM$^+$ cells (**Figure 3B**). Interestingly, the number of cells per colony was not altered in the absence of LAMTOR2 (**Figure 3B**). In line, expression of IL-7Rα was not affected by loss of LAMTOR2 (**Figure 3C**). Next, we tested whether LAMTOR2 contributed to *Ig* gene rearrangement. PCR-based analysis revealed no major

differences between distal VDJ$_H$ rearrangements in control and LAMTOR2$^{mb-1/mb-1}$ pre-B1 cells (**Figure 3D**). Expression of the pre-BCR surrogate light chains, λ5, and VpreB1, was also comparable between LAMTOR2-sufficient and LAMTOR2-deficient pre-B1 cells (**Figure 3E**). Taken together, these data indicate that LAMTOR2 was not required for IL-7 signaling or expression of the pre-BCR. Therefore, by excluding these mechanisms it is most likely that LAMTOR2 controls pre-BCR signaling and that these effects at least partially account for the developmental block in the absence of LAMTOR2.

LAMTOR2 Orchestrates BCR Downstream Signaling Pathways

In order to test whether LAMTOR2 modulated signaling through the BCR we took advantage of the partial B-lineage developmental block in LAMTOR2$^{Cd19/Cd19}$ mice. First, we analyzed phosphorylation of Erk (pErk), Syk (pSyk), and tyrosines in general (pY) after BCR triggering in both Fo B and MZ B cells. Unexpectedly, in the absence of LAMTOR2 we observed higher levels of pSyk (**Figure 4A**), pErk (**Figure 4B**), and pY (**Figure 4C**) after BCR triggering of both Fo B

FIGURE 2 | LAMTOR2 is required for the pre-B1-to-pre-B2 developmental transition. **(A)** FACS plots and quantification of pre-B1, pre-B2 cells in BM from LAMTOR2$^{fl/fl}$, LAMTOR2$^{+/mb1}$, LAMTOR2$^{Cd19/Cd19}$, and LAMTOR2$^{mb1/mb1}$ mice (pre-B1: B220^{lo}CD19$^+$CD117$^+$CD25$^-$; pre-B2: B220^{lo}CD19$^+$CD117$^-$CD25$^+$). **(B)** FACS plots and quantification of immature, transitional, and mature B cells in BM from LAMTOR2$^{fl/fl}$ and LAMTOR2$^{Cd19/Cd19}$ mice (immature B: B220^{lo}CD19$^+$IgM$^+$IgD$^-$; transitional B: B220^{lo-hi}CD19$^+$IgM$^+$IgD^{lo}; mature B: B220^{hi}CD19$^+$IgM$^+$IgD^{hi}). **(C)** Analogous to B, flow cytometric analysis and quantification of splenic B cells (follicular B: CD19$^+$CD23^{hi}CD21$^{lo/-}$; marginal zone: CD19$^+$CD23$^{lo/-}$CD21^{hi}). **(A–C)** Representative plots of three independent experiments are shown. Populations a redefined next to the respective gates. Numbers adjacent to gates indicate percentages within all B cells. Frequencies in charts are within all B cells. Pooled data of two independent experiments (mean + SD, $n = 6$–13, Rag2$^{-/-}$ $n = 3$). Statistical analysis was performed using unpaired t-test.

and MZ B cells when compared to controls. Co-treatment with H$_2$O$_2$, to inhibit phospho-tyrosine phosphatase activity, showed similar results, indicating that LAMTOR2 directly curtails certain phosphorylation events rather than promoting dephosphorylation (**Figure S3**). Next, we analyzed Ca^{2+}-flux after BCR triggering in both B cell populations. In contrast to the increase in phosphorylation, levels of Ca^{2+}-flux were reduced after BCR triggering in LAMTOR2-deficient Fo B and MZ B cells when compared to controls (**Figures 4D,E**). Note, that these effects are based on mixed populations, in which not all cells, in particular within the Fo B cell population, have lost expression of LAMTOR2. Therefore, the effects of deletion of LAMTOR2 are most likely more pronounced than indicated here. In summary, these data indicate that loss of LAMTOR2 results in a disbalance of BCR-triggered signaling pathways rather than overall weakening or strengthening of the BCR signal. As the pre-BCR shares many features of the signaling machinery with the BCR, these findings also further support the notion that the early developmental block in the absence of LAMTOR2 is, in part, due to aberrant pre-BCR signaling.
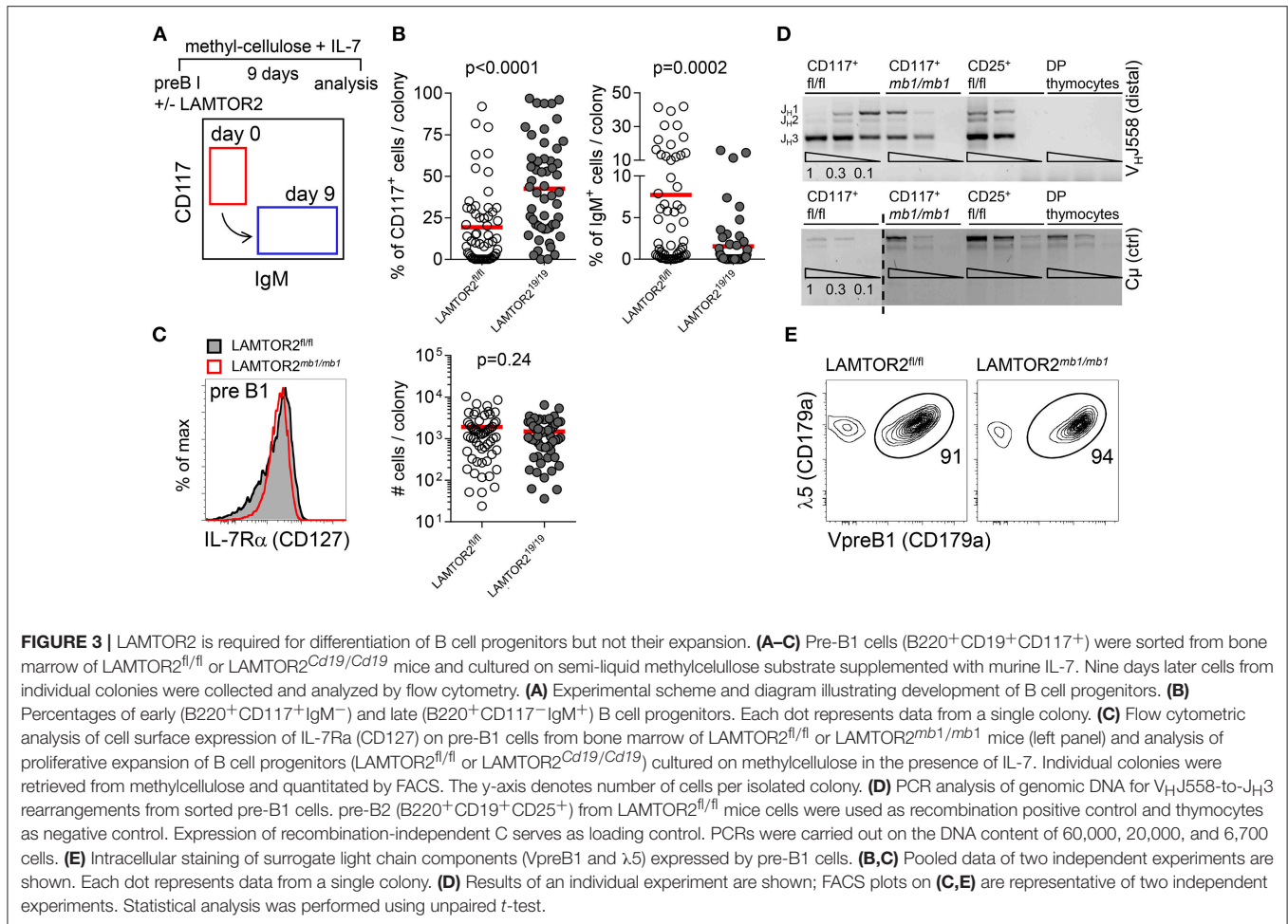
Loss of LAMTOR2 in Peripheral B Cells Results in Impaired BCR-Mediated Expansion

Next, we tested functional consequences of disbalanced BCR signaling upon loss of LAMTOR2. *In vitro* expansion was analyzed 3 days after triggering with increasing concentrations of anti-IgM antibodies. LAMTOR2-deficient B cells expanded less when compared to controls at every indicated concentration of stimulus (**Figure 5A**). The defect in BCR-dependent expansion could not be compensated by increasing levels of anti-CD40-mediated co-stimulation (**Figure 5B**). Accordingly, expansion induced by CpG or by CD40 triggering alone were unaffected by loss of LAMTOR2 in B cells (**Figures 5C,D**). Furthermore, LAMTOR2-deficiency did not impair CD40-mediated Ig class-switch (**Figure 5E**). Thus, we conclude that a disbalance in BCR downstream signaling results in impaired BCR-mediated expansion, which could not be rescued by triggering of additional proliferative signals.

LAMTOR2 Regulates Internalization and Intracellular Trafficking of the BCR

Given the role of LAMTOR2 as endosomal adapter protein, we hypothesized that disbalanced BCR signaling in the absence of LAMTOR2 might be due to alterations in BCR trafficking after stimulation. To test the hypothesis we first analyzed stimulation-dependent internalization of the BCR *in vitro*. To this end, surface BCR was labeled with anti-IgM antibodies in the cold. To assess passive internalization of the BCR cells were labeled with monovalent anti-IgM fragments in the cold and cultured at 37°C without additional stimulation. Both MZ B (**Figure 6A** and **Figure S4A**) and Fo B cells (**Figure 6B** and **Figure S4A**) from LAMTOR2$^{Cd19/Cd19}$ mice retained more BCR

FIGURE 3 | LAMTOR2 is required for differentiation of B cell progenitors but not their expansion. **(A–C)** Pre-B1 cells (B220$^+$CD19$^+$CD117$^+$) were sorted from bone marrow of LAMTOR2$^{fl/fl}$ or LAMTOR2$^{Cd19/Cd19}$ mice and cultured on semi-liquid methylcellulose substrate supplemented with murine IL-7. Nine days later cells from individual colonies were collected and analyzed by flow cytometry. **(A)** Experimental scheme and diagram illustrating development of B cell progenitors. **(B)** Percentages of early (B220$^+$CD117$^+$IgM$^-$) and late (B220$^+$CD117$^-$IgM$^+$) B cell progenitors. Each dot represents data from a single colony. **(C)** Flow cytometric analysis of cell surface expression of IL-7Ra (CD127) on pre-B1 cells from bone marrow of LAMTOR2$^{fl/fl}$ or LAMTOR2$^{mb1/mb1}$ mice (left panel) and analysis of proliferative expansion of B cell progenitors (LAMTOR2$^{fl/fl}$ or LAMTOR2$^{Cd19/Cd19}$) cultured on methylcellulose in the presence of IL-7. Individual colonies were retrieved from methylcellulose and quantitated by FACS. The y-axis denotes number of cells per isolated colony. **(D)** PCR analysis of genomic DNA for V$_H$J558-to-J$_H$3 rearrangements from sorted pre-B1 cells. pre-B2 (B220$^+$CD19$^+$CD25$^+$) from LAMTOR2$^{fl/fl}$ mice cells were used as recombination positive control and thymocytes as negative control. Expression of recombination-independent C serves as loading control. PCRs were carried out on the DNA content of 60,000, 20,000, and 6,700 cells. **(E)** Intracellular staining of surrogate light chain components (VpreB1 and λ5) expressed by pre-B1 cells. **(B,C)** Pooled data of two independent experiments are shown. Each dot represents data from a single colony. **(D)** Results of an individual experiment are shown; FACS plots on **(C,E)** are representative of two independent experiments. Statistical analysis was performed using unpaired t-test.

on their surface over a period of 120 min when compared to WT controls. Stimulation-dependent BCR internalization was assessed in a similar assay replacing monovalent by bivalent anti-IgM fragment in order to induce BCR crosslinking. Similarly, MZ B (**Figure 6C** and **Figure S4B**) and Fo B cells (**Figure 6D** and **Figure S4B**) from LAMTOR2$^{Cd19/Cd19}$ showed delayed internalization of the BCR when compared to WT controls.

Next, we employed transmission electron microscopy to assess intracellular trafficking of the BCR upon stimulation using immunogold labeling. Consistent with our finding that passive internalization was impaired in the absence of LAMTOR2 (**Figures 6A,B**), BCRs were detected in multiple subcellular compartments prior to stimulation in controls, whereas in B cells from LAMTOR2$^{Cd19/Cd19}$ mice BCRs were predominantly detected on the cell surface (**Figures 6E,F**). Within 5 min of stimulation significantly more BCRs were detectable in early endosomes from LAMTOR2$^{Cd19/Cd19}$ B cells when compared to controls, followed by accumulation in autophagosomes at 20 and 45 min after stimulation. Of note, such autophagosomes were almost absent from wild-type B cells and the frequency of B cells with a high abundance of autophagosomes in samples from LAMTOR2$^{Cd19/Cd19}$ mice correlated well with the penetrance of LAMTOR2 deletion as detected by qRT-PCR. Given that in the absence of LAMTOR2, BCR trafficking was already altered at steady state, these data suggest that loss of LAMTOR2 perturbed intracellular localization of the BCR, which, in turn, resulted in aberrant BCR signaling.

DISCUSSION

Here we demonstrated that the endosomal adaptor protein LAMTOR2 is essential for B cell development at the pre-BCR checkpoint. Loss of LAMTOR2 resulted in aberrant BCR signaling, a defect in BCR internalization and aberrant intracellular trafficking. These data highlight the critical importance of spatial organization of signaling modules in biological processes.
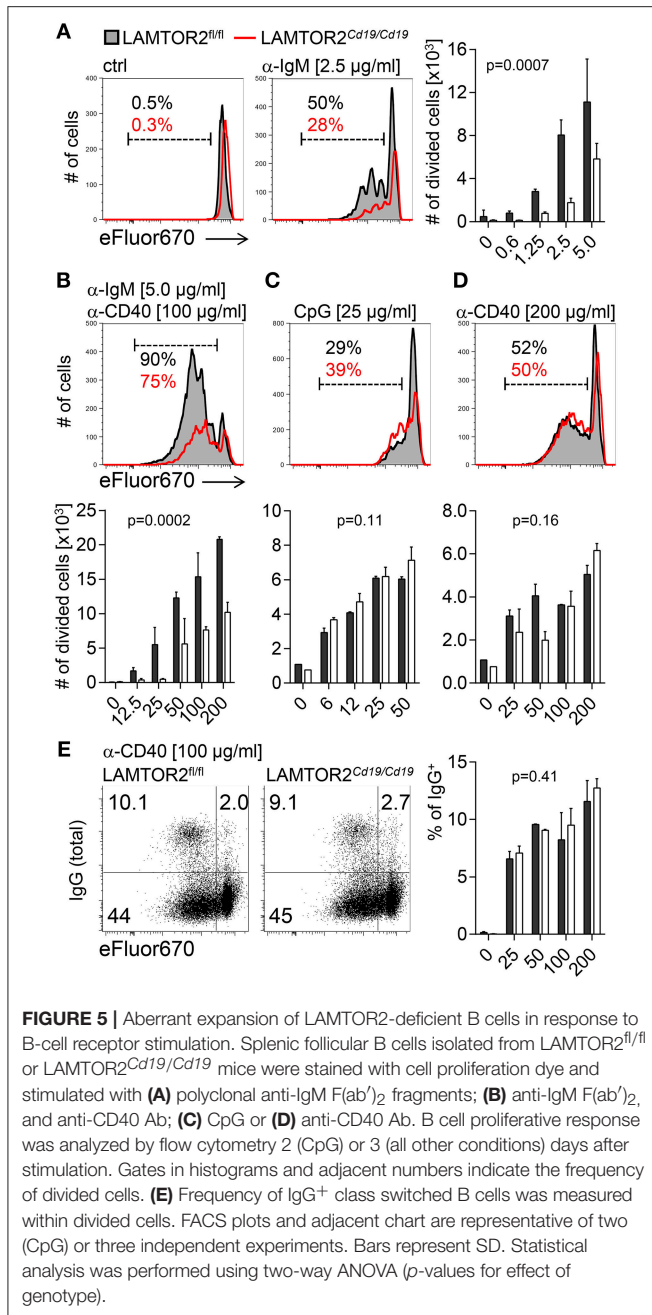
It has been previously described in multiple studies that inhibition of BCR internalization by various means results in aberrant signaling. Blocking of endocytosis resulted in increased tyrosine phosphorylation as well as increased and sustained activation of MAP kinase pathways (8, 18). In contrast, activation of the PI3-K/Akt pathway was inhibited (8). Mutation of the ITAMs in Igβ also leads to dysregulation of BCR internalization, although in this case steady-state turnover is more strongly affected than signal-induced endocytosis (19). However, despite

FIGURE 4 | Aberrant BCR-associated signaling in LAMTOR2-deficient B cells. Flow cytometric analysis of **(A)** pZap70 (pY319)/pSyk (pY352) **(B)** pERK1/2 (pT202/pY352), and **(C)** total pY in splenic B cells isolated from LAMTOR2$^{fl/fl}$ or LAMTOR2$^{Cd19/Cd19}$ mice. Starved splenocytes were left untreated (ctrl) or stimulated with anti-IgM F(ab')$_2$ for 2, 5, and 15 min. Representative histograms of three independent experiments are shown, graphs show summarized data of two independent experiments, $n = 6$ for each genotype, whiskers indicate min. to max. range of data, horizontal bars show mean value. Median fluorescence values (MFI) were normalized to ctrl (set as 100%). Statistical analysis was performed using two-way ANOVA (p-values for effect of genotype). **(D)** Total splenocytes were stimulated with anti-IgM F(ab')$_2$ and Ca^{2+}-flux was recorded flow cytometrically over time. Plots for electronically gated Fo B cells and MZ B cells are representative for 6 (ctrl) or 7 (ko) mice from two individual experiments. "anti-IgM" indicates time point of stimulation. **(E)** Bar graph shows analysis of peak Ca^{2+} flux over background from two independent experiments, each dot represents one mouse. Statistical analysis was performed using unpaired t-test.

elevated Ca^{2+} responses, sustained Erk activation and overall tyrosine hyperphosphorylation upon mutation of Igβ ITAMs, hypophosphorylation of Syk and increased activation of the PI3-K pathway were observed. Loss of LAMTOR2 analyzed here resulted in general hyperphosphorylation of Syk, Erk, and overall tyrosines but a limited Ca^{2+} response. Together, these studies imply that BCR signaling is tightly regulated through receptor internalization and compartmentalization of signaling. Opposing outcomes in different signaling modules dependent on variations in experimental setup highlight the intricate balance maintained by compartmentalization of signaling. The dual function of LAMTOR2 as mediator of endosomal trafficking as well as retention factor for the Erk module at late endosomes at present precludes a definitive conclusion as to whether spatial dislocation of Erk or aberrant BCR trafficking or both are key for aberrant signaling in the absence of LAMTOR2. Differences in passive BCR internalization in the absence of LAMTOR2 may suggest that aberrant BCR trafficking determines signaling outcomes. In addition, it has also been reported that conditional ablation results in defective homeostasis of dendritic cells due to accumulation of Flt3 on the cell surface followed by downstream

activation of Akt/mTOR signaling (20). This study indicated that aberrant endocytosis can directly result in uncoupling of signaling cascades. Alterations in endosomal trafficking in the absence of LAMTOR2 can be ascribed to destabilization of the complete LAMTOR/Ragulator complex. This complex has been reported to integrate mTOR signals which might control the composition of intracellular compartments based on metabolic needs (21). In addition, it has recently been reported that the LAMTOR/Ragulator complex is critically involved in late endosomal positioning (22). Furthermore, our observation is also consistent with a previous study directly analyzing the consequences of inhibition of endocytosis on BCR signaling (8). However, we cannot exclude that differences in tonic signaling prior to B cell isolation contribute to alterations in passive BCR internalization.

Despite the defect in BCR internalization, mutation of the ITAMs in Igβ did not result in major developmental defects (19). In contrast, we observed a complete developmental block at the pre-BCR checkpoint suggesting that the pre-BCR is particularly sensitive to aberrant compartmentalization of signaling modules. This hypothesis is consistent with the observation that only a low

FIGURE 5 | Aberrant expansion of LAMTOR2-deficient B cells in response to B-cell receptor stimulation. Splenic follicular B cells isolated from LAMTOR2$^{fl/fl}$ or LAMTOR2$^{Cd19/Cd19}$ mice were stained with cell proliferation dye and stimulated with **(A)** polyclonal anti-IgM F(ab')$_2$ fragments; **(B)** anti-IgM F(ab')$_2$, and anti-CD40 Ab; **(C)** CpG or **(D)** anti-CD40 Ab. B cell proliferative response was analyzed by flow cytometry 2 (CpG) or 3 (all other conditions) days after stimulation. Gates in histograms and adjacent numbers indicate the frequency of divided cells. **(E)** Frequency of IgG$^+$ class switched B cells was measured within divided cells. FACS plots and adjacent chart are representative of two (CpG) or three independent experiments. Bars represent SD. Statistical analysis was performed using two-way ANOVA (p-values for effect of genotype).

percentage of pre-BCR is located at the cell surface at any given time and that turnover of the pre-BCR is very high with rates of internalization of 40% within 5 min (23). However, because of low levels of surface expression, alterations of pre-BCR turnover remain difficult to quantitate in primary cells. Compared to the virtually complete block in B-cell development upon deletion of LAMTOR2, defects in BCR signaling and internalization were comparatively mild. We cannot exclude that additional signaling pathways active at the pre-BCR checkpoint were also affected by disruption of the LAMTOR complex. Signaling through the IL-7R is the second major pathway at the pre-BCR checkpoint.

However, neither clonal analysis *in vitro* nor surface expression of IL-7R suggest that this pathway was critically affected by loss of LAMTOR2. In peripheral B cells, loss of LAMTOR2 limited anti-IgM-mediated, but not anti-CD40-mediated proliferation, further indicating that BCR, and pre-BCR are the major pathways controlled by the LAMTOR complex in the B lineage. Of note, most functional experiments were performed in B cells from mice with Cd19-Cre-mediated deletion of LAMTOR2. In these mice the B-lineage developmental defect was considerably milder than in mice with mb-1-Cre-mediated deletion of LAMTOR2. This difference was due to inefficient deletion, with substantial counter-selection becoming apparent in Fo B cells.

In the periphery, Fo B cells were more strongly affected by loss of LAMTOR2 than MZ B cells. Using a Nur77-GFP reporter to monitor BCR signal strength, it was shown that MZ B cells respond differently than Fo B cells to tonic signals modulated by an allelic series of CD45 expression (24). Although it remains an open question how the complex alterations in BCR downstream signaling upon loss of LAMTOR2 translate into tuning of BCR signal strength, these differences may explain why MZ B cells were less affected by LAMTOR2-deficiency than Fo B cells.

In human patients with homozygous mutations in LAMTOR2, no complete block in B cell development but rather a defect in class-switched B cells associated with hypogammaglobulinemia was observed (14). In contrast to the knockout mice, the human mutation affected the 3′-UTR and allowed for residual protein expression (14). Nevertheless, defects in Ig class-switch recombination as well as B-cell memory formation support the idea that p14 expression controls BCR signaling in patients as well.

Thus, LAMTOR2/p14 is essential in controlling BCR trafficking and highlights a non-redundant role for the LAMTOR-complex in securing physiological differentiation of B cells.

MATERIALS AND METHODS

Mice

Flow Cytometry

Flow cytometry and cell sorting were performed on LSRII and FACSAriaIIu (BD) cytometers, respectively. Monoclonal antibodies specific for IgD (clone 11-26c), IgM (II/41), CD23 (B3B4), CD21/35 (7E9), CD179a (R3), CD179b, p-Zap70/p-Syk (p-Y319/p-Y352; 17A/P-ZAP70), p-ERK1/2 (pT202/pY204; 20A), p-Tyr (pY20), CD25 (PC61), Gr-1 (RB6-8C5), erythroid cell marker (Ter-119), CD19 (1D3), CD11b (M1/70), NK1.1 (PK136), B220 (RA3-6B2), CD117 (ACK2) were used purified
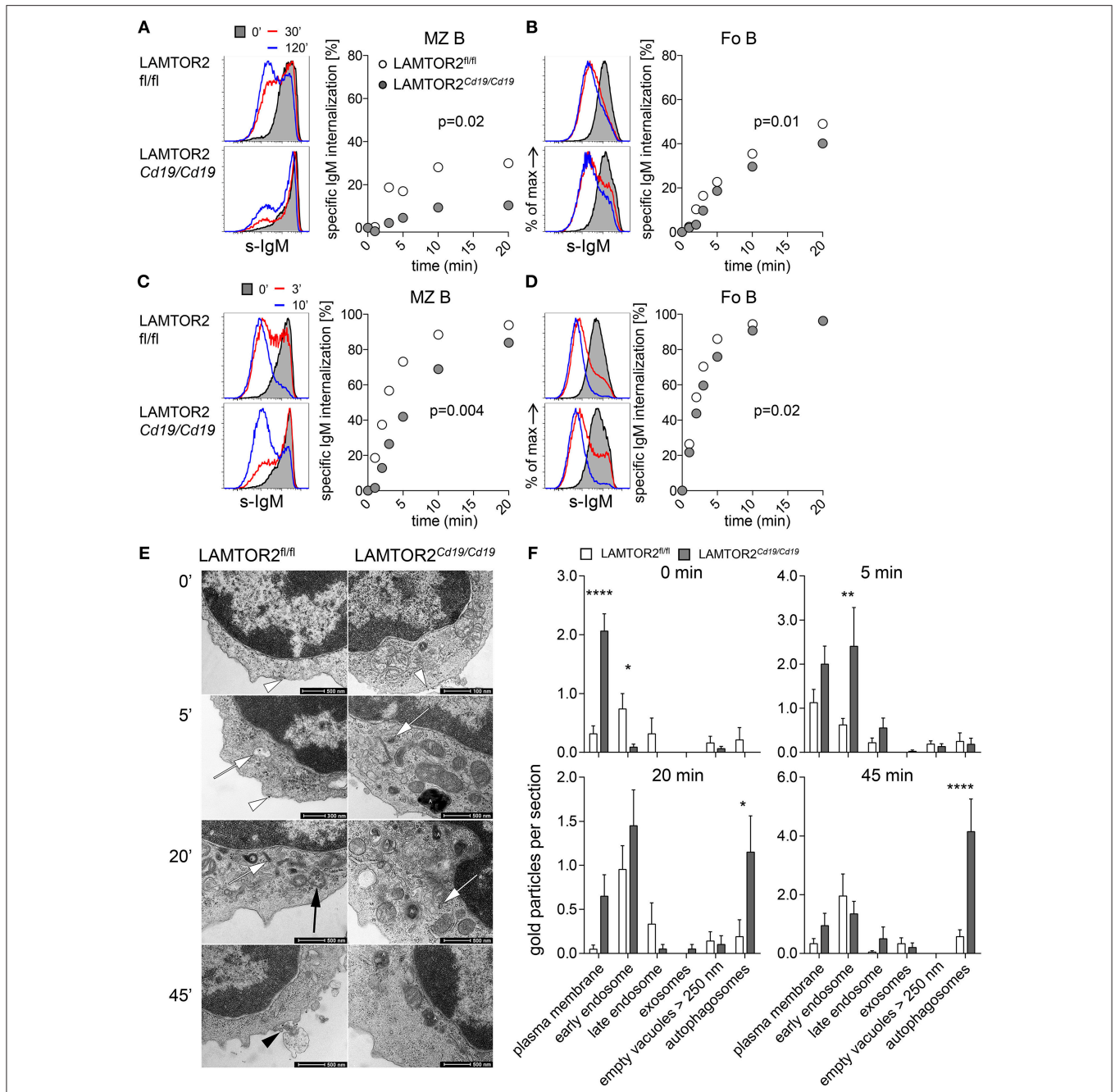
FIGURE 6 | Altered internalization and degradation of BCR in LAMTOR2-deficient B cells. FACS analysis of BCR internalization in splenic B cells. Passive BCR internalization in **(A)** MZ B, **(B)** Fo B cells or ligand-induced BCR internalization in **(C)** MZ B or **(D)** Fo B cells. Purified splenic B cells were labeled in an ice-cold environment with either monovalent **(A,B)** or bivalent **(C,D)** biotin-labeled anti-IgM Fab or F(ab')$_2$ fragments, respectively, and then BCR internalization was assessed over time at $37°$C. Plots for electronically gated cells are representative for two independent experiments. Charts summarize the first 20 min of one representative experiment out of two. **(E)** Transmission electron microscopy (TEM) analysis of ligand-induced BCR internalization and degradation in B cells of LAMTOR2$^{fl/fl}$ or LAMTOR2$^{Cd19/Cd19}$ mice. Purified B cells were stimulated with colloidal-gold labeled anti-IgM F(ab')$_2$ and analyzed at indicated time points. White arrowheads demonstrate gold particles at the cell membrane, white arrows mark early endosomes with gold-marked IgM receptors, the black arrow shows the late endosome with gold at the internal vesicles, the black arrowhead marks exosomes with attached gold particles. Autophagosomes are labeled with an "A." **(F)** Quantification of TEM data. The quantitative evaluation has been done only at cells cut through the cell center to get access directly to all cell organelles. Nineteen to thirty-eight sections per time point and genotype were analyzed. Statistical significance was assessed with 2-way ANOVA (effect for genotype is shown) and Sidak's multiple comparison test (*$p < 0.05$; **$p < 0.01$; ****$p < 0.001$).

or as various fluorescent or biotin conjugates. Antibodies were purified from hybridoma supernatants or were purchased from eBioscience, BD Biosciences, BioLegend, or Miltenyi Biotech. Flow cytometry data were analyzed in FlowJo (9.3, TreeStar).

Bone marrow B cell stages were defined as follows: pre-BI (B220$^+$CD19$^+$CD117$^+$CD25$^-$), pre-B2 (B220$^+$CD19$^+$CD25$^+$CD117$^-$), immature B (CD19$^+$IgM^{lo}IgD$^-$), transitional (CD19$^+$IgM^{hi}IgD$^{+/-}$), mature (CD19$^+$IgM$^{int/-}$IgD$^+$). Splenic B cell stages were defined as: Fo B cells (CD19$^+$CD23$^+$CD21/35$^-$), and MZ B cells (CD19$^+$CD23$^-$CD21/35$^+$).

Ex vivo Stimulation of B Cells

Single-cell suspension of splenocytes from LAMTOR2$^{fl/fl}$ and LAMTOR2$^{Cd19/Cd19}$ mice were incubated for 30–45 min in FCS free RPMI at room temperature (RT) at 10^7/mL. Next, splenocytes were incubated with or without stimulation as indicated in the figure legends. Cells were stimulated with anti-IgM F(ab')$_2$ at 10 μg/mL. Reactions were stopped by adding cell suspensions to formaldehyde at 1.5% final concentration. After 15 min of incubation at RT fixed cells were washed and permeabilized with ice-cold methanol for 30 min. Cells were then washed twice to remove residual methanol and stained for B220, CD23, and IgM as well as with phospho-specific antibodies for 30′ at RT. The protocol was adapted from (25).

Purification of B-Cell Progenitors

Lin$^-$ cells were isolated from total BM by staining cell suspensions with a lineage-specific antibody cocktail including TCRβ, IgM, CD11b, CD11c, Gr-1, Ter-119, and NK1.1 (all e-Biosciences or BioLegend) followed by incubation with sheep anti-rat IgG conjugated to magnetic beads (Dynal, Invitrogen) and immunomagnetic depletion of mature lineages. Pre-purified cells were subjected to FACS sorting.

Measurement of Intracellular Ca2$^+$ Flux in Splenic B Cells

Single-cell suspensions of splenocytes from LAMTOR2$^{fl/fl}$ and LAMTOR2$^{Cd19/Cd19}$ mice were incubated for 1 h in Ca^{2+} and Mg^{2+}-free Dulbecco's serum-free medium (Invitrogen) at room temperature at 10^7 cells/mL. Splenocytes were then loaded with Fluo-4 (3 μM) and FuraRed (6 μM) for 45 min at 37$^°$C. Further, cells were washed and stained for CD21 and CD23/35 for 15 min at 4$^°$C. Subsequently, cells were rested for 30 min at 37$^°$C. After establishing of a baseline for 30 s, B cells were stimulated with anti-IgM F(ab')$_2$, and data acquisition was continued for 4 additional minutes. To ensure cell viability, 30 s before the end of acquisition 2 μg/mL ionomycin (Sigma) was added as positive Ca^{2+}-flux control.

B Cell Proliferation Assay

Primary splenic B cells from LAMTOR2$^{fl/fl}$ and LAMTOR2$^{Cd19/Cd19}$ mice were sorted and cultured at 37°C, 5% CO$_2$. B cells were kept in complete alpha-MEM supplemented with 10% FCS and IL-4 (10 ng/ml) and stimulated with cross-linking 20 μg/mL F(ab')2 fragment goat anti-mouse IgM (Jackson Immuno Research), and/or anti-CD40 (clone FGK4T)

or fully thiolated CpG 2006 type B (24 mer 5′-TCGTCGTTT TGTCGTTTTGTCGTT-3′, TIB MOLBIO). Proliferation was assessed by staining of cells with Cell Proliferation Dye eFluor 670 according to manufacturer's instructions (eBioscience).

Methylcellulose Assay

Clonal expansion of pre-B1 cells was assessed in methylcellulose containing IL-7 (MethoCult M3630, Stemcell Technologies) according to the manufacturer's instructions with a starting cell number of 5,000–20,000 sorted cells. Cellularity and cell differentiation was assessed by picking single colonies and flow cytometric cell counting and analysis after 9 days. Cells expressing CD117 were considered as non-differentiated early progenitors, IgM positive cells were taken as differentiated cells.

BCR Internalization

BCR internalization was assessed on purified splenic B cells. Passive internalization was assessed on MZ B or Fo B cells labeled in an ice cold environment with monovalent anti-IgM–biotin Fab fragments (Jackson Immuno Research). To assess active (ligand induced) internalization of BCR cells were labeled with anti-IgM F(ab')$_2$-biotin particles. After labeling cells were kept at 37$^°$C for the indicated time, followed by fixation and detection of remaining BCR molecules with streptavidin-APC (eBioscience).

Gene Expression and Rearrangement PCR

V$_H$J558 to DJ$_H$3 rearrangement was assessed on genomic DNA. The genes belonging to the V$_H$J558 family are located at the most 5′ end of the V$_H$ locus and belong to the most frequently used V$_H$ families (26–28).Genomic DNA was isolated using QIAamp micro kit (Qiagen) and the PCR was carried out on 60,000; 20,000; and 6,700 cells using 1 nM of primers as previously described (29, 30) in 1x PCR reaction buffer (B9004S, Thermopol) for 40 cycles (annealing 59°C).

Transmission Electron Microscopy Analysis

Isolated B cells pooled of LAMTOR2$^{fl/fl}$ and LAMTOR2$^{Cd19/Cd19}$ mice were incubated at 4°C firstly with biotin SP-conjugated affiniPure F(ab')$_2$-fragment goat anti-mouse IgM followed by staining with Streptavidin-20 nm gold conjugates. The reaction was stopped immediately (0 min) and after warming up at 37°C for 5 min, 20 min as well as 45 min by fixation in 2.5% glutaraldehyde in sodium cacodylate buffer and postfixation in 2% osmium tetroxide in the same buffer. After dehydration in graded ethanol pellets were embedded in Epon. Thin sections stained with 2% uranyl acetate and lead citrate were analyzed with the Tecnai G2 200 kV. Random sections of the cell center have been selected. Because of different penetrance of the CD19-cre KO cells only cells containing autophagosomes have been analyzed (resting B cells sufficient for LAMTOR2 contain a very low number of autophagosomes) in three independent experiments. Notably, frequencies of autophagosome-containing cells corresponded almost perfectly to the penetrance of

LAMTOR2 deletion assessed by qRT-PCR. The position of the gold particles at the plasma membrane, inside the early endosomes, late endosomes, at the exosomes attached at the plasma membrane, inside empty vacuoles with a diameter larger than 250 nm as well-autophagosomes was counted separated and listed as number per cell. To avoid bias during the analysis all sample labels were temporally removed and organelles containing gold particles were identified by a person not involved in the study.

Statistics

Statistical significance of differences between two groups was analyzed using paired or non-paired t-tests where applicable. For comparison of multiple groups statistical significance was determined using two-way ANOVA and p-values for effect of genotype are shown. ANOVA analysis was followed by Sidak's multiple comparison test to assess differences between groups. To avoid bias during TEM analysis samples were quantified in blind way by a person not involved in the study.

AUTHOR CONTRIBUTIONS

MŁ, DK, NZ, CK, and AK designed the research. MŁ, DK, NZ, GB, JD, and SG performed the research. MŁ, DK, NZ, GB, CK, and AK analyzed the data. EH, MR, and LH provided vital reagents. MŁ, NZ, and AK wrote the manuscript.

SUPPLEMENTARY MATERIAL

The Supplementary Material for this article can be found online at: https://www.frontiersin.org/articles/10.3389/fimmu.2019.00497/full#supplementary-material

REFERENCES

1. Melchers F. Checkpoints that control B cell development. *J Clin Invest.* (2015) 125:2203–10. doi: 10.1172/JCI78083
2. Reth M. Oligomeric antigen receptors: a new view on signaling for the selection of lymphocytes. *Trends Immunol.* (2001) 22:356–60. doi: 10.1016/S1471-4906(01)01964-0
3. Rickert RC. New insights into pre-BCR and BCR signalling with relevance to B cell malignancies. *Nat Rev Immunol.* (2013) 13:578–91. doi: 10.1038/nri3487
4. Osmond DG, Rolink A, Melchers F. Murine B lymphopoiesis: towards a unified model. *Immunol Today.* (1998) 19:65–8. doi: 10.1016/S0167-5699(97)01203-6
5. Campbell KS. Signal transduction from the B cell antigen-receptor. *Curr Opin Immunol.* (1999) 11:256–64. doi: 10.1016/S0952-7915(99)80042-9
6. Lanzavecchia A. Receptor-mediated antigen uptake and its effect on antigen presentation to class II-restricted T lymphocytes. *Annu Rev Immunol.* (1990) 8:773–93. doi: 10.1146/annurev.iy.08.040190.004013
7. Hou P, Araujo E, Zhao T, Zhang M, Massenburg D, Veselits M, et al. B cell antigen receptor signaling and internalization are mutually exclusive events. *PLoS Biol.* (2006) 4:e200. doi: 10.1371/journal.pbio.0040200
8. Chaturvedi A, Martz R, Dorward D, Waisberg M, Pierce SK. Endocytosed BCRs sequentially regulate MAPK and Akt signaling pathways from intracellular compartments. *Nat Immunol.* (2011) 12:1119–26. doi: 10.1038/ni.2116
9. Wunderlich W, Fialka I, Teis D, Alpi A, Pfeifer A, Parton RG, et al. A novel 14-kilodalton protein interacts with the mitogen-activated protein kinase scaffold mp1 on a late endosomal/lysosomal compartment. *J Cell Biol.* (2001) 152:765–76. doi: 10.1083/jcb.152.4.765
10. Teis D, Taub N, Kurzbauer R, Hilber D, de Araujo ME, Erlacher M, et al. p14-MP1-MEK1 signaling regulates endosomal traffic and cellular proliferation during tissue homeostasis. *J Cell Biol.* (2006) 175:861–8. doi: 10.1083/jcb.200607025
11. Teis D, Wunderlich W, Huber LA. Localization of the MP1-MAPK scaffold complex to endosomes is mediated by p14 and required for signal transduction. *Dev Cell.* (2002) 3:803–14. doi: 10.1016/S1534-5807(02)00364-7
12. Morrison DK, Davis RJ. Regulation of MAP kinase signaling modules by scaffold proteins in mammals. *Annu Rev Cell Dev Biol.* (2003) 19:91–118. doi: 10.1146/annurev.cellbio.19.111401.091942
13. de Araujo MEG, Naschberger A, Furnrohr BG, Stasyk T, Dunzendorfer-Matt T, Lechner S, et al. Crystal structure of the human lysosomal mTORC1 scaffold complex and its impact on signaling. *Science.* (2017) 358:377–81. doi: 10.1126/science.aao1583
14. Bohn G, Allroth A, Brandes G, Thiel J, Glocker E, Schaffer AA, et al. A novel human primary immunodeficiency syndrome caused by deficiency of the endosomal adaptor protein p14. *Nat Med.* (2007) 13:38–45. doi: 10.1038/nm1528
15. Rickert RC, Roes J, Rajewsky K. B lymphocyte-specific, Cre-mediated mutagenesis in mice. *Nucleic Acids Res.* (1997) 25:1317–8. doi: 10.1093/nar/25.6.1317
16. Schmidt-Supprian M, Rajewsky K. Vagaries of conditional gene targeting. *Nat Immunol.* (2007) 8:665–8. doi: 10.1038/ni0707-665
17. Hobeika E, Thiemann S, Storch B, Jumaa H, Nielsen PJ, Pelanda R, et al. Testing gene function early in the B cell lineage in mb1-cre mice. *Proc Natl Acad Sci USA.* (2006) 103:13789–94. doi: 10.1073/pnas.0605944103
18. Stoddart A, Jackson AP, Brodsky FM. Plasticity of B cell receptor internalization upon conditional depletion of clathrin. *Mol Biol Cell.* (2005) 16:2339–48. doi: 10.1091/mbc.e05-01-0025
19. Gazumyan A, Reichlin A, Nussenzweig MC. Ig beta tyrosine residues contribute to the control of B cell receptor signaling by regulating receptor internalization. *J Exp Med.* (2006) 203:1785–94. doi: 10.1084/jem.20060221
20. Scheffler JM, Sparber F, Tripp CH, Herrmann C, Humenberger A, Blitz J, et al. LAMTOR2 regulates dendritic cell homeostasis through FLT3-dependent mTOR signalling. *Nat Commun.* (2014) 5:5138. doi: 10.1038/ncomms6138
21. Bar-Peled L, Sabatini DM. Regulation of mTORC1 by amino acids. *Trends Cell Biol.* (2014) 24:400–6. doi: 10.1016/j.tcb.2014.03.003
22. Filipek PA, de Araujo ME G, Vogel GF, De Smet CH, Eberharter D, Rebsamen M, et al. LAMTOR/Ragulator is a negative regulator of Arl8b- and BORC-dependent late endosomal positioning. *J Cell Biol.* (2017) 216:4199–215. doi: 10.1083/jcb.201703061

23. Salamero J, Fougereau M, Seckinger P. Internalization of B cell and pre-B cell receptors is regulated by tyrosine kinase and phosphatase activities. *Eur J Immunol.* (1995) 25:2757–64. doi: 10.1002/eji.1830251007

24. Zikherman J, Doan K, Parameswaran R, Raschke W, Weiss A. Quantitative differences in CD45 expression unmask functions for CD45 in B-cell development, tolerance, and survival. *Proc Natl Acad Sci USA.* (2012) 109:E3–12. doi: 10.1073/pnas.1117374108

25. Khalil AM, Cambier JC, Shlomchik MJ. B cell receptor signal transduction in the GC is short-circuited by high phosphatase activity. *Science.* (2012) 336:1178–81. doi: 10.1126/science.1213368

26. Connor AM, Fanning LJ, Celler JW, Hicks LK, Ramsden DA, Wu GE. Mouse VH7183 recombination signal sequences mediate recombination more frequently than those of VHJ558. *J Immunol.* (1995) 155:5268–72.

27. Hu H, Wang B, Borde M, Nardone J, Maika S, Allred L, et al. Foxp1 is an essential transcriptional regulator of B cell development. *Nat Immunol.* (2006) 7:819–26. doi: 10.1038/ni1358

28. Wu GE, Paige CJ. VH gene family utilization in colonies derived from B and pre-B cells detected by the RNA colony blot assay. *EMBO J.* (1986) 5:3475–81. doi: 10.1002/j.1460-2075.1986.tb04672.x

29. Schlissel M, Voronova A, Baltimore D. Helix-loop-helix transcription factor E47 activates germ-line immunoglobulin heavy-chain gene transcription and rearrangement in a pre-T-cell line. *Genes Dev.* (1991) 5:1367–76. doi: 10.1101/gad.5.8.1367

30. Angelin-Duclos C, Calame K. Evidence that immunoglobulin VH-DJ recombination does not require germ line transcription of the recombining variable gene segment. *Mol Cell Biol.* (1998) 18:6253–64. doi: 10.1128/MCB.18.11.6253

Supplementary Material

LAMTOR2 (p14) controls B cell differentiation by orchestrating endosomal BCR trafficking

Marcin Łyszkiewicz[1,2,*,†], Daniel Kotlarz [2,*], Natalia Ziętara[1,2,*,†], Gudrun Brandes[3], Jana Diestelhorst[2], Silke Glage[4], Elias Hobeika[5], Michael Reth[6], Lukas A. Huber[7], Andreas Krueger[1,8,#], Christoph Klein[2,#]

Correspondence: andreas.krueger@kgu.de (A.K.); Christoph.Klein@med.uni-muenchen.de (C.K.)
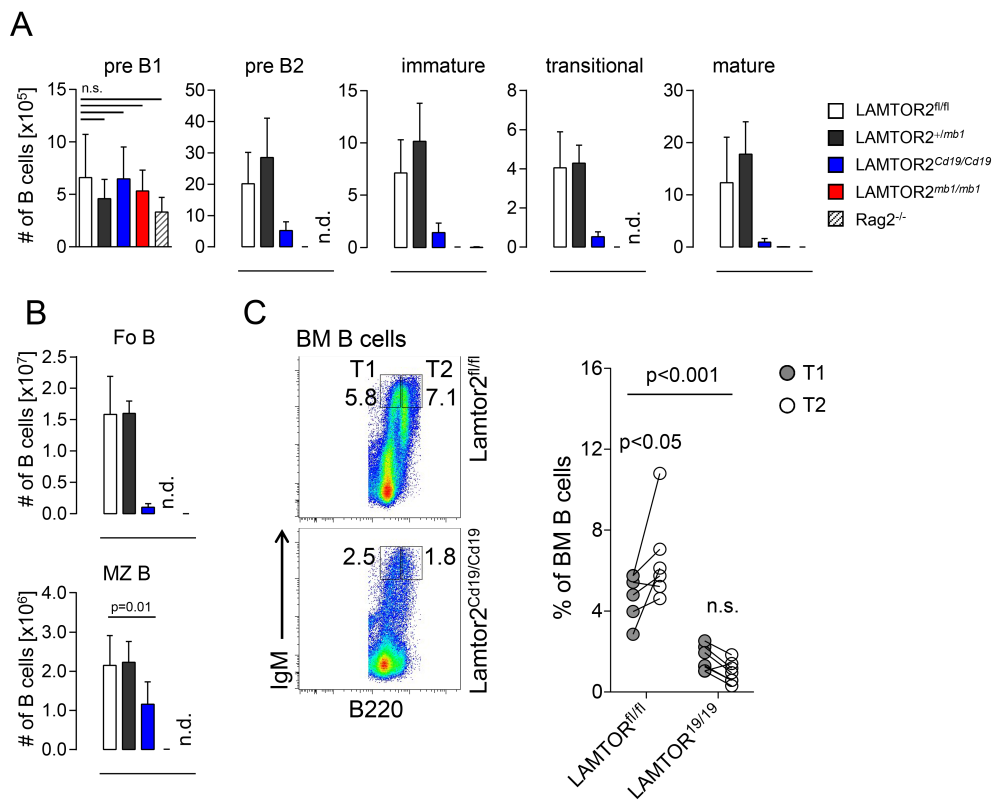
Figure S1 (related to Figure 2). Absolute numbers of B cells in spleen and BM of mice sufficient or deficient for LAMTOR2. (A) Total number of B cell progenitors in BM and (B) main B cell populations in spleen. Pooled data of one or two independent experiments, n = 5-11, Rag2$^{-/-}$ n = 3; n.d. – not detectable. (C) Representative pseudo-colour plots (left) and quantification (right) of transitional 1 (T1) and T2 B cells in BM. Statistical significance was assessed with 2-way ANOVA (effect for genotype is shown) followed by Bonferroni post-test. Pooled data of two independent experiments is shown. Each pair of dots represents data from one mouse.
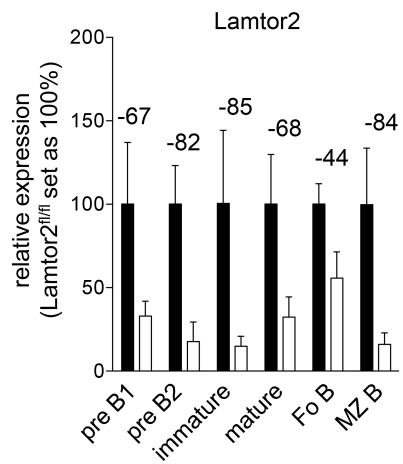
Figure S2. qRT-PCR analysis of CD19-cre mediated deletion of LAMTOR2. Purified populations of BM and splenic B cells of LAMTOR2$^{fl/fl}$ (black bars) and LAMTOR2$^{Cd19/Cd19}$ mice (open bars) were tested for expression of LAMTOR2 mRNA. Average expression in wild-type cells was set as 100%. Numbers above the bars indicate difference in expression between sufficient and deficient cells. Data of one experiment with n=3 for both genotypes is shown.
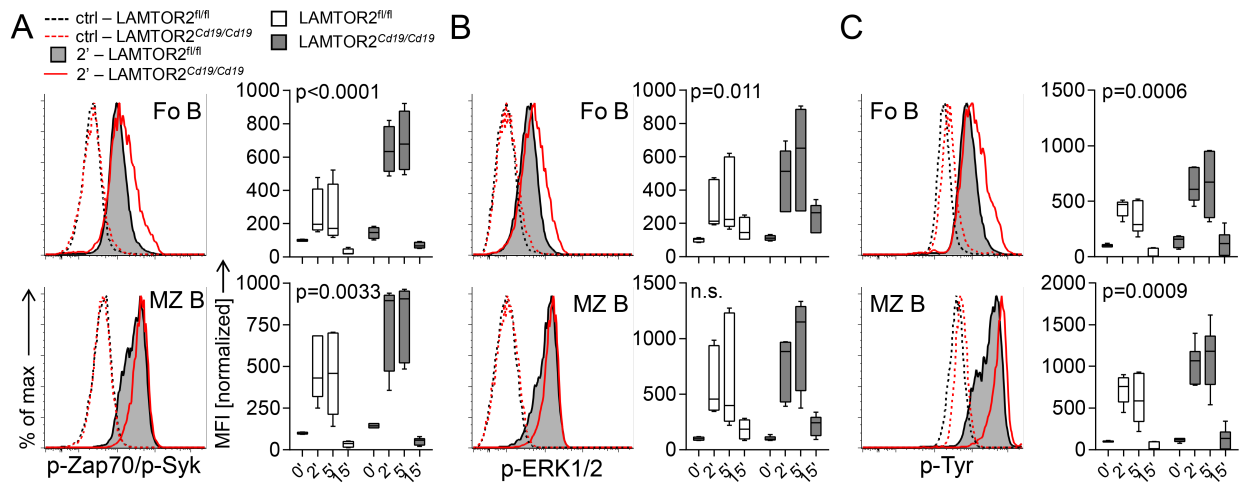
Figure S3 (related to Figure 4). Hyper phosphorylation of BCR-associated kinases in LAMTOR2-deficient B cells. Flow cytometric analysis of (A) pZap70 (pY319)/pSyk (pY352), (B) pERK1/2 (pT202/pY352), and (C) total pY in splenic B cells isolated from LAMTOR2$^{fl/fl}$ or LAMTOR2$^{Cd19/Cd19}$ mice. Starved splenocytes were left untreated (ctrl) or stimulated with anti-IgM F(ab')$_2$ and H$_2$O$_2$ for 2, 5 and 15 minutes. Representative histograms of three independent experiments are shown, graphs show summarized data of two independent experiments, n = 6 for each genotype, whiskers indicate min. to max. range of data, horizontal bars show mean value. Median fluorescence values (MFI) were normalized to ctrl (set as 100%). Statistical analysis was performed using two-way ANOVA (p-values for effect of genotype).

4
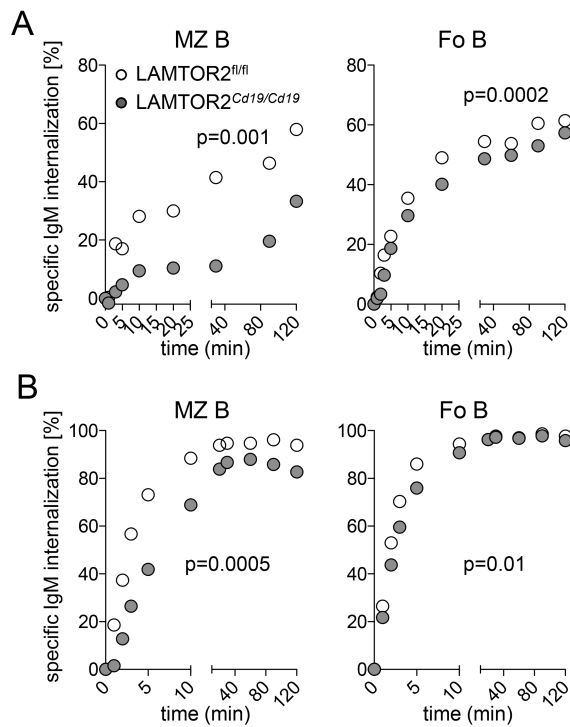
Figure S4 (related to Figure 6). Altered internalization of BCR in LAMTOR2-deficient B cells. Full-time data of the assays presented in Figure 6. (A) Passive BCR internalization in MZ B and Fo B cells or (B) ligand-induced BCR internalization in MZ B or Fo B cells. Purified splenic B cells were labelled in an ice-cold environment with either monovalent (A) or bivalent (B) biotin-labeled anti-IgM Fab or F(ab')$_2$ fragments, respectively, and then BCR internalization was assessed over time at 37°C. Plots for electronically gated cells are representative for two independent experiments. Charts summarize data of one representative experiment out of two.

Appendix 6.3.

Human FCH domain only 1 (FCHO1) deficiency reveals an essential role for clathrin-mediated endocytosis for the development and function of T cells.

Łyszkiewicz M *, **, Ziętara N *, Frey L, Pannicke U, Liu Y, Fan Y, Puchałka P, Hollizeck S, Somekh I, Rohlfs M, Yilmaz T, Ünal E, Karakukcu M, Patiroğlu T, Keller C, Karasu E, Sykora K-W, Somech R, Roesler J, Hoenig M, Schwarz K, Klein C **
* equal contribution, ** corresponding author

ARTICLE

Check for updates

Human FCHO1 deficiency reveals role for clathrin-mediated endocytosis in development and function of T cells

Marcin Łyszkiewicz[1,12,13 ✉], Natalia Ziętara[1,12,13], Laura Frey[1], Ulrich Pannicke[2], Marcel Stern[3], Yanshan Liu[1], Yanxin Fan[1], Jacek Puchałka[1,14], Sebastian Hollizeck[1], Ido Somekh[1], Meino Rohlfs[1], Tuğba Yilmaz[4], Ekrem Ünal[4], Musa Karakukcu[4], Türkan Patiroğlu[4,5], Christina Kellerer[2], Ebru Karasu[2], Karl-Walter Sykora[6], Atar Lev[7], Amos Simon[7], Raz Somech[7], Joachim Roesler[8], Manfred Hoenig[9], Oliver T. Keppler[3,10], Klaus Schwarz[2,11] & Christoph Klein[1 ✉]

Clathrin-mediated endocytosis (CME) is critical for internalisation of molecules across cell membranes. The FCH domain only 1 (FCHO1) protein is key molecule involved in the early stages of CME formation. The consequences of mutations in *FCHO1* in humans were unknown. We identify ten unrelated patients with variable T and B cell lymphopenia, who are homozygous for six distinct mutations in *FCHO1*. We demonstrate that these mutations either lead to mislocalisation of the protein or prevent its interaction with binding partners. Live-cell imaging of cells expressing mutant variants of FCHO1 provide evidence of impaired formation of clathrin coated pits (CCP). Patient T cells are unresponsive to T cell receptor (TCR) triggering. Internalisation of the TCR receptor is severely perturbed in FCHO1-deficient Jurkat T cells but can be rescued by expression of wild-type FCHO1. Thus, we discovered a previously unrecognised critical role of FCHO1 and CME during T-cell development and function in humans.

[1] Department of Pediatrics, Dr. von Hauner Children's Hospital, University Hospital, LMU, Munich, Germany. [2] Institute for Transfusion Medicine, University of Ulm, Ulm, Germany. [3] Max von Pettenkofer Institute, Virology, National Reference Center for Retroviruses, Faculty of Medicine, LMU München, Munich, Germany. [4] Department of Pediatrics, Division of Pediatric Hematology & Oncology, Erciyes University, Kayseri, Turkey. [5] Department of Pediatrics, Division of Pediatric Immunology, Erciyes University, Kayseri, Turkey. [6] Department of Pediatric Hematology/Oncology, Hannover Medical School, Hannover, Germany. [7] Pediatric Department A and the Immunology Service, Jeffrey Modell Foundation Center, Edmond and Lily Safra Children's Hospital, Sheba Medical Center, Tel Hashomer and Sackler Faculty of Medicine Tel Aviv University, Tel Aviv, Israel. [8] Department of Pediatrics, Carl Gustav Carus Technical University Dresden, Dresden, Germany. [9] Department of Pediatrics, University Medical Centre Ulm, Ulm, Germany. [10] German Center for Infection Research (DZIF), Partner Site Munich, Munich, Germany. [11] Institute for Clinical Transfusion Medicine and Immunogenetics Ulm, German Red Cross Blood Service Baden-Wuerttemberg, Hessen, Germany. [12]Present address: Institute for Immunology, Biomedical Center Munich, Ludwig-Maximilians-Universität München, Planegg-Martinsried, 82152 Munich, Germany. [13]These authors contributed equally: Marcin Łyszkiewicz, Natalia Ziętara. [14]Deceased: Jacek Puchałka. ✉email: Marcin.Lyszkiewicz@med.uni-muenchen.de; Christoph.Klein@med.uni-muenchen.de

Eukaryotic cells are characterised by a structural and functional compartmentalisation. Biological membrane systems are critically involved in the establishment and maintenance of the cellular compartments. The highly dynamic modulation of membranes is a key feature for their role in a variety of biological processes, such as endocytosis, secretion, signal transduction or migration. Clathrin, a central molecular scaffold, plays an essential role in the re-organisation of cellular membranes and the transport between compartments. Clathrin-coated vesicles (CCV), first described as "clathrin-coated pits" (CCP) in mosquito oocytes[1] and later purified from pig brain[2], control internalisation of membrane-associated proteins and protein transport from the trans-Golgi-network[3].

Clathrin-dependent endocytosis (CME) is initiated at the plasma membrane by the recruitment of adaptors (heterotetrameric AP-2 complex, AP180; clathrin assembly lymphoid myeloid leukaemia, CALM; and anchor proteins (FCH domain only 1 and 2, [FCHO1 and 2]; epidermal growth factor receptor substrate 15, [EPS15]; and intersectin)[4–6]. These factors are enriched within PIP2 (phosphatidylinositol 4,5,-biphosphate)-rich regions of the membrane and trigger the assembly of the clathrin proteins into clusters[7]. During maturation, the clathrin-enriched membrane patches undergo a local curvature and an invaginated spheric clathrin-coated pit is generated. The connection of this pit to the plasma membrane is detached by dynamin[8].

The molecular details of the formation of a new vesicle are still not fully understood. In vitro, the presence of clathrin, an adaptor protein (i.e., AP-1, AP-2) and dynamin are sufficient to form a vesicle[9]. However, in vivo, the mechanism is much more complex. It has been shown by live-cell total internal reflection fluorescence (TIRF) imaging with single-molecule EGFP sensitivity and high-temporal resolution that the formation of a vesicle can originate from two AP-2 molecules with a clathrin triskeleton[4]. In contrast, another report suggested that FCHO1 and FCHO2 need to be associated with the membrane prior to AP-2 recruitment to initiate the process[5]. FCHO1/2 interact and show similar kinetics at the membrane as the scaffold proteins EPS15 and intersectin, two factors that are important for clathrin-dependent endocytosis[6,10]. Upon downregulation of EPS15 expression by small-interfering RNA, FCHO1/2 show a diffuse pattern of distribution at the cell membrane. This observation suggests that EPS15 is critical for the specific agglomeration of FCHO1/2 on the site of the formation of clathrin-coated vesicles[5].

Since the early clinical discoveries of monogenic immune disorders by Rolf Kostmann[11] and Ogden Bruton[12], >400 primary immunodeficiency diseases have been delineated[13], many of which have opened unprecedented insights into molecular mechanisms orchestrating differentiation and function of the human immune system.

Here, we describe ten human patients with T-cell deficiency and loss-of-function mutations in FCHO1. Our experiments demonstrate that the absence of functional FCHO1 results in perturbed clathrin-mediated endocytosis in several tissues, as well as dysfunctional internalisation of the TCR. Pharmacological inhibition of CME during in vitro T-cell development results in marked delay of T-cell differentiation. In summary, we identify an essential and non-redundant role for the clathrin adaptor FCHO1 in T-cell differentiation and function, linking CME to the function of the human immune system.

Results

Clinical phenotype and molecular genetics. We collected seven pedigrees with ten patients presenting with features of T-cell immunodeficiency (Fig. 1a and Supplementary Fig. 1). All patients suffered from severe bacterial, viral or fungal infections indicative of a primary immunodeficiency disorder. Three patients (B1, C1, D1) developed B-cell lymphoma prior to allogeneic hematopoietic stem cell transplantation, and three patients (A1, D1, E1) had neurological disease (Table 1). Immunological parameters were ranging from a moderate decrease in peripheral CD4+ T cells (F2 and G1) to severe combined immunodeficiency with virtually absent B- and T-cells (A1, B1, E1). With the exception of G1, all patients had hypogammaglobulinemia (Supplementary Table 1). Thus, the common immunophenotypic denominator for all these patients was CD4+ T-cell deficiency.

In order to identify the underlying genetic defect, we performed whole-exome sequencing (WES) followed by Sanger sequencing of candidate genes on patients and family members (see Online Methods). We have identified six distinct, novel and segregating homozygous mutations in FCHO1 in seven pedigrees (Fig. 1b and Supplementary Figs. 2 and 3; Table 1 and Supplementary Table 2). At the DNA level, the mutation in kindred A results in a nucleotide substitution at the position c.2036 G > C, in kindred B in a nucleotide substitution at the position c.100 G > C, whereas the mutations of the pedigrees C and D (not known to be connected by kinship) are insertions c.2023insG resulting in a frameshift and premature termination of the protein (Fig. 1b, c). The mutations of kindred E (changing the first nucleotide of intron 8 c.489 + 1 G > A) and kindred F (contained in the intron 6 splice acceptor site; c.195-2 A > C) affect splicing of pre-mRNA (Fig. 1c and Supplementary Fig. 2). Effects on FCHO1 transcripts in fibroblasts, peripheral blood mononuclear cell (PBMC) and EBV-LCL are shown in Supplementary Figs. 2 and 3. No bands corresponding to wild-type FCHO1 were detected in these analyses. In kindred G, a single-nucleotide substitution at position c.1948C > T results in a predicted premature stop codon at amino acid position 650. All identified patient-associated mutations are summarised in Supplementary Table 2.

FCHO1 consists of three main segments organised into two major domains (Fig. 1c). The N-terminal F-BAR domain (also known as extended FCH), which is responsible for membrane binding, is followed by a structurally less organised and evolutionary poorly conserved segment that binds the adaptor protein AP-2. The C-terminal part (~270 amino acids) forms a μ homology domain (μHD), which directly binds to epidermal growth factor receptor pathway substrate 15 (EPS15) and EPS15-like 1 (EPS15L1) also known as EPS15R[5].

The mutation in kindred A results in an Arg to Pro substitution at the position 679 in the μHD domain. The crystal structure of the Danio rerio μHD domain of Fcho1 has been resolved together with a fragment of EPS15 allowing for direct modelling the effect of the amino acid substitution on this structure (Fig. 1d)[14]. Although the patient-associated mutations are not directly located at the protein-binding trough, replacing the charged side chain of Arg with a nonpolar and rigid ring of Pro may result in steric alterations in the μHD subdomain A and thus affect interaction with its binding partners (Fig. 1d).

The point mutation in kindred B results in an amino acid substitution in the alpha-helix structure of the F-BAR domain (p. Ala34Pro). The F-BAR domain of FCHO1 has not been crystallised. However, the structure of its functional and structural paralogue FCHO2 has been resolved, which allows for modelling of the patient-associated mutation[14]. The substitution of Ala with Pro at position 34 is likely to result in a disruption of the alpha-helix structure, which in turn may lead to alterations in the membrane-binding properties of the entire domain (Fig. 1e).

In addition to mutations resulting in amino acid substitutions, we identified three distinct variants resulting in a premature stop
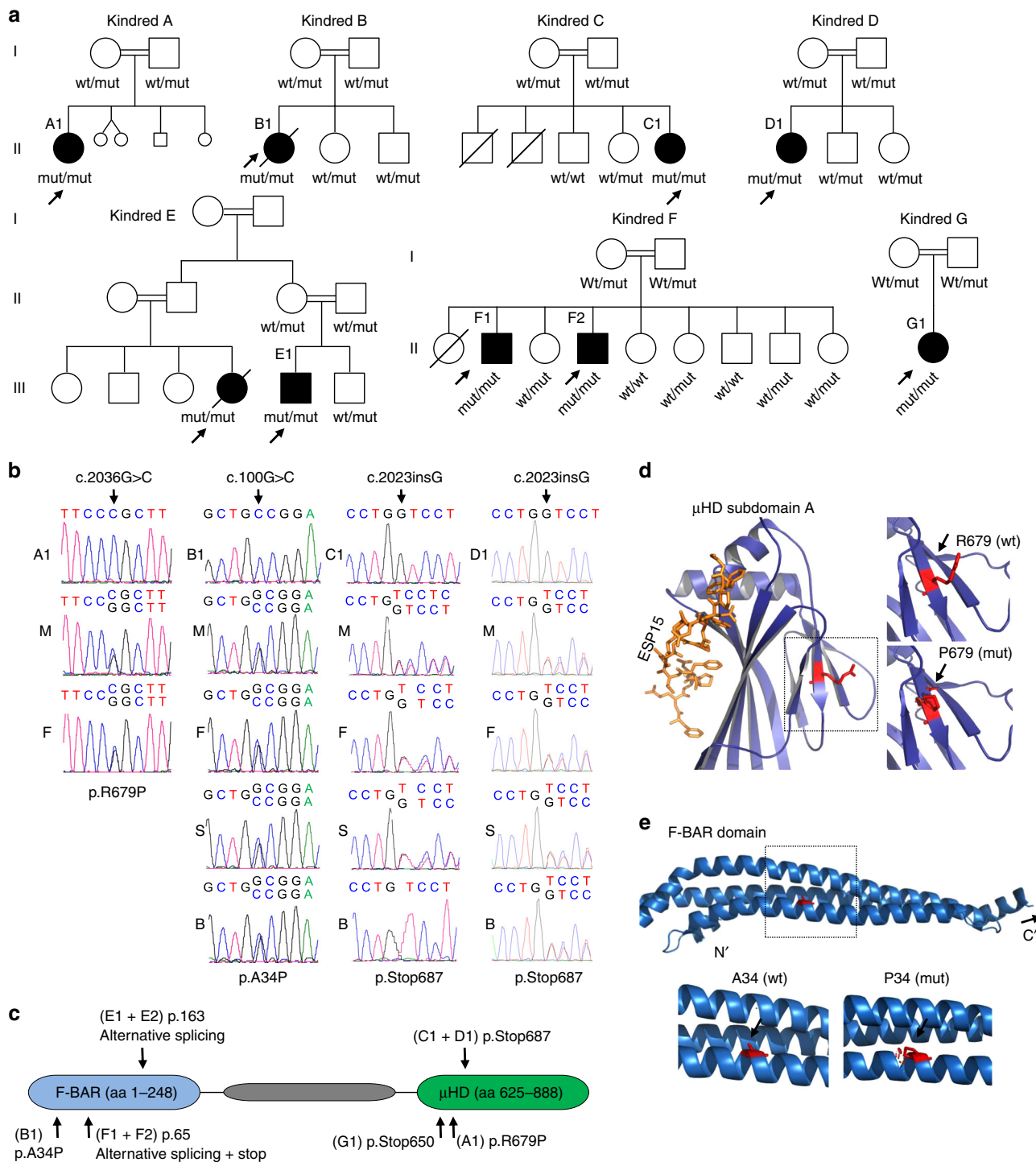
Fig. 1 Homozygous mutations in the *FCHO1* gene segregate with patients' lymphopenia. a Pedigrees of seven unrelated families show ancestral segregation of mutations in the *FCHO1* locus. Generations are assigned by Roman numerals from I to III. Index cases are marked with an arrow, small circles and squares denote spontaneous abortions and crossed symbols deceased individuals. mut, mutation; wt, wild-type. **b** Sanger sequencing chromatograms indicating homozygous mutation c.2036 G > C in index cases of kindred A, c.100 G > C in kindred B and c.2023insG in kindred C and D. Families C and D are not connected by kinship. A–D, index cases; M' mother; F, father; S, sister; B, brother. Additional kindred analyses are exhibited in Supplementary Figs. 2 and 3. **c** Schematic representation of FCHO1 protein indicating two main domains and localisation of family-associated mutations. **d**, **e** Computed crystal structures with indicated point mutations in μHD domain (**d**) and F-BAR domain (**e**).

codon. The two identical mutations in the unrelated families C and D result in a frameshift and premature stop codon at amino acid position 687 (p.Val675GlyTer13, referred to as p.Stop687). Similarly, the mutation associated with kindred G results in a premature stop codon at amino acid position 650 (p.Stop650). In both variants virtually the entire μHD domain is truncated, which presumably alters interaction with the FCHO1-binding partners. The point mutation in kindred E affects a splice donor and thereby results in a shortening of the FCHO1 by 51 amino acid encoded by exon 8 (Supplementary Fig. 2). Given the localisation

Table 1 Summary of clinical features of patients carrying mutations in *FCHO1*.

Patient	Origin	Genetic variant[a]	Consequences of mutation	Immunological findings	Infections	Other clinical findings	Therapy and outcome
A1	Germany	*FCHO1* c.2036 G > C	aa substitution in µHD domain (p.R679P)	• T- and B-cell lymphopenia • hypogammaglo-bulinemia	• Recurrent pneumonia and viral gastroenteritis • Relapsing oro-genital mycoses • Bronchiolitis obliterans • Postpneumonic pulmonary fibrosis • Otitis media	• Moya-Moya syndrome • Transient left hemiparesis upon cerebral ischaemia • Failure to thrive • Microcephaly	Reduced cardiopulmonary performance, stable Moya-Moya 9 years after HLA-matched HSCT
B1	Turkey	*FCHO1* c.100 G > C	aa substitution in F-BAR domain (p.A34P)	• T- and B-cell lymphopenia • hypogammaglo-bulinemia	• Recurrent pneumonia • Recurrent fungal infections • CMV infection	• DLBCL • Renal metastases	Deceased as consequence of DLBCL, age 16 years
C1	Turkey	*FCHO1* c.2023insG	Truncated (p.Stop687)	• CD4+ T-cell lymphopenia • hypogammaglo-bulinemia	• Recurrent pulmonary infections • Recurrent fungal infections • Otitis media	• EBV+ Hodgkin lymphoma • Failure to thrive • hepatosplenomegaly • Renal masses • Xanthogranulomatous pyelonephritis	IVIG replacement and antibiotics; awaiting allo-HSCT
D1	Turkey	*FCHO1* c.2023insG	Truncated (p.Stop687)	• CD4+ T-cell lymphopenia • hypogammaglo-bulinemia	• Recurrent pneumonia • HSV infection	• DLBCL stage IV • Liver lesions • Spleen lesions • Lung lesions • Aphthous stomatitis • Gingivitis • Encephalitis	Deceased, age 10 years
E1	Palestine	*FCHO1* c.489 + 1G > A	Alternative splicing IVS8 splice donor	• CD4+ T-cell and B-lymphopenia • hypogammaglo-bulinemia	• Recurrent pneumonia • Chronic diarrhoea • CMV infection • Fungal infection	• Mild brain atrophy	IVIG replacement and antibiotics; awaiting allo-HSCT
E2	Palestine	*FCHO1* c.489 + 1G > A	Alternative splicing IVS8 splice donor	• not available	• Recurrent pneumonia • Chronic diarrhoea		Deceased after cardiac arrest, age 2 years
E3	Palestine	*FCHO1* c.489 + 1G > A	Alternative splicing IVS8 splice donor	• CD4+ T-cell lymphopenia • hypogammaglo-bulinemia	• Recurrent pneumonia • Chronic diarrhoea • EBV infection		IVIG replacement and antibiotics; awaiting allo-HSCT
F1	Saudi Arabia	*FCHO1* c.195-2 A > C	Alternative splicing IVS6 splice acceptor	• CD4+ T-cell lymphopenia • hypogammaglo-bulinemia	• Recurrent pneumonia • Chronic diarrhoea • Cryptosporidiosis • Recurrent stomatitis (HSV)	• Failure to thrive	HSCT at age 5 yrs (no conditioning), MFD (mother), a+cGvHD, complete donor chimerism, normal immune function, off IVIG, 10 yrs follow up
F2	Saudi Arabia	*FCHO1* c.195-2 A > C	Alternative splicing IVS6 splice acceptor	• CD4 + T-cell lymphopenia	• Recurrent pneumonia • Chronic diarrhoea • Cryptosporidiosis • Multiple viruses (adenovirus, RSV, enterovirus)		HSCT at age 1.5 yrs, (no conditioning), MSD, no GvHD, post-transplant intracranial EBV-PTLD and atypical mycobacterium-associated mastoiditis; mixed chimerism (T-cells 100% donor, non-T-MNCs 5-10% donor, red cells recipient), normal immune function, off IVIG, 12.5 yrs follow up
G1	Algeria	*FCHO1* c.1948C > T	Truncated p.R650X p. Stop650	• CD4 + T-cell lymphopenia • Weak response to vaccination	• Recurrent broncho-pulmonary infections • Candidiasis • CMV infection	• Failure to thrive	HSCT (MFD) at age 5 years, doing well

EBV Epstein-Barr virus, *DLBCL* diffuse large B-cell lymphoma, *PTLD* post-transplant lymphoproliferative disorder, *HLA* human leucocyte antigen, *HSCT* haematopoietic stem cell transplantation, *MFD* matched family donor, *IVIG* intravenous immunoglobulin, *a* +*cGvHD* acute and chronic graft versus host disease.
[a]Sequence of coding DNA is given from the first nucleotide of the translation start codon.
[b]Sequence of protein is given from the first amino acid.

of these amino acids, it is likely that, in case a protein is stably expressed, it disrupts the alpha-helix structure of the F-BAR domain. Finally, the kindred F-associated mutation in the splice acceptor region gives rise to three possible splice variants, each of them resulting in a premature stop codon shortly downstream of exon 6. It prevents correct splicing and by prediction presumably leads to expression of a very short (~7.1 kDa), non-functional form of FCHO1 (Supplementary Fig. 3b–e).

Effects of patient-associated mutations on FCHO1 function. Based on CADD and PolyPhen-2 scores, all patient-associated mutations are deleterious for the FCHO1 protein function (Supplementary Table 2). To test this, we first established a heterologous system, where HEK239T cells were transiently transfected with vectors carrying wild-type (wt) or mutated versions of the *FCHO1* complementay DNA (cDNA). None of the herein tested mutations altered protein stability, albeit p.Stop687 resulted in the expression of a shorter protein (Fig. 2a and Supplementary Fig. 4). The encoded proteins were tested for co-immunoprecipitation with their direct interacting partners EPS15 and its homologue EPS15R. Recovery of the EPS15 and EPS15R was strongly reduced in both mutants affecting the μHD domain (c.R679P and p.Stop687). In contrast, the FCHO1 mutant affecting the F-BAR domain (p.A34P) did not alter the interaction with EPS15 and EPS15R (Fig. 2a).

The function of FCHO1 critically depends not only on its biochemical interaction with partner proteins but also on the spatiotemporal organisation of its interactome. Nucleation of FCHO1-mediated clathrin-coated vesicles (CCV) occurs only at the plasma membrane[5]. We, therefore, set out to test whether the identified *FCHO1* mutations altered the subcellular location of the corresponding protein. We employed SK-MEL-2 cells expressing a RFP-tagged clathrin light chain from one allele of its endogenous locus[15]. In order to circumvent confounding effects of the endogenously encoded FCHO1 protein, the *FCHO1* gene was deleted using CRISPR/Cas9-mediated gene editing. Transient expression of wt FCHO1-GFP fusion protein in knockout (ko) cells showed scattered bright puncta associated with the plasma membrane as previously reported[5,14] (Fig. 2b–d and Supplementary Figs. 5–7). In contrast, expression of the F-BAR mutated (p.A34P) FCHO1 form resulted in the formation of large plasma membrane-dissociated agglomerations (Fig. 2b–d and Supplementary Figs. 5–7).

Further, both pR679P and p.Stop687 μHD mutants failed to form any punctated structures. These mutants appeared as a diffuse network, mostly dissociated from the plasma membrane (Fig. 2b–d and Supplementary Fig. 5). In accordance with the co-immunoprecipitation results, only wt and p.A34P FCHO1 colocalized with their partners EPS15 and adaptin (Fig. 2b–c, and for quantification Fig. 2e). Importantly, all mutants failed to colocalize with endogenous clathrin (Fig. 2d–e). We chose a model system with physiological expression levels of FCHO1. While this is advantageous in many respects[5], it is limited with respect to poor signal-to-noise ratio. To improve signal intensities, we additionally transduced SK-MEL-2 cells to stably over-express RFP-tagged clathrin light chains. As shown in Supplementary Fig 7, these data confirm that only wild-type FCHO1, but none of the mutants, colocalize with clathrin.
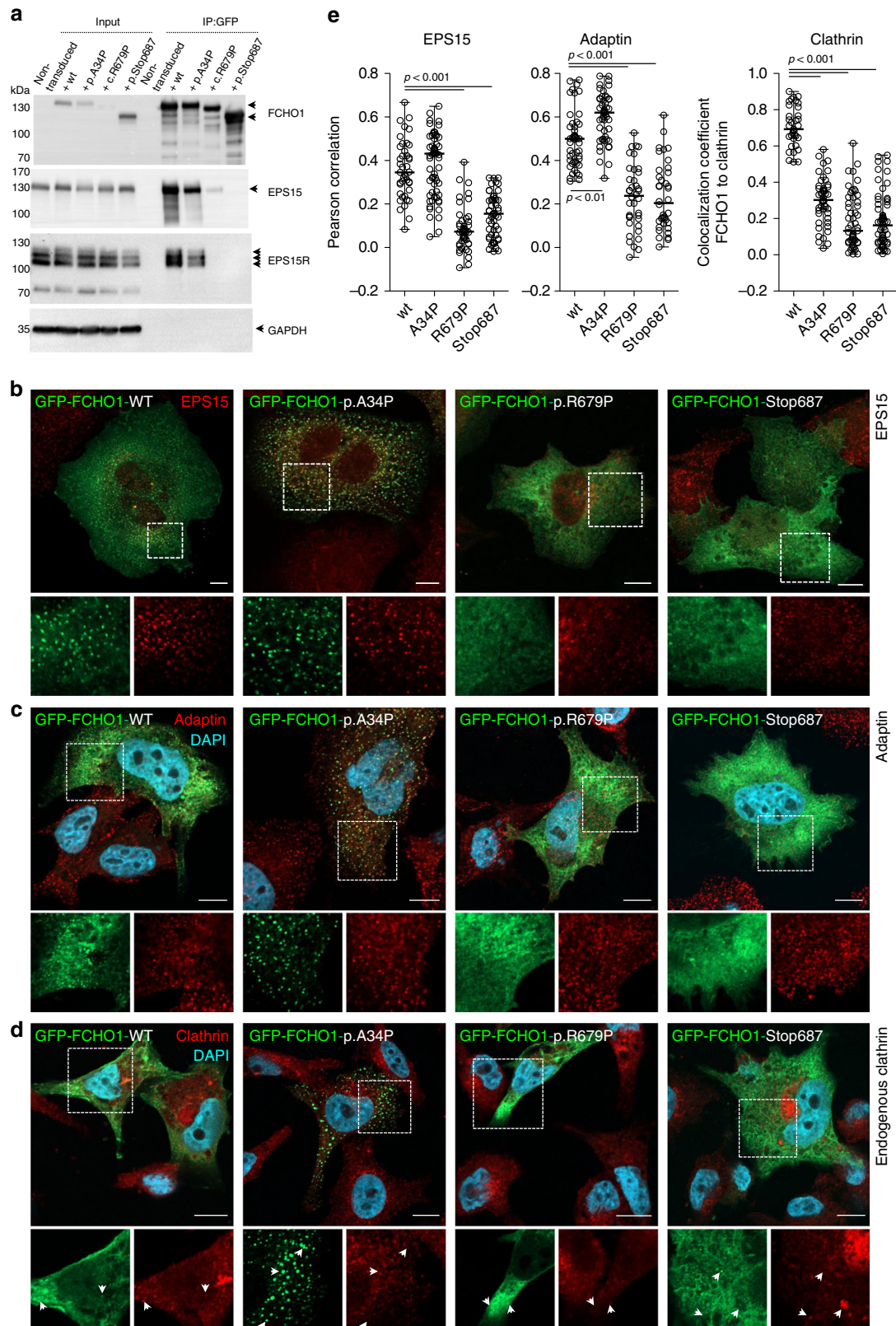
Nucleation of CCV is a highly dynamic process. To measure the dynamics of protein–protein interaction between FCHO1 and clathrin, we established live-cell imaging models. Here, we followed wt FCHO1 and both point mutants (p.R679P and p.A34P). As anticipated, wt GFP-FCHO1 initiated the formation of clathrin-coated pits, whereas both mutants failed to do so (Fig. 3a–c and Supplementary Movies 1–3). FCHO1 carrying the

μHD-associated p.R679P mutation prevented the formation of productive pits and thus failed to facilitate the formation of CCV. Since the sensitivity of the confocal microscope does not allow to discriminate single molecules, we cannot exclude that small, abortive pits may have been formed. However, we failed to detect any aggregation of FCHO1 carrying this mutation. In striking contrast, the F-BAR-associated mutation p.A34P resulted in the formation of fast moving, large aggregates of GFP-FCHO1 fusion proteins. Moreover, such membrane-dissociated aggregates tended to merge, leading to the formation of cytoplasmic protein intrusions (Supplementary Fig. 5). These pits appeared to be abortive, since they failed to interact with clathrin (Fig. 3a–c).

These results illustrate that the identified mutations in *FCHO1* constitute loss-of-function alleles: whereas the mutation in the μHD domain results in loss-of-interaction with its main interacting partners and partial dissociation from the plasma membrane, the mutation in the F-BAR domain alters the subcellular localisation of the FCHO1 protein. Irrespective of their nature, all mutations ultimately result in inefficient nucleation of CCV.

FCHO1 regulates endocytosis of the T-cell receptor. The *FCHO1* mutations identified in our patients predominantly result in a severe T-cell defect while other cells of the immune system appear largely unaffected. The key designate of T-cell fate during ontogeny is the quality and strength of the T-cell receptor (TCR) signal[16–18]. The TCR has no intrinsic catalytic activity. TCR-dependent signal propagation requires a multi-protein complex comprises TCR α- and β-chains non-covalently coupled to immunoreceptor tyrosine-based activation motif (ITAM)-rich CD3 ε, γ, δ and ζ molecules. Internalisation of the CD3:TCR complex depends on the formation of CCP[19–24]. We hypothesised that FCHO1 may be involved in TCR internalisation during T-cell activation. To test this, we took advantage of the CD4-positive human Jurkat T-cell lymphoma line in which we deleted the endogenous *FCHO1* gene using CRISPR/Cas9 gene editing. FCHO1-deficient Jurkat clones were reconstituted with either wt or mutated FCHO1 using retroviral vectors encoding a bicistronic FCHO1 and GFP cDNA separated by an internal ribosomal entry site (IRES). In order to understand the effect of FCHO1 on TCR internalisation and clustering, we analysed TCR distribution upon stimulation using confocal microscopy. After 60 min of TCR triggering by an α-CD3 monoclonal Ab, large intracellular CD3-positive puncta were formed in wt cells, whereas in FCHO1 ko clones CD3 molecules remained in diffuse form (Fig. 4a and Supplementary Fig. 8). Knockout clones reconstituted with wt FCHO1 formed large CD3-positive puncta, essentially indistinguishable from those in wt cells. In contrast, none of the FCHO1 mutants were able to rescue the phenotype and thus nearly all CD3 molecules remained diffused upon TCR-activation (Fig. 4a). We also noted plasma membrane invagination and nucleus segmentation in FCHO1-deficient Jurkat cells. This effect was not observed in SK-MEL-2 cells (Figs. 2b–d and 4a, and Supplementary Fig. 5). It is therefore possible, that FCHO1 deficiency has a more general effect on plasma membrane structure in T cells.

To assess TCR internalisation in a quantitative manner, we next measured the intracellular accumulation of CD3:TCR complexes upon anti-CD3-mediated TCR triggering over time using flow cytometry. Consistent with our confocal microscopy studies, we noted that FCHO1 ko cells accumulated approximately two-fold less CD3:TCR complexes when compared to wt cells (Fig. 4b). Finally, as the TCR cross-linking and its subsequent internalisation are essential for quality and strength of the triggered signal, we assessed whether FCHO1 directly

a — Input / IP:GFP western blots (Non-transduced, + wt, + p.A34P, + c.R679P, + p.Stop687) probed for FCHO1, EPS15, EPS15R, GAPDH.

e — EPS15, Adaptin, Clathrin colocalization scatter plots (wt, A34P, R679P, Stop687); $p < 0.001$, $p < 0.01$.

b — GFP-FCHO1-WT / EPS15, GFP-FCHO1-p.A34P, GFP-FCHO1-p.R679P, GFP-FCHO1-Stop687.

c — GFP-FCHO1-WT / Adaptin / DAPI and mutant panels.

d — GFP-FCHO1-WT / Clathrin / DAPI and mutant panels (Endogenous clathrin).

modulated TCR responsiveness. To this end, Jurkat cells sufficient or deficient for FCHO1 were stimulated with an α-CD3 antibody and assessed for release of intracellular Ca^{2+}. When compared to controls, FCHO1-deficient cells released less Ca^{2+} upon CD3: TCR triggering (Fig. 4c). Furthermore, only reconstitution with

wt but not mutated forms of FCHO1 restored normal levels of Ca^{2+}, directly demonstrating that physiological TCR signalling depends on FCHO1.

During CME adaptor proteins recognise cargoes at the cell surface and direct them to the clathrin pits. FCHO1 binds its

Fig. 2 Patient-associated mutations alter either binding properties or subcellular localisation of the FCHO1 protein. a Whole-cell lysates from HEK293T cells overexpressing either wt or indicated mutant GFP-FCHO1 fusion proteins were used for immunoprecipitation. Specific bands are indicated with arrows. Anti-FCHO1 or anti-GFP antibodies were used independently to detect FCHO1-specific bands. Representative data of three independent experiments are shown. Uncropped blots are shown in Supplementary Fig. 4. **b–d** FCHO1-deficient SK-MEL-2 cells expressing RFP-tagged clathrin light chain from endogenous locus (CLTA$^{RFP/wt}$) were transiently transfected with either wt or mutated GFP-FCHO1 and fixed 24 to 36 h post transfection. Representative confocal microscopy pictures show that the F-BAR-domain-associated mutation p.A34P alters the subcellular localisation of FCHO1 and leads to the formation of large aggregates dissociated from the plasma membrane. The µHD domain-associated mutations (p.R679P and p.Stop687) abolish the interaction of FCHO1 with its interacting partners EPS15, and adaptin. All mutations obliterate interaction with endogenous clathrin. Enlarged and colour-separated regions corresponding to boxed areas are shown below each main picture. In **d** arrows indicate presumptive interaction of clathrin with wild-type FCHO1 and lack of such interaction for all tested mutants. Scale bar represents 5 µm for main pictures and 10 µm for enlarged regions. Colour code: **b–d** GFP-FCHO1, green; DAPI, blue, **b** EPS15, **c** adaptin, **d** clathrin–red. **e** Quantification of data shown in **b** to **d**. Pearson correlation or co-localisation coefficients of FCHO1 wild-type and all tested mutants with EPS15, adaptin and clathrin. Pooled data of two to three independent experiments are depicted. Each symbol represents one region of 25 µm^2. Up to three regions per cells were quantified. Horizontal lines indicate the median, whiskers indicate the range (min to max). Statistical analysis of significance was performed using one-way ANOVA test followed by Tukey's multiple comparison test to assess differences between groups. Source data are provided as a Source Data file.
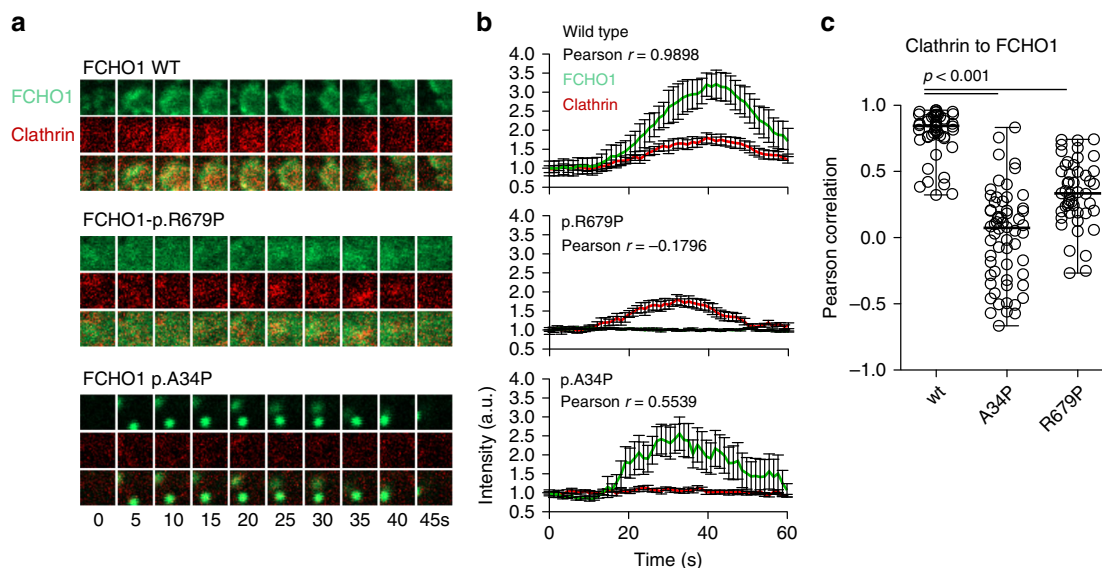
Fig. 3 Mutations in both µHD and F-BAR domains of FCHO1 prevent nucleation of clathrin-coated pits (CCP). a The dynamics of FCHO1-mediated nucleation of CCP in FCHO1-deficient SK-MEL-2 cells expressing RFP-tagged clathrin light chain from endogenous locus (CLTA$^{RFP/wt}$) transduced with either wild-type (upper panel), µHD-mutated (p.R679–middle panel) or F-BAR-mutated (p.A34P–bottom panel) GFP-FCHO1 fusion protein. Two micrometre-wide sections of representative movies are shown. Full movies are available in supplemental materials. In the middle panel, contrast was reduced and brightness was increased as to show a diffused signal of GFP at the plasma membrane. **b** Time dependence of the fluorescent intensity of FCHO1 (green) and endogenous clathrin (red) averaged from nine independent movies. Only the fluorescence of wild-type but not mutant FCHO1 correlates with clathrin. Each channel was normalised to the background and the initial fluorescence was set to 1. Error bars represent SEM of mean fluorescence intensity, $n = 9$ biologically independent cells from minimum three independent experiments. **c** Pearson correlation of FCHO1 and clathrin from individual movies. Pooled data from three independent experiments. Each symbol represents one square region of 25 µm^2. Up to three regions per cells were quantified. Horizontal lines indicate the median. Statistical analysis of significance was performed using one-way ANOVA test followed by Tukey's multiple comparison test to assess differences between groups Source data are provided as a Source Data file.

cargo through its µHD domain[25,26]. It has been proposed that Syp1, the yeast FCHO1 homologue, recognises DxY motifs on its cargo[26]. We hypothesised that human FCHO1 may also recognise its cargo via DxY motifs, in particular since CD3ε and CD3γ have DxY motifs in their cytoplasmic domain (Supplementary Fig. 9a). While we could confirm interaction of FCHO1 and EPS15 in Jurkat cells stably transduced with N'- or C'-flag FCHO1 fusion proteins, we could not observe any direct interaction with either of the CD3 molecules (Supplementary Fig. 9c–f). Thus, although CD3 molecules possess the putative sorting motifs recognised by FCHO1, we could not provide experimental evidence for direct FCHO1-CD3 interaction.

In sum, we provide evidence that FCHO1 plays a role in TCR-dependent T-cell activation. It affects TCR clustering upon

receptor triggering and modulates its internalisation. Finally, FCHO1 deficiency results in impaired mobilisation of Ca^{2+}, directly linking the FCHO1 to TCR-associated signalling.

FCHO1 deficiency does not affect entry of VSV-G pseudotyped HIV-1. Infection of cells with vesicular stomatitis virus (VSV) is strongly dependent on CME. CME of VSV particles is initiated after interaction of the viral glycoprotein (VSV-G) with the cellular LDL (low-density lipoprotein) receptor[27]. Entry of VSV or VSV-G pseudotyped lentiviruses into the cytoplasm occurs after endosomal acidification, which induces a conformational change of VSV-G followed by fusion of viral and cellular membranes[28].

To evaluate whether the absence of FCHO1 in Jurkat T cells has an impact on CME-dependent virus infection, Jurkat wt and
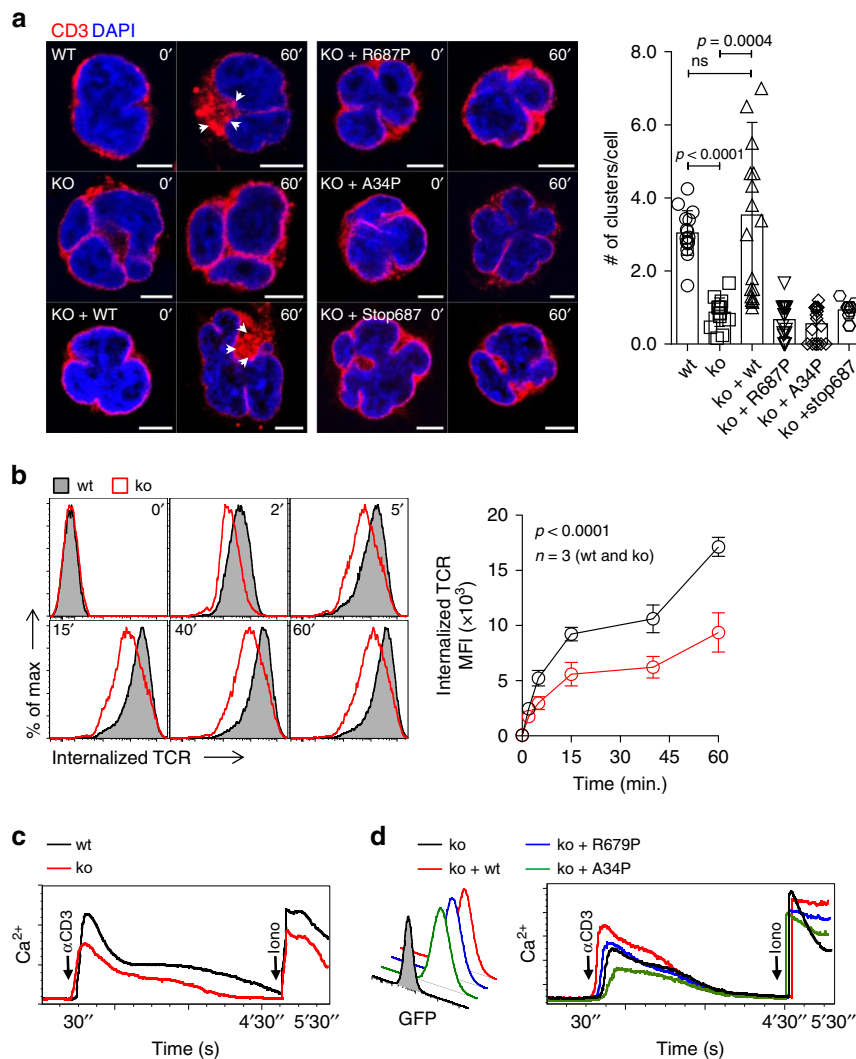
Fig. 4 FCHO1 deficiency impairs TCR internalisation. a FCHO1-sufficient and -deficient clones of Jurkat cells were used in the heterologous system, in which ko clones were left either non-transduced or stably transduced with wt or FCHo1 construct carrying one of the patient-associated mutations, as indicated. Cells were mock-treated (0′) or stimulated with anti-CD3 Ab (60′) at 37 °C, fixed and stained for CD3 and DAPI. Representative confocal microscopy pictures show that only wt FCHO1 facilitates the formation of CD3 puncta upon stimulation. Scale bar 5 μm. White arrowheads indicate CD3 puncta. The chart summarises data of three independent experiments in which an average number of CD3 puncta per cell is shown. Each point indicates an average number of puncta per cell that could be found in one field of view. Statistical analysis of significance was performed using ANOVA test followed by Sidak's multiple comparison test to assess differences between groups, whiskers indicate the range (5–95 percentile). **b** FACS analysis of TCR internalisation in wt or FCHO1 ko Jurkat clones. Jurkat cells were stained with anti-CD3 Ab in cold and then TCR internalisation was assessed over time at 37 °C in the presence of anti-mouse F(ab′)$_2$ fragments labelled with Ax647. At indicated time points remaining surface TCRs were stripped, thus fluorescent signal corresponds to the internalised TCR only. The chart summarises data of one representative experiment out of three, $n = 3$ clones per genotype. **c** Intracellular Ca^{2+} flux upon TCR stimulation. Wt or FCHO1 ko Jurkat clones were loaded with Ca^{2+}-sensitive FuraRed and Fluo-4 dyes and stimulated with anti-CD3 Ab and then Ca^{2+} flux was recorded flow cytometrically over time. α-CD3 and Iono indicate time points of respective stimulations. Data are representative of three independent experiments in which minimum three different clones of each genotype were analysed. **d** Ca^{2+} flux of FCHO1-deficient clones upon reconstitution with either wt or indicated mutants of FCHO1. GFP histogram indicates transduction efficiency. Intracellular Ca^{2+} flux was assessed as in **c**, representative data of two independent experiments are shown. Two FCHO1-deficient clones were analysed. **b**, **e** Statistical analysis was performed using two-way ANOVA (p-values for the effect of the genotype). Source data are provided as a Source Data file.

FCHO1 ko clones were challenged with HIV-1 particles, that are devoid of their own envelope glycoprotein but had been pseudotyped with VSV-G. The interaction of T cells with VSV-G HIV-1 was monitored using two established readouts, i.e., virion fusion and productive HIV-1 infection. The quantitative assessment of fusion of virions is based on the incorporation of a BlaM-Vpr chimeric fusion protein into VSV-G HIV-1 particles and their subsequent delivery into the cytoplasm of T cells as a result of virion fusion. Cleavage of the fluorescent CCF2 dye,

which is loaded into target cells, allows for detection of fusion events by flow cytometry[29–31]. The successful infection of VSV-G HIV-1 pseudotypes can be quantified by intracellular staining for HIV-1 p24 antigen[32].

Jurkat wt and FCHO1 ko clones were challenged with different multiplicities of infection of either VSV-G HIV-1ΔEnv (BlaM-Vpr) (Fig. 5a and Supplementary Fig. 10a) or VSV-G HIV-1ΔEnv (Fig. 5b and Supplementary Fig. 10b). FCHO1-deficient Jurkat T clones displayed a susceptibility to VSV-G pseudotyped HIV-1,
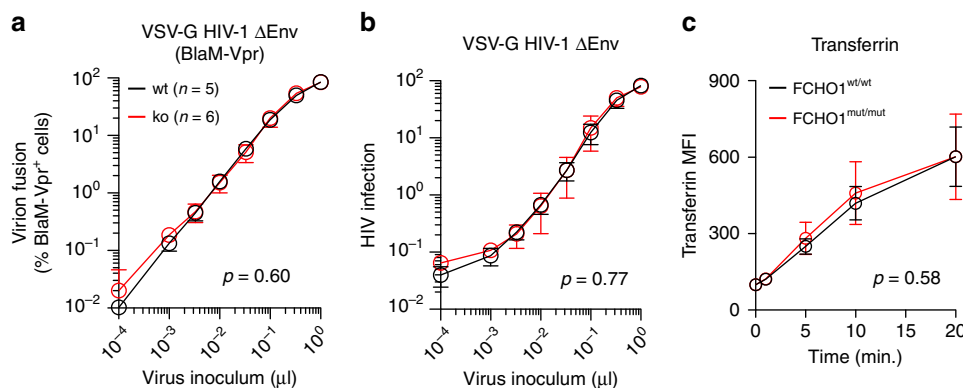
Fig. 5 FCHO1 deficiency does not alter global clathrin-mediated endocytosis. a, **b** Fusion of VSV-G HIV-1ΔEnv (BlaM-Vpr) virions (**a**) or infection by VSV-G HIV-1ΔEnv (**b**) of Jurkat cells. Wt or FCHO1-deficient clones were challenged with increasing volumes of the indicated VSV-G HIV-1ΔEnv. Virion fusion was monitored by flow cytometry as previously reported[29–31] and the percentage of cleaved $CCF2^+$/BlaM-Vpr$^+$ cells is plotted relative to the virus inoculum. Infection of VSV-G HIV-1ΔEnv was monitored by intracellular HIV-1 p24 staining two days post challenge and the relative percentage of p24-positive cells is plotted relative to the virus inoculum[32]. Arithmetic means and standard errors are shown of results obtained for the indicated number of clones from either virion fusion (**e**) or infection (**f**). **c** Patient fibroblast or healthy donor fibroblast were subjected to the transferrin uptake assay. Cells were exposed to fluorescently labelled transferrin for the indicated time at 37 °C and subsequently analysed by FACS. Data are pooled of four independent assays; error bars represent standard deviation. **a–c** Statistical analysis was performed using two-way ANOVA (p-values for the effect of the genotype). Source data are provided as a Source Data file.

monitored by both virion fusion and productive infection, that was indistinguishable from that of wt clones. As controls of specificity, fusion of HIV-1 wt, but not of VSV-G HIV-1 ΔEnv, was inhibited by the peptidic HIV-1 fusion inhibitor T20 (Supplementary Fig. 11a) and, importantly, infection by VSV-G HIV-1 ΔEnv was blocked by the V-ATPase inhibitor bafilomycin A1, which prevents endosome acidification (Supplementary Fig. 11b).

Taken together, FCHO1 deficiency in Jurkat T cells does not functionally impair CME in the context of VSV-G-mediated entry and infection of a lentivirus pseudotype.

FCHO1 deficiency does not alter global endocytosis. To further assess whether FCHO1 deficiency has a global impact on CME, we tested transferrin receptor internalisation, a well-recognised model of a clathrin-dependent process[33]. To this end, we incubated patient and healthy donor fibroblasts with fluorescently labelled transferrin in the cold and, following a temperature shift, its internalisation was monitored over time. Both wild-type and FCHO1-deficient primary cells were able to internalise transferrin through the TfR comparably (Fig. 5c), suggesting that FCHO1 deficiency does not affect general CME endocytosis, but selectively CME endocytosis of certain molecules.

FCHO1 modulates function of primary human T cells. The paucity of T cells in peripheral blood of most FCHO1-deficient patients precluded an in-depth investigation of primary lymphocytes. However, we were able to test functional consequences of FCHO1 deficiency on T cells isolated from the patient of kindred C. We assessed proliferation of T cells and their capacity to produce cytokines in response to TCR stimulation. First, we determined the frequency of T cells in peripheral blood of patient C1 (Fig. 6a). Although largely reduced in number when compared to her heterozygous siblings, peripheral blood T cells were abundant enough to perform a functional assay. To this end, PBMCs were labelled with CFSE and stimulated with α-CD3 and α-CD28 Abs. Cell proliferation and cytokine production were assessed after 3 and 5 days. At both time points, CD4 and CD8 T cells of healthy siblings responded vigorously to the stimulation whereas patient T cells failed to proliferate (Fig. 6b). Similarly,

FCHO1-deficient T cells produced considerably lower levels of IL-2 and IFN-γ. In contrast, secretion of TNF-α was comparable to healthy control cells, and IL-4 secretion was only marginally dependent of FCHO1 function (Fig. 6c). Of note, T cells from the heterozygous mother (and to a lesser extent the father) produced less cytokines when compared to FCHO1$^{wt/wt}$ control T cells. The reason for this observation remains unclear. While a mild dominant-negative effect cannot be excluded, there is no in vivo evidence of T-cell dysfunction in healthy parents. (Fig. 6c).

In summary, FCHO1 deficiency impairs T-cell development and responsiveness to TCR stimulation.

Inhibition of CME arrests development of murine T cells in vitro. Our data highlighted a mechanistic link between impaired CME and ensuing T-cell deficiency. To further validate this notion, we employed OP9-DL1 and OP9 co-culture systems allowing us to study in vitro T-cell differentiation, as well as differentiation of B cells and myeloid cells[34]. Purified thymus-derived, T-cell-committed double-negative (DN) three progenitors were co-cultured with OP9 DL1 cells for 10 days until ~50% of them co-expressed CD4 and CD8 co-receptors (double-positive, DP). At day 5 of culture, we exposed the cells to chlorpromazine, a known inhibitor of CME[35] (Fig. 7a). In a concentration-dependent manner, we observed inhibition of developmental transition between DN3 to DP stage. Whereas > 50% of cells reached the DP stage in the absence of CME inhibition, only 30–35% of chlorpromazine-treated showed progression to the DP stage. Even though minuscule surface expression levels of pre-TCR at this stage of thymocyte development prevented any direct measurements of TCR internalisation, it is known that thymocyte differentiation from DN3 to DP strongly depends on the quality of pre-TCR signal[36,37].

To exclude the general cytotoxic effect of chlorpromazine we co-cultured bone marrow-derived lineage-Sca-1$^+$CD117$^+$ (LSK) cells, the most versatile progenitors, which in similar conditions develop to nearly all hematopoietic lineages (albeit with different kinetics), and assessed how chlorpromazine affects development of various lymphoid and non-lymphoid cells. To this end, LSK co-cultured on OP9-DL1 cells gave rise to all pre-TCR independent thymocyte populations in an indistinguishable
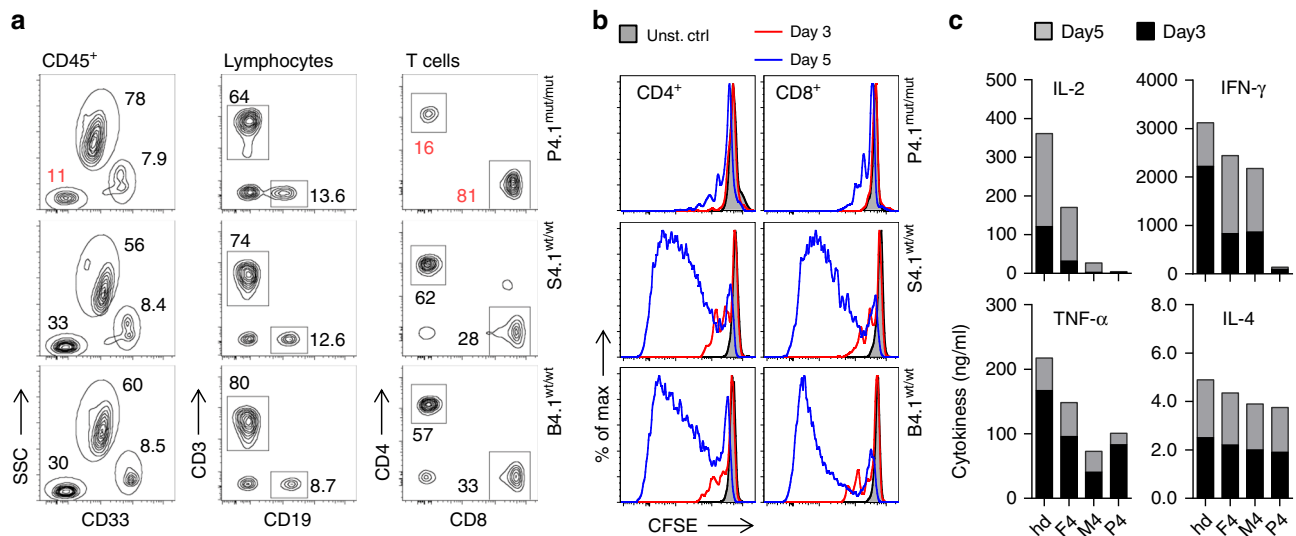
Fig. 6 Patient-associated mutation in *FCHO1* gene alters development and activation of T lymphocytes. a Density plots of blood leucocytes (CD45+) of the index case (upper row) homozygous for a mutation in the *FCHO1* locus and her siblings carrying the heterozygous mutation (middle and bottom rows). T helper cells were defined as CD45hiCD33−SScloCD3+CD4+ and cytotoxic T cells were CD45hiCD33−SScloCD3+CD8+. Numbers adjacent to the gates indicate percentages. **b** Histograms of CFSE-labelled T lymphocytes stimulated with anti-CD3 and anti-CD28 Ab for 3 (red line) or 5 (blue line) days. Unstimulated controls are depicted in grey. **c** Cytokine production by lymphocytes of patient and family members after anti-CD3 and anti-CD28 stimulation for the indicated periods of time. IL-2, IFN-γ, TNF-α and IL-4 were determined using cytometric bead assays. **a–c** Data are representative of two independent experiments, except data of day 3 shown in **c**, which was assessed once. Source data are provided as a Source Data file.

manner irrespective of presence or absence of chlorpromazine (Fig. 7b). Similarly, presence or absence of chlorpromazine in LSK and OP9 co-culture did not interfere with development of neither B220+CD19+ B-cell committed progenitors nor CD11b+Gr-1+ neutrophilic granulocytes (Fig. 7c, d).

Thus, chlorpromazine, a chemical inhibitor of CME, shows rather selective effects on the DN3-DP transition of thymocyte differentiation, known to be particularly vulnerable to disturbances of pre-TCR-signalling strength[36,37]. Taken together, these data indirectly support our concept that T-cell differentiation in FCHO1 deficiency is at least partially dependent on perturbed TCR internalisation/signalling.

Discussion

Here, we identify autosomal recessive FCHO1 deficiency as a human genetic defect associated with combined immunodeficiency (CID). We show that six different mutations in the *FCHO1* gene, either point mutations resulting in amino acid substitutions, premature stop codons or affecting pre-mRNA splicing are deleterious for FCHO1 function. T-cell deficiency predisposes affected patients to severe and persistent viral and fungal infections. Hypogammaglobulinemia is seen in all patients, except G1. It remains currently unclear whether B-cell defects are intrinsic or strictly dependent on defective T cells.

FCHO1 deficiency predisposes not only to infections but also to lymphoma[13]. Several patients died secondary to malignancies before definitive therapy in form of an allogeneic hematopoietic stem cell transplant could be done. Thus, FCHO1 deficiency warrants rapid genetic diagnosis and provision of access to definitive cure.

Our studies have provided insights into the structural and functional biology of FCHO1. In a structure-guided prediction, Ma and colleagues[14] concluded that a minimum of two aa substitutions in FCHO1 (at positions K877E + R879A), located directly in the peptide-binding groove, are required to abolish interaction of the domain with its main interacting partner EPS15. Here, we show that a single substitution at R679P,

spatially distant from the groove, is sufficient to severely alter this interaction. Although localised opposite of the groove, replacement of the charged side chain of Arg with a nonpolar and rigid ring of Pro is sufficient to alter the domain function. Three mutations resulting in a premature stop codon at the beginning of μHD domain further strengthen their significance for FCHO1 function. Alterations in the F-BAR domain also prove to be deleterious, yet in a different mode. Substitution of Ala at position 34 with Pro, a known alpha-helix breaker, leads to dissociation of the FCHO1 homodimers from the plasma membrane and hence abolishes the function. Although not directly tested, it is plausible that alternative splicing resulting in loss of 51 aa located within the F-BAR domain disrupts the protein structure. From a clinical point of view, the severity of the immunodeficiency, however, cannot directly be correlated to the type of the *FCHO1* mutation.

Given the central role of FCHO1 for the formation of clathrin-coated pits and endocytosis it is surprising that FCHO1 deficiency results in T-cell immunodeficiency rather than more global defects of development. In contrast, *Caenorhabditis elegans* deficient for FCHO show body malformation and uncoordinated locomotion[38]. FCHO interacts with AP-2 and induces a conformational change, leading to AP-2 activation. Mutations in either FCHO or AP-2 result in a strikingly similar phenotype, indicating that the severe defects seen in FCHO-deficient worms are caused by aberrant activation of AP-2. In vertebrates, however, the interplay between AP-2 and FCHO is more complex. Morpholino-mediated knock-down of Fcho1 in *Danio rerio* causes dorsoventral patterning defects and severe malformation at an early developmental stage, whereas transcriptional silencing of Fcho2 is associated with notochord and somite malformations[38]. In zebrafish, AP-2 deficiency results in a more severe, broader and earlier developmental phenotype than combined Fcho1/2 deficiency, suggesting that AP-2 function is, at least in part, Fcho1/2-independent[39]. The idea that the functional relevance of FCHO has changed during evolution is supported by the observation that a) two FCHO paralogs have emerged[40] and b) FCHO may act as receptor-specific adaptors (e.g., BMP-mediated signalling in zebrafish) rather than universally
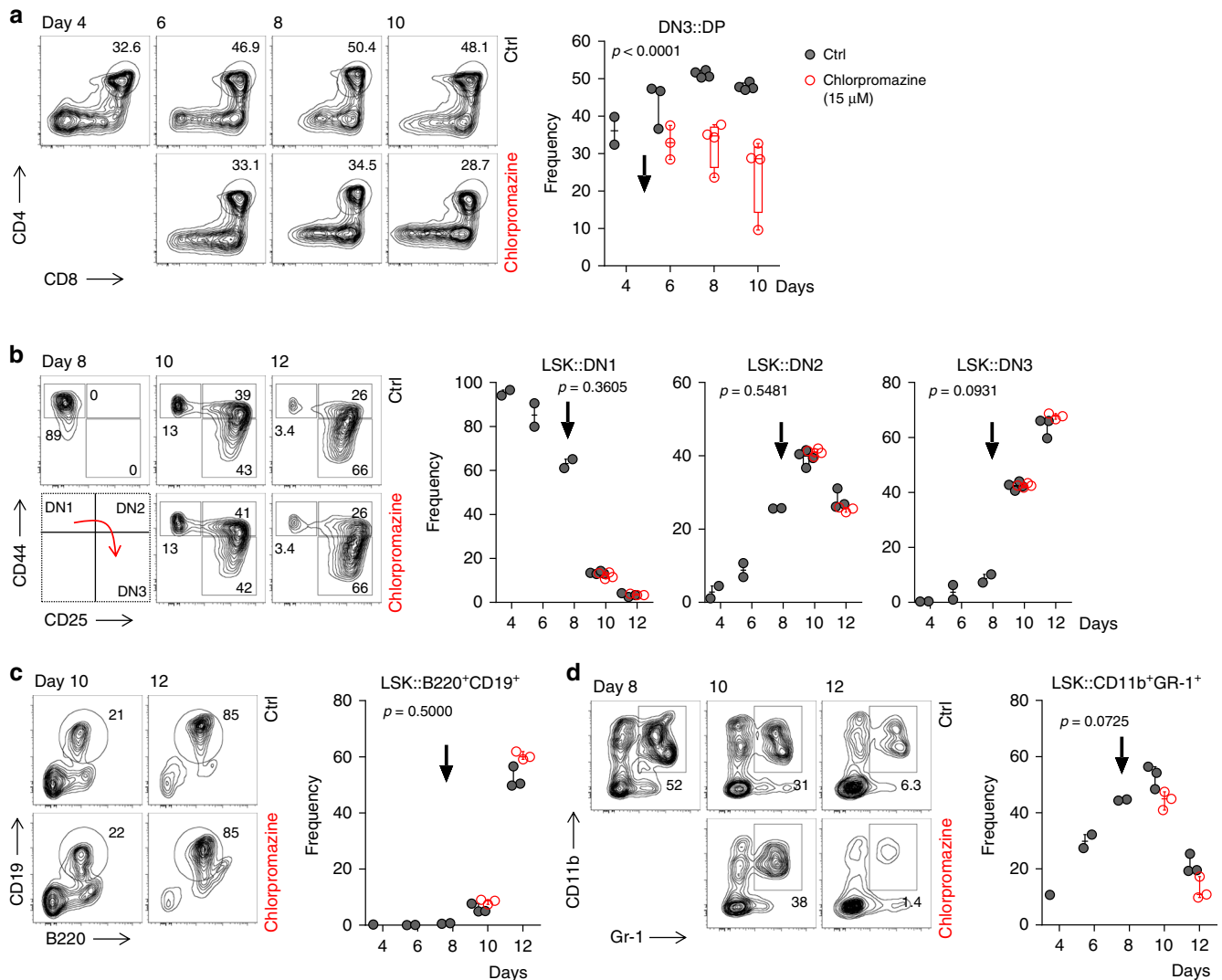
Fig. 7 Chlorpromazine-induced inhibition of CME arrests development of thymocytes. a Thymi-derived double-negative three progenitors (DN3: CD4$^-$CD8$^-$CD44$^+$CD25$^-$) were sorted and cultured on OP9-DL1 stroma cells in the presence of Flt-3L, SCF and IL-7. At day 5 of co-culture cells were left untreated (ctrl) or treated with chlorpromazine (15 μM) to partially inhibit CME (chlorpromazine IC$_{50}$ for CME was established at 17.4 μM[35]). Subsequently, development of double-positive (DP: CD4$^+$CD8$^+$) progenitors was assessed by FACS (left) and quantified (right). **b** Bone marrow-derived LSK progenitors (lineage$^-$Sca-1$^+$CD117$^+$) were sorted and cultured on OP9-DL1 stroma cells in the presence of Flt-3L, SCF and IL-7. Analogous to **a**, at day 8 of culture cells were left untreated (ctrl) or treated with 15 μM chlorpromazine. Effect of partial CME inhibition on early-thymocyte development was assessed by FACS. Double-negative (DN) cells were defined as follows: DN1-CD44$^+$CD25$^-$; DN2-CD44$^+$CD25$^+$ and DN3-CD44$^-$CD25$^+$. **c, d** Bone marrow-derived LSK progenitors (lineage$^-$Sca$^+$1$^-$CD117$^+$) were sorted and cultured on OP9 stroma cells in the presence of Flt-3L, SCF and IL-7. At day 8 of culture cells were left untreated (ctrl) or treated with chlorpromazine (15 μM) to partially inhibit CME. Subsequently, development of **c** B-cell committed progenitors defined as B220$^+$CD19$^+$ and **d** granulocytes (CD11b^{int-hi}Gr-1$^+$) was assessed by FACS (left) and quantified (right). **a–d** Density FACS plots and charts are representative of two independent experiments where one to four wells were measured at each indicated time point. Number adjacent or within the gates indicate frequency. Each dot on the chart represents one well. Whiskers indicate the range (min to max). Arrows indicate time points when chlorpromazine was added. Statistical analysis was performed using two-way ANOVA (p-values for effect of chlorpromazine). Source data are provided as a Source Data file.

important initiators of clathrin-mediated endocytosis[39]. This notion is also supported by the lack of functional consequences of FCHO1 deficiency observed on both VSV-G-mediated virus entry and TfR endocytosis in T cells. Both processes strictly rely on CME[27,33], but are apparently not affected in FCHO1-deficient cells. We conclude that FCHO1 deficiency does not generally affect cellular processes that require CME, underscoring a selective role of FCHO1.

This concept is further corroborated by a series of other studies focusing on central elements orchestrating clathrin-mediated endocytosis. Defects in prime molecules such as clathrin, epsin, AP-2 and dynamin, result in embryonic lethality in model organisms (reviewed in ref. [5]). Mutations in proteins that are deemed to

be less pivotal for the clathrin-mediated endocytosis have been linked to a variety of diseases such as cancer, neuro-psychiatric disorders, metabolic syndromes, but not to inherited defects of the immune system[8]. Of note, a large number of FCHO1 and FCHO2 interacting partners have been identified, yet none of them have been linked to the adaptive immune system[5,25,38,39,41,42].

The quality of signal transmitted by pre-T-cell receptor (pre-TCR) and TCR is essential for T-cell development and homoeostasis. During T-cell ontogeny, there are three stages in which such signal is critically required for selection, differentiation and commitment of developing thymocytes, respectively (reviewed in refs. [43,44]).

The precise localisation of the TCR that is continuously internalised and recycled back to the plasma membrane is of critical importance for the quality of signal transduction. The TCR can be internalised via clathrin-dependent[19–21,45] or clathrin-independent mechanisms[46]. This process may be ligand-dependent or ligand-independent[19,20,22,44,47,48]. Even though previous studies have linked TCR internalisation to a di-leucine sorting motif present in the CD3γδ subunit of the TCR:CD3 complex[49,50], we could not provide definitive evidence that FCHO1 directly binds to the CD3γδ sorting motifs. Nevertheless, we have shown that FCHO1 deficiency results in impaired TCR internalisation. Our data thus suggest that (a) we were not in the position to prove FCHO1/CD3 interaction using crude biochemical methods or (b) that FCHO1 interacts with other membrane-bound molecules to indirectly induce TCR internalisation.

In theory, FCHO1-dependent TCR internalisation can serve several purposes: (1) activation signals could be amplified via the scaffolding on early endosomes, (2) activation signals could be attenuated via lysosomal degradation of the TCR or (3) recirculation of the TCR to immune synapses via recycling endosomes may modulate TCR-dependent activation signals upon encountering antigen presenting cells. Integrating signal strengths relies on spatiotemporal organisation of the TCR and associated signalling molecules. Although the quality of the signal provided by TCR is essential for the outcome of thymopoiesis, our studies in FCHO1 deficiency do not provide definitive answers on detailed mechanisms of FCHO1 in T-cell differentiation. Indirectly, the link between CME and TCR-signalling is highlighted by our in vitro T-cell differentiation studies. In the presence of chlorpromazine, a chemical inhibitor of CME, we observed a rather specific effect of differentiation blockade at the DN3-DP transition. This step is known to be highly dependent on TCR-signalling strength[36,37].

Very recently, Calzoni et al.[51] published a short letter and reported biallelic mutations in FCHO1 in four families. The phenotypes of these patients resembled the phenotype of our patients, but no functional experiments or proof-of-causality was provided. Based on experiments in activated T-cell blasts, the authors concluded that in the absence of FCHO1, CME is globally affected. In contrast, our data support the concept that FCHO1 does not globally affect CME.

In sum, our studies unravel a previously unrecognised role of FCHO1 in orchestrating the T-cell development and function. Our discovery also exemplifies how systematic studies of patients with inherited disorders help to uncover genes and pathways that were previously not associated with the function of the immune system. FCHO1 deficiency thus highlights a critical role of clathrin-mediated endocytosis for the development and function of human T cells.

Methods

Patients. Patients were referred to the clinical and scientific team of Professor Christoph Klein for further investigations. Informed consent/assent for the genetic and immunological studies, as well as their publication was obtained from all legal representatives and patients. Genetic and functional studies on biosamples from patients and their relatives were performed under the framework of a scientific project entitled "Genetic characterisation of congenital bone marrow failure and immunodeficiency syndromes". This study was approved in 2011 by the ethics committee at LMU (438-11) and includes permission to publish the results.

Whole-exome sequencing and variant filtering. For family A we performed whole-exome sequencing (WES) for patient and father using Agilent V4 + UTR library preparation and a SOLiD sequencing platform. WES for the patient from the family B, the patient from family C, as well as for patient, mother and siblings (from family D) was performed after Agilent library preparation (V5 + UTR or V6 + UTR (SY265)) using an IlluminaNextSeq 500 platform. BWA (version 0.7.15) was used to align short reads to the human reference genome Grch37.p13. Variants were called and recalibrated according to the best practice pipeline by GATK (version 3.6). The final variants were then annotated with VEP release 85. A custom in-house database was used to filter variants to be rare (not reported in gnomAD or ExAC), as well as severe effects according to the Ensembl guidelines.

Effects of filtered variants on protein were predicted with SIFT[52] and PolyPhen-2[53]. The remaining variants were compiled and filtered for rare homozygous and compound heterozygous mutations following a pattern of autosomal recessive inheritance. Whole-exome sequencing of genomic DNA of kindred F patients was conducted using Illumina sequencing platforms. Bioinformatics analysis for detection of rare sequence variants following Mendelian inheritance patterns were performed as described previously[54].

Sanger sequencing. *FCHO1* Sanger sequencing was performed to confirm WES-detected variants and their segregation with the clinical phenotype across the family members. Genomic DNA was PCR-amplified using OneTaq Polymerase (NEB), specific primers are provided in Supplementary Table 3. Amplicons were sequenced either in-house or by using the commercial service of Eurofins Genomics.

Structural analysis of FCHO1 mutants. Crystal structures of FCHO1 domain were modelled using PyMol software with the mutalyzer wizard[55]. Mu homology domain of *Danio rerio* with bound Eps15 peptide (5JP2; https://doi.org/10.2210/pdb5JP2/pdb) and human FCHO2 F-Bar domain (2v0O; https://doi.org/10.2210/pdb2V0O/pdb) were chosen as template for structure modelling. To calculate effect of point mutations on the structures, rotamer configurations of the highest probability were chosen.

Cell lines. The SK-MEL-2 cell line, engineered using zinc finger nucleases (ZNF) genome editing to stably express RFP under the endogenous human clathrin light chain A locus (CLTA-RFP), was kindly provided by David G. Drubin, University of Berkeley[15]. The cell line with only one RFP-tagged CLTA locus was used to minimise putative side effects. Cells were maintained in Dulbecco's modified Eagle medium (DMEM)/F12 medium (ThermoFisher Scientific) supplemented with 10% fetal calf serum (FCS) (ThermoFisher Scientific), 100 U/ml of both penicillin and streptomycin (Gibco). Jurkat cells were purchased from ATCC, USA. They were maintained in RPMI1640 medium (ThermoFisher Scientific) supplemented with 10% FCS (ThermoFisher Scientific), 100 U/ml of both penicillin and streptomycin (Gibco) and 2 mM glutamine (Gibco). In all, 100 U/ml of penicillin and streptomycin (Gibco) HEK293T cells and NIH-3T3 cells (both from DSMZ–German Collection of Microorganisms and Cell Cultures) were maintained in DMEM (ThermoFisher Scientific) supplemented with 10% FCS (ThermoFisher Scientific), 100 U/ml each of penicillin and streptomycin (Gibco). Patient fibroblasts were grown in Iscove's Modified Dulbecco's Medium supplemented with 10% FCS. EBV-LCL were maintained in RPMI with 10% FCS. All cell lines were routinely tested for mycoplasma and were mycoplasma-negative throughout the study.

Plasmid DNA cloning. Full-length cDNA of the human *FCHO1* isoform b (IMAGE 5757146), cloned into the pEGFP-C3 vector with modified MCS (EcoRI/SalI) was kindly provided by Emmanuel Boucrot (UCL London) and Harvey McMahon (MRC-LMB, Cambridge, UK)[5]. Patient mutations were introduced by site-directed PCR mutagenesis using Q5 site-directed mutagenesis kit (NEB) according to manufacturer's instruction with specific primers designed with NEBase Changer (NEB). Wt and mutated *FCHO1* cDNAs were cloned as either GFP fusion proteins or as IRES-containing bicistronic lentiviral pRRL vectors with or without GFP as a reporter gene, respectively. Full-length cDNA of human clathrin light chain tagged with mRFP was kindly provided by Klemens Rottner from Technical University in Braunschweig[56]. It was cloned to lentiviral pRRL vector for production of virus particles. The correctness of the sequences was routinely monitored by Sanger sequencing.

CRISPR/Cas9 genome editing. The genomic locus of *FCHO1* (transcript ENST00000594202.1) was designated for gene disruption by inducing double-strand breaks in exon 7 (T1: 5′-GGACGTTCTCCGCTACGGCG AGG-3′) and intron 7 (T2: 5′-GTGTCGTGGGCGCCGCCCAG CGG-3′). Genome editing of SK-MEL-2 and Jurkat cells was done cells using the Alt-R CRISPR-Cas9 technology (IDT technology, Belgium). Upon coincubation of crRNA and ATTOTM 550 (ATTO-TEC, Germany) fluorescent dye-labelled tracRNA, the RNA duplexes were electroporated into target cells along with Cas9 nuclease (SG Cell Line 4D-Nucleofector X Kit and 4D-NucleofectorTM System Lonza, Switzerland). Red fluorescent protein (RFP)-positive cells were single-sorted using a BD FACSAria flow sorter (BD Bioscience, USA).

As endogenous expression of FCHO1 is too low for faithful assessment by western blot, deletion of FCHO1 was confirmed by PCR. The following primer pair was used for validation: (F: 5′-GTGAGCCTGATGAACCCTGGGTGTG-3′, R: 5′-TGCATGTGGGTGACAGAGTGAGAC-3′). Cells carrying homozygous mutations are expected to have a long deletion, spanning between exon 7 and intron 7. A minimum of five clones carrying homozygous mutations resulting in frameshift were used for subsequent experiments (Supplementary Fig. 12). Unmodified clones were used as a FCHO1-positive control. To ensure deletion specificity, the ten most probable off-target sites were tested using direct Sanger sequencing, showing no signs of unspecific cuts.

Transient transfection. FCHO1 ko SK-MEL-2 cells and FCHO1 ko Jurkat cells were transfected using calcium phosphate transfection kit (Sigma, USA) and 0.1–1 µg of the various lentiviral plasmids carrying either wt or mutant FCHO1 cDNAs. Cells were typically incubated 24 h to express the constructs before imaging.

Lentiviral vector particles production and cell transduction. For production of vesicular stomatitis virus G glycoprotein (VSV-g)-pseudotyped lentiviral particles HEK293T cells were transfected using calcium phosphate transfection kit (Sigma, USA) and 5 µg respective lentiviral vector, 12 µg pcDNA3.GP.4xCTE (which expresses HIV-1 gag- pol), 5 µg pRSV-Rev and 1.5 µg pMD.G (which encodes VSV-g) in the presence of 25 µM chloroquine (Sigma, USA). Eight hours after transfection, medium was exchanged and supernatant containing lentiviral particles was collected after 24, 48 and 72 h post transfection. Viral titre were determined on 3T3 cells.

FCHO1 ko SK-MEL-2 cells and FCHO1 ko Jurkat cells were transduced with lentiviral particles through centrifugation at $900 \times g$ for 4 h at 32 °C in the presence of polybrene (8 µg/ml) (Sigma, USA).

Production of HIV-1 stocks. The HIV-1$_{NL4-3}$wt plasmid was obtained from Nathaniel Landau (Alexandria Centre for Life Science, NYU, USA), the HIV-1$_{NL4-3}$ΔEnv plasmid was a kind gift of Oliver T. Fackler (Universitätsklinikum Heidelberg, Germany) and the BlaM-Vpr plasmid was a gift from Thomas J. Hope (Northwestern University, Chicago, USA). HIV-1$_{NL4-3}$ΔEnv and HIV-1$_{NL4-3}$ΔEnv (BlaM-Vpr), both VSV-G pseudotyped, or HIV-1$_{NL4-3}$wt (BlaM-Vpr) stocks were produced by PEI co-transfection of HEK293T cells. Forty-eight hours later, supernatants were collected and filtered through a 0.45 µm Stericup (Millipore). After sucrose cushion (25% in 1x phosphate-buffered saline (PBS_) purification at 24,000 rpm at 4 °C for 1.5 h (Sorvall WX + Ultra series; rotor: SW32, Beckmann Coulter), virus pellets were resuspended in PBS and stored at −80 °C until use.

Immunoprecipitation and western blot. To test for protein–protein interactions, FCHO1-deficient cell lines were used. SK-MEL-2 cells overexpressing different variants of GFP-FCHO1 fusion proteins were starved in serum-free medium for 1 h at 37 °C prior the assay. Jurkat lines were starved for 1 h and subsequently stimulated with an α-CD3 antibody (OKT3, 1 mg/ml, BD Biosciences) cross-linked by a goat α-mouse polyclonal antibody (0.5 mg/ml, Jackson ImmunoResearch) for 2 to 20 min at 37 °C. Stimulation was terminated by addition of ice-cold PBS. Cell pellets were lysed in RIPA buffer containing phenylmethylsulfonyl fluoride protease inhibitors for 30 min in cold. Next, the supernatants were collected for further analysis. GFP-tagged FCHO1 proteins were pulled-down by GFP-Trap magnetic beads (ChromoTek GmbH) and N' or C' Flag-tagged FCHo1 by anti-Flag M2 Affinity Gel (Sigma). After incubation, beads were collected and washed two times in RIPA buffer and the pellet was boiled in sample buffer containing SDS for 10 min at 95 °C. Equal amounts of protein were separated by SDS polyacrylamide gel electrophoresis and blotted onto polyvinylidene difluoride (PVDF) membranes using the Trans-Blot Turbo Transfer System (Bio-Rad). Membranes were blocked for 1 h at room temperature in 5% non-fat milk before staining. Following primary antibodies were used: FCHO1–rabbit, polyclonal, PA5-31603, lot Q12081994A, Thermo Scientific or rabbit, polyclonal, 84740, lot GR214150−4, Abcam; EPS15–rabbit, clone D3K8R, Cell Signalling; EPS15R–rabbit, clone EP1146Y, Abcam; adaptin–mouse, clone AP6, Abcam; CD3epsilon–rat, clone OKT3, ThermoFisher Scientific; CD3delta–rabbit, polyclonal, ThermoFisher Scientific; CD3 gamma–rabbit, polyclonal, ThermoFisher Scientific; GAPDH–mouse, clone 6C5, Santa Cruz. All antibodies used are summarised in Supplementary Table 4.

After washing in PBS-T, the PVDF membranes were exposed to horseradish peroxidase-conjugated secondary anti-mouse (BD), anti-rat (CS), or anti-rabbit (CST) Ig antibodies for 1 h at room temperature (RT). Western blots were detected using a chemiluminescent substrate (Pierce Technology) and images were captured on a Chemidoc XRS Imaging System (Bio-Rad Laboratories). Blots were stripped between exposures to different antibodies using a Restore Western Blot Stripping Buffer (Thermo Scientific). Data analysis was performed using Quantity One or Image Lab software (Bio-Rad Laboratories). Uncropped immunoblots are shown in Supplementary Figures.

Confocal microscopy analysis of fixed samples. To minimise dominant-negative effects on CCP dynamics resulting from prolonged overexpression of FCHO1 protein, only FCHO1-deficient SK-MEL-2 cell line transiently transduced with N-terminally tagged versions of GFP-FCHO1 were used for experiments. Cells with a low expression of FCHO1 were analysed typically 16 to 20 h post transfection. Cells were plated on glass coverslips (Karl Hecht, 0.13–0.16 mm thickness, diameter 20 mm) in 24-well tissue culture plates and cultured in complete DMEM/F12 medium for min 12 h to facilitate attachment. Coverslips were rinsed with PBS and fixed with 3% formaldehyde (Electron Microscopy Sciences) for 10 min at RT. Next, cells were washed in PBS and autofluorescence was quenched for 15 min using 50 mM NH$_4$Cl at RT. Coverslips were washed once in PBS and incubated for 30 min at RT in PBS containing 0.1% (w/v) bovine serum albumin (BSA; Sigma Aldrich), 0.05% (w/v) saponin (Sigma Aldrich). Further blocking solution was removed and cells were stained with the following primary antibodies: rabbit-α-Eps15 (clone D3K8R, Cell Signalling) or mouse-α-Adaptin (AP6, Abcam) at 4 ºC, overnight.

Subsequently, cells were washed in PBS containing 0.05% (w/v) saponin (Sigma Aldrich), three times for 5 min each. The following secondary antibodies coupled to fluorochromes were used: goat-α-rabbit IgG, AlexaFluor 405 (Invitrogen) and goat-α-mouse IgG, AlexaFluor 633 (Invitrogen).

WGA (wheat germ agglutinin) staining was performed on transfected cells fixed with 3% formaldehyde (Electron Microscopy Sciences) for 10 min at RT. After extensive washing with phenol red free 1xHBSS, WGA conjugated to AlexaFluor 633 (Invitrogen) was added to the cells at concentration 1.25 µg/ml (in phenol red free 1xHBSS) and incubated for 5 min.

Some samples were co-stained with 300 nM DAPI (Invitrogen) for 2 min at RT. Cells were mounted on glass slides using Fluoromount-G (SouthernBiotech) and dried at RT in darkness for minimum 12 h before imaging. Samples were analysed by confocal fluorescent microscopy using the Zeiss LSM880 and Zeiss LSM800 inverted microscopes. Images were collected using 63×/1.4 NA or 40×/1.4 NA oil objectives (Zeiss). Four solid-state 5 and 10 mW laser (405, 488, 561, 640 nm) were used as light source; scanner frequency was 400 Hz; line-averaging 2. All images were obtained with GaAsP high-sensitivity detectors. Pearson correlation or co-localisation coefficient was assessed on 16-bits raw digital files on Zen Blue software (Zeiss). Representative cells from two to three independent experiments were chosen for analysis. Two to four 25 µm^2 square regions were selected and minimum ten cells per condition were analysed. To avoid bias during analysis, only one fluorescent channel was active while selecting regions.

Live-cell imaging. For live-cell imaging experiments stably transduced SK-MEL-2 cell lines were used. Cells were seeded on µ-dish 35 mm, high Glass Bottom (IBIDI, glass coverslip no.1.5 H, selected quality, 170 µm + /− 5 µm) in complete DMEM/F1224h before imaging. Medium was exchanged directly before start of the experiment. During the experiment dishes were placed into a temperature-controlled chamber on the microscope stage with 95% air, 5% CO$_2$ and 100% humidity. Live-cell imaging data were acquired using a fully motorised inverted confocal microscope (Zeiss LSM800) using either 40×/1.4 NA or 63 × /1.4 NA oil objectives (Zeiss) under control of Definite Focus for Axio Observer Z1 (Zeiss). Sixteen-bits digital images were obtained with GaAsP high-sensitivity detectors, confocal module and 488 and 561 nm laser lines and a dual (525/50; 605/70) BP filters. Cell regions were selected to allow for 500–950 ms-lasting intervals. Time dependence of the fluorescent intensity of FCHo1 and endogenous clathrin were assessed on movies from three independent experiments, using Zen Blue software (Zeiss). Up to three 25 µm^2 regions per cells were quantified. Both GFP and RFP channels were normalised to the background and initial fluorescence was set to 1.

Fusion of VSV-G pseudotyped HIV-1 ΔEnv to Jurkat T cells. The virion fusion assay was performed in principle as reported[29] employing HIV-1 particles carrying the HIV-1 Vpr protein fused to β-lactamase (BlaM-Vpr). In brief, after fusion of virus particles to target cells, the incorporated BlaM-Vpr protein is released into the cytoplasm and is able to cleave the CCF2 dye. This leads to a shift of the dye's emission maximum from 520 to 447 nm, which can be detected and quantified by flow cytometry. Jurkat T cells were plated at a density of 2×10^5 cells per well (96-well conical plate, Corning, New York, USA). Where indicated, the HIV-1 fusion inhibitor T20 (50 µM, enfuvirtide, Roche, Rotkreuz, Switzerland) was added 1 h prior to virus challenge. Serial dilutions of VSV-G HIV-1$_{NL4-3}$ΔEnv (BlaM-Vpr) were performed in PBS. 4 h following challenge with either VSV-G HIV-1$_{NL4-3}$ ΔEnv (BlaM-Vpr) or HIV-1$_{NL4-3}$ (BlaM-Vpr), Jurkat T cells were washed and incubated with the CCF2 dye as previously reported[30,31]. The following day, cells were fixed for 90 min with 4% PFA/PBS and analysed by flow cytometry.

Infection of Jurkat T cells with VSV-G HIV-1 ΔEnv. Jurkat T cells were plated at a density of 2×10^5 cells per well. T20 (50 µM), the V-ATPase inhibitor bafilomycin A1 (100 nM, Sigma Aldrich, St. Louis, USA) or PBS were added 1 h prior to virus challenge. Cells were challenged with VSV-G HIV-1$_{NL4-3}$ΔEnv and 4 h later, 200 µl of fresh culture medium were added. 48 h later, cells were fixed for 90 min in 4% PFA/PBS and HIV infection was monitored using an intracellular p24 staining (anti-p24 antibody, clone KC57-FITC, Beckmann Coulter, Brea, USA) in principle as reported[32].

Transferrin uptake. Fibroblasts from healthy donor (HD) and patient (kindred E) were detached using PBS containing 10 mM EDTA and serum-starved for 30 min in DMEM at 37 °C. Cells and transferrin conjugated to AlexaFluor 633 (ThermoFisher Scientific) were washed in glucose buffer (PBS supplemented with 20 mM Glucose and 1% BSA) and cooled down on ice. 25 µg/ml AlexaFluor 633-conjugated transferrin were added to cells and incubated on ice for 10 min. Cells were then transferred to 37 °C for indicated periods of time. Upon indicated time, surface-bound transferrin was stripped by acid wash (PBS supplemented with 0.1 M glycine and 150 mM NaCl at pH 3) and uptake of fluorescent transferrin was determined by flow cytometry. Data are pooled from four independent experiments. Error bars indicate mean ± SD. Statistical analysis using two-way ANOVA followed by Sidak's multiple comparisons test revealed no significant difference in transferrin uptake between HD and patient fibroblasts.

Flow cytometry. Blood samples were washed with PBS and stained with the following antibodies for 20 min at RT: α-CD45 BV711 or APC (HI30), α-CD33 PE-Cy7 (P67.6), α-CD3 PE (HIT3a), α-CD19 FITC (HIB19), α-CD8α APC (RPA-T8), α-CD4 PE-Cy7 (A161A1) all from Biolegend. All antibodies used are summarised in Supplementary Table 4. Red blood cells were lysed using 1 × BD FACS Lysing Solution (BD Biosciences) according to the manufacturer's instructions. The samples were acquired using a LSRFortessa (BD Bioscience) cytometer. Data were analysed using FlowJo Software (TreeStar), v9 and v10. Gating strategy to assess frequency of blood leucocytes is shown in Supplementary Fig. 13. Virion fusion and HIV infection of Jurkat T cells were recorded on a BD FACSLyric (BD Biosciences, Franklin Lakes, USA).

In vitro stimulation of PBMCs. PBMC were isolated from blood samples by Ficoll-Hypaque (Pharmacia) density gradient centrifugation. Cells were labeled with 1 μM CFSE (eBioscience) according to the manufacturer's protocol. They were resuspended in complete RPMI1640, plated on 96-well flat bottom plates and stimulated with α-CD3-coupled beads (bio-α-CD3, clone OKT3 (eBioscience) coupled with α-biotin MACSiBeads (MiltenyiBiotec)) at a ratio 10:1, in the presence of 1 mg/ml of soluble α-CD28, clone CD28.2 (eBioscience). Proliferative response was measured after 3 and 5 days. Gating strategy to assess T-cell proliferation is shown in Supplementary Fig. 14. Supernatants (four technical replicates) were tested for the presence of IL-2, IL-4, IFN-γ and TNF-α using human FlowCytomix beads (eBioscience) according to the manufacturer's instructions.

Assessment of intracellular calcium flux. Up to five different FCHO1-sufficient or -deficient Jurkat clones were incubated for 1 h in Ca^{2+}- and Mg^{2+}-free Dulbecco's serum-free medium (Invitrogen) at room temperature at a density of 10^7 cells/ml. Cells were then loaded with Ca^{2+}-sensitive dyes, either Indo-1 or Fluo-4 (3 μM) and FuraRed (6 μM) for 45 min at 37 °C. Further, cells were rested for 30–45 min at 37 °C. After establishing a baseline for 30 s, cells were stimulated with α-CD3 antibody (OKT3, 1 mg/ml, BD Biosciences) and goat-α-mouse polyclonal antibody (0.5 mg/ml, Jackson ImmunoResearch) to allow cross-linking and data acquisition was continued for four additional minutes. To ensure cell viability, 1 min before the end of acquisition, 2 μg/ml ionomycin (Sigma) was added as positive Ca^{2+}-flux control. Gating strategy to assess Ca^{2+} release is shown in Supplementary Fig. 15.

TCR internalisation assays on Jurkat cell lines. Confocal microscopy: FCHO1-sufficient or -deficient, or stably transduced (with wt or mutant FCHO1 viruses) Jurkat FCHO1$^{-/-}$ cell lines were used to visualise TCR internalisation. Cells were plated on poly-D-lysine (0.1 mg/ml, Sigma Aldrich) and α-CD3 (clone OKT3, 0.5 mg/ml, eBioscience) coated glass coverslips (Karl Hecht, 0.13-0.16 mm thickness, diameter 20 mm) in 24-well tissue culture plates and incubated for indicated time points. Coverslips were rinsed with PBS and cells were fixed in 3% formaldehyde (Electron Microscopy Sciences) for 10 min at RT. Next, cells were washed in PBS and autofluorescence was quenched for 15 min at RT using 50 mM NH_4Cl. Coverslips were washed once in PBS and incubated for 30 min at RT in PBS containing 0.1% (w/v) BSA (Sigma Aldrich), 0.05% (w/v) saponin (Sigma Aldrich). Further, blocking solution was removed and cells were stained with mouse-α-CD3 (OKT3, eBioscience) and goat-α-mouse IgG, AlexaFluor 633 (Invitrogen). Samples were co-stained with 300 nM DAPI (Invitrogen) for 2 min at RT. Cells were mounted on glass slides using Fluoromount-G (SouthernBiotech) and dried at RT in darkness for at least 12 h before imaging. Samples were analysed by confocal fluorescent microscopy using the ZEISS LSM800 inverted microscopes (ZEISS) as described above. We used Fiji software[57] to quantify the number of CD3 puncta/cell. The number of puncta/cell was averaged on several random fields of view.

Flow cytometry: FCHO1-sufficient or -deficient Jurkat cells were stained with α-CD3 Ab (OKT3) in cold and TCR internalisation was assessed over time at 37 °C in the presence of anti-mouse F(ab')2 fragments labelled with Ax647. After 2, 5, 15, 45 and 60 min of stimulation the remaining surface TCRs were stripped, thus fluorescent signal corresponds only to the internalised TCR. Gating strategy to assess TCR internalisation is shown in Supplementary Fig. 16.

Statistics. Statistical analysis was performed using GraphPadPrism software v.6. Pearson correlation and colocalization coefficient on selected cell fragments were assessed on raw files using Zen Blue software (Zeiss). Cell regions or entire cells are referred to as n unless indicated otherwise. No method of randomisation was used, and no samples were excluded from analysis. To avoid bias during analysis, cell regions were selected based on the signal from only one fluorescent channel. No statistical method was used to predetermine sample size for analyses. Two-way analysis of variance (ANOVA) or ANOVA analysis followed by Sidak's multiple comparison test were used to assess differences between groups. p-values < 0.05 were considered to be statistically significant.

Reporting summary. Further information on research design is available in the Nature Research Reporting Summary linked to this article.

Data availability

References

1. Roth, T. F. & Porter, K. R. Yolk protein uptake in the oocyte of the mosquito *Aedes Aegypti. L. J. Cell Biol.* **20**, 313–332 (1964).
2. Pearse, B. Clathrin: a unique protein associated with intracellular transfer of membrane by coated vesicles. *Proc. Natl Acad. Sci. USA* **73**, 1255–1259 (1976).
3. Robinson, M. S. Forty years of clathrin-coated vesicles. *Traffic* **16**, 1210–1238 (2015).
4. Cocucci, E., Aguet, F., Boulant, S. & Kirchhausen, T. The first five seconds in the life of a clathrin-coated pit. *Cell* **150**, 495–507 (2012).
5. Henne, W. M. et al. FCHo proteins are nucleators of clathrin-mediated endocytosis. *Science* **328**, 1281–1284 (2010).
6. Pechstein, A. et al. Regulation of synaptic vesicle recycling by complex formation between intersectin 1 and the clathrin adaptor complex AP2. *Proc. Natl Acad. Sci. USA* **107**, 4206–4211 (2010).
7. Di Paolo, G. & De Camilli, P. Phosphoinositides in cell regulation and membrane dynamics. *Nature* **443**, 651–657 (2006).
8. McMahon, H. T. & Boucrot, E. Molecular mechanism and physiological functions of clathrin-mediated endocytosis. *Nat. Rev. Mol. Cell Biol.* **12**, 517–533 (2011).
9. Dannhauser, P. N. & Ungewickell, E. J. Reconstitution of clathrin-coated bud and vesicle formation with minimal components. *Nat. Cell Biol.* **14**, 634–639 (2012).
10. Koh, T. W. et al. Eps15 and Dap160 control synaptic vesicle membrane retrieval and synapse development. *J. Cell Biol.* **178**, 309–322 (2007).
11. Kostmann, R. Hereditär reticulos––en ny systemsjukdom. *Sven. Läkartidningen* **47**, 2861 (1950).
12. Bruton, O. C. Agammaglobulinemia. *Pediatrics* **9**, 722–728 (1952).
13. Picard, C. et al. International union of immunological societies: 2017 primary immunodeficiency diseases committee report on inborn errors of immunity. *J. Clin. Immunol.* **38**, 96–128 (2018).
14. Ma, L. et al. Transient Fcho1/2Eps15/RAP-2 nanoclusters prime the AP-2 clathrin adaptor for cargo binding. *Dev. Cell* **37**, 428–443 (2016).
15. Doyon, J. B. et al. Rapid and efficient clathrin-mediated endocytosis revealed in genome-edited mammalian cells. *Nat. Cell Biol.* **13**, 331–337 (2011).
16. Lyszkiewicz, M. et al. miR-181a/b-1 controls thymic selection of Treg cells and tunes their suppressive capacity. *PLoS Biol.* **17**, e2006716 (2019).
17. Zietara, N. et al. Critical role for miR-181a/b-1 in agonist selection of invariant natural killer T cells. *Proc. Natl Acad. Sci. USA* **110**, 7407–7412 (2013).
18. Gaud, G., Lesourne, R. & Love, P. E. Regulatory mechanisms in T cell receptor signalling. *Nat. Rev. Immunol.* **18**, 485–497 (2018).
19. Telerman, A. et al. Internalization of human T lymphocyte receptors. *Eur. J. Immunol.* **17**, 991–997 (1987).
20. Dietrich, J., Hou, X., Wegener, A. M. & Geisler, C. CD3 gamma contains a phosphoserine-dependent di-leucine motif involved in down-regulation of the T cell receptor. *EMBO J.* **13**, 2156–2166 (1994).
21. Boyer, C. et al. T cell receptor/CD3 complex internalization following activation of a cytolytic T cell clone: evidence for a protein kinase C-independent staurosporine-sensitive step. *Eur. J. Immunol.* **21**, 1623–1634 (1991).
22. Crotzer, V. L., Mabardy, A. S., Weiss, A. & Brodsky, F. M. T cell receptor engagement leads to phosphorylation of clathrin heavy chain during receptor internalization. *J. Exp. Med.* **199**, 981–991 (2004).
23. Dietrich, J., Kastrup, J., Nielsen, B. L., Odum, N. & Geisler, C. Regulation and function of the CD3gamma DxxxLL motif: a binding site for adaptor protein-1 and adaptor protein-2 in vitro. *J. Cell Biol.* **138**, 271–281 (1997).
24. Balagopalan, L., Barr, V. A. & Samelson, L. E. Endocytic events in TCR signaling: focus on adapters in microclusters. *Immunol. Rev.* **232**, 84–98 (2009).
25. Reider, A. et al. Syp1 is a conserved endocytic adaptor that contains domains involved in cargo selection and membrane tubulation. *EMBO J.* **28**, 3103–3116 (2009).
26. Apel, A. R. et al. Syp1 regulates the clathrin-mediated and clathrin-independent endocytosis of multiple cargo proteins through a novel sorting motif. *Mol. Biol. Cell* **28**, 2434–2448 (2017).

27. Finkelshtein, D., Werman, A., Novick, D., Barak, S. & Rubinstein, M. LDL receptor and its family members serve as the cellular receptors for vesicular stomatitis virus. *Proc. Natl Acad. Sci. USA* **110**, 7306–7311 (2013).

28. Kim, I. S. et al. Mechanism of membrane fusion induced by vesicular stomatitis virus G protein. *Proc. Natl Acad. Sci. USA* **114**, E28–E36 (2017).

29. Cavrois, M., De Noronha, C. & Greene, W. C. A sensitive and specific enzyme-based assay detecting HIV-1 virion fusion in primary T lymphocytes. *Nat. Biotechnol.* **20**, 1151–1154 (2002).

30. Michel, N., Allespach, I., Venzke, S., Fackler, O. T. & Keppler, O. T. The Nef protein of human immunodeficiency virus establishes superinfection immunity by a dual strategy to downregulate cell-surface CCR5 and CD4. *Curr. Biol.* **15**, 714–723 (2005).

31. Venzke, S., Michel, N., Allespach, I., Fackler, O. T. & Keppler, O. T. Expression of Nef downregulates CXCR4, the major coreceptor of human immunodeficiency virus, from the surfaces of target cells and thereby enhances resistance to superinfection. *J. Virol.* **80**, 11141–11152 (2006).

32. Homann, S. et al. Determinants in HIV-1 Nef for enhancement of virus replication and depletion of CD4+ T lymphocytes in human lymphoid tissue ex vivo. *Retrovirology* **6**, 6 (2009).

33. Mayle, K. M., Le, A. M. & Kamei, D. T. The intracellular trafficking pathway of transferrin. *Biochim Biophys. Acta* **1820**, 264–281 (2012).

34. Schmitt, T. M. & Zuniga-Pflucker, J. C. Induction of T cell development from hematopoietic progenitor cells by delta-like-1 in vitro. *Immunity* **17**, 749–756 (2002).

35. Daniel, J. A. et al. Phenothiazine-derived antipsychotic drugs inhibit dynamin and clathrin-mediated endocytosis. *Traffic* **16**, 635–654 (2015).

36. von Boehmer, H. Unique features of the pre-T-cell receptor alpha-chain: not just a surrogate. *Nat. Rev. Immunol.* **5**, 571–577 (2005).

37. Gascoigne, N. R., Rybakin, V., Acuto, O. & Brzostek, J. TCR signal strength and T cell development. *Annu Rev. Cell Dev. Biol.* **32**, 327–348 (2016).

38. Hollopeter, G. et al. The membrane-associated proteins FCHo and SGIP are allosteric activators of the AP2 clathrin adaptor complex. *Elife* **3**, 1–23 (2014).

39. Umasankar, P. K. et al. Distinct and separable activities of the endocytic clathrin-coat components Fcho1/2 and AP-2 in developmental patterning. *Nat. Cell Biol.* **14**, 488–501 (2012).

40. Dergai, M., Iershov, A., Novokhatska, O., Pankivskyi, S. & Rynditch, A. Evolutionary changes on the way to clathrin-mediated endocytosis in animals. *Genome Biol. Evol.* **8**, 588–606 (2016).

41. Mulkearns, E. E. & Cooper, J. A. FCH domain only-2 organizes clathrin-coated structures and interacts with Disabled-2 for low-density lipoprotein receptor endocytosis. *Mol. Biol. Cell* **23**, 1330–1342 (2012).

42. Henne, W. M. et al. Structure and analysis of FCHo2 F-BAR domain: a dimerizing and membrane recruitment module that effects membrane curvature. *Structure* **15**, 839–852 (2007).

43. Brownlie, R. J. & Zamoyska, R. T cell receptor signalling networks: branched, diversified and bounded. *Nat. Rev. Immunol.* **13**, 257–269 (2013).

44. Miosge, L. & Zamoyska, R. Signalling in T-cell development: is it all location, location, location? *Curr. Opin. Immunol.* **19**, 194–199 (2007).

45. Ohno, H. et al. Interaction of tyrosine-based sorting signals with clathrin-associated proteins. *Science* **269**, 1872–1875 (1995).

46. Compeer, E. B. et al. A mobile endocytic network connects clathrin-independent receptor endocytosis to recycling and promotes T cell activation. *Nat. Commun.* **9**, 1597 (2018).

47. Monjas, A., Alcover, A. & Alarcon, B. Engaged and bystander T cell receptors are down-modulated by different endocytic pathways. *J. Biol. Chem.* **279**, 55376–55384 (2004).

48. Finetti, F., Onnis, A. & Baldari, C. T. Regulation of vesicular traffic at the T cell immune synapse: lessons from the primary cilium. *Traffic* **16**, 241–249 (2015).

49. Krangel, M. S. Endocytosis and recycling of the T3-T cell receptor complex. The role of T3 phosphorylation. *J. Exp. Med.* **165**, 1141–1159 (1987).

50. Dietrich, J. et al. Ligand-induced TCR down-regulation is not dependent on constitutive TCR cycling. *J. Immunol.* **168**, 5434–5440 (2002).

51. Calzoni, E. et al. F-BAR domain only protein 1 (FCHO1) deficiency is a novel cause of combined immune deficiency in human subjects. *J. Allergy Clin. Immunol.* **143**, 2317–2321 e12 (2019).

52. Kumar, P., Henikoff, S. & Ng, P. C. Predicting the effects of coding non-synonymous variants on protein function using the SIFT algorithm. *Nat. Protoc.* **4**, 1073–1081 (2009).

53. Adzhubei, I., Jordan, D. M. & Sunyaev, S. R. Predicting functional effect of human missense mutations using PolyPhen-2. *Curr. Protoc. Hum. Genet.* **Chapter 7**, Unit7.20 (2013).

54. Field, M. A., Cho, V., Andrews, T. D. & Goodnow, C. C. Reliably detecting clinically important variants requires both combined variant calls and optimized filtering strategies. *PLoS ONE* **10**, e0143199 (2015).

55. DeLano, W. L. Pymol: an open-source molecular graphics tool. *CCP4 Newsl. Protein Crystallogr.* **40**, 82–92 (2002).

56. Benesch, S. et al. N-WASP deficiency impairs EGF internalization and actin assembly at clathrin-coated pits. *J. Cell Sci.* **118**, 3103–3115 (2005).

57. Schindelin, J. et al. Fiji: an open-source platform for biological-image analysis. *Nat. Methods* **9**, 676–682 (2012).

Acknowledgements

Author contributions

M.Ł. and N.Z. initiated the project, designed the studies, performed experiments and analysed the data (pedigrees A-D); L.F. performed IP and microscopy experiments, analysed the data (pedigrees A-D); U.P. designed and performed experiments, analysed the data (pedigree F); M.S performed HIV infection experiments and analysed the data; Y.L. designed and performed CRISPR/Cas9 knockout experiments; Y.F. performed IP experiments (pedigrees A-D); J.P. and S.H. performed bioinformatical analysis of WES data (pedigrees A-D); I.S. performed genotyping and WB experiments, analysed the data (pedigree E); M.R. performed Sanger sequencing and in silico prediction analyses of mutations (pedigrees A-D); K.-W.S. provided clinical data (pedigree A); O.T.K designed and analysed HIV infection experiments; E.Ü provided patient material, clinical data (pedigree C); M.K., T.P. provided patient material, clinical data (pedigree B, D); A.L., A.S. and R.S. provided patient material, clinical data and genetic analysis (pedigree E); M.H. J.R. and K.S. designed the studies, provided patient material, clinical data and genetic analysis (pedigree F and G); C.Ke. and E.K. performed family analyses, RNA and protein detection (Pedigree F). C.K. initiated the project, designed the studies and provided clinical and laboratory resources; (pedigrees A-E); M.Ł., N.Z. and C.K. wrote the manuscript.

Competing interests

The authors declare no competing interests.

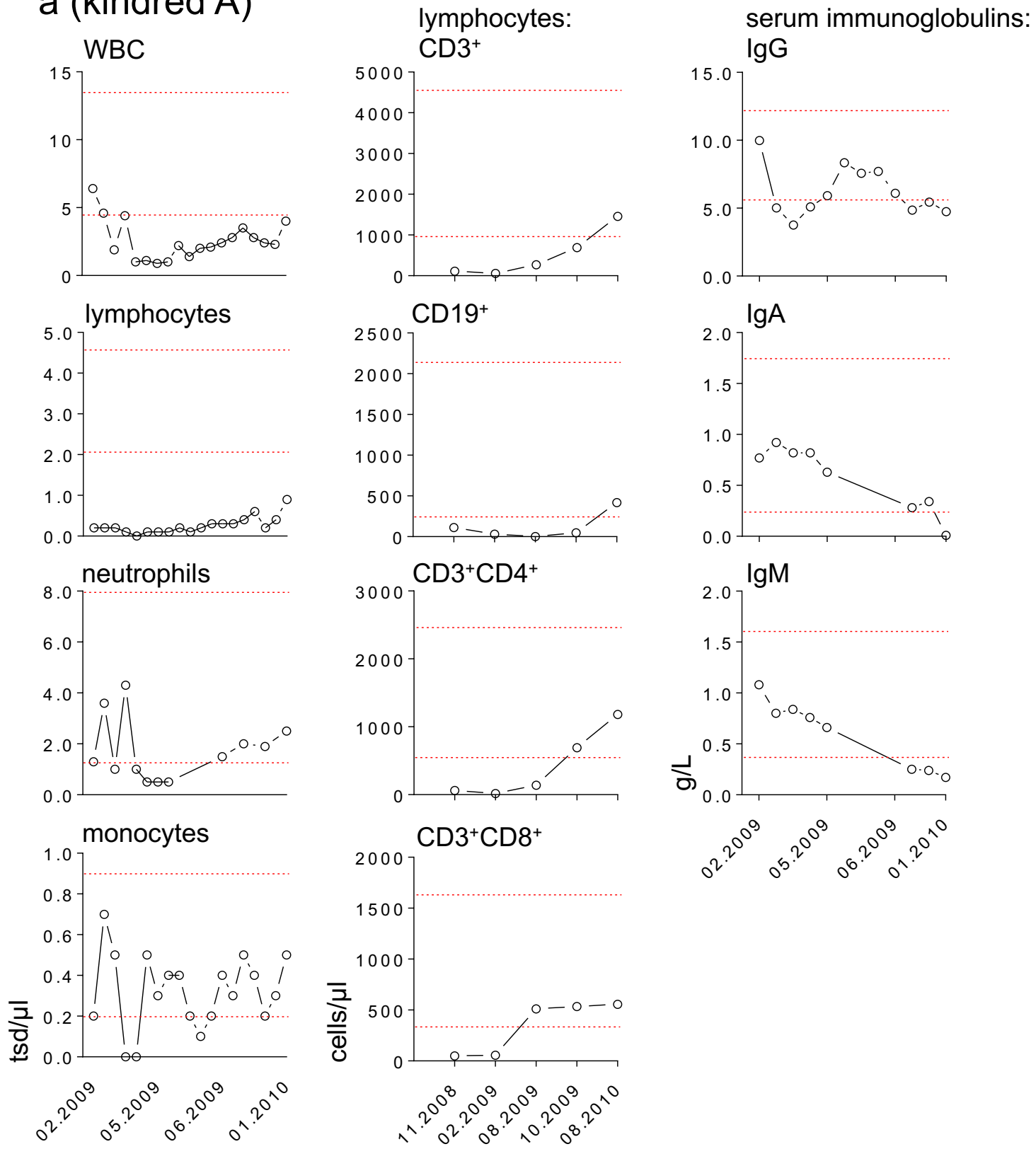## Additional information

Human FCHO1 deficiency reveals role for clathrin-mediated endocytosis in development and function of T cells
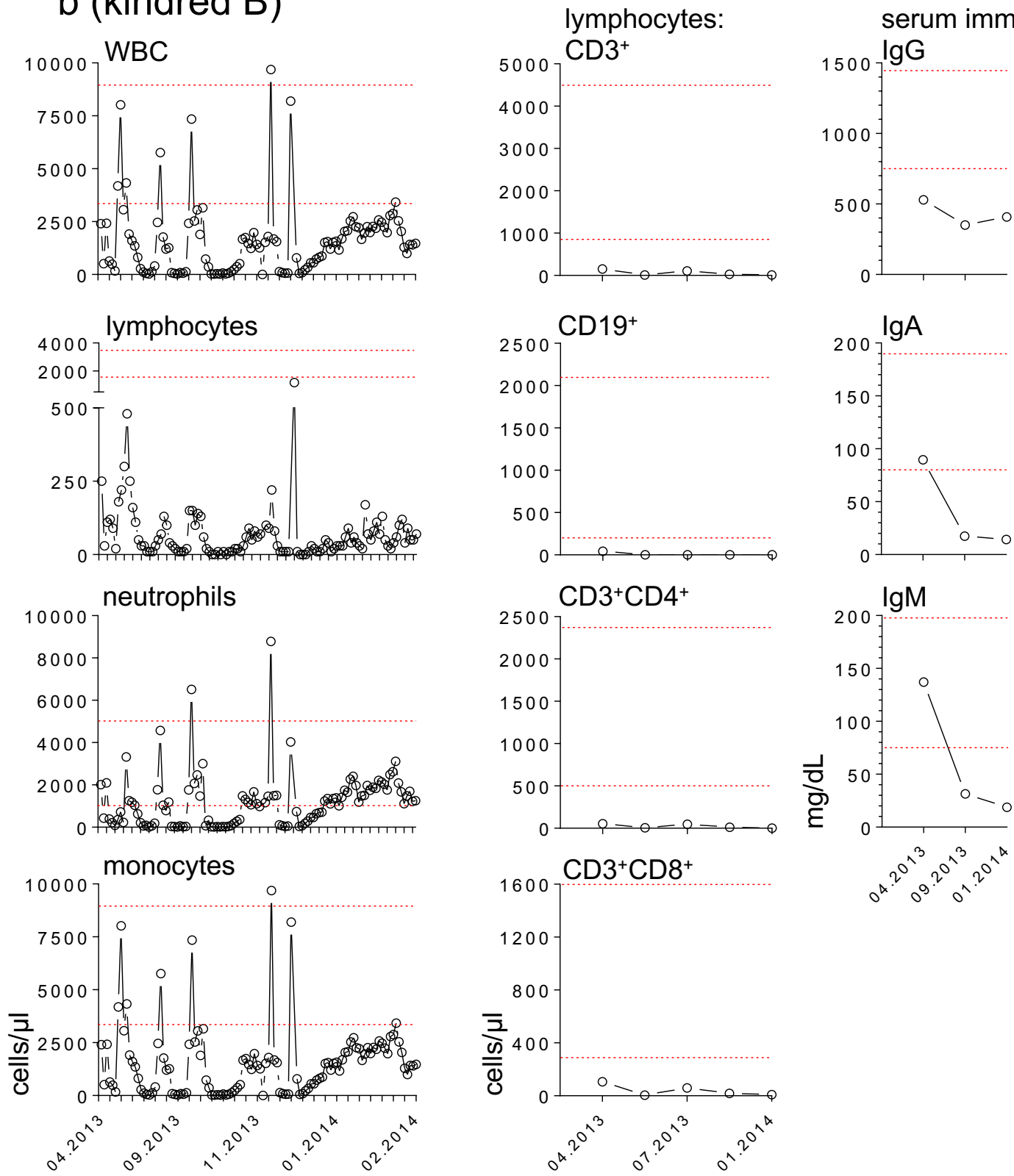
Łyszkiewicz and Ziętara et al.
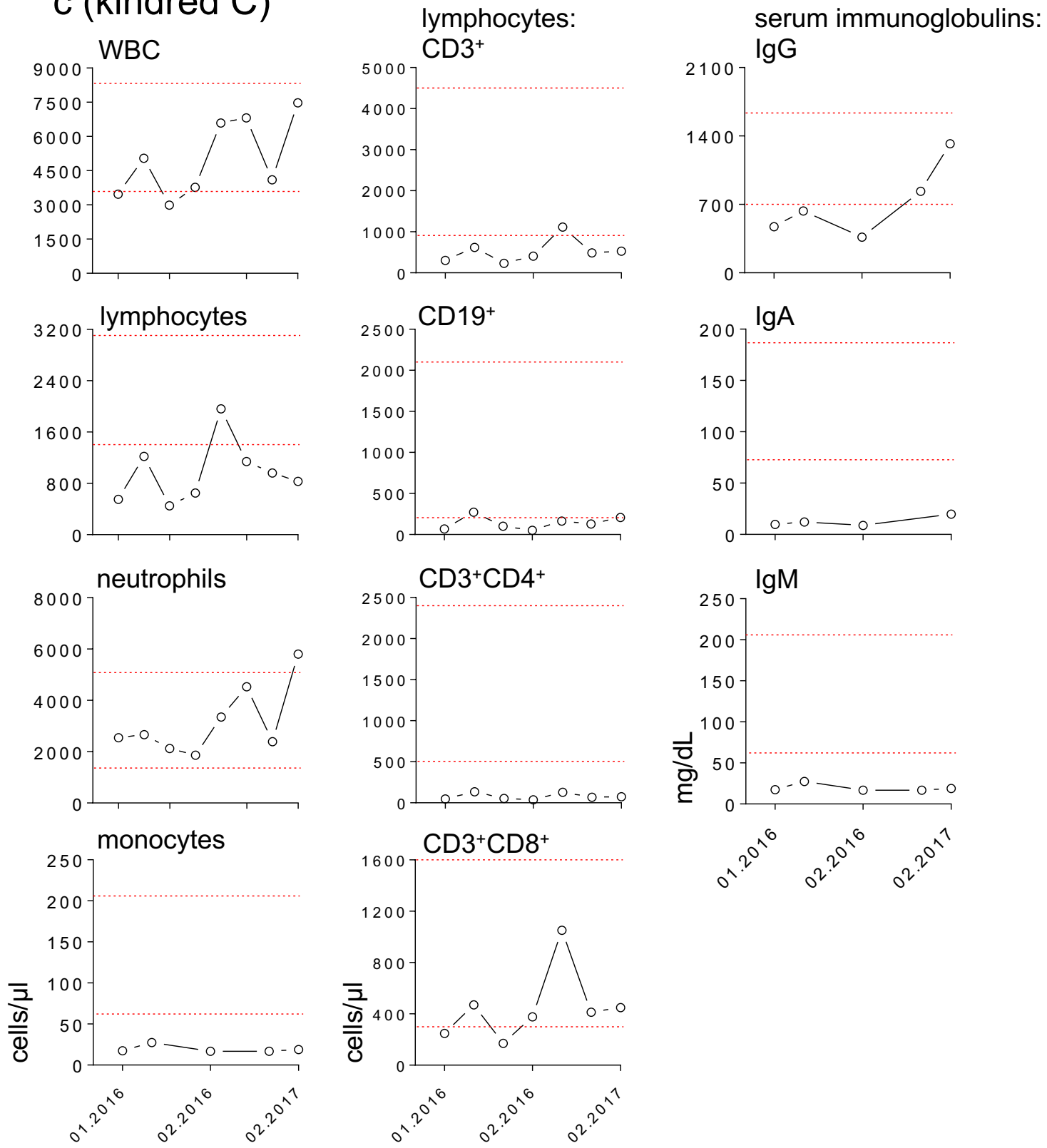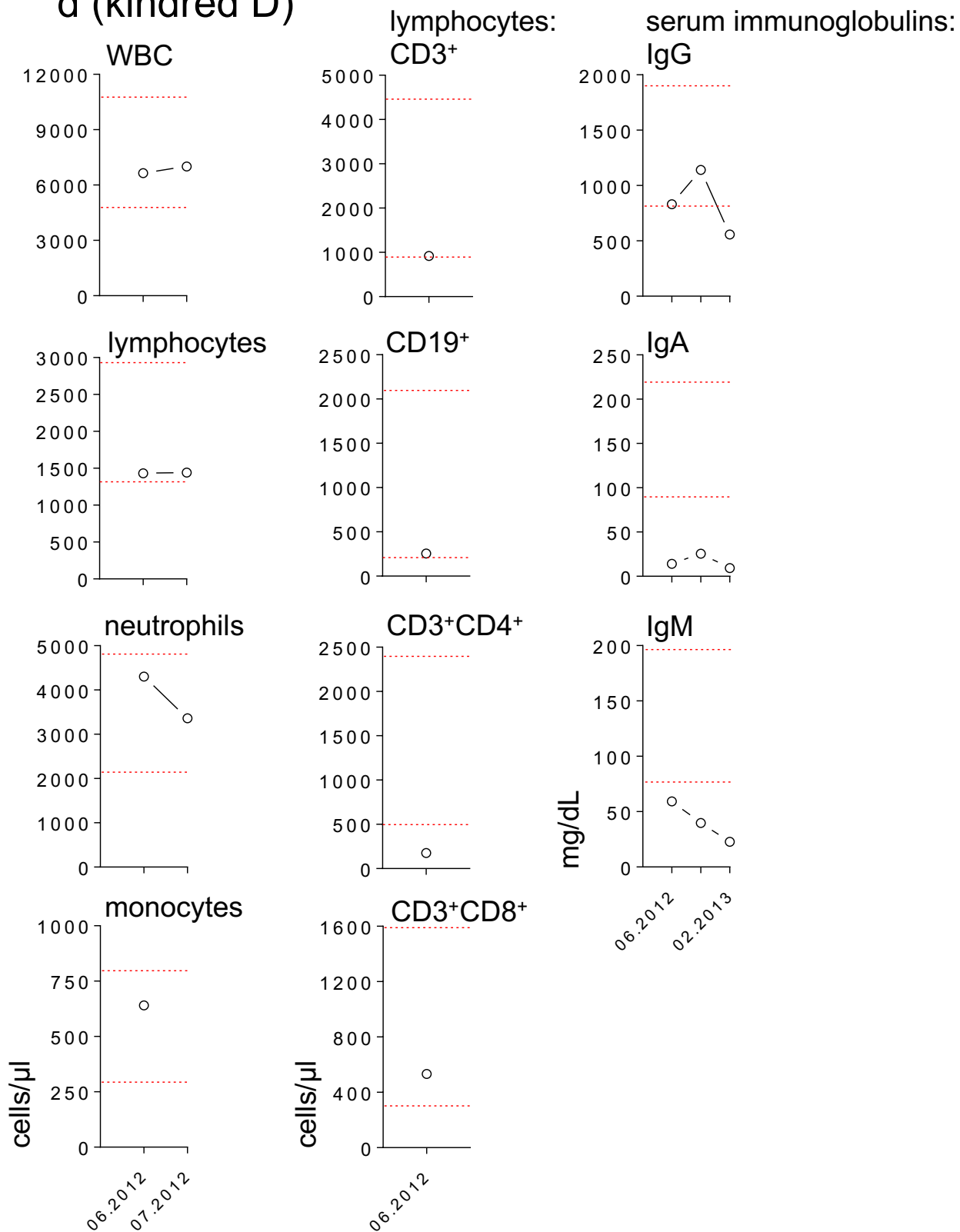
Sup Figure 1
a (kindred A)

Sup Figure 1
b (kindred B)

Sup Figure 1
c (kindred C)

WBC

lymphocytes: CD3⁺

serum immunoglobulins: IgG

lymphocytes

CD19⁺

IgA

neutrophils

CD3⁺CD4⁺

IgM

monocytes

CD3⁺CD8⁺

Supplementary Figure 1. SCID-like lymphopenia phenotype in patients carrying homozygous mutations in the *FCHO1* locus. (a-d) Absolute numbers of total white blood cells (WBC) and main populations of leukocytes (left column), main populations of peripheral blood lymphocytes (central column) and serum immunoglobulins (right column) of index cases from kindred A to D. (a) Please note recovery of both T and B lymphocytes upon allogeneic hematopoietic stem cell transplantation (indicated by arrow). The normal range of serum immunoglobulin levels can be attributed to IVIg therapy. (a-d) All presented data were obtained from certified clinical diagnostic laboratories. Red lines on charts show the normal range.
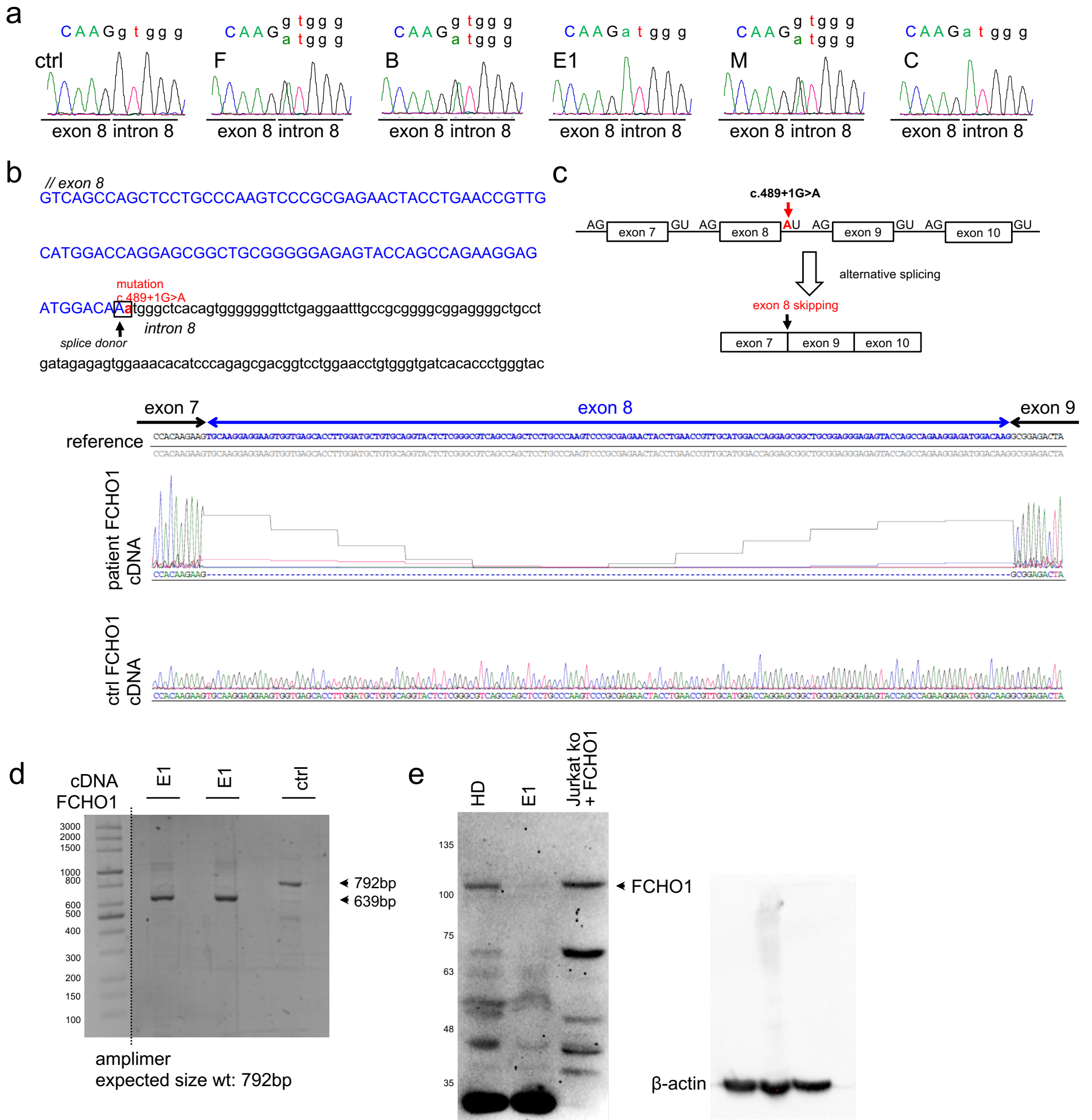
Supplementary Figure 2. Kindred E-associated mutation affects FCHO1 splicing. (a) Sanger sequencing chromatograms indicating a homozygous mutation in exon 7 of index patient c.489+1G>A. (b) A sequence of pre-spliced mRNA with indicated mutation (red). (c) Scheme showing the putative effect of c.489+1G>A mutation on mRNA splicing. Please note skipping of 153 nucleotides of exon 8, resulting in an in-frame protein shortened by 51 aa (6 kDa). (d) FCHO1 cDNA from patient fibroblasts (E1). Wild-type and alternatively spliced cDNA fragments are indicated with arrows. (e) FCHO1 Western blot performed on lysates of a healthy donor and patient fibroblasts.
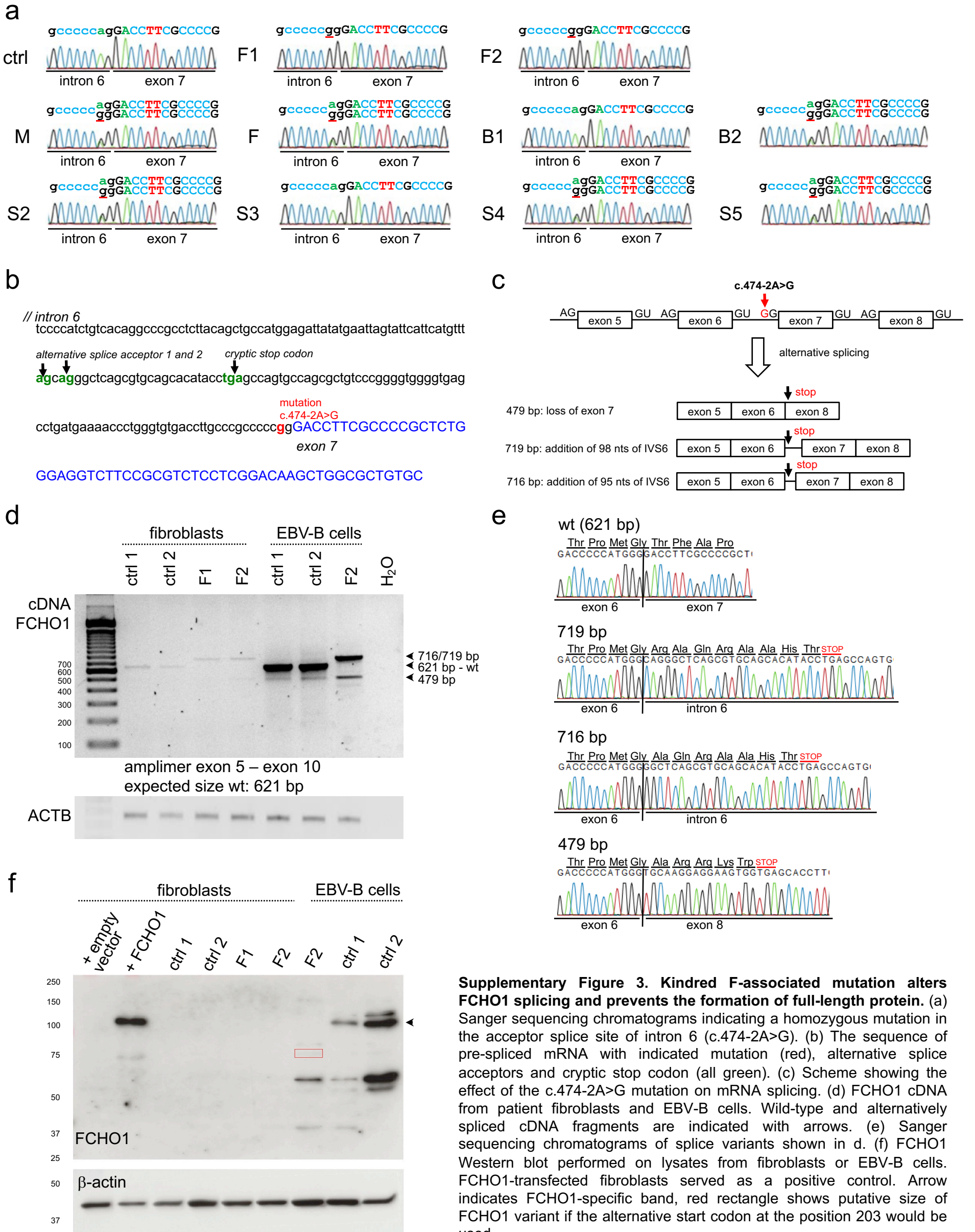
Supplementary Figure 3. Kindred F-associated mutation alters FCHO1 splicing and prevents the formation of full-length protein. (a) Sanger sequencing chromatograms indicating a homozygous mutation in the acceptor splice site of intron 6 (c.474-2A>G). (b) The sequence of pre-spliced mRNA with indicated mutation (red), alternative splice acceptors and cryptic stop codon (all green). (c) Scheme showing the effect of the c.474-2A>G mutation on mRNA splicing. (d) FCHO1 cDNA from patient fibroblasts and EBV-B cells. Wild-type and alternatively spliced cDNA fragments are indicated with arrows. (e) Sanger sequencing chromatograms of splice variants shown in d. (f) FCHO1 Western blot performed on lysates from fibroblasts or EBV-B cells. FCHO1-transfected fibroblasts served as a positive control. Arrow indicates FCHO1-specific band, red rectangle shows putative size of FCHO1 variant if the alternative start codon at the position 203 would be used.
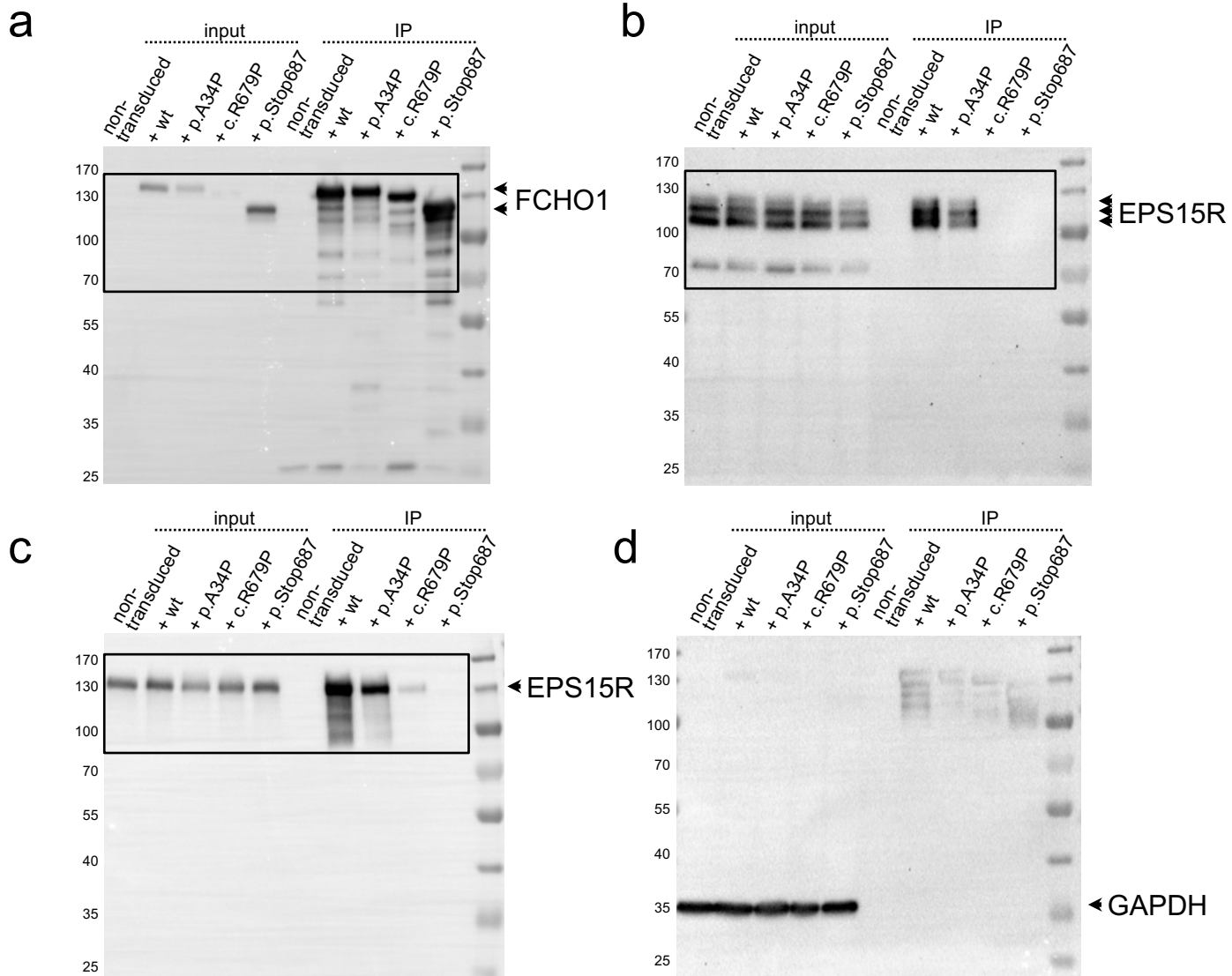
Supplementary Figure 4. Uncropped Western blots images corresponding to data shown in Figure 2. Frames show the fragments displayed in the main figure. The molecular mass of proteins is shown in kDa.
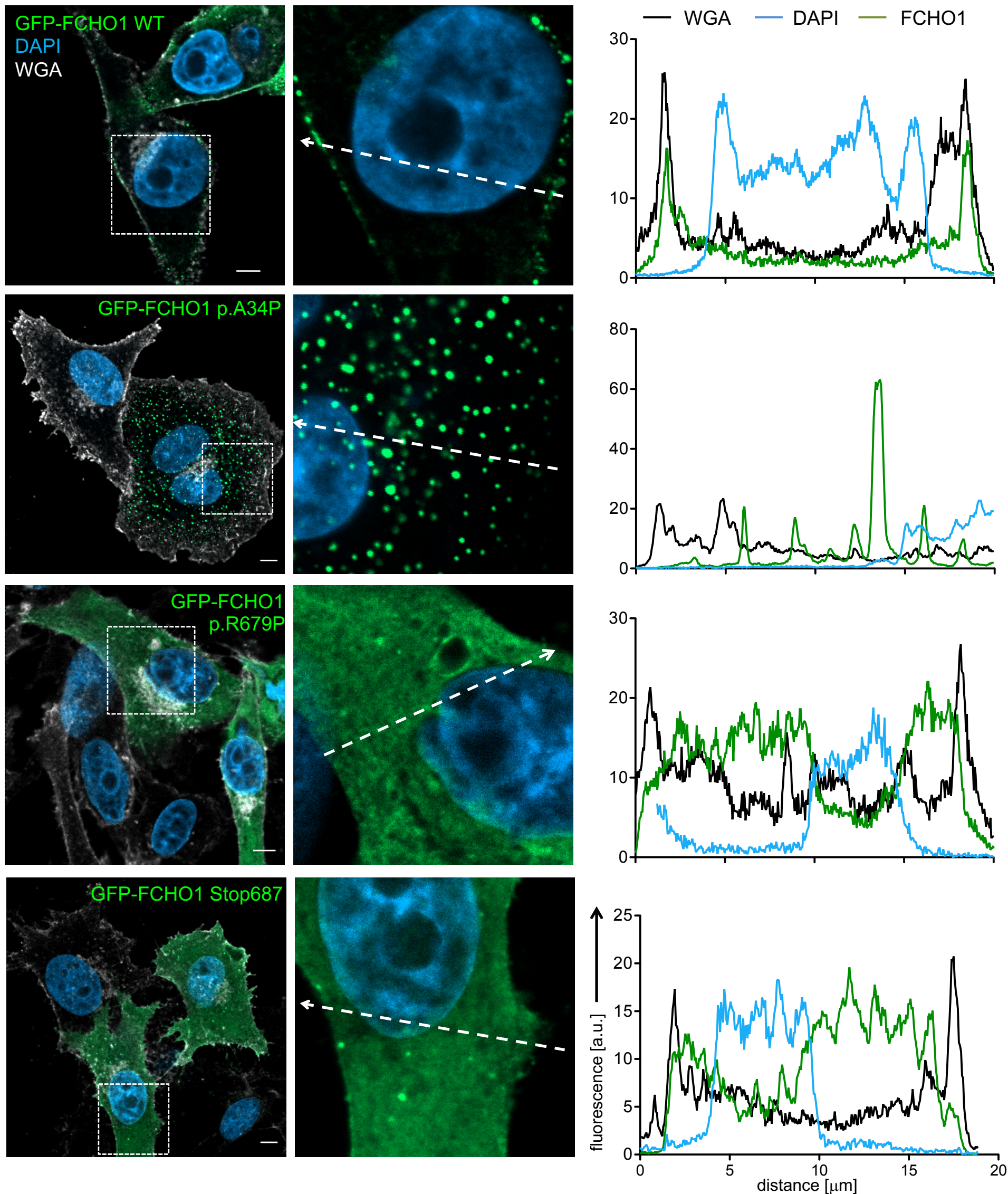
Supplementary Figure 5. Mutations in FCHO1 lead to dissociation of protein from the plasma membrane, yet do not affect overall plasma membrane organization. FCHO1$^{-/-}$ SK-MEL-2 cells were transiently transfected with GFP-fusion protein constructs, carrying indicated mutants of FCHO1 (green on both image and fluorescence plots). Cells were co-stained with WGA (Wheat Germ Agglutinin) conjugated to Alexa Fluor 647 (white on the image, black line on the fluorescence plot) to visualize plasma membrane and DAPI (blue on both image and fluorescence plots) to visualize nucleus. Only wt GFP-FCHO1 almost perfectly correlates with WGA staining of the plasma membrane, whereas both F-BAR domain (pA34P) and µHD domain (p.R679P and Stop687) mutants do not, and the p.A34P mutant is completely dissociated from the plasma membrane (second panel from the top). Data are representative of two independent experiments (two independent transfections). Scale bars 5 µm, enlarged boxes 20 µm, length of the arrows 20 µm.
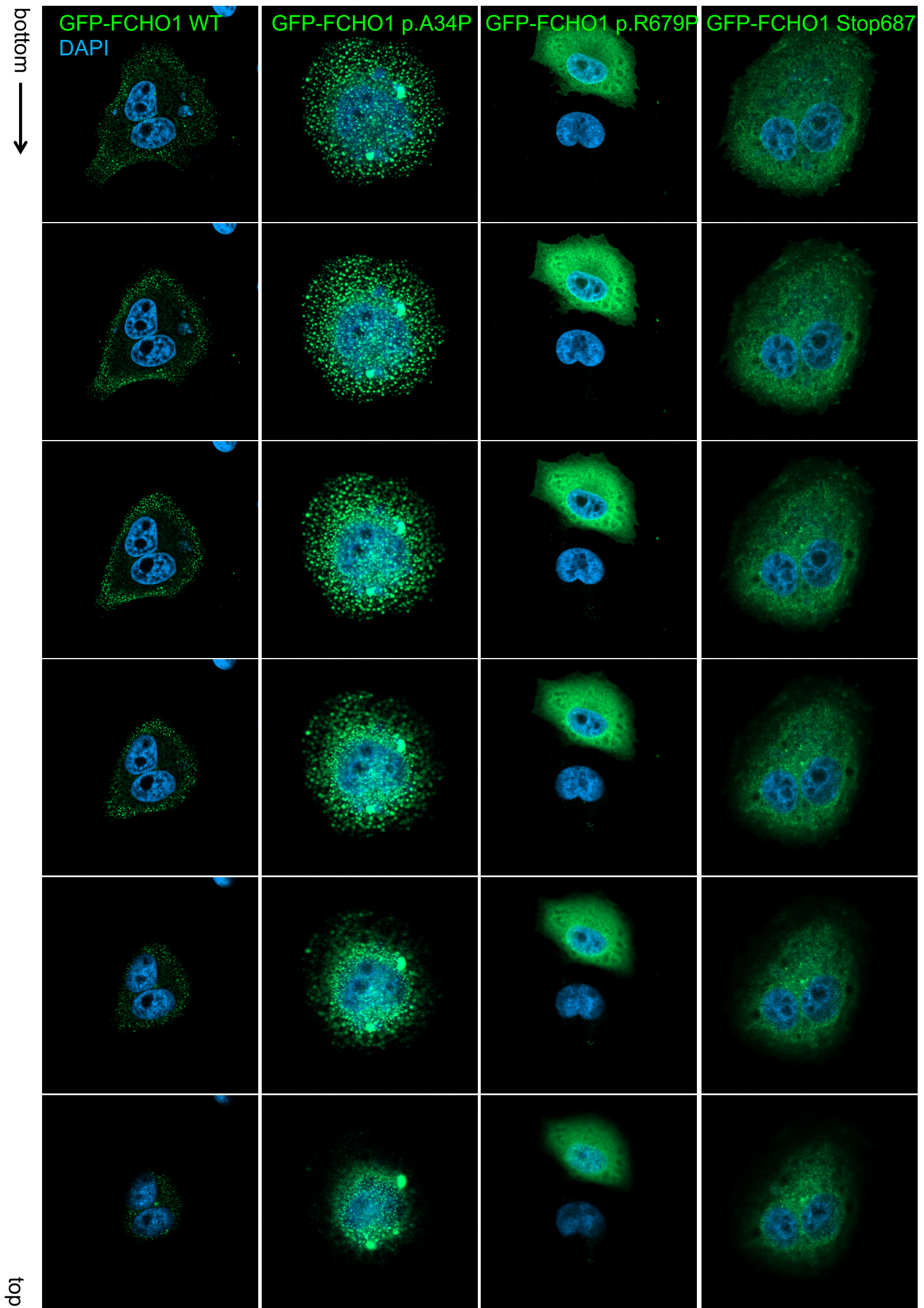
Supplementary Figure 6. Mutations in FCHO1 lead to dssociation of protein from the plasma membrane.
Optical sections (Z-stacks every 40 μm) for 3-D reconstruction and six selected optical sections from whole depth of the cells from the bottom to the top. FCHO1^{-/-} SK-MEL-2 cells were transiently transfected with GFP-fusion protein constructs, carrying indicated mutants of FCHO1. Optical sections visualize dissociation of all FCHO1 mutants from the plasma membrane as compared to wt GFP-FCHO1. Data are representative of two independent biological experiments (two independent transfections).
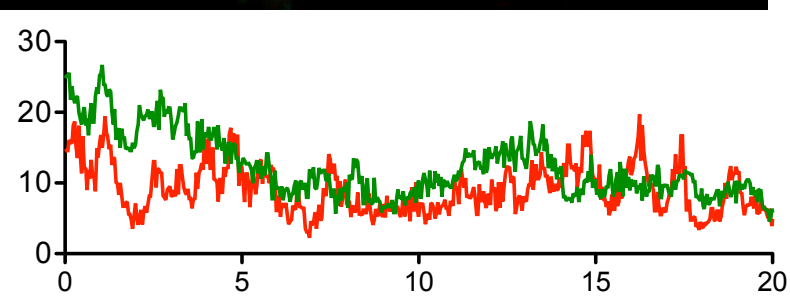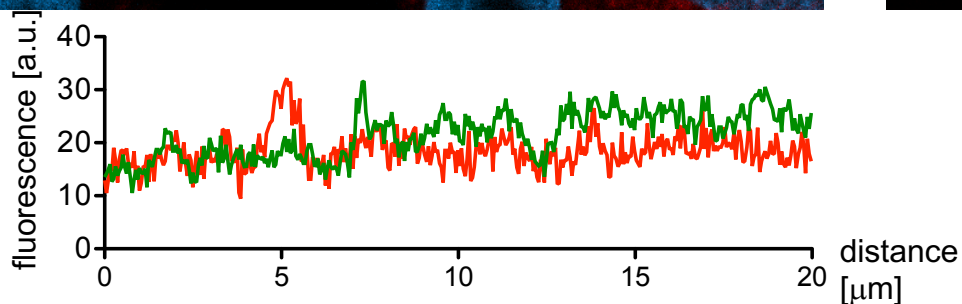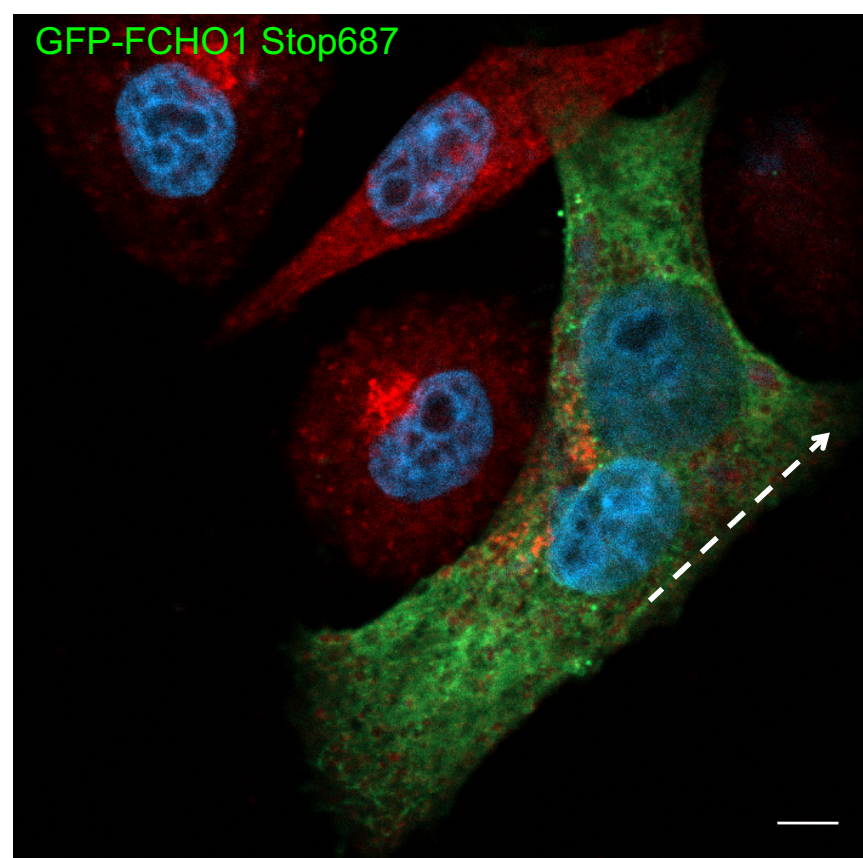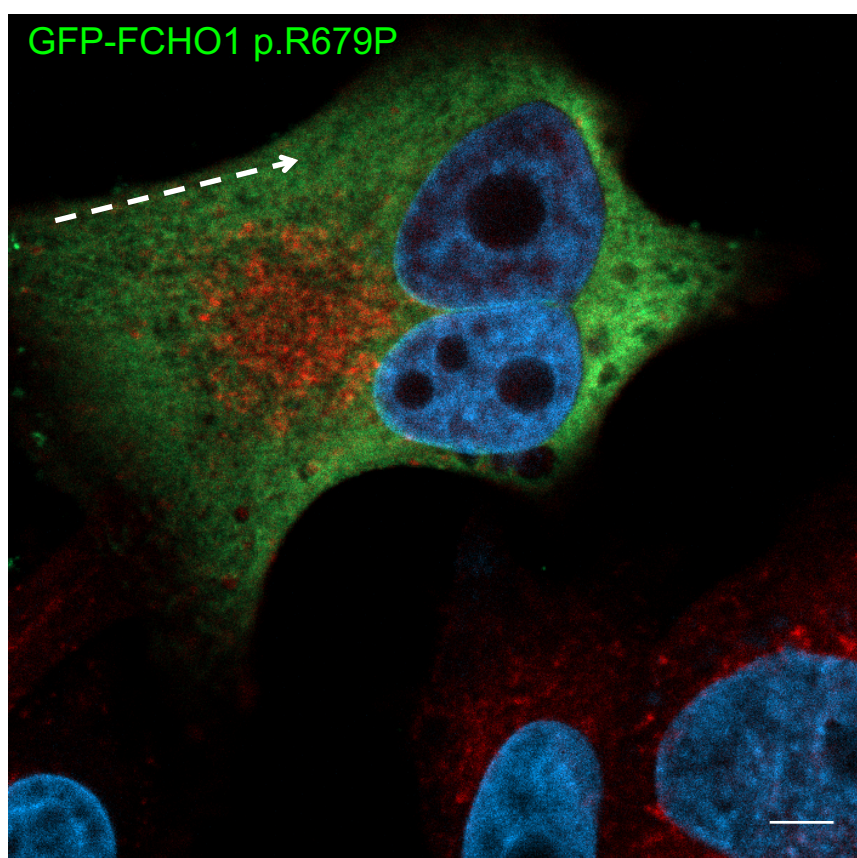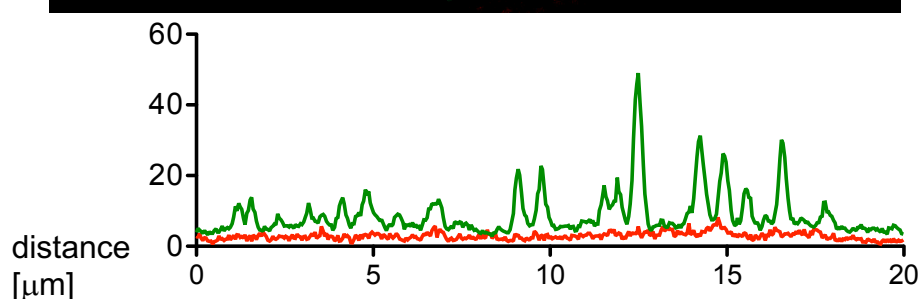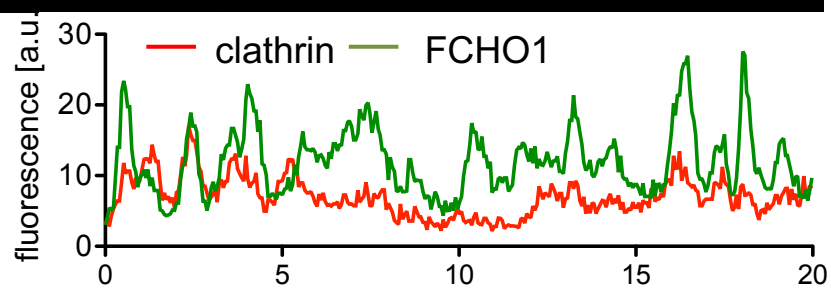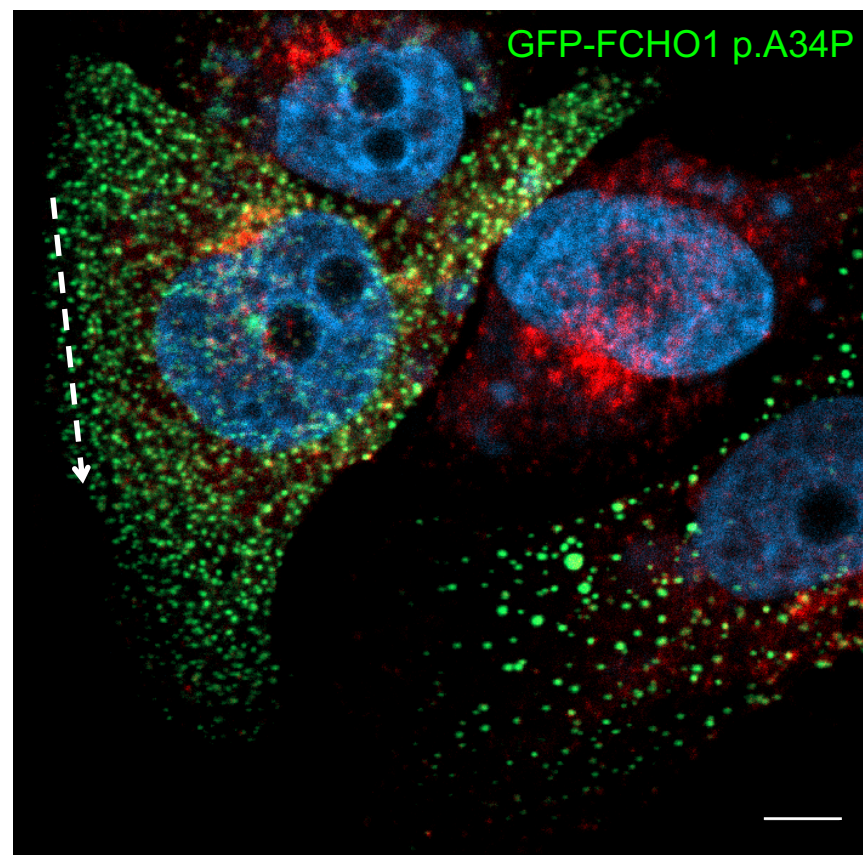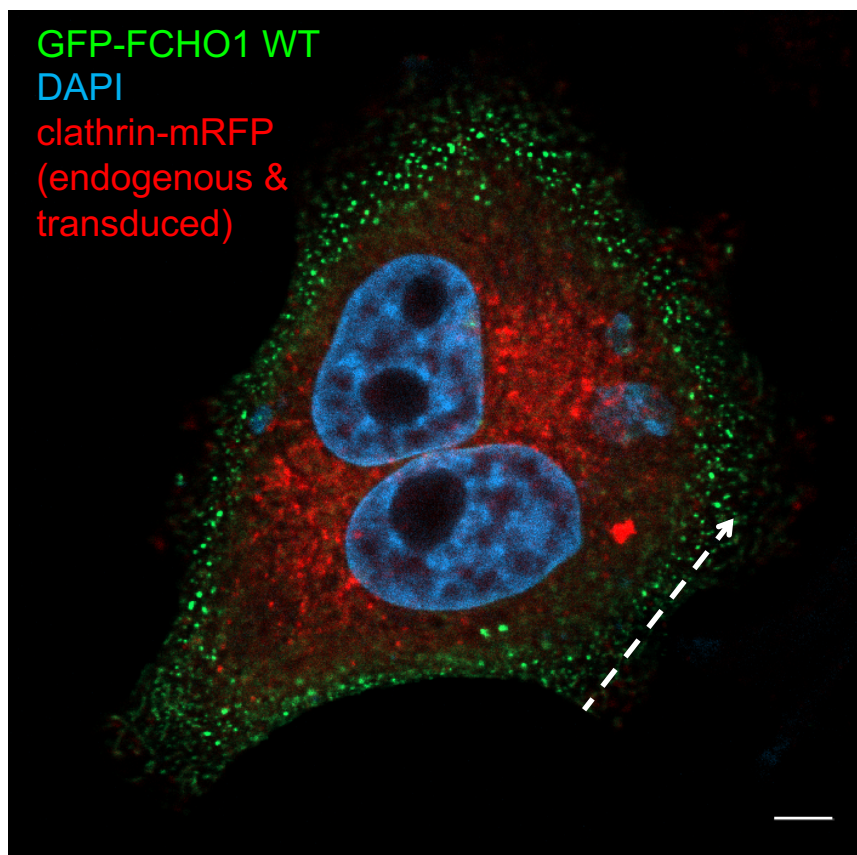
Supplementary Figure 7. FCHO1 mutants fail to colocalize with clathrin. In order to improve clathrin signal-to-noise ratio, FCHO1$^{-/-}$ SK-MEL-2 cells expressing RFP-tagged clathrin light chain from endogenous locus (CLTA$^{RFP/wt}$) were stably transduced with retroviral particles encoding clathrin light chain tagged with mRFP and subsequently transiently transfected with various GFP-FCHO1 plasmids. Representative confocal microscopy pictures show that all mutants but not wt FCHO1 fail to colocalize with clathrin. Arrows indicate regions where both RFP and GFP fluorescence intensities have been displayed on histograms below each image. In contrast to SK-MEL-2 cells engineered to express RFP from a single native locus of endogenous clathrin light chain A (used in all other experiments), additional overexpression of the clathrin-mRFP fusion protein leads to non-physiological accumulation of RFP signal near the nucleus.
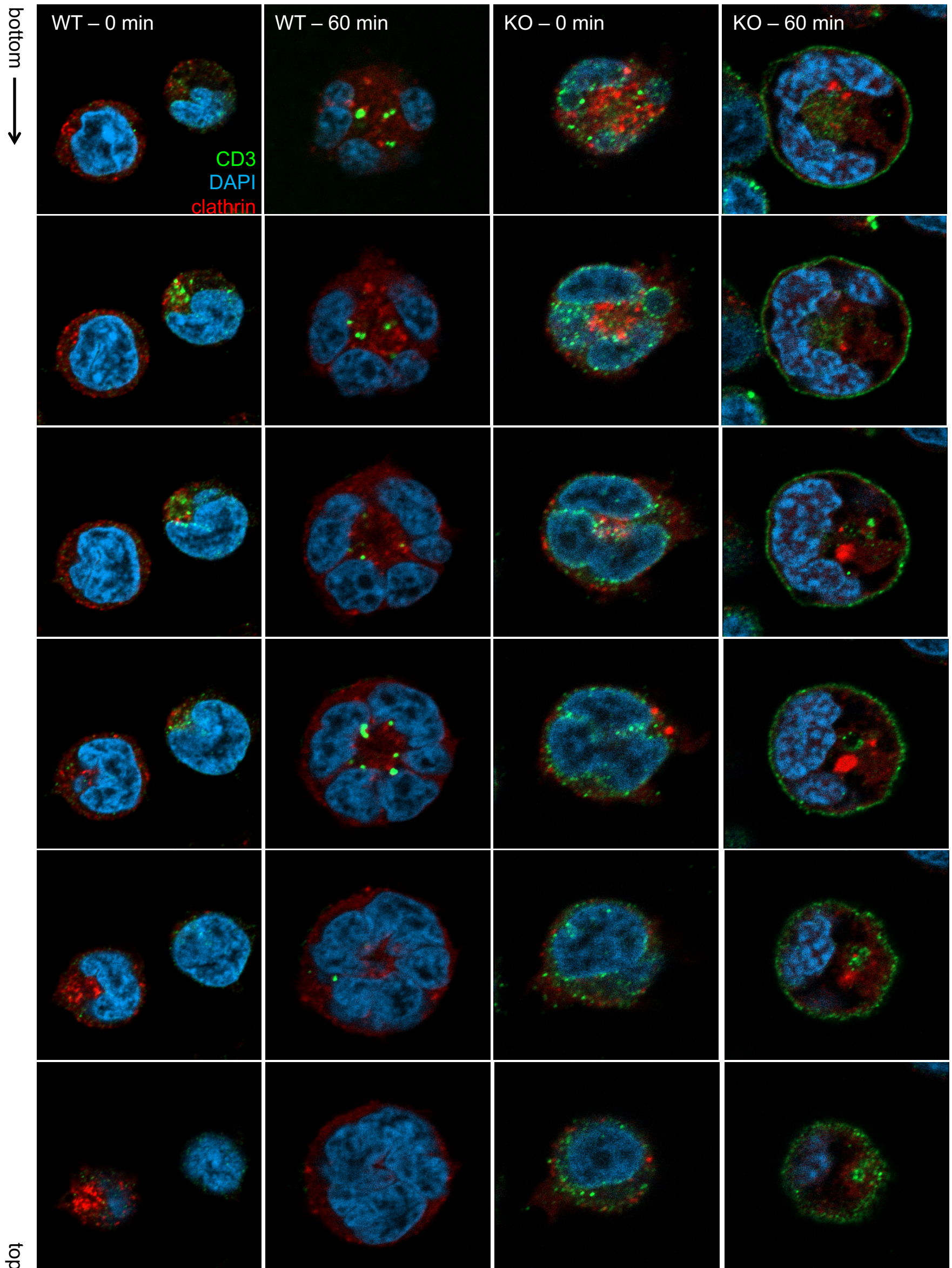
Supplementary Figure 8. This data supplements the 2D data presented on Figure 4a and shows that in the absence of FCHO1 surface CD3 is not efficiently internalised from the plasma membrane. Z-stack for 3-D reconstruction and six selected optical sections from whole length of the cells bottom to the top. Jurkat wt and FCHO1^{-/-} clones were stably transduced with RFP-clathrin and stimulated for 60 min with glass-bound anti-CD3 antibody (OKT-3). It supplements 2D data presented on Figure 4a and shows that in the absence of FCHO1 surface CD3 is not efficiently internalised form the plasma membrane.

Supplementary Figure 9. FCHO1 does not bind to CD3 ε, g, and d subunits of the TCR complex. Immunoprecipitation experiments with lysates prepared from FCHO1-deficient Jurkat cells stably overexpressing N' or C'-Flag wt FCHo1 fusion protein. Prior to immunoprecipitation cells were starved for a minimum 45' at 37°C and subsequently stimulated as indicated with anti-CD3 Ab to induce clustering of TCR complexes. Non-transduced Jurkat FCHO1-deficient cells served as negative control. (a) Amino acid sequence of CD3 ε, d and d. Cytoplasmic motif is marked in green, DxY or DxxY putative sorting motifs in red. (b) FCHO1 and (c) EPS15 served as positive immunoprecipitation controls. (d-f) Western blots of CD3 ε, d and d components of the TCR complex. The molecular mass of proteins is shown in kDa. Specific bands as well as Ig heavy (IgH) and Ig light (IgL) chains are indicated with arrows. Representative data of two independent experiments are shown.
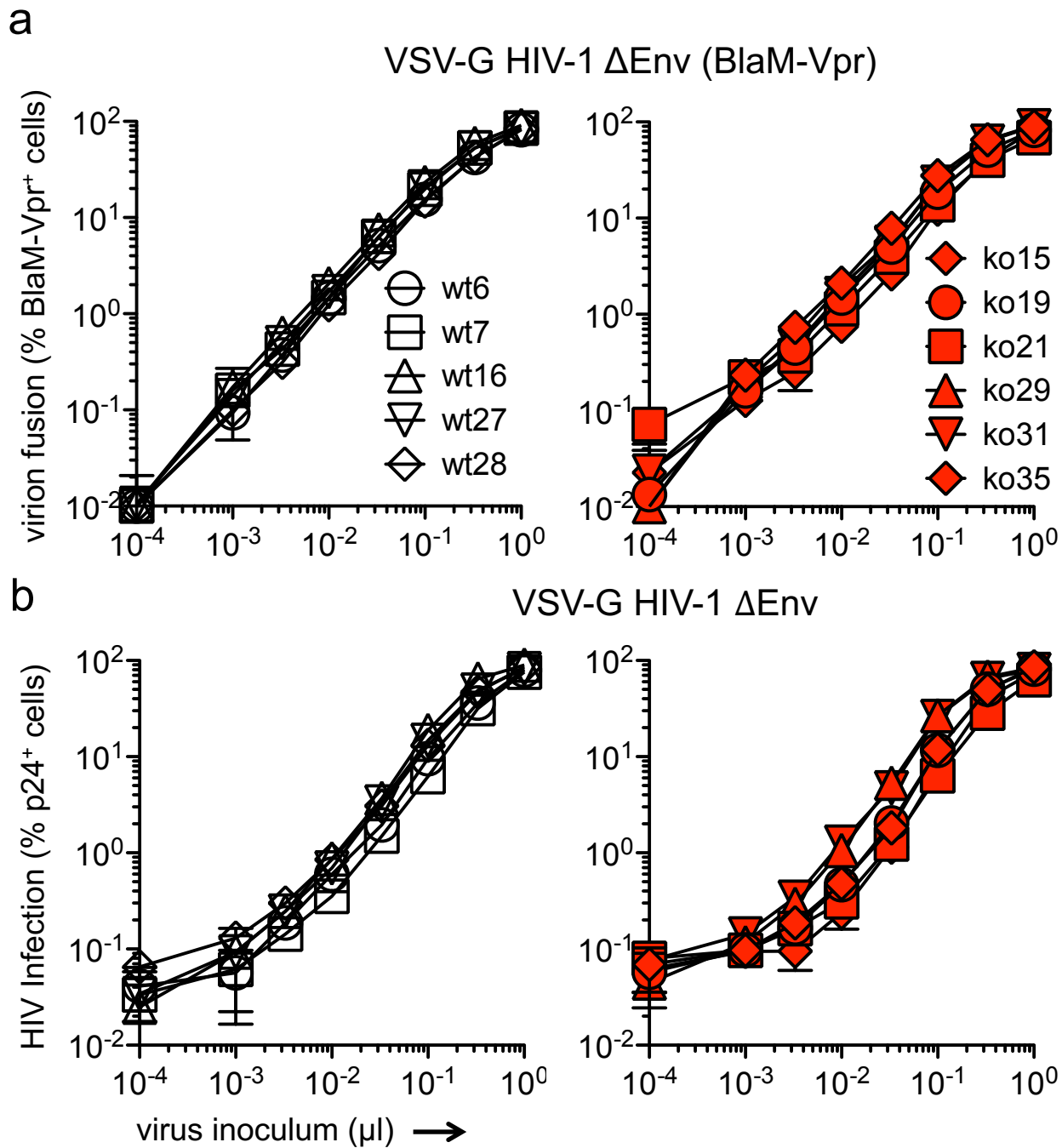
Supplementary Figure 10. FCHO1 ko in Jurkat T cells does not affect fusion and infection by HIV-1ΔEnv pseudotyped with VSV-G. (a) Virion fusion of VSV-G HIV-1ΔEnv (BlaM-Vpr) or (b) infection by VSV-G HIV-1ΔEnv of five Jurkat wt and six FCHO1 ko clones. (a, b) Jurkat wt and FCHO1 ko clones were challenged with increasing volumes of the indicated VSV-G-pseudotyped HIV-1ΔEnv. Virion fusion was monitored by flow cytometry and the percentage of cleaved CCF2+/BlaM-Vpr+ cells is plotted relative to the virus inoculum. Infection of VSV-G HIV-1 ΔEnv was monitored by intracellular HIV-1 p24 staining two days post challenge and the relative percentage of p24-positive cells is plotted relative to the virus inoculum. Values represent the arithmetic means of technical triplicates.
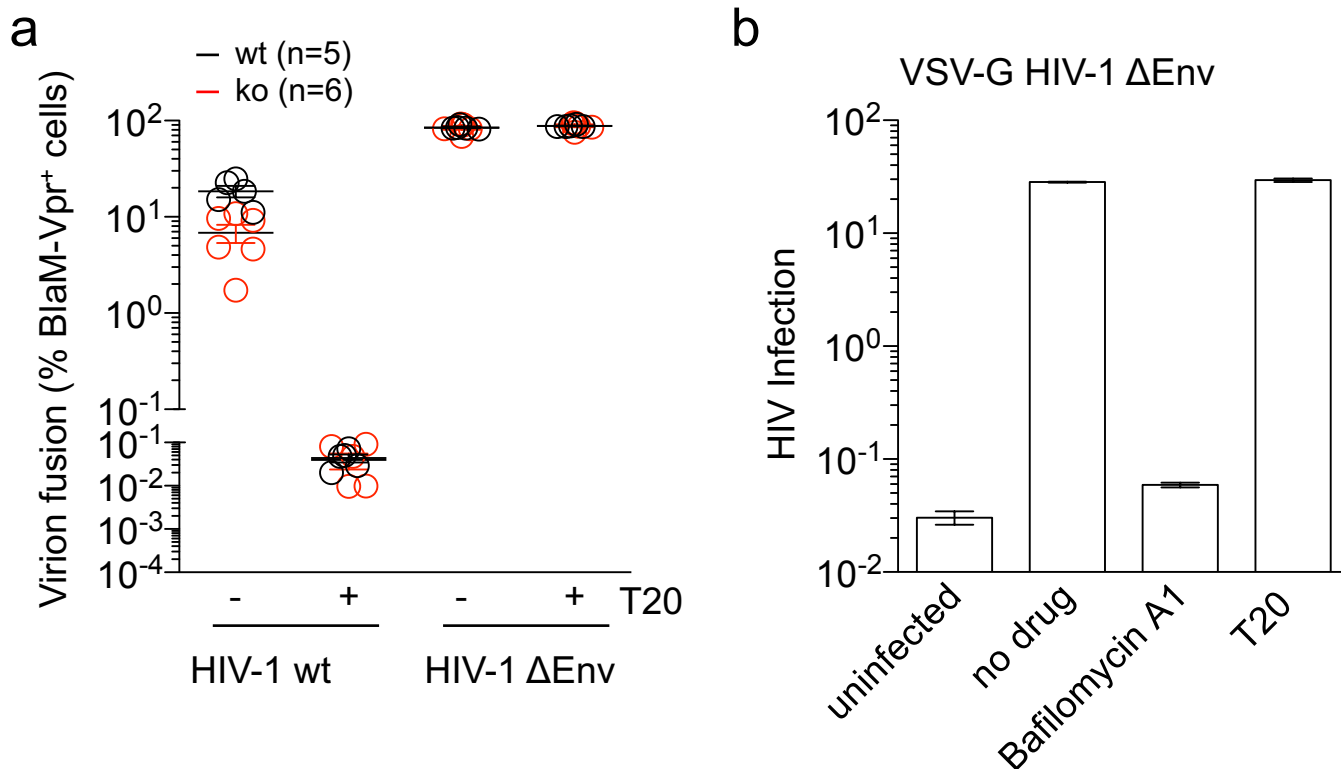
Supplementary Figure 11. **CME-dependent infection with VSV-G-pseudotyped HIV-1 is inhibited by bafilomycin A1, but not by the lack of FCHO1.** (a) Jurkat wt and FCHO1 ko clones were pre-incubated for 1 h either with the HIV-1-specific fusion inhibitor T20 or PBS and then challenged with HIV-1wt (BlaM-Vpr) or VSV-G HIV-1ΔEnv (BlaM-Vpr). Virion fusion was monitored by flow cytometry and the relative percentage of cleaved CCF2+/BlaM-Vpr+ cells is given. The symbols depicted represent the arithmetic means + standard deviations of technical triplicates from one representative experiment for five Jurkat wt clones (red circles) or six FCHO1 ko clones (grey squares). (b) Jurkat T cells were pre-treated with either bafilomycin A1, T20 or PBS (no drug) and subsequently challenged with VSV-G HIV-1ΔEnv. Two days later, cells were analyzed for the percentage of HIV-1 p24-positive cells by flow cytometry. Uninfected cells served as a reference. Histogram bars represent the arithmetic mean + standard deviation of three technical replicates from one representative experiment.

CRISPR/Cas9 cut   CRISPR/Cas9 cut

↓c.310   ↓c.(336+24)

ACGTTCTCCGCTACGGCG……//…….GAag……//…….cggctgggtgggtgtg

exon 7   intron 7

expected sequence after cut: ACGTTCTCCGCTACGGCGcggctgggtgggtgtg

exon 7   intron 7

Clone J15   allele 1: ACGTTCTCCGCTACG*CGA*cggctgggtgggtgtg
                allele 2: ACGTTCTCCGCTACG*GA*cggctgggtgggtgtg

Clone J19   allele 1: ACGTTCTCCGCTACG*CCC*cggctgggtgggtgtg
                allele 2: ACGTTCTCCGCTAC*CC*cggctgggtgggtgtg

Clone J21   allele 1: ACGTTCTCCGCTACG*CG*cggctgggtgggtgtg
                allele 2: ACGTTCTCCGCTACcggctgggtgggtgtg

Clone J29   allele 1: ACGTTCTCCGCTAC*NNNN*cggctgggtgggtgtg
                allele 2: ACGTTCTCCGCTACG*N*cggctgggtgggtgtg

Clone J35   allele 1: ACGTTCTCCGCTAC*GG*cggctgggtgggtgtg
                allele 2: ACGTTCTCCGCTACGcggctgggtgggtgtg

Supplementary Figure 12. Examples of CRISPR/Cas9-mediated deletion damaging FCHO1 locus at exon7 – intron 7 junction. Deletion at an intron-exon junction ensures aberrant splicing of the pre-mRNA transcript, whereas the deletion at an exon distant from the beginning of the protein prevents from usage of an alternative start codon.

Supplementary Figure 13. Example of gating strategy to assess frequency of leukocytes in human peripheral blood. CD45 staining was used to discriminate between leukocytes and remaining erythrocytes and platelets. FSC-A and FSC-H parameters were used to exclude doublets.
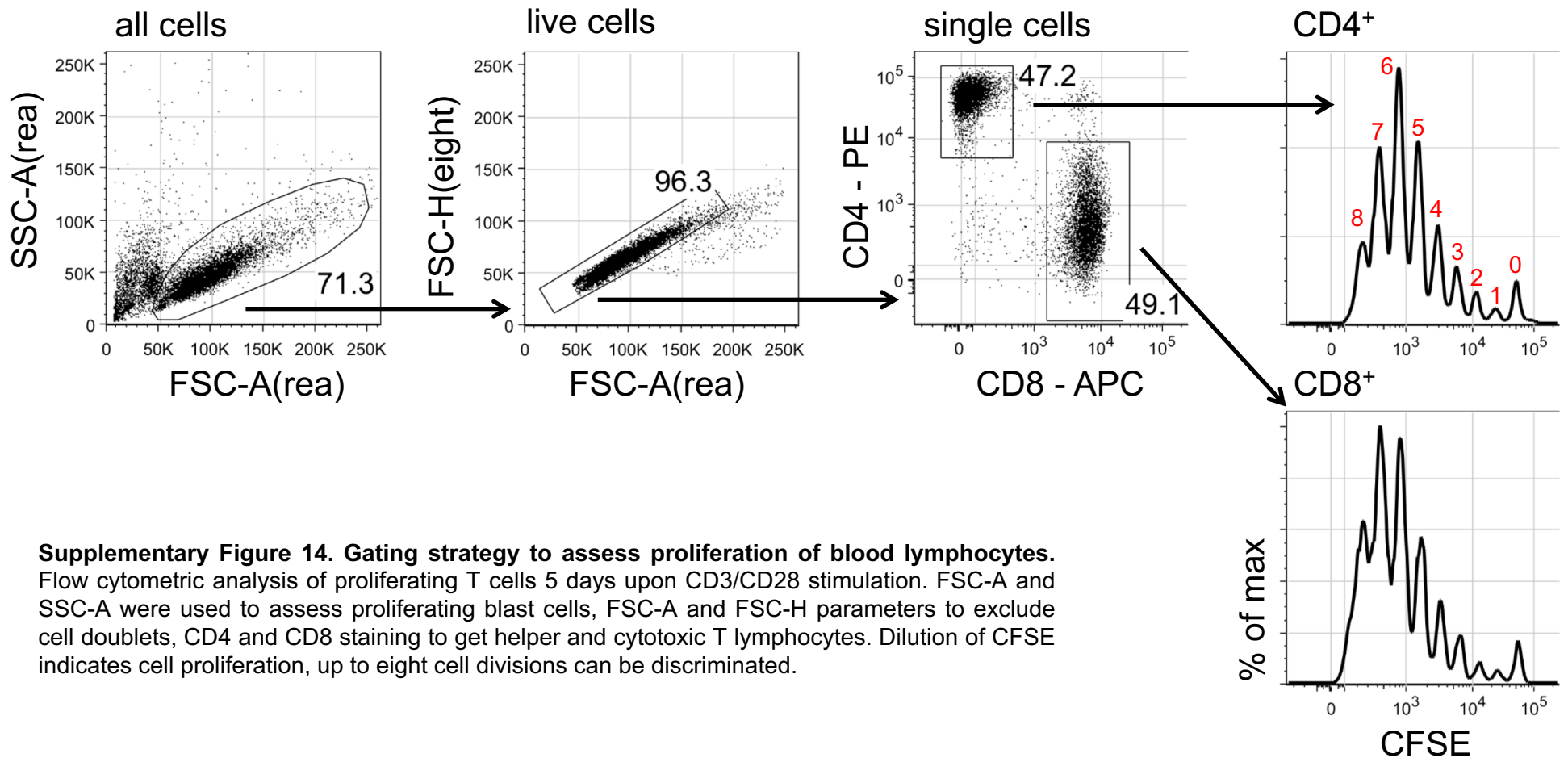
Supplementary Figure 14. Gating strategy to assess proliferation of blood lymphocytes. Flow cytometric analysis of proliferating T cells 5 days upon CD3/CD28 stimulation. FSC-A and SSC-A were used to assess proliferating blast cells, FSC-A and FSC-H parameters to exclude cell doublets, CD4 and CD8 staining to get helper and cytotoxic T lymphocytes. Dilution of CFSE indicates cell proliferation, up to eight cell divisions can be discriminated.
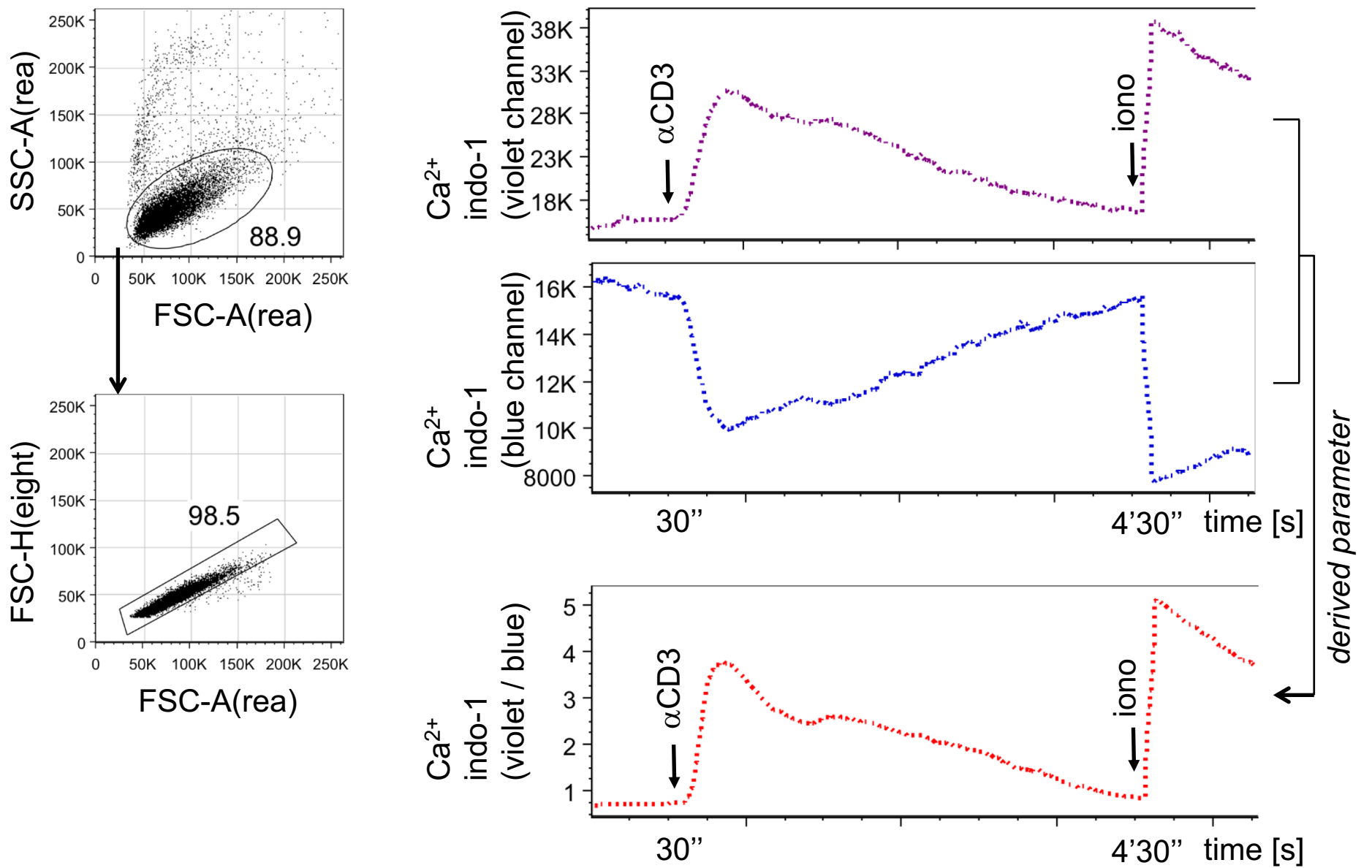
Supplementary Figure 15. Flow cytometry work flow to assess Ca²⁺ release from ER upon CD3 stimulation. Prior to CD3 stimulation Jurkat cells were loaded with an indo-1, Ca²⁺-sensitive dye. Changes in cytoplasmic concentration of Ca²⁺ can be followed due to the fact the emission of indo-1 shifts from about 475 nm without Ca²⁺ ("blue" channel) to about 400 nm ("violet" channel) with Ca²⁺ when excited at about 350 nm. Usage of 400/475 ratio parameter (red line) reduces the effect of uneven dye loading between the samples, uneven size of the cells, photobleaching etc.
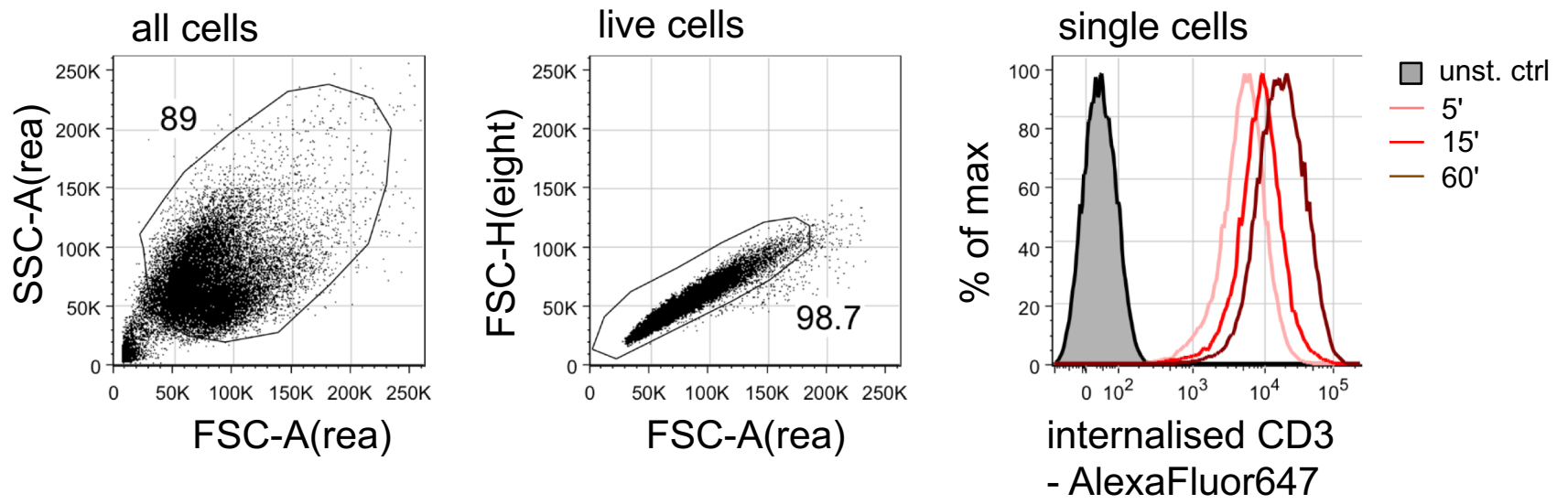
Supplementary Figure 16. Gating strategy to assess TCR-internalisation. FSC-A and SSC-A parameters were used to discriminate between cells and debris, FSC-A and FSC-H parameters to exclude cell doublets. Internalisation of TCR was followed over time after striping of remaining surface TCR.

	A1	B1	C1	D1	E1	E2	E3	F1	F2	G1
					blood cells count					
White blood cells (WBC)	2400/µl	2400/µl [4800-10800/µl]	3470/µl [4800-10800/µl]	6640/µl [4800-10800/µl]	2920	NA	4360/µl	7200/µl [5200-11000]	8600/µl [5200-11000]	3890/µl [5500-14000/µl]
Neutrophils	55%	83.5% [43-65%]	73.2% [43-65%]	64.8% [43-65%]	61% [40-67%]	NA	42% [40-67%]	74% [45.5-73.1]	62% [0.14-1.59]	40% [30-53%]
Lymphocytes	8.3%	10.3% [20.5-45.5%]	15.9% [20.5-45.5%]	21.5% [20.5-45.5%]	18.6% [33-60]	NA	46% [33-60]	14% [22.3-49.9]	16% [22.3-49.9]	27% [37-52%]
Monocytes	10%	3.8% [5.5-11.7%]	6.3% [5.5-11.7%]	9.6% [5.5-11.7%]	10% [4.7-12.5%]	NA	8.8% [4.7-12.5%]	2% [0.7-7.5]	12% [0.7-7.5]	7.3% [0-5%]
Eosinophils	26.3%	0.3% [0.9-2.9%]			5% [0-7%]	NA	3% [0-7%]	10% [0.0-4.4]	10% [0.0-4.4]	1.6% [0-4%]
Basophils⋅	0.4%	0.3% [0.2-1%]			1.9 [0-1.5%]	NA	0.3%[0-1.5%]	0% [0.2-1.2]	0% [0.2-1.2]	0.3% [0-1%]
					lymphocytes					
CD3⁺	58/µl (30%)	151/µl (61.3%) [60-85%]	305/µl (55.3%) [60-85%]	917/µl (64.1%) [60-85%]	489 (90%) [60-85%]	NA	891/µl (65%) [60-85%]	554/µl [1400-3700]	247/µl [1400-3700]	1164/µl (65.4%)
CD4⁺	17/µl (9%)	53/µl (21.6%) [29-59%]	46/µl (8.3%) [29-59%]	177/µl (12.4%) [29-59%]	81 (15%) [36-63%]	NA	137/µl (10%) [36-63%]	100/µl [700-2200]	178/µl [700-2200]	78/µl (4.4%)
CD8⁺	56/µl (29%)	104/µl (42.2%) [19-48%]	247/µl (44.9%) [19-48%]	532/µl (37.2%) [19-48%]	396 (73%) [15-40%]	NA	754/µl (55%) [15-40%]	443/µl [490-1300]	68/µl [490-1300]	981/µl (55%)
CD19⁺	31/µl (16%)	42/µl (17.1%) [11-16%]	67/µl (12.2%) [11-16%]	256/µl (17.9%) [11-16%]	0 (0%) [5-25%]	NA	625/µl (31%) [5-25%]	372/µl [390-1400]	756/µl [390-1400]	290/µl (16%) [7-23%]
CD16⁺	88/µl (46%)	54/µl (22%) [5-20%]	164/µl (29.8%) [5-20%]	237/µl (16.6%) [5-20%]	105 (20%) [5-20%]	NA	400/µl (25%) [5-20%]	40/µl [100-600]	247/µl [100-600]	279/µl (15%)
					immunoglobulins					
IgG	3.76 g/l [5.7 – 15.5 g/l] substituted	529 mg/dL [740-1450 mg/dL] substituted	471 mg/dL [700-1630 mg/dL] substituted	581 mg/dL [700-1630 mg/dL] substituted	420 mg/dL [470-1230 mg/dL] substituted	NA	316 mg/dL [470-1230 mg/dL] substituted	8.5 g/L Substituted [3.45-12.36]	9.0 g/L Substituted [3.45-12.36]	1400 mg/dL [500-1300 mg/dL]
IgM	0.25 g/l [0.6 – 3.0 g/l]	137 mg/dL [76-195 mg/dL]	17.4 mg/dL [65-206 mg/dL]	59.3 mg/dL [65-206 mg/dL]	20 mg/dL [45-169 mg/dL]	NA	114 mg/dL [45-169 mg/dL]	0.23 g/L [0.43-2.07]	0.36 g/L [0.43-2.07]	700 mg/dL [400-1800 mg/dL]
IgA	0.77 g/l [0.5 – 2.3 g/l]	89.6 mg/dL [80-190 mg/dL]	9.77 mg/dL [73-187 mg/dL]	14.1 mg/dL [73-187 mg/dL]	0 mg/dL [21-145 mg/dL]	NA	49 mg/dL [21-145 mg/dL]	0.57 g/L [0.14-1.59]	0.13 g/L [0.14-1.59]	25mg/dL [40-180 mg/dL]

Supplementary Table 1. Clinical laboratory investigations for patients A1-G1. Presented data were collected during initial admission of patients to the wards and before starting any treatment. Data in the square brackets indicate normal values for respective measurement. Frequencies of lymphocytes in the brackets were calculated in the reference to CD45⁺ cells.

patient	chromosome	position	reference allele	alternative allele	gene	cDNA (ENST00000594202)	protein
A1	19	17893924	G	C	FCHO1	c.2036G>C	p.Arg679Pro
B1	19	17873643	G	C	FCHO1	c.100G>C	p.Ala34Pro
C1 & D1	19	17893910	T	TG	FCHO1	c.2023insG	p.Val625GlyfsTer13
E1, E2, E3	19	17881387	G	A	FCHO1	c.489+1G>A	*unknown, IVS8 splice donor*
F1, F2	19	17877476	A	C	FCHO1	c.195-2A>C	*unkown, IVS6 splice acceptor*
G1	19	17893836	C	T	FCHO1	c.1948C>T	p.Arg650Ter

Mutation Significance Cutoff (MSC) Scores (http://pec630.rockefeller.edu:8080/MSC/)

patient	CADD Score	MSC-CADD score	MSC-CADD impact prediction	PolyPhen2 score	PolyPhen2 prediction	MSC-PolyPhen2 Score	MSC-PolyPhen2 impact prediction
A1	32.000	5.744	high	0.999	probably damaging	0.239	high
B1	28.700	5.744	high	1.000	probably damaging	0.239	high
C1 & D1	35.000	5.744	high	NA	NA	0.239	NA
E1, E2, E3	25.700	5.744	high	NA	NA	0.239	NA
F1, F2	24.500	5.744	high	NA	NA	0.239	NA
G1	43.000	5.744	high	NA	NA	0.239	NA

Supplementary Table 2. Chromosomal localization of all identified genetic variants (upper panel) and predicted influence of those mutations on protein function (bottom panel).

Western Blot

antigen	dilution	source	catalog number
beta-actin	1:1000	Santa Cruz	sc-47778 HRP
FCHO1	1:1000	Thermo Fisher Scientific	PA5-31603, polyclonal
FCHO1	1:1000	Abcam	ab84740, polyclonal
EPS15	1:2000	Cell Signaling	12460S, clone D3K8R
EPS15R	1:1000	Abcam	ab76004, clone EP1146Y
Adaptin	1 :1000	Abcam	ab2730, clone AP6
CD3 epsilon	1:1000	Cell Signaling	4443S, clone CD3-12
CD3 delta	1:500	Thermo Fisher Scientific	PA5-28313, polyclonal
CD3 gamma	1:500	Thermo Fisher Scientific	PA5-29387, polyclonal
GAPDH	1:1000	Santa Cruz	sc-32233, clone 6C5
anti-mouse HRP	1:2000	BD Biosciences	554002, polyclonal
anti-rabbit HRP	1:2000	Cell Signaling	7074S, polyclonal
anti-rat HRP	1:2000	Cell Signaling	7077S, polyclonal

flow cytometry

antigen	conjugate	dilution	source	catalog number
CD45	BV711	1:50	BD Biosciences	564358, clone HI30
CD45	APC	1:50	BioLegend	304012, clone HI30
CD33	PE-Cy7	1:100	BioLegend	366618, clone P67.6
CD3	PE	1:200	BioLegend	300308, clone HIT3a
CD19	FITC	1:50	BioLegend	302206, clone HIB19
CD8a	APC	1:50	BD Biosciences	555369, clone RPA-T8
CD4	PE-Cy7	1:50	BioLegend	357410, clone A161A1
CD45	APC	1:50	BioLegend	304012, clone HI30

Supplementary Table 3. List of antibodies used in Western Blot and FACS.

Appendix 6.4.

Niche availability promotes intrathymic dendritic-cell development from Early T lineage Progenitors

Łyszkiewicz M, Ziętara N, Föhse L, Puchałka J, Diestelhorst J, Witzlau K, Prinz I, Schambach A, Krueger A.

Regular Article

HEMATOPOIESIS AND STEM CELLS

Limited niche availability suppresses murine intrathymic dendritic-cell development from noncommitted progenitors

Marcin Łyszkiewicz,[1] Natalia Ziętara,[1] Lisa Föhse,[1] Jacek Puchałka,[2] Jana Diestelhorst,[1] Katrin Witzlau,[1] Immo Prinz,[1] Axel Schambach,[3,4] and Andreas Krueger[1]

[1]Institute of Immunology, Hannover Medical School, Hannover, Germany; [2]Dr von Haunersches Kinderspital, University Children's Hospital, Munich, Germany; [3]Institute of Experimental Hematology, Hannover Medical School, Hannover, Germany; and [4]Division of Hematology and Oncology, Boston Children's Hospital, Harvard Medical School, Boston, MA

Key Points

- DCs and T-lineage cells in the thymus have separate origins.
- Availability of microenvironmental niches in the thymus determines lineage fate.

The origins of dendritic cells (DCs) and other myeloid cells in the thymus have remained controversial. In this study, we assessed developmental relationships between thymic dendritic cells and thymocytes, employing retrovirus-based cellular barcoding and reporter mice, as well as intrathymic transfers coupled with DC depletion. We demonstrated that a subset of early T-lineage progenitors expressed CX3CR1, a bona fide marker for DC progenitors. However, intrathymic transfers into nonmanipulated mice, as well as retroviral barcoding, indicated that thymic dendritic cells and thymocytes were largely of distinct developmental origin. In contrast, intrathymic transfers after in vivo depletion of DCs resulted in intrathymic development of non–T-lineage cells. In conclusion, our data support a model in which the adoption of T-lineage fate by noncommitted progenitors at steady state is enforced by signals from the thymic microenvironment unless niches promoting alternative lineage fates become available. (*Blood*. 2015;125(3):457-464)

Introduction

T-cell development in the thymus is tightly regulated through the interactions of thymocytes with nonthymocytes, such as thymic epithelial cells and thymic dendritic cells (tDCs). tDCs consist of plasmacytoid DCs (pDCs) and two distinct populations of conventional DCs (cDCs) that can be distinguished based on differential expression of CD8α and Sirpα.[1] In secondary lymphoid organs, both CD8α[+] and CD8α[−] cDCs are derived from a common developmental pathway. This pathway is comprised of various progressively lineage restricted intermediates ranging from myeloid progenitors (MPs) via macrophage/DC progenitors (MDPs) and common DC progenitors (CDPs) to pre-DCs.[2]

However, the developmental origin of tDCs within the thymus has remained controversial. Thus, the discovery of $D_H J_H$ immunoglobulin rearrangements in tDCs, but not in splenic CD8α[+] DCs supported a lymphoid origin of tDCs.[3] In addition, both human and mouse tDCs have been reported to express the pre-TCRα chain.[4,5] Furthermore, early T-lineage progenitors (ETPs), which constitute the earliest detectable intrathymic T-cell precursors, have been shown to retain DC potential and CD8α[+] tDCs develop intrathymically with kinetics paralleling those of T cells.[6-10] However, analysis of mouse models expressing lineage-specific reporter genes or Cre recombinase to allow genetic fate mapping in vivo provided evidence for separate origins of thymocytes and tDCs. Thus, using *Il7r*-based fate mapping, which labels virtually all thymocytes, Schlenner et al showed that among tDCs, the majority of pDCs but only minor frequencies of other tDC subsets, were derived from progenitors with a history of *Il7r* expression.[11] Consistently, fate

mapping based on *Ptcra* expression showed that tDCs were not derived from T-lineage committed cells.[12] An intrathymic DC progenitor population that is likely to be of independent origin from ETPs was identified in mice expressing a CD207(Langerin)-green fluorescent protein (GFP) reporter gene.[13] In addition, these progenitors already expressed CD11c and low levels of MHC-II, and appeared therefore to be more mature than peripheral pre-DCs of the canonical DC developmental pathway.

To date, it remains difficult to reconcile these divergent findings. Whereas some experimental approaches, such as analysis of lineage potential ex vivo have directly been contested,[14] some experiments supporting either one model or the other remain compelling.[15] Lineage fate mapping, in combination with simultaneous deletion of *Notch1* in mice indicated that in vivo, in the absence of Notch signaling, ETPs can be diverted to become tDCs.[16] Absence of Notch1 is likely to lift Hes1-dependent repression of the key myeloid transcription factor gene, *Cebpa*.[17] These experiments support the notion that ETPs are basically equipped with DC potential, but do not adopt DC fate in a microenvironment rich in Notch ligands, such as the thymus. However, this hypothesis remains to be tested with ETPs that retain an intrinsic capacity to develop into T cells.

In this study, we have assessed whether a pro-T-cell–derived DC progenitor exists in the thymus that can be diverted into the DC lineage in vivo. We identified and characterized a subset of ETPs expressing CX3CR1. Retroviral barcoding in combination with next-generation sequencing suggested that at steady state tDC and T-cell development are largely independent. Finally, we demonstrated

that various progenitors, including ETPs and MP/MDPs can give rise to tDCs in vivo upon depletion of endogenous tDCs, but not in their presence. Taken together, our data support a model in which the thymic microenvironment provides a strong inductive force for T-cell development, thereby preventing diversion into alternative lineages. However, liberation of bona fide tDC niches generates a permissive state for intrathymic DC development from various progenitors, including pro-T cells.

Methods

Mice

C57BL/6J mice (CD45.2) and B6.SJL-$Ptprc^aPepc^b$/BoyJ mice (termed "B6 CD45.1" throughout this study) were purchased from Charles River. CD11c.DOG mice expressing diphtheria toxin receptor under the control of the CD11c promoter were described previously[18] and crossed to B6 CD45.1 to become CD45.1/CD45.2 heterozygous. All experiments were performed with heterozygous mice for the DOG construct. B6.129P-CX3CR1^{tm1Litt}/J (CX3CR1$^{GFP/+}$) reporter mice[19] and C57BL/6J x B6 CD45.1 F1 mice (CD45.1/CD45.2 heterozygous) were bred at the animal facility of the Hannover Medical School. Animals were maintained under specific pathogen-free conditions. All animal experiments were conducted in accordance with local and institutional guidelines.

Antibodies and flow cytometry

Monoclonal antibodies specific for CD4 (RM4-5, GK1.5), CD8 (53-6.7), CD25 (PC61), CD44 (IM7), Gr-1 (RB6-8C5), erythroid cell marker (Ter-119), CD19 (1D3), CD11b (M1/70), pan-NK (DX5), CD45.1 (A20), CD45.2 (104), B220 (RA3-6B2), CD117 (ACK2), Sca-1 (E13-161.7), CD135 (A2F10), CD127 (A7R34), Ki-67 (B56), Sirpα (P84), and CD115 (AFS98) were used purified or as various fluorescent or biotin conjugates. Antibodies were purified from hybridoma supernatants or were purchased from eBioscience, BD Biosciences, or BioLegend. Phycoerythrin-Cy7 conjugated streptavidin (BD Biosciences) was used to reveal staining with biotinylated monoclonal antibody. Data were analyzed with FloJo software (Tree Star). Lin$^-$ cells were isolated from total bone marrow (BM) by staining cell suspensions with a lineage-specific antibody cocktail (anti-CD4, anti-CD8, anti-CD19, anti-CD11b, anti-Gr-1, Ter-119, and DX5), followed by incubation with anti-rat-IgG-conjugated magnetic beads (Dynal, Invitrogen) and magnetic-bead depletion of mature lineages. Double-negative (DN) thymocytes were enriched by complement lysis of double-positive (DP) and single-positive (SP) cells using anti-CD4 and anti-CD8 antibodies (clones RL1.72 and 31M), followed by incubation with Low-Tox-M rabbit complement (Cedarlane). Complement lysis based on this protocol did not affect cells expressing low levels of CD4.

Cell lines

OP9 BM stromal cells expressing the Notch ligand Delta-like ligand 1 (OP9-DL1) and OP9-control cells (OP9-GFP) were provided by J.C. Zúñiga-Pflücker (University of Toronto, Toronto, Canada).[20] BaF3 cells were cultured in RPMI medium supplemented with 10% fetal calf serum, 100 U/mL penicillin, 0.1 mg/mL streptomycin, and IL-3 (10 ng/mL).

OP9 cocultures

OP9 coculture assays were essentially performed as described.[20] Precursors were plated at an initial density of 1 to 5×10^2 cells onto subconfluent OP9-GFP or OP9-DL1 monolayers at 5×10^4 cells/well in a 24-well plate. All cocultures were performed in the presence of 1 ng/mL IL-7, 5 ng/mL Flt3 ligand (Flt3-L), and 10 ng/mL stem cell factor (SCF) for OP9-DL1 assays and 0.1 ng/mL IL-7, 100 ng/mL Flt3-L, 10 ng/mL SCF and 5% of granulocyte macrophage (GM)–colony-stimulating factor (CSF) supernatant prepared in house (corresponding to 12-22 ng/mL as assessed by enzyme-linked

immunosorbent assay) for OP9-GFP cocultures. Fifty percent of medium was exchanged at days 4 and 7 of coculture.

Intrathymic transfers

Two to 10×10^3 CX3CR1$^-$ ETPs, CX3CR1$^+$ ETPs, or MP/MDPs isolated from CX3CR1$^{GFP/+}$ mice were injected into thymi of nonirradiated B6 CD45.1/CD45.2 or CD11c.DOG mice 1 day after diphtheria toxin (DT) (8 μg/gbw) treatment. Thymi were analyzed for donor-derived cells 21 days after transfer.

Barcoded vector library

Design of the barcode library was performed analogous to the method described by Verovskaya et al.[21] Briefly, bar code oligonucleotides of the sequence: GTACAAGTAANNATCNNGATSSAAANNGGTNNAACNNTGTAAAA CGACGGCCAGTGAC (see supplemental Figure 1A, available on the *Blood* Web site) were inserted into the 3′UTR of the coding sequence for eGFP in the gammaretroviral SF91 vector.[22,23] Approximately 6000 clones were collected. Re-transformation followed by Sanger sequencing of 86 clones revealed one duplicate and near-equal distribution of all variable bases (supplemental Figure 1B), indicating a depth of the library of at least 4000 barcodes.

Transduction of cells

For production of retroviral vectors, HEK293T cells were transfected with pCL-Eco (coexpressing gag, pol, and env derived from murine leukemia virus) and library-containing SF91 plasmids. Eight hours after transfection, medium was exchanged and supernatant containing retroviral particles was collected after 24, 48, and 72 hours posttransfection. Retroviral transductions of BaF3 cells were performed in 24-well plates (Sarstedt, Germany) in the presence of 8 μg/mL of polybrene (Sigma-Aldrich). Lin$^-$Sca-1$^+$CD117^{hi} (LSK) cells were sorted from lineage-depleted BM and cultured overnight in α-minimum essential medium supplemented with SCF (50 ng/mL), IL-7 (25 ng/mL), Flt-3L (25 ng/mL), and IL-6 (20 ng/mL). LSK cells were then transferred into 96-well plates (Sarstedt, Germany) preloaded with retroviral vector attached to RetroNectin (Takara, Japan) according to the manufacturer's protocol.

BM chimeras and cell analysis

Some 48 hours after transduction with library vector, GFP^{lo} LSKs were sorted and a minimum of 50 000 LSK cells were IV transferred into lethally irradiated (9 Gy) C57BL/6 recipients. BM, spleen, and thymic cells were isolated 8 to 10 weeks after transfer. tDCs (CD11c$^+$MHC-II$^+$) were sorted after CD11c-allophycocyanin staining and positive enrichment using anti-allophycocyanin MicroBeads (Miltenyi Biotec). Other thymic populations included: DN (lin$^-$CD4$^-$CD8$^-$), DP (CD4$^+$CD8$^+$), and SP (TCRβ$^+$CD4$^+$ CD8$^-$) thymocytes. Splenic leukocyte populations included: DCs (CD11c$^+$ MHC-II$^+$), T cells (TCRβ$^+$), and B cells (IgM$^+$). BM precursors were defined as Lin$^-$CD117^{hi} cells.

Next-generation sequencing

Messenger RNA from sorted cells was isolated by RNeasy Plus Micro Kit (Qiagen), and then reversely transcribed into complementary DNA using SuperScript II Reverse Transcriptase (Invitrogen). Individual samples for each sequencing run were amplified with primers carrying multiplex identifiers. Sequences are available on request. Amplification was performed using recombinant Taq DNA polymerase (Invitrogen). Amplicons were purified by agarose gel electrophoresis and quantified by Quant-iT dsDNA HS Assay Kit (Invitrogen). Next-generation sequencing was performed on the Genome Sequencer FLX System (454, Roche Applied Sciences) as described before.[24]

Statistical analysis

All analysis was performed using GraphPad Prism or Excel software. Morisita-Horn index (MHI) and unsupervised hierarchical clustering based on the MHI was calculated based on in-house developed macros.
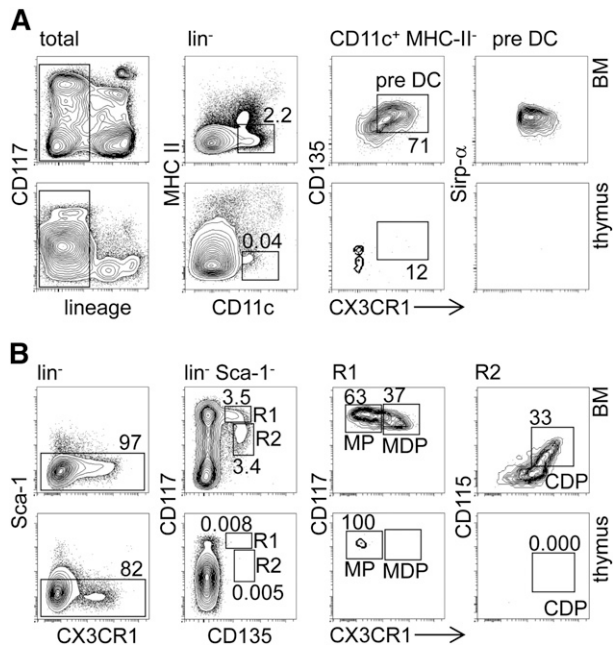
Figure 1. Canonical early DC progenitors are absent from the adult thymus. (A) BM (upper panel) and thymic (lower panel) cells from CX3CR1$^{GFP/+}$ reporter mice were labeled with antibodies against lineage markers (CD19, TCR-β, NK1.1, CD11b, and Gr-1), along with CD11c, MHC-II, and CD135 and analyzed by FACS to detect pre-DCs (CD11c$^+$MHC-II$^-$). Representative FACS density plots indicate the pre-DC population in the BM and thymus. Numbers next to gates indicate the percentage of cells. (B) Similar to (A), the BM and thymic cells from CX3CR1$^{GFP/+}$ reporter mice were stained with lineage markers (CD19, TCR-β, NK1.1, CD11b, CD11c, and Gr-1), as well as Sca-1, CD135, CD117, and CD115 antibodies to visualize MPs (Lin$^-$Sca-1$^-$CD117^{hi}CD135$^+$ CX3CR1$^-$), MDPs (CD117^{hi}CD135$^+$CX3CR1$^+$), and CDPs (CD117$^+$CD135$^+$ CX3CR1$^+$CD115$^+$) in the BM (upper panel) and thymus (lower panel). Representative FACS density plots indicate frequencies of MP, MDP, and CDP. Results are representative of 3 independent experiments with at least 3 mice per group.

Results

Canonical early DC progenitors are absent from the adult thymus

In order to assess whether the thymus contained DC progenitors that were less mature than the previously characterized CD11c$^+$ CD207$^+$MHC-II^{lo} cells,[13] such as MPs, MDPs, CDPs, or MHC-II$^-$ pre-DCs, we employed CX3CR1^{GFP} mice. MDPs, CDPs, and pre-DCs, which were readily detectable in BM, were completely absent from the thymus (Figure 1A-B). In addition, we found minute numbers of cells phenotypically corresponding to MPs, which might constitute background signals. In conclusion, the adult thymus is virtually devoid of canonical DC progenitors.

CX3CR1^{GFP} reporter expression is common for MDPs, CDPs, as well as pre-DCs, suggesting that potential noncanonical DC progenitors might also express CX3CR1. Indeed, we identified a subset of CX3CR1$^+$ cells that otherwise phenotypically overlapped with ETPs and constituted approximately 10% of all ETPs (Figure 2A). Further phenotypic characterization for CD135, CD115, CD11c, and CD11b showed no differences between CX3CR1$^+$ and canonical CX3CR1$^-$ ETPs (termed ETPs throughout this study) (Figure 2B). Differential expression of CD24 among thymocyte subsets that are considered to be most immature revealed 5 distinct populations designated DN1a-e.[25] Within these populations, a subset

of DN1c cells, which do not constitute physiological T-lineage progenitors, was identified as a CD207$^+$ DC precursor.[13] Analysis of CD24 expression on CX3CR1$^+$ ETPs showed that the majority of these cells were DN1a/b cells, consistent with a function as physiological pro-T cells (Figure 2C). Of note, when compared with canonical CX3CR1$^-$ ETPs, CX3CR1$^+$ ETPs expressed slightly lower levels of CD117 and slightly higher levels of CD24, suggesting that these cells might be able to generate DN1c cell progeny (Figure 2C-D). However, the lack of expression of CD11c clearly distinguished CX3CR1$^+$ ETPs from DN1c tDC progenitors.
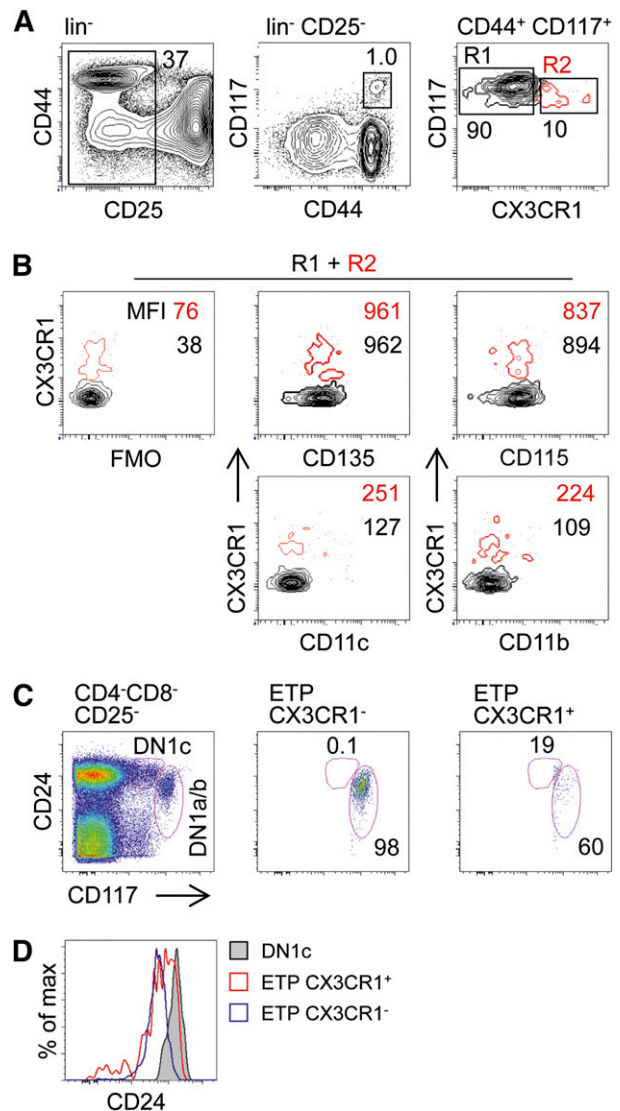

Figure 2. Identification of ETPs expressing CX3CR1. (A) Thymocytes from CX3CR1$^{GFP/+}$ reporter mice were depleted of CD4 and CD8 positive cells and subsequently stained with lineage antibodies (CD19, TCR-β, NK1.1, CD11b, CD11c, and Gr-1), as well as CD44, CD25, and CD117. Representative FACS density plots show ETPs (lin$^-$CD44$^+$CD25$^-$CD117^{hi}) negative and positive for CX3CR1. (B) ETPs prepared as in (A) positive (red, R1) or negative (black, R2) for CX3CR1 and were tested for expression of markers associated with myeloid precursors: CD135, CD115, CD11c, and CD11b. FMO controls were used to visualize background fluorescence. (C) Thymocytes were prepared and stained as in (A) and antibodies against CD24 to discriminate DN1 subsets according to the DN1a-e scheme. (D) Levels of CD24 on DN1 cells. Numbers inside contour plots indicate median fluorescent intensities of the respective surface antigens. Data are representative of 6 (A) and 2 (B-D) independent experiments. FMO, fluorescence-minus-one.
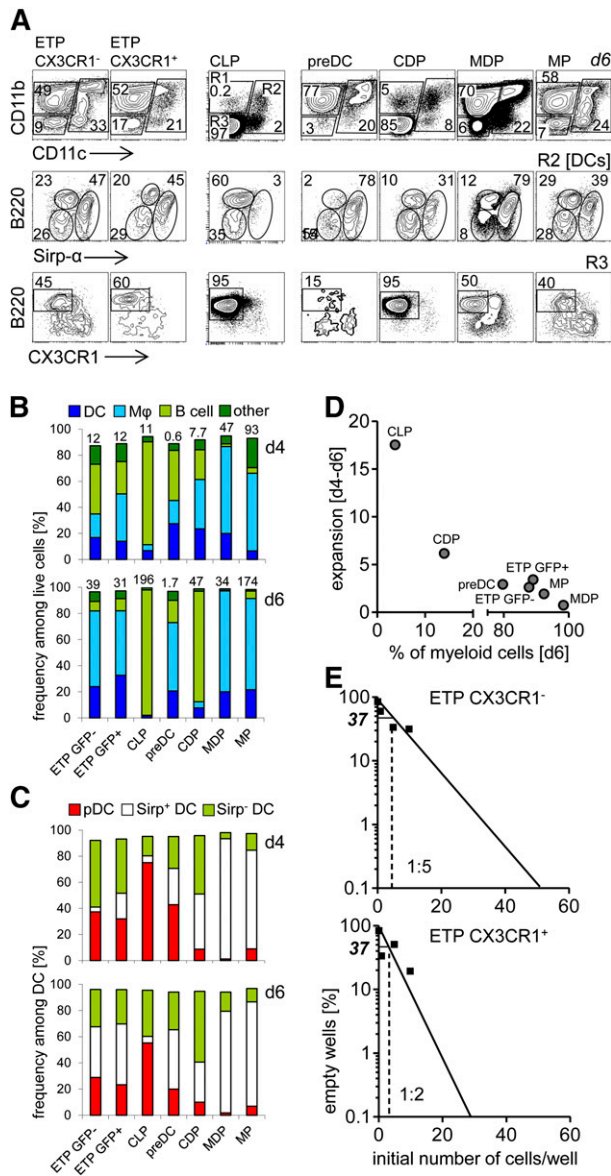
Figure 3. CX3CR1+ and CX3CR1− ETPs have comparable DC potential in vitro. (A) BM-derived progenitors (CLPs, pre-DCs, CDPs, MDPs, and MPs) and thymic progenitors (CX3CR1+ and CX3CR1− ETPs) were sorted from CX3CR1GFP/+ reporter mice. Progenitors were sorted according to gates shown in Figures 1 and 2. CLPs were defined as lin−Sca-1+CD117intCD127− CD135+. Purified precursors were cultured on OP9 stromal cells in the presence of Flt-3L, SCF, IL-7, and GM-CSF, and analyzed at days 4 and 6 to assess their myeloid and B-lineage potential. Cells derived from these precursors were defined as DC, based on expression of CD11c, along with Sirpα and B220. Bona fide macrophages were identified as CD11b+CD11c−, while B220 cells were defined as CD11c−CD11b−B220+CX3CR1−. (B) Quantification of data shown in (A) at day 4 (upper panel) and day 6 (bottom panel) of culture. Numbers above the columns indicate fold expansion of precursors compared with day 0. (C) Quantification of DC populations shown in (A, middle panel) at day 4 (upper panel) and day 6 (bottom panel) of culture. Development of 3 major DC populations was assessed: CD11c+Sirpα+, CD11c+Sirpα−, and CD11c+B220+ (pDC). (D) Expansion of precursors between days 4 to 6 inversely correlated to the frequency of myeloid cells generated by day 6. (E) The potential of CX3CR1+ and CX3CR1− ETPs to develop toward the myeloid or B lineages was assessed by limiting dilution assay on OP9 stromal cells in the presence of Flt-3L, SCF, IL-7, and GM-CSF. (A-E) Data are representative of 2 independent experiments.

CX3CR1+ and CX3CR1− ETPs have comparable DC potential in vitro

Next, we employed the OP9 coculture system to compare the propensity of CX3CR1+ ETPs to differentiate into non-T cells with

that of their CX3CR1− counterparts, as well as other canonical lymphoid and DC progenitor populations.[26] After 4 days of culture CX3CR1+ ETPs, ETPs, pre-DCs, and CDPs displayed a very similar distribution of DC, macrophage, and B-lineage progeny (Figure 3A-B) with ETPs generating slightly fewer Sirpα+ DCs and CDPs generating only a few pDCs (Figure 3C). After 6 days of culture, ratios of progeny were shifted toward myeloid populations in cultures of CX3CR1+ ETPs, ETPs, and pre-DCs. In contrast, CDP-derived cultures consisted predominantly of B cells, whereas MPs and MDPs generated mostly DCs and macrophages, and the majority of DCs were Sirpα+ (Figure 3B-C). Common lymphoid progenitors (CLPs) predominantly gave rise to B cells, and limited but detectable numbers of macrophages and DCs, the latter consisting mostly of pDCs and very limited numbers of Sirpα+ DCs (Figure 3C).

Of note, cultures originating from the various progenitors expanded to different extents during differentiation (Figure 3B). MPs and MDPs displayed the strongest expansion within 4 days of culture, followed by CDPs, CLPs, and ETP subsets, all of which expanded approximately 10-fold. In contrast, pre-DCs failed to expand during this interval. After 6 days of culture, MP- and CLP-derived cultures had expanded close to 200-fold, whereas CDP and ETP-derived cultures had expanded 30- to 50-fold. Notably, no additional expansion was observed in MDP- and pre–DC-derived cultures after 6 days when compared with 4 days of culture. Whereas early expansion is likely to indicate more the potential of the input progenitors to proliferate and/or survive under these culture conditions, further expansion between days 4 and 6 of culture inversely correlated with the frequency of myeloid cells in these cultures, consistent with their state of terminal differentiation (Figure 3D). Comparison of CX3CR1+ ETPs and ETPs in limiting dilution analysis revealed a slightly higher precursor frequency within the ETPs in OP9 cocultures (Figure 3E). In conclusion, all progenitors, including CLPs, displayed myeloid potential in vitro. In turn, somewhat unexpectedly, B-lineage potential, albeit to different degrees, was found in all populations as well. In addition, limiting dilution analysis showed that CX3CR1+ ETPs contained a higher frequency of myeloid-lineage progenitors when compared with their canonical counterparts.

T-lineage differentiation can be elicited from various myeloid lineage-committed or DC-committed progenitors

Given the lymphoid lineage potential of DC progenitor populations detected in vitro, we next assessed whether these populations carried the potential to differentiate into T-lineage cells as well. To this end, we employed the OP9-DL1 coculture system.[20] CLPs and both ETP subsets gave rise predominantly to T-lineage cells after 6 days of culture (Figure 4A-B). Consistent with previous work,[27] ETPs displayed a more rapid developmental progression when compared with CLPs (Figure 4A,C). Both subpopulations of ETPs displayed a similar T-lineage progenitor frequency in limiting dilution analysis with a higher frequency in ETPs (Figure 4D). As expected, MPs yielded mostly DC-like and macrophage-like cells at this time point, but we could also detect some CD25+ DN2 cells in each culture (supplemental Figure 2 and Figure 4A-B). Of note, after 6 days of culture, T-lineage cells constituted the majority irrespective of the starting population and most of these cells displayed a CD25+ DN2 or DN3 phenotype (Figure 4A,C). However, cultures from canonical lymphoid progenitors, including CX3CR1+ ETPs, expanded 40- to 223-fold. In contrast, cultures from myeloid-lineage progenitors (with the exception of MP-derived cultures) expanded considerably less (Figure 4B). Pre–DC-derived
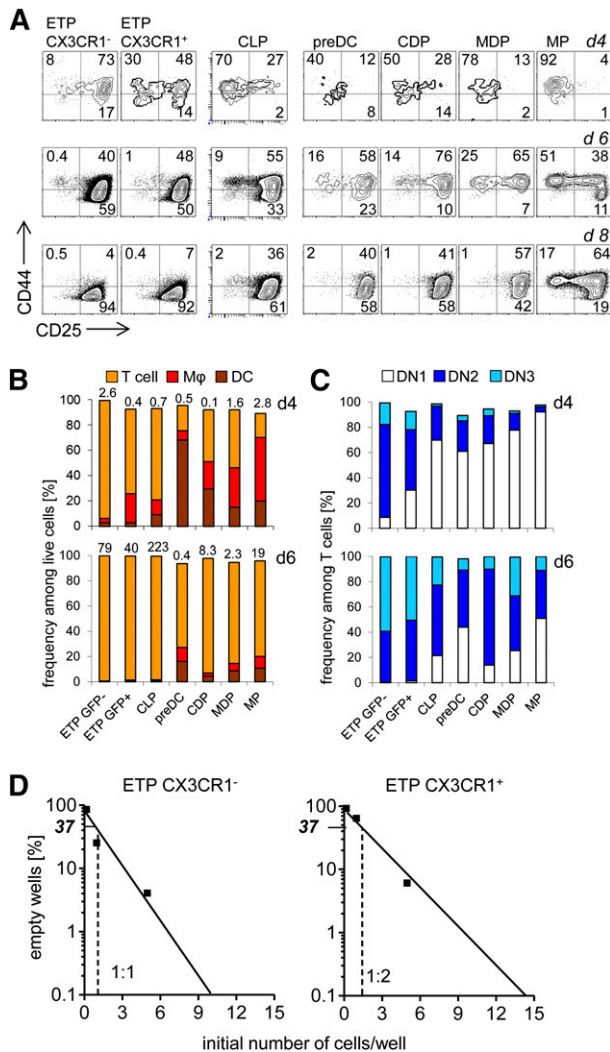
Figure 4. T-lineage differentiation can be elicited from various myeloid–lineage-committed or DC-committed progenitors. (A) BM-derived and thymic progenitors were sorted from CX3CR1$^{GFP/+}$ reporter mice. Purified precursors were cultured on OP9-DL1 stromal cells in the presence of Flt-3L, SCF, and IL-7, and analyzed at days 4, 6, and 8 to assess their myeloid- and T-lineage potential. DCs were considered as CD11c$^+$, while macrophages were CD11b$^+$CD11c$^-$. T-cell–committed precursors were negative for myeloid markers (CD11c, CD11b, and CX3CR1) and further subdivided into 3 DN populations based on the surface expression of CD25 and CD44. DN1 were CD44$^+$CD25$^-$, DN2 CD44$^+$CD25$^+$, and DN3 CD44$^-$CD25$^+$. (B) Quantification of data shown in (A) at day 4 (upper panel) and day 6 (bottom panel) of culture. Numbers above the columns indicate fold expansion of precursors. (C) Quantification of T-lineage–committed DN populations shown in (A) at day 4 (upper panel) and day 6 (bottom panel) of culture. (D) The potential of CX3CR1$^+$ and CX3CR1$^-$ ETPs to develop toward the T lineage was assessed by limiting dilution assay on OP9-DL1 stromal cells in the presence of Flt-3L, SCF, and IL-7. (A-D) Data are representative of 2 independent experiments.

cultures even underwent a twofold contraction during the culture period of 6 days. Taken together, we conclude that all DC progenitor populations tested, ranging from MPs to pre-DCs, have robust T-lineage potential in vitro. These data suggest that inductive signals from the environment may critically contribute to DC vs T-lineage fate decisions in the thymus.

Limited lineage relationship of tDCs and thymocytes revealed by retroviral barcoding

In order to test in vivo whether tDCs and thymocytes are developmentally related, we employed retroviral barcoding combined with next-generation sequencing as an independent approach to determine potential lineage relationships. We hypothesized that limited colonization of the thymus by BM-derived progenitors would allow us to determine whether thymocytes and tDCs shared a common intrathymic progenitor. Barcodes consisted of semi-random oligonucleotide duplexes, in which 6 pairs of random nucleotides were separated by fixed triplets, with a theoretical diversity of more than 10^6 (supplemental Figure 1A).[28]

In order to gain an estimate on the sensitivity of our barcoding approach, we transduced the lymphoid cell line BaF3 and generated 50 clones carrying defined individual barcodes. These clones were then mixed at a defined ratio of 50:49:48:…:3:2:1 into one single culture (Figure 5A). After 3 days of culture, 50 000 cells were randomly harvested from this culture and subjected to next-generation sequencing. Comparison of the expected frequencies of barcodes ranging from 3.9% to 0.08% for the most and the least abundant ones, respectively, with the barcodes recovered from the sequencing experiment showed that our system is sufficiently sensitive to faithfully detect small differences in clone sizes and to recover clones of very low abundance (Figure 5B).

To determine lineage relationships in vivo, LSK cells were transduced so that the vast majority of cells contained one individual barcode.[29] Barcoded cells were sorted based on eGFP expression and used to generate BM chimeras. After 8 weeks, complementary DNA from fluorescence-activated cell sorter (FACS)-sorted tDCs, splenic DCs, B and T cells, DN, DP, and SP thymocytes, as well as BM-derived Lin$^-$CD117$^+$ precursors was subjected to next-generation sequencing (Figure 5C). Analysis of the frequency of individual recovered barcodes revealed a high similarity between tDCs, splenic DCs, and BM-derived progenitors. In addition, DP and SP thymocytes had a comparable distribution of bar codes, which was clearly distinct from that of DCs (Figure 5D). The MHI is a measure of similarity, which scores identical populations as 1 and completely distinct populations as 0.[30] In order to quantify clonal relationships between sorted populations, we compared each possible pair of populations and subjected the resulting MHIs to unsupervised hierarchical clustering (Figure 5E). These calculations substantiated the initial impression of a close lineage relationship between DCs, irrespective of their origin, as well as BM-derived progenitors (Figure 5E). In contrast, all lymphoid populations were distinct from those 3 subsets. The closest linkage was observed between DP and SP thymocytes, consistent with a close temporal developmental relationship. DN thymocytes were less related to other thymocytes, possibly reflecting a heterogeneous mixture of populations undergoing dynamic changes during its lifespan. Interestingly, DN thymocytes were most closely related to splenic B cells, which might reflect their simultaneous generation from the same small population of common progenitors. In conclusion, these data indicate that a large majority of tDCs do not arise from the same intrathymic progenitor as T cells. Rather, tDCs and splenic DCs are likely to share a common origin.

Generation of a niche for DCs permits intrathymic DC development

Our data suggested that limited lineage relationships between tDCs and thymocytes in vivo despite multipotentiality of progenitors might be due to strong inductive signals, such as via Notch ligands in OP9-DL1 cultures. Therefore, we next addressed the question whether the thymic microenvironment transmits such inductive signals and whether it can be manipulated toward being permissive to non–T-lineage differentiation. To this end, we transferred congenically
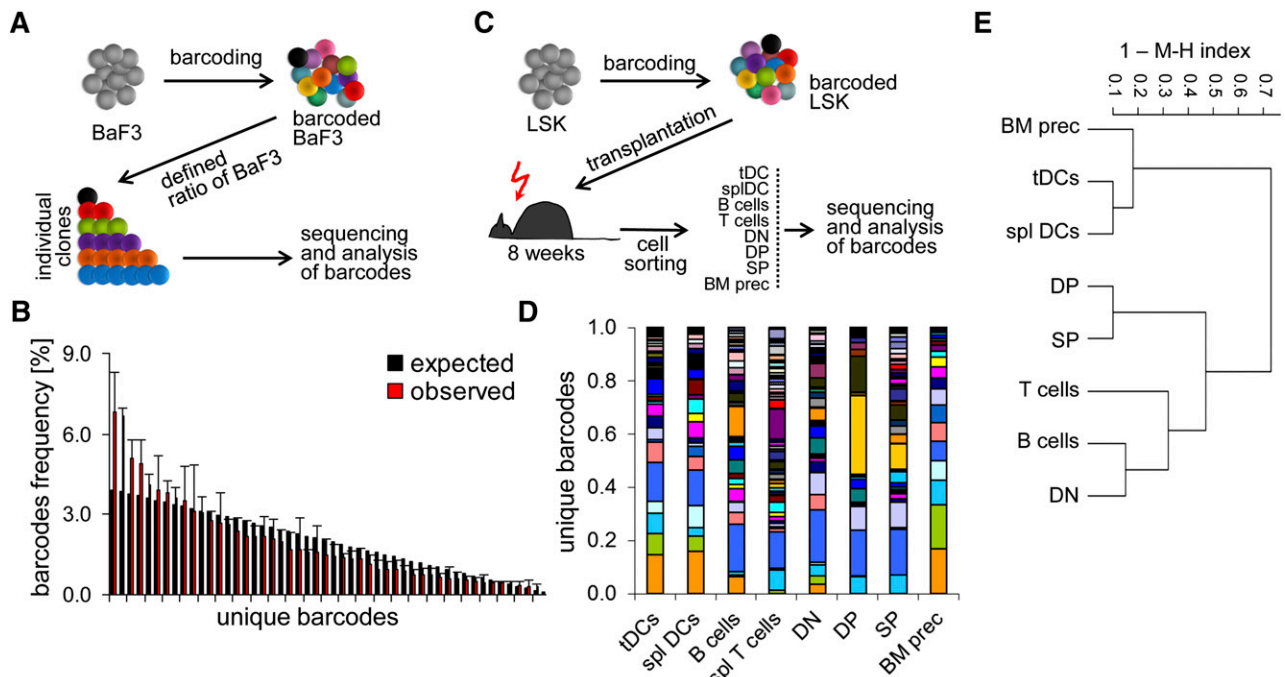
Figure 5. Limited lineage relationship of tDCs and thymocytes revealed by retroviral barcoding. (A) Experimental setup. Fifty individually barcoded BaF3 cells were clonally expanded in vitro. Bar coded BaF3 clones were then mixed at defined ratios of 50:49:48 … 3:2:1 and 50 000 cells of these mixed cultures were subjected to bar code analysis by 454 sequencing. (B) Distribution of individual barcode sequences in BaF3 test sample. Expected frequencies of individual bar codes are shown in black. Observed frequencies of individual barcodes after sequencing are displayed in red. (C) Experimental setup to assess lineage relationship between tDCs, splenic DCs, and thymocytes. LSK cells were transduced with retroviral vectors encoding the barcode library at a multiplicity of infection, on average generating a single integration event per cell. Tagged LSK were FACS-sorted based on GFP expression and injected into lethally irradiated recipients to generate BM chimeras. About 8 to 10 weeks after transplantation, indicated populations of cells were sorted (50 000 cells) and sequenced as described in (A). (D) The distribution of unique barcodes was assessed for tDCs, splenic DCs, splenic B and T cells, DN, DP, and SP thymocytes, as well as BM lin⁻CD117⁺ precursors. Each color represents a unique barcode. (E) Unsupervised hierarchical clustering based on the MHI to reveal lineage relationships between sorted populations. (B,D-E) Data are pooled of 2 independent experiments with a total number of 6 mice analyzed.

marked (CD45.1) ETPs, CX3CR1⁺ ETPs, or mixed MP/MDP cells directly into the thymus of nonmanipulated mice and assessed their capacity to generate T-lineage or DC-lineage progeny after 21 days. ETPs readily gave rise to DP thymocytes, whereas CX3CR1⁺ ETPs generated much fewer DP thymocytes (Figure 6A). None of the two populations generated DC-lineage progeny under these conditions (Figure 6A). Interestingly, transferred MP/MDP also gave rise to T-lineage cells, but not DC-lineage cells under these conditions, suggesting that the nonmanipulated thymus transmits strong inductive signals to drive progenitor cells into the T lineage.

Next, we tested whether it was possible to induce intrathymic DC differentiation from different progenitors by altering the thymic microenvironment. To this end, we employed CD11c-DOG mice where DCs can be depleted by injection of DT.[18] ETPs, CX3CR1⁺ ETPs, or MP/MDP from congenic (CD45.1) donors were transferred intrathymically into DC-depleted CD11c-DOG mice and their progeny was analyzed after 21 days. Similar to transfers into nonmanipulated recipients, all donor populations gave rise to T-lineage progeny (Figure 6B). Notably, the frequencies of donor-derived DP thymocytes in DC-depleted animals were higher after transfer of CX3CR1⁺ ETPs and MP/MDPs than after transfer into nonmanipulated recipients, suggesting that these cells are initially dependent on niches occupied by DCs (Figure 6C). In addition, in DC-depleted mice, all donor populations gave rise to CD11c⁺, as well as CD11b⁺ myeloid progeny with ETPs, showing a reduced capacity to generate myeloid cells when compared with CX3CR1⁺ ETPs and MP/MDP cells (Figure 6B-C). Thus, the depletion of DCs generates a

permissive state for myelopoiesis and DC differentiation in the thymus.

Discussion

The origin of thymus-resident cDCs, as well as that of other myeloid cells in the thymus has been controversially discussed. Experimental evidence exists that supports both common and separate origins as thymocytes. Although some of these conflicting data may be explained by high sensitivity of stromal cocultures to elicit non–T-lineage fate from T-cell progenitors (possibly due to limited availability of Notch ligands),[14,31] others are more difficult to explain. Synchronized intrathymic development of tDCs and thymocytes might be explained by a general gate opening process generating a permissive state for thymus colonization by progenitor cells irrespective of their developmental potential.[32] A pre-thymic transient convergence of developmental pathways appears to be required to explain immunoglobulin rearrangements in thymic myeloid cells.[14] However, why only thymic myeloid cells should carry these rearrangements in such a scenario is difficult to fathom.

Identification of a common DC–T-cell progenitor would constitute a prerequisite if at least some tDCs and thymocytes shared a common intrathymic origin. Because canonical DC precursors were absent from the thymus, we focused on the characterization of a subset of ETPs expressing CX3CR1, which can be described as a hallmark of DC
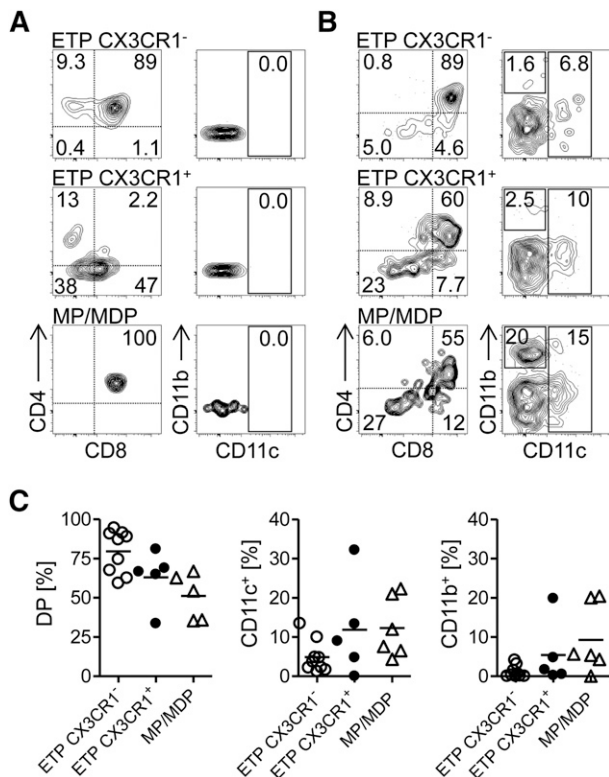
Figure 6. Generation of a niche for DCs permits intrathymic DC development. (A) Sorted thymic CX3CR1$^+$ ETPs, CX3CR1$^-$ ETPs, and BM MP/MDP precursors were injected intrathymically into congenic (CD45.1$^+$CD45.2$^+$), nonmanipulated mice. The development of myeloid cells and T cells was assessed 21 days after transfer. CD45.2$^+$ T-cell–committed precursors were either DP or SP for CD4 and CD8. Myeloid cells were CD4/CD8 DN and expressed CD11c (DC), or were CD11c$^-$CD11b$^+$ (macrophages). (B) Precursors sorted as in (A) were injected intrathymically into CD11c-DOG (CD45.1$^+$CD45.2$^+$) mice, in which DCs were depleted 24 hours prior to progenitor injection. Development of T cells and myeloid cells was assessed 21 days after transfer. (C) Quantification of data shown in (B). (A-B) Representative plots of 2 independent experiments and (C) pooled data of 2 independent experiments, with each point representing an individual mouse.

progenitors. Ten percent of all ETPs were CX3CR1^{GFP} positive, a frequency consistent with that showing no history of *Il7r* expression in a previous fate mapping study.[11] This subset displayed a marginally higher precursor frequency in non–T-lineage promoting limiting dilution assays, as well as a slightly higher capacity to generate tDCs in DC-depleted animals when compared with CX3CR1$^-$ ETPs. Given the apparent absence of ETP-derived development of tDCs in vivo, CX3CR1 expression might reflect a state of aborted lineage diversion at steady state.

Viral barcoding has emerged as a new technology to retrospectively track the behavior of cells at the clonal level. This approach has been proven useful to track differential clonal expansion of T cells during an immune response, as well as to determine hematopoietic lineage relationships.[28,33-35] Here, we have employed this method to assess lineage relationships between tDCs and thymocytes in the thymus. This experiment was based on the assumption that thymus colonization represents a bottle neck in T-cell development,[36] and that, therefore, thymocytes carry a limited set of barcodes, which is distinct from all other hematopoietic subsets. Our data showed that tDCs and splenic cDCs were closely related, whereas all T-cell subsets analyzed clustered together and displayed little similarity in terms of barcodes when compared with either set of DCs. These data support the notion that tDCs and thymocytes do not share an intrathymic progenitor, although several caveats remain to be considered. It constitutes one caveat that because of low cell numbers

amenable to analysis, heterogeneous populations had to be subjected to sequencing. Thus, the analysis of total conventional tDCs rather than CD8α$^+$ DCs might result in an underestimation of a putative thymocyte-DC relationship, because only these DCs are thought to be generated in situ.[37] Furthermore, DN thymocytes combined might contain cells originating from sequential colonization events, as thymocytes remain DN for up to 18 days.[38] This notion is consistent with our finding that total DN cells were overall more closely related to B cells than to the more mature DP and SP thymocytes, which in part have already undergone selection events. Thus, the similarity in barcode distribution between DN thymocytes and B cells possibly reflects their recent common origin from a lymphoid progenitor. Ultimately, we cannot completely exclude that the observed difference between barcodes recovered from tDCs and DN thymocytes is also caused by selection of a minor subset of DN cells to develop into tDCs. However, such a scenario would still not explain the high degree of similarity observed between splenic DCs and tDCs. Taking into account these caveats, the high degree of dissimilarity of all DCs to thymocytes and the closer relationships of DN thymocytes to more mature thymocyte lineages, as well as peripheral T and even B cells, nevertheless provide no indication for a common tDC-thymocyte progenitor.

Depletion of endogenous DCs using DT generated a permissive state for intrathymic DC development originating from various progenitors, including MP/MDPs and ETPs. These data are consistent with a previous report that showed that ablation of Notch1 in T-cell progenitors allowed their diversion into the DC lineage.[16] This study suggested that the thymic microenvironment provided inductive signals via Dll4-Notch1 interactions to prevent lineage diversion of T-lineage progenitors. Our study indicates that even wild-type progenitors are able to escape inductive signaling, once space, which is otherwise occupied by tDCs, is provided. The nature of a putative niche devoid of Dll4 yet remains elusive. However, the absence of DCs might result in high local concentrations of Flt3-L promoting intrathymic DC reconstitution. This hypothesis is consistent with the role of Flt3-L as a rheostat for DC homeostasis in the periphery.[18] Given the absence of early myeloid and uncommitted DC progenitors in the thymus, empty tDC niches could potentially be filled by ETPs provided they escape Notch signaling. Genetic ablation of *Notch1* or depletion of DCs constitute massive alterations of the thymic microenvironment, which might, similar to highly sensitive in vitro assays, reveal developmental potential that might not be elicited in a physiological situation at steady state.[14,31] Consistently, previous work based on fate mapping, as well as our barcoding approach, suggest that T-lineage progenitors generating tDCs might be a rare event at best.[11] Rather, empty tDC niches are likely to be filled by dedicated committed intrathymic progenitors, such as DN1c cells, although their prethymic origins remain to be characterized.[13]

In conclusion, our study supports a model in which the majority of thymus-resident DCs are generated from already committed progenitors, whereas noncommitted progenitors are forced into the T lineage due to strong inductive signals from the thymic microenvironment. These findings are consistent with recent fate mapping experiments.[11,12,16] Liberation of niches occupied by tDCs generates a permissive state for T-lineage progenitors to adopt an alternative fate, although the extent to which this alternative pathway of DC development operates in different physiological scenarios remains to be investigated. Of note, the presence of immunoglobulin gene rearrangements exclusively in thymic but not in other cDC subsets suggests, at least in some instances, that tDCs might be generated through this alternative pathway. Taken together, our study underscores the plasticity of the thymus to support the development of a balanced pool of cell types that is essential for its function.

Acknowledgments

Authorship

Contribution: M.Ł., N.Z., A.S., and A.K. designed research; M.Ł., N.Z., L.F., J.D., K.W., and A.S. performed research; M.Ł., N.Z., L.F., J.P., I.P., and A.K. analyzed data; and M.Ł. and A.K. wrote the manuscript.

Conflict-of-interest disclosure: The authors declare no competing financial interests.

Correspondence: Andreas Krueger, Institute of Immunology, OE5240, Hannover Medical School, Carl-Neuberg-Strasse 1, 30625 Hannover, Germany; e-mail: krueger.andreas@mh-hannover.de.

References

1. Wu L, Shortman K. Heterogeneity of thymic dendritic cells. *Semin Immunol.* 2005;17(4): 304-312.

2. Geissmann F, Manz MG, Jung S, Sieweke MH, Merad M, Ley K. Development of monocytes, macrophages, and dendritic cells. *Science.* 2010; 327(5966):656-661.

3. Corcoran L, Ferrero I, Vremec D, et al. The lymphoid past of mouse plasmacytoid cells and thymic dendritic cells. *J Immunol.* 2003;170(10): 4926-4932.

4. Wu L, D'Amico A, Hochrein H, O'Keeffe M, Shortman K, Lucas K. Development of thymic and splenic dendritic cell populations from different hemopoietic precursors. *Blood.* 2001;98(12): 3376-3382.

5. Res PC, Couwenberg F, Vyth-Dreese FA, Spits H. Expression of pTalpha mRNA in a committed dendritic cell precursor in the human thymus. *Blood.* 1999;94(8):2647-2657.

6. Ardavin C, Wu L, Li CL, Shortman K. Thymic dendritic cells and T cells develop simultaneously in the thymus from a common precursor population. *Nature.* 1993;362(6422):761-763.

7. Wu L, Vremec D, Ardavin C, et al. Mouse thymus dendritic cells: kinetics of development and changes in surface markers during maturation. *Eur J Immunol.* 1995;25(2):418-425.

8. Bell JJ, Bhandoola A. The earliest thymic progenitors for T cells possess myeloid lineage potential. *Nature.* 2008;452(7188):764-767.

9. Wada H, Masuda K, Satoh R, et al. Adult T-cell progenitors retain myeloid potential. *Nature.* 2008; 452(7188):768-772.

10. Donskoy E, Goldschneider I. Two developmentally distinct populations of dendritic cells inhabit the adult mouse thymus: demonstration by differential importation of hematogenous precursors under steady state conditions. *J Immunol.* 2003;170(7):3514-3521.

11. Schlenner SM, Madan V, Busch K, et al. Fate mapping reveals separate origins of T cells and myeloid lineages in the thymus. *Immunity.* 2010; 32(3):426-436.

12. Luche H, Nageswara Rao T, Kumar S, et al. In vivo fate mapping identifies pre-TCRα expression as an intra- and extrathymic, but not prethymic, marker of T lymphopoiesis. *J Exp Med.* 2013; 210(4):699-714.

13. Luche H, Ardouin L, Teo P, et al. The earliest intrathymic precursors of CD8α(+) thymic dendritic cells correspond to myeloid-type double-negative 1c cells. *Eur J Immunol.* 2011;41(8): 2165-2175.

14. Schlenner SM, Rodewald HR. Early T cell development and the pitfalls of potential. *Trends Immunol.* 2010;31(8):303-310.

15. Krueger A. A missing link in thymic dendritic cell development. *Eur J Immunol.* 2011;41(8): 2145-2147.

16. Feyerabend TB, Terszowski G, Tietz A, et al. Deletion of Notch1 converts pro-T cells to dendritic cells and promotes thymic B cells by cell-extrinsic and cell-intrinsic mechanisms. *Immunity.* 2009;30(1):67-79.

17. De Obaldia ME, Bell JJ, Wang X, et al. T cell development requires constraint of the myeloid regulator C/EBP-α by the Notch target and transcriptional repressor Hes1. *Nat Immunol.* 2013;14(12):1277-1284.

18. Hochweller K, Miloud T, Striegler J, Naik S, Hämmerling GJ, Garbi N. Homeostasis of dendritic cells in lymphoid organs is controlled by regulation of their precursors via a feedback loop. *Blood.* 2009;114(20):4411-4421.

19. Jung S, Aliberti J, Graemmel P, et al. Analysis of fractalkine receptor CX(3)CR1 function by targeted deletion and green fluorescent protein reporter gene insertion. *Mol Cell Biol.* 2000; 20(11):4106-4114.

20. Schmitt TM, Zúñiga-Pflücker JC. Induction of T cell development from hematopoietic progenitor cells by delta-like-1 in vitro. *Immunity.* 2002;17(6): 749-756.

21. Verovskaya E, Broekhuis MJ, Zwart E, et al. Heterogeneity of young and aged murine hematopoietic stem cells revealed by quantitative clonal analysis using cellular barcoding. *Blood.* 2013;122(4):523-532.

22. Hildinger M, Abel KL, Ostertag W, Baum C. Design of 5′ untranslated sequences in retroviral vectors developed for medical use. *J Virol.* 1999; 73(5):4083-4089.

23. Schambach A, Wodrich H, Hildinger M, Bohne J, Kräusslich HG, Baum C. Context dependence of different modules for posttranscriptional enhancement of gene expression from retroviral vectors. *Mol Ther.* 2000;2(5):435-445.

24. Föhse L, Suffner J, Suhre K, et al. High TCR diversity ensures optimal function and homeostasis of Foxp3+ regulatory T cells. *Eur J Immunol.* 2011;41(11):3101-3113.

25. Porritt HE, Rumfelt LL, Tabrizifard S, Schmitt TM, Zúñiga-Pflücker JC, Petrie HT. Heterogeneity among DN1 prothymocytes reveals multiple progenitors with different capacities to generate T cell and non-T cell lineages. *Immunity.* 2004; 20(6):735-745.

26. Cho SK, Webber TD, Carlyle JR, Nakano T, Lewis SM, Zúñiga-Pflücker JC. Functional characterization of B lymphocytes generated in vitro from embryonic stem cells. *Proc Natl Acad Sci USA.* 1999;96(17):9797-9802.

27. Krueger A, Garbe AI, von Boehmer H. Phenotypic plasticity of T cell progenitors upon exposure to Notch ligands. *J Exp Med.* 2006;203(8): 1977-1984.

28. Gerrits A, Dykstra B, Kalmykowa OJ, et al. Cellular barcoding tool for clonal analysis in the hematopoietic system. *Blood.* 2010;115(13): 2610-2618.

29. Kustikova OS, Wahlers A, Kuhlcke K, et al. Dose finding with retroviral vectors: correlation of retroviral vector copy numbers in single cells with gene transfer efficiency in a cell population. *Blood.* 2003;102(12):3934-3937.

30. Magurran AE. Ecological Diversity and Its Measurement. Princenton, NJ: Princenton University Press; 1988:192.

31. Richie Ehrlich LI, Serwold T, Weissman IL. In vitro assays misrepresent in vivo lineage potentials of murine lymphoid progenitors. *Blood.* 2011;117(9): 2618-2624.

32. Foss DL, Donskoy E, Goldschneider I. The importation of hematogenous precursors by the thymus is a gated phenomenon in normal adult mice. *J Exp Med.* 2001;193(3):365-374.

33. Schumacher TN, Gerlach C, van Heijst JW. Mapping the life histories of T cells. *Nat Rev Immunol.* 2010;10(9):621-631.

34. Naik SH, Perié L, Swart E, et al. Diverse and heritable lineage imprinting of early haematopoietic progenitors. *Nature.* 2013; 496(7444):229-232.

35. Lu R, Neff NF, Quake SR, Weissman IL. Tracking single hematopoietic stem cells in vivo using high-throughput sequencing in conjunction with viral genetic barcoding. *Nat Biotechnol.* 2011;29(10): 928-933.

36. Scollay R, Smith J, Stauffer V. Dynamics of early T cells: prothymocyte migration and proliferation in the adult mouse thymus. *Immunol Rev.* 1986; 91:129-157.

37. Li J, Park J, Foss D, Goldschneider I. Thymus-homing peripheral dendritic cells constitute two of the three major subsets of dendritic cells in the steady-state thymus. *J Exp Med.* 2009;206(3): 607-622.

38. Lind EF, Prockop SE, Porritt HE, Petrie HT. Mapping precursor movement through the postnatal thymus reveals specific microenvironments supporting defined stages of early lymphoid development. *J Exp Med.* 2001; 194(2):127-134.

Limited niche availability suppresses murine intrathymic dendritic-cell development from non-committed progenitors

Figure S1

A

GTACAAGTAA**NN**ATC**NN**GAT**SS**AAA**NN**GGT**NN**AAC**NN**TGTAAAA
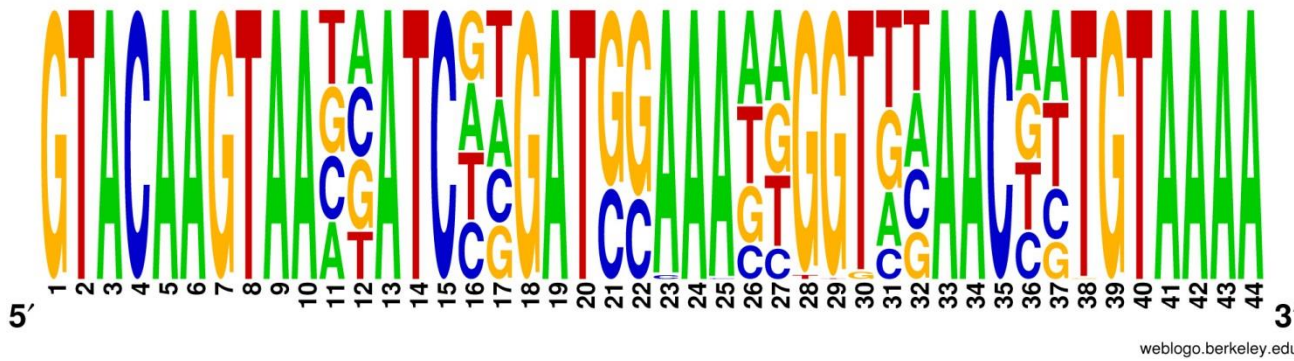
B

Figure S1. Retroviral barcode library. (A) Nucleotide sequence of barcodes. (B) Distribution of barcodes after retransformation of the library and analysis of 86 clones by Sanger sequencing. Image was generated using http://weblogo.berkeley.edu/logo.cgi.
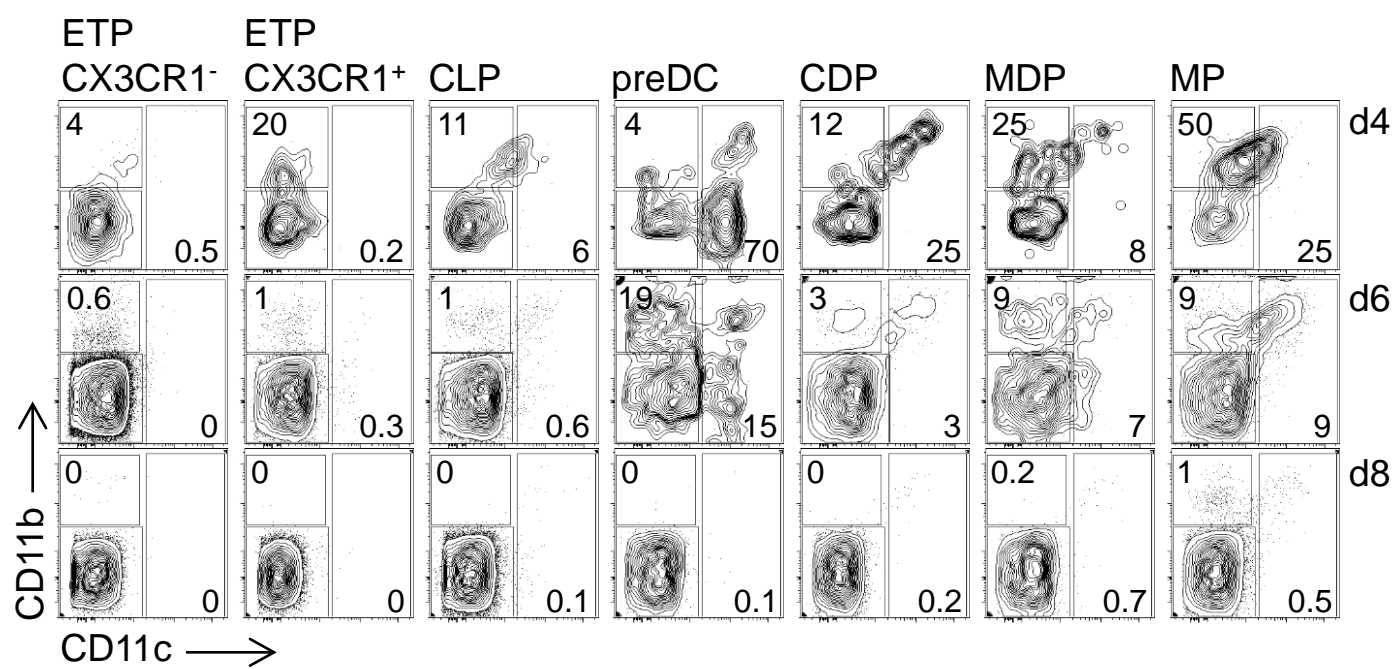
Figure S2

Figure S2. Gating strategy to assess frequency of T cell, DC and macrophage precursors in OP9-DL1 co-cultures. T cell precursors were defined as CD11c⁻CD11b⁻ cells, DC were $CD11c^+CD11b^{+/-}$ and macrophages were defined as $CD11b^+CD11c^-$ cells.